38. Erosion of natural sediments from The Netherlands

Analysis of laboratory experiments

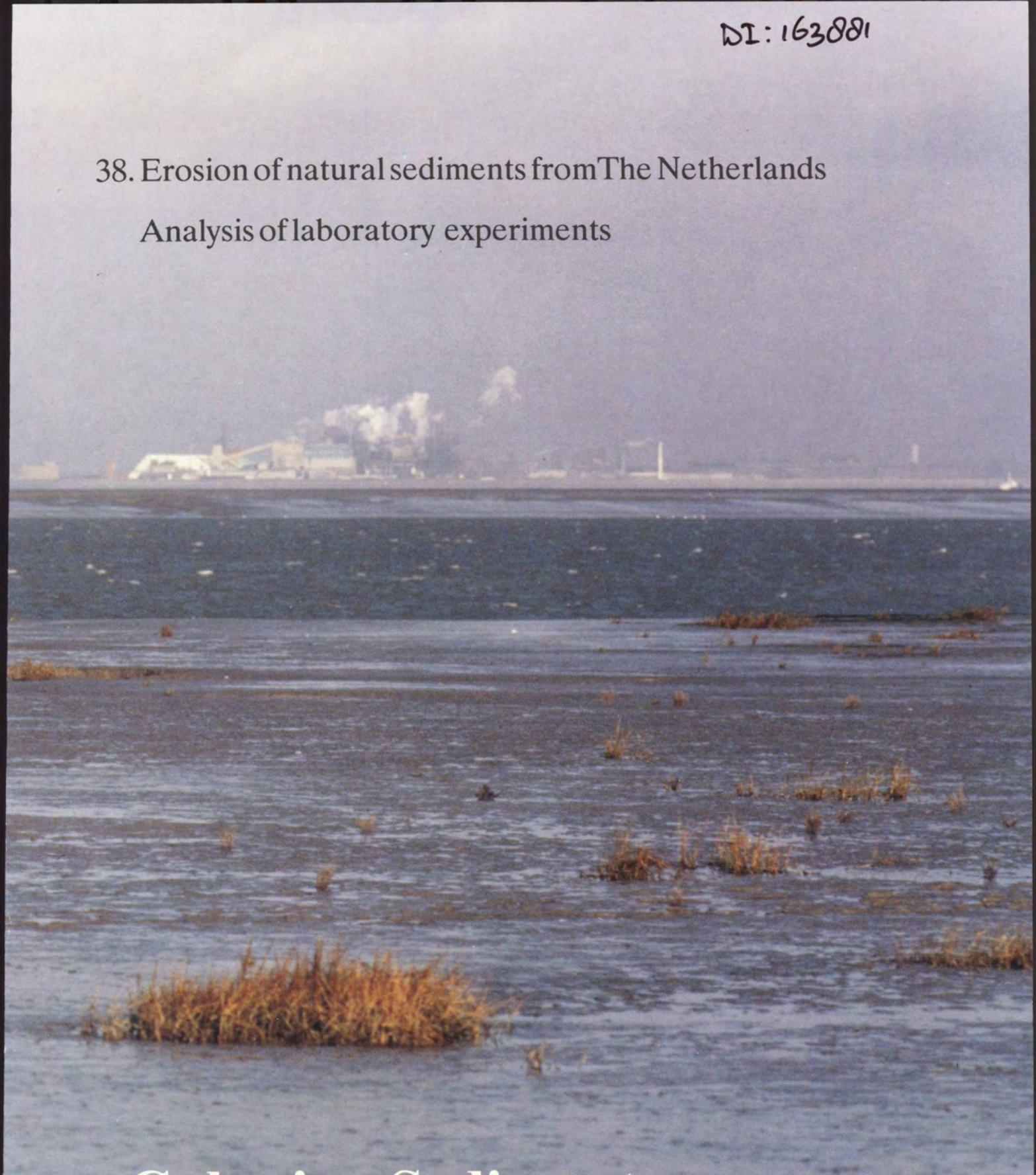

Cohesive Sediments

Rijkswaterstaat

Delft Hydraulics

Report 38. Erosion of natural sediments from The Netherlands
Analysis of laboratory experiments

J.C. Winterwerp
J.M. Cornelisse
C. Kuijper

March 1992

Cohesive Sediments

Rijkswaterstaat

Delft Hydraulics

Summary and Conclusions.

This report presents a first analysis of the experiments carried out with mud samples from the Hollandsch Diep (Sassenplaat and Moerdijkbrug), the Western Scheldt (Breskens), Lake Ketelmeer (Lake Ketel), the Meuse (Belfeld), the Eems-Dollard (Delfzijl Harbour), Loswal Noord (North Sea) and the Biesbosch (Spijkerboor). It describes mutual relations between the various physico-chemical bulk parameters, and analyses of surface erosion and tidal experiments in the annular flume. As a first step, the methodology of the experiments and their analyses and the formula used are adapted from well-known procedures encountered in literature. The study has led to the following conclusions:

1. There is some correlation between the specific surface of the sediments and the lutum fraction.

2. The dynamic viscosity of the sediments decreases with increasing sand content at concentration beyond about 300 kg/m^3.

3. The yield strength increases with increasing sediment concentration. The rate of this increase is a function of the sediment concentration; the results agree with results published by Krone, Owen and Migniot.

4. The yield strength increases with increasing specific surface and with increasing Cation Exchange Capacity.

5. The height of the interface H during consolidation experiments can be described with a formula due to Krone:

$$H/H_e - 1 = (k/t)^{nHt}$$

where H_e is the final equilibrium height, t = time in minutes, and k and nHt are parameters in the range of $30 < k < 170$ and $0,5 < nHt < 1,2$. The consolidation curves sometimes show a kink at the transition between hindered settling and consolidation (point of contraction).

6. The measurements of the sediment concentration within the bed are not accurate enough to assess the sediment concentration distribution in the upper (1 cm) part of the bed in detail. This is a big constraint in the analysis of the erosion experiments.

7. Large sand contents in the mud samples (> 50 %?) hamper the analyses and interpretation of the results considerably. For instance, the deposited bed from Loswal Noord mud shows a layered structure, and sorting effects take place during the experiments in the annular flume.

8. The sediment concentration profiles within the bed show a similarity behaviour, i.e. the shape of the profiles are similar throughout the consolidation process. This similarity behaviour can be described by:

$$c/\bar{c} = kcz\ (z/H)^{-ncz}$$

with $\bar{c}$ is mean concentration of the bed with thickness H, and kcz and ncz are parameters in the range $0,1 < kcz < 0,8$ and $0,3 < ncz < 1,7$; ncz increasing with increasing sand content.

9. The depth mean concentration $\bar{c}$ can be related to the consolidation time T_c through:

$$\bar{c} = c_{ref}\ T_c^{nct}$$

with $120 < c_{ref} < 360$, depending on the sand content, and nct = 0,1 à 0,2.

10. During the consolidation process, a light coloured, thin layer of oxidized material is formed on the bed surface. The mechanical properties of this layer differ from the properties of the lower anaerobic bed: this oxidized layer is eroded first before the remaining non-oxidized layer is been eroded.

11. The critical shear strength against erosion τ_e appears to increase with increasing sediment concentration c_b. This however could not be quantified in detail, because of the inaccuracies in c_b.

12. The critical shear strength against erosion τ_e varies largely within the upper 10 - 20 % of the bed from about 0,1 to 0,7 Pa for a consolidation time of 1 day and from about 0,2 to 0,8 Pa for a consolidation time of 7 days.

13. The data on the erosion rates show a large scatter, comparable to the scatter encountered in literature. For a first approximation the surface erosion rate E observed during the present experiments can be described as by:

$$E = E_f \exp\{\alpha(\tau_b - \tau_e)\}$$

with the floc erosion rate $E_f \approx 10^{-5}$ kg/m^{2}s and $\alpha \approx 30$ Pa^{-1}, though the scatter is large: $0{,}5.10^{-6} < E_f < 52.10^{-6}$ kg/m^{2}s and $27 < \alpha < 60$ Pa^{-1}). These parameters are in the range encountered in literature.

14. The floc erosion rate E_f and the maximum erosion rate E_m seem to show an asymptotic increase with increasing bed shear stress τ_b.

15. The variation in τ_e for the various samples is not very large. However, the variation (accuracy) in E_f is huge, and in fact larger than the variation in physico-chemical properties of the samples.

16. During the tidal experiments with a maximum bed shear stress of 0,2 Pa only very little sediment could be re-entrained from the bed into suspension.

17. During the tidal experiments with a maximum bed shear stress of 0,4 Pa a dynamic equilibrium in the flocculation, deposition, consolidation and re-entrainment/erosion processes occurred after about 10 tidal cycles.

18. The effective settling velocity during the depositional phase of the tide is affected by the processes of flocculation and hindered settling, comparable to observations reported in literature. During this phase a soft fluid mud layer is formed.

19. The erosion/re-entrainment phase during accelerating tide is governed by two different processes. Initially the soft fluid mud layer is eroded by entrainment processes at the interface. After some time, the interface becomes stable and smooth surface erosion is observed.

20. The entrainment processes mentioned above are very similar to those observed in stratified two layer fresh-saline water flows. The observed rate of entrainment however is much lower.

21. The observed surface erosion can be described with the classical formula by Parchure mentioned under conclusion 13.

22. It is hypothesized that this two mode response of the bed is caused by a secondary compaction of the bed due to the internal waves at the interface and/or the character of the instabilities themselves.

Table of contents.

		Page
	Summary and conclusions.	1
	Table of contents.	4
	List of symbols.	6
1.	Introduction.	8
2.	Summary of physico-chemical properties.	9
3.	Bed development.	16
3.1	Water-bed interface.	16
3.2	Bed concentration profiles.	18
4.	Steady state erosion experiments in the annular flume.	23
4.1	General observations and remarks.	23
4.2	Method of analysis.	25
4.3	Strength distribution within the bed.	27
4.4	Erosion rate.	29
5.	Tidal experiments in the annular flume.	33
5.1	General.	33
5.2	Phenomenological description of the processes during tidal cycle.	34
5.3	Resuspension by entrainment - a literature review.	35
5.4	Series 1 Tidal experiments ($\tau_{b,max}$=0,2 Pa).	39
5.5	Series 2 Tidal experiments ($\tau_{b,max}$=0,4 Pa): Deposition.	40
5.6	Series 2 Tidal experiments ($\tau_{b,max}$=0,4 Pa): Erosion.	42
	Acknowledgements.	49
	Literature.	50
	Table 2.1: Physical-chemical properties of the water and sediment.	
	Figures.	

Appendix A: Test programme to determine the flow induced erosion and sedimentation behaviour of natural muds encountered in The Netherlands.

Appendix B: Method of analysis of erosion experiments.

Appendix C: Correlations between erosion rate and some functions of the bed shear stress.

Appendix D: Summary of entrainment experiments described in literature.

List of symbols.

		Units
c	sediment concentration	kg/m^3
$\bar{c}$	depth mean sediment concentration	kg/m^3
c_0	initial sediment concentration	kg/m^3
c_b	sediment concentration within the bed	kg/m^3
c_e	final sediment concentration after consolidation	kg/m^3
c_{pa}	sediment concentration of primary aggregates	kg/m^3
c_{rel}	relative sediment concentration; $c_{rel} = c/c_e$	-
c_s	sediment concentration of the suspension	kg/m^3
c_v	sediment concentration by volume	-
CEC	Cation Exchange Capacity	meq/100gr
D	particle diameter	m
D	deposition rate	kg/m^2s
E	erosion rate	kg/m^2s
E_f	floc erosion rate	kg/m^2s
E_{max}	observed maximum erosion rate	kg/m^2s
E_p	potential erosion rate (Parchure´s formula)	kg/m^2s
E_v	entrainment rate; $E_v = u_e/U$	-
E_{v*}	entrainment rate: $E_{v*} = u_*/U$	-
F_l	lutum fraction	-
g	acceleration of gravity	m/s^2
H	thickness of sediment bed	m
H_e	final thickness of sediment bed after consolidation	m
h	water depth	m
k	coefficient in equ. (3.1)	-
k	wave number: $k = 2\pi/\lambda$	1/m
k_1	coefficient in equ. (5.9)	-
k_2	coefficient in equ. (5.9)	-
kcz	coefficient in equ. (3.3)	-
M	erosion parameter	kg/m^2s
Ms	mass per unit area of sediment within bed	kg/m^2
n	coefficient in equ. (5.9)	-
nct	coefficient in equ. (3.5)	-
ncz	coefficient in equ. (3.3)	-
ncτ	coefficient in equ. (2.4)	-
nHt	coefficient in equ. (3.1)	-
O_s	specific surface of sediment	m^2/gr
Ri	gradient Richardson number	-
Ri_0	overall Richardson number	-
Ri_u	overall Richardson number; see equ.(5.21)	-

Ri_*	overall Richardson number; see equ.(5.18)	-
SAR	sodium adsorption ratio	meq/l
T	temperature	°C
T_c	consolidation time	min
t	time	sec
U	mean velocity in suspension	m/s
u	velocity	m/s
u_e	entrainment velocity	m/s
u_*	shear velocity	m/s
W_s	effective settling velocity	m/s
W_{s0}	reference settling velocity	m/s
z	vertical coordinate	m
z_{rel}	relative vertical coordinate within bed: $z_{rel}=z/H$	-
α	erosion coefficient in equ.(4.5)	Pa^{-1}
β	erosion coefficient in equ.(4.5)	-
β	coefficient in equ.(5.9)	-
δ_u	thickness of layer with velocity gradient	m
δ_ρ	thickness of layer with concentration gradient	m
ε	parameter describing ratio δ_u and δ_ρ of mixing layer	-
ζ	amplitude internal waves	m
λ	length internal waves	m
μ	dynamic viscosity sediment suspension	mPas
μ_d	effective viscosity sediment suspension	mPas
μ_0	dynamic viscosity of pore water	mPas
ρ	density	kg/m^3
ρ_b	density within bed	kg/m^3
$\Delta\rho$	density difference	kg/m^3
σ	celerity of internal waves	m/s
τ_B	upper Bingham strength of sediment	Pa
τ_b	bed shear stress	Pa
$\tau_{b,max}$	maximum bed shear stress during a tidal experiment	Pa
τ_e	critical shear stress for erosion	Pa
τ_y	yield strength of sediment	Pa

1. Introduction.

In commission of and in collaboration with Rijkswaterstaat (Ministry of Transport and Public Works, The Netherlands), Dienst Getijdewateren (Tidal Waters Division) and RIZA (Inland Water Division) Delft Hydraulics is performing a long term basic study into the behaviour of cohesive sediments. A part of this programme was dedicated to studying the erosion and deposition characteristics of sediments from various locations in The Netherlands (see Table 2.1 for a summary). This was done through the execution of a "Standard experimental programme" (see Appendix A) involving experiments in the annular flume and measurements of various physico-chemical bulk parameters. This work was carried out in 1989 and 1990 and the results were presented in a series of reports - see Kuijper et al [1990], [1991].

The present report gives a first analysis of the results from the erosion and tidal experiments and comparisons between the properties of the various sediment samples. The data are mainly compared with other, well-established data encountered in literature, and for the analyses existing, often used formula are applied. The present study therefore should be regarded only as a step towards a better understanding of the processes. Moreover, many of the existing data were not yet explicitly used in the analyses.

In Chapter 2 possible relations between the physico-chemical bulk-parameters are discussed. In Chapter 3 the (density) structure of the deposited beds are studied. This is a basic part of the report, as all the results presented in the Chapters 4 and 5 are highly affected by the accuracy of the sediment concentrations within the bed. The erosion characteristics of the bed were measured during experiments in the annular flume by increasing the bed shear stress in successive steps. The results are discussed in Chapter 4. Finally, two preliminary experiments were conducted under tidal flow conditions (i.e. a sinusoidally varying flow velocity). These are discussed in Chapter 5. A major part of the analyses of these tidal experiments were carried out before the analyses of the steady state erosion experiments. As a result, Chapter 4 and 5 are not entirely consistent everywhere.

2. Summary of physico-chemical properties.

During the Standard Programme on mud characteristics, various physico-chemical properties were measured. These properties are summarized in Table 2.1.
The table shows that the samples can be classified with respect to the salinity of their environment. The chlorinity of the North Sea amounts to about 17 to 20 kg/m^3. Thus the samples from the Western Scheldt (Breskens), Eems-Dollard (Delfzijl Harbor) and Loswal Noord (North Sea) were taken in saline water, whereas the samples from the Hollandsch Diep (Sassenplaat and Moerdijkbrug), Lake Ketel, Meuse (Belfeld) and Biesbosch (Spijkerboor) were taken in fresh water.

From a mineralogical point of view, the various sediments do not differ much. All sediments contain a considerable amount of illite and chlorite clays, and a major fraction of quartz and feldspar minerals. Remarkable is the absence of the highly cohesive montmorillonite in the sediments. Even a small fraction of this clay will have a large effect on the sediment properties.
The mineralogical composition was assessed with the röntgen-diffraction method. The sediment is first dispersed and then sieved through a 150 µm sieve. However, it should be remarked that at this moment the accuracy of determining the mineralogical components is not well understood. This is subject of further studies.

The organic content of all samples is fairly high (about 5 to 12 %), except of those taken in Delfzijl Harbor and at Loswal Noord. The oxygen content of the sediments is fairly low to nil, indicating reduced conditions (this in contrast to the high oxygen concentrations in the water samples). This agrees with the values of the Redox Potential E_h which are strongly negative, characteristic for sediments with high organic content (Zobell [1946]). A remarkable anomaly is the combination of a relatively high oxygen content and negative redox potential observed for the samples from Hollandsch Diep (Moerdijkbrug) and Breskens. No explanation was found for this behaviour.

The sand fraction ($D > 63$ µm) of the sediment samples varies widely, with a very high content for the samples from Delfzijl Harbor and Loswal Noord. This causes considerable interpretation problems, as well as experimental problems: it is difficult to obtain a homogeneous sample, characteristic for that specific sediment, sand grains can disturb the

proper functioning of the rheometer, the sediment is likely to sort during experiments in the annular flume, etc.
Also the fraction of lutum (D < 2 μm) varies by about a factor 2 between 14 and 30 %. Verreet [1988] suggests a correlation between the lutum fraction F_1 and the specific surface O_s [m^2/gr] of the sediment. To get a feeling of the values to be expected, this relation can be established for spheres and clay plates of one diameter.
For a fraction F_1 of spherical particles of diameter D, $O_s = 2{,}26.10^{-6}/D * F_1$; hence for example for D = 2 μm, $O_s = 1{,}13\ F_1$, and for D = 0,5 μm, $O_s = 4{,}5\ F_1$. Typical values for O_s for various clay minerals are: chlorite: $5 < O_s < 50$ m^2/gr, kaolinite: $25 < O_s < 50$ m^2/gr, illite: $75 < O_s < 125$ m^2/gr and montmorillonite: ca 750 m^2/gr.
The diameter d of illite clay varies between 0,1 and 2 μm, and its thickness amounts to about 0,1 d. Hence, for example d = 0,5 μm, $O_s = 18\ F_1$.
The values of the Dutch sediments and those of Verreet given in Figure 2.1 showing the correlation:

$$O_s \propto 2{,}5 * F_1 \qquad (2.1)$$

with F_1 in [%]. For the sub-sample of Dutch estuarine sediments and Dutch inland water sediments other correlations can be established:

$$O_s \propto 8 * F_1 \qquad \text{for marine mud} \qquad (2.1a)$$

$$O_s \propto 5 * F_1 \qquad \text{for inland water mud} \qquad (2.1b)$$

The large scatter in the data points is due to the presence of both clay, plate-like particle and the more spherical quartz particles in the samples with D < 2 μm.

Another measure for cohesion are the rheological properties. These are being measured in a rotating cylinder "applied strain" rheo-meter. A typical result for sediments from the Hollandsch Diep (Sassenplaat) is given in Figure 2.2, showing a general-plastic (shear thinning) character with thixotropic behaviour for concentrations beyond c = 100 kg/m^3. This general-plastic behaviour is characterised by a yield strength τ_y, which is defined as the shear stress at which deformation starts. It can be argued (Otsubo [1985], James [1987]) that τ_y is related to the strength of the bed against erosion. Unfortunately, it cannot be measured unambiguously with an applied strain rheo-meter, as the measured value is a function of the acceleration of the cylinders. A

more unambiguous parameter is the Bingham shear strength τ_B, which is defined as the intercept of the straight part of the flow curve with the vertical axis. The rheological behaviour is then approximated by a Bingham plastic model. The accelerating curve depicts an overshoot; the decelerating curve is smoother. The overshoot is caused by changes in the structure of the sediment, resulting in different curves: the so-called thixotropic effects (see Blom et al [1986]). The magnitude of this overshoot is probably a function of the acceleration of the rheometer; this was however not elaborated.

Rheological measurements are fairly subjective in the sense that the results are affected by the choice of the rheo-meter and the measuring cylinders, the acceleration of the cylinders, preparation of the samples, etc. These aspects will be subject of another study.
The present results were obtained with a Haake RV100 rheometer. An acceleration period of 1 minute was applied, achieving a maximum shear rate of 150 s^{-1}. All measurements were carried out at 20 ^{o}C. Data were sampled at a frequency of 4 Hz. The following sensors were used:

sediment from	low conc. sensor	high conc. sensor
H-Diep (Sasspl)	≤ 200: CV100, DA45	≥ 200: CV100, ME15
H-Diep (Moerdb)	≤ 250: CV100, DA45	
W´Scheldt	≤ 300: CV100, DA45	≥ 200: RV100, MEII
Lake Ketel	≤ 300: CV100, DA45	≥ 300: RV100, MEII
Meuse	≤ 400: CV100, DA45	≥ 400: CV100, Q30/2
Eems-Dollard	≤ 300: CV100, DA45	≥ 400: CV100, Q30/2
Loswal Noord	≤ 230: CV100, DA45	≥ 220: CV100, Q30/2
Biesbosch	≤ 250: CV100, DA45	≥ 250: CV100, Q30/2

Table 2.2: Sensors used with Haake RV100 rheo-meter for rheological measurements (N.B. CV100 is a special configuration of the measuring sensor. DA45, ME15 and MEII are cylindrical elements and Q30/2 is a plate-like element)

A final remark concerns the small vibration of the curves. This is probably due to sand particles in the sample, which cause occasional additional friction within the rheo-meter.

The Figures 2.3a and 2.3b show the measured dynamic viscosity μ_d as a function of sediment concentration; μ_d is defined as the slope of the straight part of the decelerating flow curve. At sediment concentrations below c = 200 kg/m^3 the various curves coincide well, and no significant

trend with any of the physico-chemical properties can be deduced. At higher concentrations larger differences are observed. At c = 400 kg/m^3 μ_d apparently is directly related to the sand content - see Figure 2.4a. Though this seems plausible, it is not clear why this behaviour is not observed at smaller concentrations.
For clear water at T = 20 °C, μ_{dw} = 1 mPas, which is taken as the reference value in the following analysis by considering the behaviour of the relative viscosity μ_d/μ_{dw}.
Einstein [1906] considered the effect of elastic, spherical particles in dilute suspensions. He reasoned that the flow will be accelerated and decelerated around the particles, which will result in effective internal strains due to non-linear effects. Together with the additional friction between fluid and particles, an effective viscosity for the fluid as a function of particle concentration can be deduced:

$$\mu_d = \mu_0 \, (1 + 2{,}5 \, c_v) \qquad (2.2)$$

where c_v is the concentration of the particles by volume [-] and μ_0 the dynamic viscosity [Pas] for $c_v = 0$ (i.e. $\mu_0 = \mu_{dw}$). For c = 100 kg/m^3 ($c_v \approx 0{,}04$) $\mu_d = 1{,}09 \, \mu_0$. Lee [1969] gives another formula based on numerous experiments with rigid, incompressible particles of various shape up to high concentrations:

$$\mu_d = \mu_0 \, (1 - c_v)^{-(2{,}5 + 1{,}9 \, c_v + 7{,}7 \, c_v^2)} \qquad (2.3)$$

yielding $\mu_d = 1{,}10 \, \mu_0$ for c = 100 kg/m^3. Figure 2.3a shows that for mud, $\mu_d \approx 3 \, \mu_0$ for c = 100 kg/m^3. In the examples above, c_v is taken as the volume concentration of the primary particles. It would make more sense to use the volume concentrations of the particle aggregates. These are not known however. On the other hand, from equ. (2.3) it follows that c_v should be 0,27 to get $\mu_d = 3 \, \mu_0$. This seems a reasonable value (see also Table 2.3).
From this analysis it is clear that it is not only the cohesive bonds between the particles, but also the presence of the grains themselves which affect the viscosity of the suspensions.

Figure 2.4b shows a comparison of the results with data from other sources (Ross [1988]). The sediments from Brunswick Harbor (CEC = 38 meq/100 gr) contain kaolinite, montmorillonite, chlorite, illite, quartz and feldspar, the sediments from Wilmington District (CEC = 32 meq/100 gr) kaolinite, montmorillonite, vermiculite and quartz, and the

sediments from San Francisco Bay (CEC = 34 meq/100 gr) contain kaolinite, montmorillonite and illite and some quartz and chlorite. The difference with the results by Krone is striking. This can be explained only partly by the presence of the strong cohesive montmorillonite. A second (major?) reason lies in the data used by Ross. Also in the original results by Krone a large scatter for the various tests is observed. However, Ross only presented the results with the highest viscosities. Other data by Krone agree better with the present results.

The results of the yield strength τ_y are plotted against the sediment concentration c in the Figures 2.5a and 2.5b; τ_y is defined as the intercept of the decelerating flow curve with the vertical-axis.[1] It is interesting to compare the results with those given by Krone [1986], Owen [1975] and Migniot [1968], [1989], [1989]. This is done graphically in Figure 2.5a. The difference in functional behaviour observed by these three authors becomes clear at once: within the range of concentrations the experiments were performed, their results do not disagree - they merely do not overlap. Hence:

$$\tau_y \propto c^{nc\tau} \qquad (2.4)$$

with $2,5 < nc\tau < 6$, depending on the sediment concentration. However, the physical mechanisms behind this behaviour are presently not clear.

Verreet [1988] tried to correlate τ_B with several physico-chemical bulk parameters. He favoured the specific surface of the particles O_s. This is shown in Figure 2.6:

$$\tau_B \ (c = 300 \text{ kg/m}^3) \propto O_s^{2,8} \qquad (2.5)$$

Figure 2.7 shows that τ_y and the Cation Exchange Capacity CEC are not well correlated.

Another relation often encountered in literature is due to Krone [1986]:

$$\tau_B(c_{pa}) = 0,39 + 0,084 \ (CEC\text{-}clay) \qquad (2.6)$$

---

1. In the following analyses, τ_y is compared with values of τ_B encountered in literature. Though the variations of τ_y and τ_B with various other parameters are expected to be similar, the magnitudes may differ considerably, as τ_y is always smaller than τ_B, and sometimes $\tau_y \ll \tau_B$. It is therefore recommended to define also τ_B from the existing flow curves.

CEC-clay is defined as the Cation Exchange Capacity for the smallest clay particles:

$$\text{CEC-clay} = \frac{\text{CEC of sediment sample (incl. sand)}}{\text{lutum fraction } (< 2\ \mu m)} \qquad (2.7)$$

The CEC-values were measured on the complete sample, i.e. including organic material at pH = 7. This value can be corrected for organic material through:

$$\text{CEC}_{\text{no org.}} = \text{CEC}_{\text{with org.}} - \alpha.[\%\ \text{org. matter}]$$

where $1,5 < \alpha < 6,5$ depending on the organic content, with a mean value of about $\alpha = 3,5$.
Typical values for the CEC are: chlorite: 20 meq/100 gr, kaolinite: 5 - 10 meq/100 gr, illite: 20 - 40 meq/100 gr and montmorillonite: 80 to 125 meq/100 gr.
τ_B (c_{pa}) is the Bingham shear strength of the primary aggregates of the sediment, which can be obtained with a procedure explained in detail in Krone [1986]. A summary is given here.

For infinite dilute suspensions, i.e. a suspension containing one particle, equ. (2.2) can be applied. If a second particle is added, the viscosity becomes:

$$\mu_d' = \mu_d\ (1 + 2,5\ c_v') \qquad (2.8)$$

This can be elaborated for a third, fourth particle, etc. yielding eventually:

$$\mu_d = \mu_0\ \exp\{2,5\ c_v\} \qquad (2.9)$$

Also the experimental viscosity curves in Figure 2.3b can be described with an exponential curve:

$$\mu_d = \mu_0\ \exp\{k.c\} \qquad (2.10)$$

From equs. (2.9) and (2.10) and the experimental slopes k, c_v can be established as a function of the concentration c. The slopes k from the experimental curves shown in Figure 2.3b are given in Table 2.3, varying between about 0,004 and 0,01. This would yield a volume concentration for for example c = 100 kg/m^3 of c_v = 0,16 to 0,4. This is in the range of the results discussed above.

sediment from	slope k m^3/kg	conc. c_{pa} prim. aggr.	Yield. str. τ_y (c_{pa})
H-Diep (Sasspl)	0,0106	235 kg/m^3	1,4 Pa
H-Diep (Moerdb)	0,0075	334	1,9
W´Scheldt	0,0075	334	0,7
Lake Ketel	0,0078	319	2,1
Meuse	0,0071	353	0,7
Eems-Dollard	0,0057	441	1,1
Loswal Noord	0,0037	668	6,0
Biesbosch	0,0096	259	1,8

Table 2.3: Yield strength for primary particles (c_v = 1).

Next, the primary particle aggregates are defined as those aggregates for which c_v = 1. Using the experimental slope k, obtained for low sediment concentrations, Krone could obtain the high concentrations of the primary aggregates through extrapolation. Thus, his results are obtained from experimental results with a capillary visco-meter for sediment concentrations below c ≈ 80 kg/m^3, and extrapolating these to concentrations up to several hundred kg/m^3.

For the present study, c_{pa} can be read directly from Figure 2.3a (from μ_d/μ_0 = exp {2,5}), and τ_y (c_{pa}) from Figure 2.5b. The results are listed in Table 2.3 and shown in the Figures 2.8 and 2.9. It can be seen that the results of the present study show no correlation with CEC. The values however are in the range of the values given by Krone, though lower. This latter is probably due to the fact that in general $\tau_y < \tau_B$. However, this could not be quantified.

3. Bed development.

3.1 Water-bed interface.

During the formation of the bed from deposition of a suspension of fine-grained, cohesive sediments in the annular flume and/or the consolidation column, the lowering of the water-bed interface was monitored. The results are shown in the Figures 3.1a through 3.7a. The last part of the curves are redrawn in the Figures 3.1b through 3.7b in an H vs 1/t plot, similar to the representation by Krone [1962]. These curves are fairly straight for about $0,1 < 1/t < 0,01$, which is comparable to the results Krone obtained in a 36 cm high consolidation column - see Figure 3.8. This phase is called primary consolidation and the relevant processes are comparable to the processes of hindered settling. At smaller values of 1/t, a significant deviation is observed. This is due to a second phase of consolidation when the pore water is squeezed out by the weight of the sediment particles (self weight-consolidation).[2]

Krone [1962] found that this consolidation process could be described as:

$$\frac{H}{H_e} - 1 = \left(\frac{k}{t}\right)^{nHt} \qquad (3.1)$$

where H(t) = height interface, H_e = is ultimate interface height after complete consolidation, t = time [min], and k and nHt are parameters. The Figures 3.1 through 3.7 are replotted in the Figures 3.9 through 3.15. A linear fit is drawn through the data; for three sediments two curves are given. The resulting coefficients k and nHt are compared in Table 3.1 with the results by Krone for San Francisco Bay mud - see also Figure 3.8.

Relation (3.1), with nHt = 1 represents Krone´s results up to about 100 to 200 min. (1/t = 0,01 to 0,005) fairly well - see Figure 3.8. At

2. N.B. Unfortunately there is some unambiguity in the terminology: the first consolidation phase is often referred to as the phase of hindered settling, whereas the second phase is called "primary consolidation"; secondary consolidation is then the final phase during which (a part of) the aggregates are broken up, the thickness of the bed continues to decrease slightly and chemical processes become important. In general however, the strength of the bed increases largely during this "secondary consolidation" process.

larger times, a significant deviation is observed. It should be remarked that for large t the results become inaccurate, as H approaches H_e.

Mud source	Curve	c_0 [kg/m^3]	k	nHt
San Francisco Bay (Krone [1962])	-	8,6	28	1
	-	14	31	1
	-	20	45	1
	-	25	54	1
	-	40	36	1
H´Diep (Sassenplaat)	-	57	72	0,5
H´Diep (Moerdijkbrug)	first	49	31	0,5
	second	49	73	0,9
W´Scheldt (Breskens)	first	56	155	0,5
	second	56	171	0,8
Lake Ketel	first	56	47	0,7
	second	56	62	1,2
Meuse (Belfeld)	-	53	22	0,6
E-Dollard (Delfzijl)	-	60	79	0,5
Loswal Noord (North Sea)	-	60	76	0,6

Table 3.1: Bed-water interface during consolidation.

Figure 3.9 through 3.15 show that some of the consolidation curves of Dutch mud show a kink between 100 and 300 min. This kink corresponds to the transition between the processes of hindered settling of a mud suspension and consolidation of a mud bed, as explained above. This is schematically shown in Figure 3.16. The transition point is called contraction point after Sills [1986]. During the present experiments the lower branch of the consolidation curve (the "density step change" between the bed and the suspension - see Figure 3.16) were not recorded. It is recommended to include this in future experiments.
The first part of the curves, which should correspond to Krone´s observations, show $0,5 < nHt < 0,7$, hence lower than Krone. This is probably due to the fact that nHt should not be a constant: the processes of hindered settling are a function of the (initial) sediment concentration and bed thickness, c.q. column height, though these don´t differ too much.

From the schematic diagram it should be expected that all curves would show a kink. However, 4 out of the 7 curves (H´Diep/Sassenplaat, Meuse,

E-Dollard/Delfzijl and Loswal Noord) do not show this trend. A possible explanation might be found in the sand content, which is high for the sediments from the Meuse, Eems-Dollard and Loswal Noord. A high sand content may promote the outflow of pore water (f.i. through small channels along the wall of the consolidation column), which will accelerate the consolidation process. Hence, only the right hand part of the consolidation curves (beyond the point of contraction) are found. This will be subject of future studies.

3.2 Bed concentration profiles.

The concentration profiles measured in the various cohesive beds are shown in the Figures 3.17 through 3.24. These profiles can be presented in a non-dimensional form by defining:

$$\text{Relative concentration} = c_{rel} = c / \bar{c}$$
$$\text{Relative depth} = z_{rel} = z / H \qquad (3.2)$$

where $\bar{c}(t)$ = depth-averaged concentration [kg/m^3], and H(t) = bed thickness [m]. These non-dimensional profiles are shown in the Figures 3.25a through 3.32a to collapse reasonably into one curve, except for the mud from Loswal Noord. This is probably due to the high sand content of the Loswal Noord samples. This causes a layered structure of the bed - see the zig-zag curve in Figure 3.23.
Next, the non-dimensional profiles are replotted on logarithmic scale in the Figures 3.25b through 3.32b. Apparently, most of the profiles can be described by:

$$\frac{c}{\bar{c}} = kcz \left(\frac{z}{H}\right)^{-ncz} \qquad (3.3)$$

This relation was used before by for instance Owen [1975], Thorn and Parson [1980] and by Mehta et al [1982]. The results are summarized in Table 3.2.

The Figures 3.33 through 3.40 compare the predicted and measured bed concentration profiles. It is shown that the agreement between the empirical fits and the experimental data is fair, except near the bed surface for the sediments from Hollandsch Diep, Lake Ketel and Biesbosch. The data suggest a fairly smooth concentration gradient near

the bed surface for these sediments, which is not represented by (3.3). However, the accuracy of the measurements here is questionable, as the diameter of the acoustic probe is 0,5 cm, hence beyond the required resolution to measure within the top of the layer. It will be argued in Chapter 4, that the results of the analyses of the erosion experiments are very sensitive to the concentration distribution within this top layer. It is therefore recommended to carry out additional experiments, focussed on measuring the bed concentration within this top layer.

Mud source	c_0 [kg/m^3]	$\bar{c}_e$ [kg/m^3] ac.m	intf	H_e [m]	ncz	kcz
H´Diep (Sassenplaat 1)	57	253	248	0,069	0,3	0,75
H´Diep (Sassenplaat 2)	57	271	287	0,060	0,3	0,75
H´Diep (Moerdijkbrug)	49	300	288	0,051	0,3	0,7
W´Scheldt (Breskens)	56	305	365	0,046	0,8	0,45
Lake Ketel	56	302	262	0,064	0,3	0,65 0,55
Meuse (Belfeld)	53	415	418	0,038	0,5	0,5 0,4
E-Dollard (Delfzijl)	60	495	450	0,040	0,6	0,3
Loswal Noord (North Sea)	134	867	1517	0,040	1,7	0,1 0,15
Biesbosch (Spijkerboor)	55	248	254	0,065	0,4	0,6
Avonmouth (Owen [1975])	7,7	253 *)		0,293	0,3	0,8
	15,4	198 *)		0,775	0,3	0,8
	17,3	-		-	0,3	0,8
Brisbane (Thorn [1980])	-	150-200 *)		0,25-,41	0,3	0,8
Grangemouth (Thorn [80])	-	150-200 *)		0,25-,41	0,3	0,8
Belawan (Thorn [1980])	-	150-200 *)		0,25-,41	0,3	0,8

Table 3.2: Density profiles (equ 3.3) *) = cons. period of 48 hrs. The second value for kcz applies for T_c = 7 days.

Table 3.2 gives two columns for the final concentration $\bar{c}_e$: "ac.m", indicating the integration by trapezium rule of the bed concentrations measured with the acoustic probe, and "intf", indicating computation of the depth mean concentration from the initial conditions and the thickness of the bed. The differences for mud from the Western Scheldt and Lake Ketel are probably due to inaccuracies inherent to the acoustic

probe; the large difference for Loswal Noord mud is due to the extreme sand content of the sample and the segregation during deposition. A visual comparison finally is given in the Figures 3.41a and 3.41b, showing a similar behaviour for all sediments. From these graphs it can be concluded that the mean bed concentration increases with increasing sand content, as expected.

Owen [1975] and Thorn and Parson [1980] found that the concentration profiles measured in a consolidation column could be desribed reasonably with:

$$c = 0{,}8\ \bar{c}\ (\frac{z}{H})^{-0{,}3} \quad , \text{ for } z > 0{,}1\ H \qquad (3.3)$$

(N.B. The sum of kcz and ncz should be unity to match the mass balance. This can be shown as follows. Let:

$$c = kcz\ \bar{c}\ (\frac{z}{H})^{-ncz}$$

Then, by definition: $\bar{c} = \frac{1}{H} \int^{H} c\ dz$, from which it follows that ncz + kcz = 1. However, the coefficients in Table 3.2 were chosen such that the empirical fit (3.3) agrees reasonably with the experimental data in the upper part of the bed.)

Parchure [1984] studied the consolidation of China Clay (kaolinite) in tap and salt water and Lake Mud (source unknown) and found an exponential relation, reading for the Lake Mud:

$$c_b = 0{,}38\ \bar{c}_b\ \exp\{1{,}73.\frac{z}{H_e}\} \qquad (3.4)$$

Though this relation differs from the power relations (3.2) and (3.3), Parchure also found similarity in the density profiles.

The coefficient ncz is a "profile parameter" giving the slope of the concentration profiles. It can be argued that steeper slopes are to be expected for more graded sediments, thus for instance with increasing sand content. This is shown in Figure 3.42. It should be remarked that the sand content in the consolidating sample may differ from the content measured in the original sample; due to sorting effects it is difficult to get a homogeneous mixture.

Plotting the depth mean concentration $\bar{c}$ versus the consolidation time T_c [hrs] (see Figure 3.43) shows again a remarkable similarity: the curves can be described with:

$$\bar{c} \approx c_{ref} . T_c^{nct} \qquad (3.5)$$

This formula is comparable to equ (3.1), but not identical. This can be shown as follows: $\bar{c}.H = \alpha$ should be constant because of continuity. Hence from equ (3.5) it follows that:

$$H = \frac{\alpha}{c_{ref}} T_c^{-nct},$$

and from equ (3.1) it follows that:

$$H = k\, H_e\, t^{-nHt} + H_e$$

Both formulations are similar, except the constant H_e in the second one. This is due to the empirical character of the studies.

The coefficients of equ (3.5) are summarized in Table 3.3. It should be remarked that though this seems an attractive description, the upper 10 % (or less) of the bed is not included in this formulation. This may give constraints for practical applications.

Mud source	c_{ref} [kg/m^3]	nct
H´Diep (Sassenplaat 1)	120	0,2
H´Diep (Sassenplaat 2)	120	0,2
H´Diep (Moerdijkbrug)	130	0,2
W´Scheldt (Breskens)	140	0,2
Lake Ketel	140	0,1
Meuse (Belfeld)	140	0,1
E-Dollard (Delfzijl)	220	0,2
Loswal Noord (North Sea)	360	0,1
Biesbosch (Spijkerboor)	140	0,2

Table 3.3: Consolidation curves (see equ (3.5)).

As a first approximation the curves can be described with:

$$\bar{c} \propto T_c^{0,2} \qquad (3.6)$$

The depth mean concentration $\bar{c}$ and bed thickness H (and of course $\bar{c}_e$ and H_e) are directly related to each other. A closer look at the curves for Hollandsch Diep, Western Scheldt and Lake Ketel mud in Figure 3.43 indeed shows kinks similar to those observed in the Figures 3.11 through 3.17. These kinks are however far less pronounced, which is due to less data points.

$\bar{c}$ can be determined from the lowering of the interface, and ncz will be a function of the sediment properties, among which sand content appears to be significant. These parameters will have to be measured during deposition/consolidation experiments.

It can be concluded that equ. (3.3) seems to give a useful relation to describe the density structure of a cohesive bed. Equ. 3.5 can be used to describe the development in time, for instance during non-steady conditions.

The physical reasoning why these relations seem to work, and the exact influence of the physico-chemical properties will be subject of another study.

4. Steady state erosion experiments in the annular flume.

4.1 General observations and remarks.

During the erosion (and consolidation) experiments a number of general features were observed. These are summarized in this chapter.
As explained earlier, beds were formed by deposition from a suspension. Within about 2 hours after the start of this bed formation a thin, light coloured layer was formed on top of the bed. This was observed during most experiments. These observations are summarized in Table 4.1:

Table 4.1: Observations of top layer on sediment.

Sediment source	Cons. time	Observations of top layer
Holl. Diep Sassenplaat	1 day	Thin white top layer of about 3 mm
	7 day	idem
Holl. Diep Moerdijkbrug	1 day	Thin white top layer of about 2 mm
	7 day	idem
West. Scheldt	1 day	No top layer observed
Lake Ketel	1 day	No top layer
	7 day	Yellow-brown layer of 2 mm on top of black-brown bed [3]
Meuse	1 day	Light-brown top layer of 2-3 mm; after this layer was eroded, a new top layer was formed different from the first one
	7 day	Initial top layer of 2 mm, after erosion white top layer of about 1 cm; shows dark spots after some time
Eems-Dollard	1 day	White thin top layer
Loswal Noord	1 day	Light-brown top layer of 1 mm, very soft
	7 day	No top layer
Biesbosch	1 day	Top layer of about 5 mm; after erosion of of this layer, the bed starts to change colour again
	7 day	idem

Probably these top layers are not formed as a result of sorting effects, but as a result of oxidizing processes of the sediments. The time scale

3. During field surveys by Toet [1991], this top layer was found to be greyish in general.

of these processes is of the order of minutes. Hence, the oxidizing rate of the entire layer (i.e. the change in colour) is governed by the availability of oxygen and the diffusion processes within the bed. However, no confirming data on the oxygen content within the bed are available.

The erosional behaviour of this top layer differed for the various sediments.

For Hollandsch Diep (Sassenplaat) mud, T_c = 1 days, the top layer was eroded gradually. At τ_b = 0,35 Pa, the top layer was completely resuspended. At τ_b = 0,55 Pa a deep scour hole (about 6 cm long and 2 cm deep) was observed, growing up to about 10 cm in the final step with τ_b = 0,65 Pa.

For Hollandsch Diep (Sassenplaat) mud, T_c = 7 days, the top layer started to erode suddenly in large fractions, an hour after the bed shear stress was raised to τ_b = 0,35 Pa. During the following sub-test (τ_b = 0,4 Pa), hardly any further erosion took place. During the next step, at τ_b = 0,55 Pa, the top layer was resuspended completely.

For Hollandsch Diep (Moerdijkbrug) mud, T_c = 1 day, erosion was fairly smooth, and the top layer was eroded completely at τ_b = 0,45 Pa. For T_c = 7 days, the top layer started to erode locally at τ_b = 0,25 Pa, and was gone at τ_b = 0,45 Pa. At τ_b = 0,75 Pa, mass erosion resulted in local scour holes of about 1 cm depth.

The bed of Western Scheldt mud was not entirely flat; however, smooth surface erosion occurred.

Lake Ketel mud, T_c = 1 day was also eroded smoothly. For T_c = 7 days, the top layer was eroded completely at τ_b = 0,35 Pa.

Meuse mud was eroded smoothly. For T_c = 1 day, the top layer was eroded completely at τ_b = 0,55 Pa. During the next step, mass erosion occurred (bed failure).

At τ_b = 0,55 Pa, Eems-Dollard mud started to show mass erosion through some large scour holes, mainly near the inner wall of the flume. The erosion rate of such a scour hole seems to be considerably larger than the erosion rate of the undisturbed bed.

A main problem with the interpretation of the experiments with Loswal Noord mud was the high sand content. As a result, it was not possible to take identical samples for the consolidation experiments and the two erosion experiments. For example, the bed thickness varied between 40 and 60 mm for the various samples. For T_c = 7 days large (ca 4 mm), dilute aggregates were observed to wander over the bed.

The top layer of Biesbosch mud, T_c = 1 day erodes irregularly between τ_b = 0,31 Pa and 0,38 Pa. At τ_b = 0,48 Pa, the remaining bed starts to

change colour again. For T_c = 7 days, the top layer collapses at τ_b = 0,3 Pa. Again, at τ_b = 0,48 Pa, the remaining bed starts to change colour.

During and at the end of some tests (some) mass erosion was observed. This implies that clusters of aggregates are torn out of the bed. It is not likely that these clusters, especially when they are large, can be sampled properly with the sampling tubes and pumps presently installed in the annular flume. Hence, one of the consequences is that the concentration measurements cannot be accurate when mass erosion occurs.

4.2 Method of analysis.

The experiments were carried out by increasing τ_b in successive steps of 1 to 1,5 hours each. These steps are called sub-tests in this report.

The analyses of the experimental data are carried out in two separate steps. First, the vertical distribution of the bed strength (critical shear stress for erosion) τ_e is deduced from the data. Next the erosion rate E is determined.

The bed strength τ_e is determined in 6 steps:

1. The measured bed concentration profile $c_b(z)$ is approximated with the empirical fit (3.3) and the parameters listed in Table 3.2. This was discussed in Chapter 3 and shown in the Figures 3.33 through 3.40.

2. By integrating (3.3) over the depth, the mass distribution Ms(z) per unit area within the bed is found:

$$Ms(z) = \int_{z_b}^{H} c_b(z)\, dz = \frac{\bar{c}_b\, kcz\, H}{1 - ncz} \left[1 - (z_b/H)^{1-ncz}\right] \quad (4.1)$$

   where $z_b(t)$ = actual thickness of the bed during the erosion process (erosion depth) [m], and H = initial thickness of the bed [m] prior to erosion.

3. The measured suspended sediment concentration $c_s(t)$ measured in the annular flume at mid depth is used to determine the mass per unit area Ms(t) of the sediment in suspension:

$$Ms(t) = c_s.(H - z_b) \qquad (4.2)$$

4. From Ms(z) = Ms(t), the erosion depth z_b is found, as is shown in the sketch.

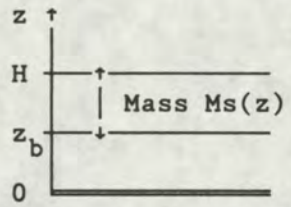

5. The erosion rate E(t) [kg/m^2s] is obtained from differentiating c_s:

$$E = (h - H)\frac{dc_s}{dt} \qquad (4.3)$$

where h = depth of annular flume. Hence, E(t) is related to $c_s(t)$ and thus to Ms(t). During a sub-test, the bed first erodes rapidly. After some time $t = t_f$, E becomes constant. It is assumed that this happens when the bed strength $\tau_e(z)$ becomes equal to the actual bed shear stress $\tau_b(t)$. The small remaining erosion at rate E_f is called floc erosion and is due to a slow, but continuous weakening of the bed and/or the fluctuations of the turbulent shear stresses (e.g. Winterwerp [1989]).
By substituting $t = t_f$ in Ms(t), Ms(z) is found and thus $z_b(t_f)$.

6. At $t = t_f$ it is assumed that $\tau_e = \tau_b$, and thus the vertical distribution of $\tau_e(z)$ is obtained.

This procedure is similar to the procedure applied by Mehta et al [1982] and by Parchure [1984]. The results are shown and discussed in Chapter 4.3. It is obvious that the results of the analyses are highly influenced by the form of the bed concentration distribution that is chosen.

For the analysis of the erosion rate E some simple empirical correlations were tried by plotting the floc erosion rate E_f and the maximum observed erosion rate E_{max} against τ_e, $\tau_b - \tau_e$, etc. The results are shown and discussed in Chapter 4.4.
Mehta et al [1982] and Parchure [1984] generate additional data for the erosion rate E within one sub-test by a special interpolation procedure. This procedure is described in Appendix B. It has two major disadvantages. First, the accuracy is very low: the experimental data are differentiated numerically and interpolated within some (a fraction of a?) mm of the bed. A second, more important problem is that this procedure does not really give additional data, but only spurious correlations. This is also further elaborated in Appendix B.

4.3 Strength distribution within the bed.

The distribution of the strength against erosion (critical shear stress for erosion τ_e) within the bed is shown in the Figures 4.1 through 4.8 for the various sediments. The vertical z-coordinate (left hand axis) is made dimensionless with the bed thickness H prior to erosion. The results show that the strength distribution can only be established for the upper 10 to 20 % of the bed (which is of the order of at most 1 cm for the present experiments). This is a consequence of the applied experimental procedure. However, within this 1 cm, τ_e increases rapidly by several factors. The graphs also show that an increase in consolidation time T_c results in an overall increase of τ_e by about 0,1 Pa, more or less evenly over the depth. A more pronounced difference further down in the bed would be expected, as was observed by for instance Mehta et al [1982] and Parchure [1984].
The right hand vertical axis of the Figures 4.1 - 4.8 yield the bed concentration c_b. Hence these graphs also show the τ_e vs c_b relation, yielding the following relation:

$$\tau_e \propto c_b^{ncb} \qquad (4.4)$$

with ncb of the order of 10. This is much larger than the value given by Owen [1970], who reported ncb ≈ 2,3. However, it is clear from the results that the results are not very accurate: a small variation in c_b will yield a large variation in τ_e and the accuracy of c_b near the bed surface is questionable. Hence, it is not recommended to use these results.

The results are summarized in the Figures 4.9 through 4.12. The Figures 4.9 and 4.10 show no significant differences between the various sediments, though the sediments from Eems-Dollard seem to be slightly stronger, and those from the Biesbosch slightly weaker than the other sediments. This could however not be related to the bulk properties of the sediments.
The results presented are a direct function of the empirical fit (equ. 3.3) used to interpolate and extrapolate the bed concentration data. Equ. (3.3) seems to agree better with the data for the sediments from the Western Scheldt, Lake Ketel, Meuse, Eems-Dollard and Loswal Noord. However, no significant difference between this group of sediments and the other group is found.
Apparently it can be concluded, that the strength distribution in the upper part of the bed does not vary much for the 8 sediment samples

presently studied. An increase in consolidation time from 1 to 7 days yields an increase in τ_e by about 0,1 Pa, more or less evenly distributed over the bed. However, it should be kept in mind that the beds presently studied were all made in the same way, and all experienced the same history.

The Figures 4.11 and 4.12 show the τ_e vs c_b relations. The bed concentration c_b does not vary much, which of course is again a consequence of the empirical fit (3.3) used. The graphs show a significant difference between the curves for the fresh water sediment and the marine sediments: marine sediments show the same strength at much lower concentrations. This observation is in agreement with the diffusive double layer theory (e.g. Winterwerp [1989]). Adding salt to the (pore) water causes the diffusive double layer to become thinner. Hence, the attraction by the Van Der Waals forces becomes stronger. Thus, marine sediments in suspension will form more flocs prior to and during bed formation, resulting in larger aggregates, containing more water. Hence the (upper part of the) bed of a marine sediment will have a larger water content then fresh water sediments (the pore water cannot escape from the aggregates). Moreover, the mutual bonds between the aggregates within the bed are also stronger for marine sediments. As a result, salinity does increase the strength of the bed.
The mutual difference in the behaviour of the fresh water sediments and of the marine sediments can be defined through the bed concentration c_b at τ_e = 0,3 Pa. These values are listed in Table 4.2.
A close inspection of Table 4.2 and Figure 4.11 reveals that for instance for the fresh water sediments the mud from the Meuse is stronger than the mud from Lake Ketel (though this picture might be clouded by the accuracy of the concentration profiles). However, from Figure 2.5 it is expected that the latter mud would be stronger. This is another indication that the relation between yield strength and erosion strength is not yet clear.

As mentioned before, the accuracy of the bed concentration profiles is questionable, and therefore the accuracy of the strength profiles. It is therefore recommended to repeat the analyses by using more detailed and accurate data on the sediment concentration in the upper part of the bed. For the time being, the strength distributions shown in the Figures 4.9 and 4.10 can be used for practical purpose. At the moment it is not necessary to distinguish between the various sediments presently studied.

Table 4.2: Bed concentration at τ_e = 0,3 Pa.

Sediment source	Cons. time	Bed concentr. cb [kg/m3]
Holl. Diep	1 day	167
Sassenplaat	7 day	211
Holl. Diep	1 day	157
Moerdijkbrug	7 day	211
West. Scheldt	1 day	124
Lake Ketel	1 day	179
	7 day	190
Meuse	1 day	146
	7 day	-
Eems-Dollard	1 day	121
Loswal Noord	1 day	104
	7 day	94
Biesbosch	1 day	156
	7 day	167

4.4 Erosion rate.

In this chapter only surface erosion is treated; the experiments are not suitable to analyse the mass erosion processes occasionally observed.

The following definitions are used:

1) Erosion rate E [kg/m^{2}s]:

$$E = h \frac{dc_s}{dt} \qquad (4.3)$$

2) Floc erosion E_f is the erosion rate E observed during a sub-test when $\tau_e = \tau_b$, i.e. when E(t) becomes constant (occasionally zero).

3) Maximum erosion E_m is the maximum erosion rate observed during a sub-test, i.e. when $\tau_b - \tau_e$ has about its maximum value.

During the course of the analyses, several empirical relations were studied, based on well-known relations found in literature:

$$E = E_f \exp \{\alpha(\tau_b - \tau_e(z))^\beta\} \qquad (4.5)$$

$$E = M \frac{\tau_b - \tau_e}{\tau_e} \qquad (4.6)$$

The Figures 4.13 and 4.14 show that the floc erosion rate E_f increases with bed shear stress τ_b. A similar correlation was found by Parchure [1984], but this was not explicitly mentioned in his report. The graphs suggest that E_f does not increase unlimited with increasing τ_b, but approaches some asymptotic value. This behaviour will be discussed below.
Also the observed maximum erosion rate E_m can be correlated to the bed shear stress τ_b, as shown in the Figures 4.15 and 4.16, and again the graphs suggest an asymptotic behaviour.

It is interesting to note that Lavelle et al [1984] found that E can be related to τ_b, which they concluded from a reanalysis of data from 10 experiments by Lavelle et al, Fukuda and Lick, Sheng and Lick, Lee et al, Gularte et al and Partheniades. This relation reads:

$$E = E_0 \tau_b^\eta \qquad (4.7)$$

in which E_0 is an erosion rate parameter, its value varying between $1{,}9.10^{-8}$ and $3{,}7.10^{-5}$ kg/m^{2}s, and η varies between 1,2 and 5. This result is shown in Figure 4.17a.

The Figures 4.18 and 4.19 show the relation between the maximum erosion rate E_m and the maximum value of $(\tau_b - \tau_e)_{max}$. Though the scatter is huge, some correlation, indicated by the solid lines in the graphs, could be deduced:

$$T_c = 24 \text{ hrs}: \quad E_m \approx 8{,}5.10^{-6} \exp \{36(\tau_b - \tau_e)_{max}\} \qquad (4.8)$$

$$T_c = 7 \text{ days}: \quad E_m \approx 14{,}1.10^{-6} \exp \{27(\tau_b - \tau_e)_{max}\} \qquad (4.9)$$

The regression coefficient for (4.8) and (4.) are respectively r = 0,81 and r = 0,75. The scatter in the results is indicated by the broken lines in the Figures 4.18 and 4.19, yielding:

$$E_m = (0{,}5 - 52).10^{-6} \exp\{(60 - 27)(\tau_b - \tau_e)_{max}\} \quad (4.8a)$$

$$E_m = (2{,}9 - 20).10^{-6} \exp\{(34 - 20)(\tau_b - \tau_e)_{max}\} \quad (4.9a)$$

By comparing the value for E_f of 8,5 to $14{,}1.10^{-6}$ kg/m^{2}s with the results presented in the Figures 4.13b and 4.14b, the fits (4.8) and (4.9) agree well. Another remark concerns the scatter of the data. This scatter is apparently inherent to the experimental procedure applied, as it is comparable to the scatter in the data obtained by Parchure and Mehta [1985] - see Figure 4.17b. The obtained values for E_f, α and β (see equ.(4.5)) are also in the range reported in literature (see Winterwerp [1989]).
As equ.'s (4.8) and (4.9) should be representative for the entire erosion process, the following empirical formula is recommended for practical use, describing the erosion of soft deposited beds of sediments from one of the locations presently studied:

$$E = 10^{-5} \exp\{30(\tau_b - \tau_e)\} \quad (4.10)$$

The accuracy of the results is too low to distinguish between the various sediments and/or to correlate the results to one of the physico-chemical bulk parameters.
Finally, it is shown in Appendix C, that no correlation could be found between E, or E/E_f and $(\tau_b - \tau_e)/\tau_e$, indicating that the simple formula (4.6) is not applicable for describing the erosion of deposited beds.

The observed behaviour is in agreement with the rate process theory, in which the excess bed shear stress determines the activation energy. This theory was advocated by Parchure [1984], and recently by Mehta [1991].
Another conceptual frame work however can be found by considering erosion as an inverse consolidation or swell process. The idea is that the turbulent shear stress and pressure (fluctuations) weaken and/or loosen the aggregates within the bed, and that these aggregates are transported into the main flow through turbulent movement. The propagation velocity of the swelling into the bed then defines the maximum possible erosion rate. This is expected to be a function of the permeability of the bed, its water content (sediment concentration), the cohesive properties of the sediment and of course the turbulent structure of the eroding fluid. The dependency of E_f and E_m on τ_b is consistent with this theory. It is proposed to elaborate on this framework in a following phase of the study.

From the present analysis, it should be concluded that more detailed measurements of the sediment concentration in the upper part of the bed are required. Only then it may be possible to quantify the observed erosion processes in more detail.

5. Tidal experiments in the annular flume.

5.1 General.

Tidal experiments were conducted in the annular flume with mud from the Western Scheldt and from the Eems-Dollard (Delfzijl Harbor). The flow velocity was varied sinusoidally with bed shear stresses between -0,2 and +0,2 Pa for the first series of experiments, and between -0,4 and +0,4 Pa for the second series of experiments. A bed was formed from deposition of a homogeneous water-sediment suspension with an initial concentration of about 60 kg/m^3 (see Table 2.1). The bed was allowed to consolidate for 6 hours before the tidal experiments started by increasing the bed shear stress from zero to its maximum value, and decreasing it again. The experiments were continued until a dynamic equilibrium occurred, which was achieved after about 10 tidal cycles.[4]

The results of the four experiments given in the Figures 5.1, 5.3, 5.5 and 5.7 show the observed variation in time of the concentration in the water column measured at mid depth, and the Figures 5.2, 5.4, 5.6 and 5.8 show the variation in concentration as a function of the bed shear stress.

In the first series of experiments, the bed shear stress did only slightly exceed the critical threshold for erosion (see Chapter 4). Consequently the observed sediment concentrations in the water column were very low, varying between 0,1 and 0,35 kg/m^3 for Western Scheldt mud and between 0,25 and 0,4 kg/m^3 for Eems-Dollard mud. Assuming a sediment concentration of 50 kg/m^3 in the upper part of the bed (see Chapter 5.6), this would yield the erosion of about 1 mm of the bed during the tidal cycle.
Though the concentrations in the water column are much higher than those observed in nature, one should realize that the depth of the annular flume is only 0,3 m, i.e. at least an order of magnitude smaller that the depth of natural water systems. This brings the erosion processes observed in the annular flume in the range of those observed in nature.

4. During preliminary experiments with China Clay, dynamic equilibrium was not achieved, even after 1000 (!) tidal cycles. This was attributed to the consolidation time of 7 days that was applied - see Cornelisse et al [1990].

The maximum concentrations observed during the second series of experiments ($\tau_{b,max}$ = 0,4 Pa) are much higher, ranging from about 0 to 10 kg/m^3, corresponding to an erosion depth of several centimetre. The large difference in behaviour between the two series of experiments is due to the formation of a fluid mud layer. This is elaborated further in the following section. It is emphasized that the present tests have a preliminary character and that the analyses are based on a number of hypotheses. This implies that the results are merely qualitative.

5.2 Phenomenological description of the processes during a tidal cycle.

In this paragraph a phenomenological description of the sediment behaviour in the annular flume during a tidal cycle is given. For convenience, this description is restricted to the experiments with sediment from the Western Scheldt; a similar picture can be drawn for the experiments with sediment from the Eems-Dollard.

The sediment exchange between the bed and the water column during the first series of experiments ($\tau_{b,max}$ = 0,2 Pa) is governed by the common erosion and deposition processes. This implies that during decelerating tide, when the flow velocity becomes sufficiently small, the sediment in the water column can settle on the bed. Around slack water, the flow velocity is small, and the deposited sediment can consolidate. After slack tide, the flow velocity increases again, and the bed is eroded smoothly. This smooth erosion process is also observed during steady state experiments when the excess bed shear stress is not too large and it is known as surface erosion.

During the second series of experiments ($\tau_{b,max}$ = 0,4 Pa) a different picture is observed - see Figure 5.3. From about t ≈ 180 min. to t ≈ 300 min, the concentration in the water column is almost constant and the sediment particles are small. When τ_b decreases and becomes smaller than about 0,15 Pa, the deposition process starts up slowly. A more important process during this period is the formation of fairly large flocs of about 1 mm diameter in size. These were observed visually, but could not be recorded photographically. The settling velocity of the sediment now becomes large, and a high concentration layer is formed. This layer consolidates during about 1 hour in the slack water period. Pore water flows out of the layer through small irrigation channels until these small channels are compressed by self-weight consolidation and/or by the increasing flow itself. The sediment concentration within this layer

amounts to about 50 kg/m^3 (see Figure 5.26). At about t ≈ 400 min, τ_b > 0,1 Pa, internal waves are observed at the fluid-bed interface - see Figure 5.9a. The upper part of the layer is shown to contain large pores filled with water; the internal waves can penetrate down into this layer. The lower part of the layer is more homogeneous and is not deformed by the waves. When τ_b is increased further, the amplitude of the internal waves was observed to increase first, and then to decrease again - see Figure 5.9b. At about t ≈ 430 min, τ_b = 0,3 Pa, the waves have disappeared completely and smooth surface erosion occurs. Apparently a four layer system develops, consisting of:

- -a fixed bed (non-erodible layer) up to z = 632 mm, that is not affected by the tide,
- -a dense fluid-mud layer up to about z = 648 mm, that is not affected by the internal waves; the erosion of this layer proceeds smoothly at a moderate rate, like in steady flow,
- -a loose very soft fluid-mud layer, that is affected strongly by the internal waves; the erosion rate of this layer is very high, the processes resemble those occurring during the mixing of two fluid layers of different density, and
- -a suspension in the water column.

This change in resuspension process, and thus resuspension rate is also observed in the concentration-time curves in Figure 5.3. A typical feature of this dual-mode response of the bed is the kink in the c - τ_b curve in Figure 5.4. During the other series of experiments with $\tau_{b,max}$ = 0,2 Pa, only smooth surface erosion did occur, and no kink was observed in the c - τ_b curve (Figure 5.2). A close inspection of the results of the tidal experiments presented by Umita et al [1984] shows a small tendency of the accelerating curve to kink, indicating that some entrainment could have occurred, though nothing was mentioned in their paper.

In the following paragraphs this qualitative picture is further analysed. This is done by studying the various processes separately. This analysis is preceded by a short literature review concerning the entrainment processes in two-layer flow systems.

5.3 Resuspension by entrainment - a literature review.

Entrainment is defined as the mixing processes between fluid layers with different turbulence intensity. For the present study the situation is relevant that the lower layer is stagnant and the upper layer is

flowing. The turbulent motions in the upper layer erode the lower layer and mixes the lower layer fluid into the upper layer. Thus, the lower layer becomes thinner. When the two layers are also of different density, buoyancy effects become important as these will oppose the mixing processes.
The hydrodynamics of two-layer flow systems of fluids with different density is well studied in literature (e.g. Turner [1973]). The stability of these systems can be described by the gradient Richardson number Ri:

$$Ri = - \frac{g \, (\partial\rho/\partial z)}{\rho \, (\partial u/\partial z)^2} \qquad (5.1)$$

For large Ri (Ri > 0,25 according to classical stability theory) a stable stratification will occur, i.e. interfacial instabilities will decay. For small Ri unstable stratification occurs, i.e. interfacial instabilities will grow.

Mixing processes in stratified flows are often related to an overall Richardson number Ri_o. It is defined as:

$$Ri_o = \frac{g \, \Delta\rho \, \ell}{\rho \, \chi^2} \qquad (5.2)$$

where ℓ is a typical length scale and χ a typical velocity scale. For appropriate choices of ℓ and χ, Ri_o can be regarded as the ratio between the potential energy required to establish mixing (or the buoyancy effect opposing mixing) and the kinetic energy available for mixing.
The mixing processes themselves are defined by the entrainment rate E_v, which is the ratio between the entrainment velocity (here, the thinning of lower layer) and some characteristic flow velocity. Various definitions are used in literature. From many experiments it was concluded that E_v is correlated to an overall Richardson number. A number of these experiments are summarised in Appendix D. Several conclusions may be drawn from these studies:

1. From the experiments where one of the layers is flowing (i.e. not the stirring grid experiments) the entrainment of fresh/clear water into saline/turbid water is given by:

$$E_v \propto Ri_o^{-n}, \quad \text{where } 0,5 < n < 1,2 \qquad (5.3)$$

2. The scatter of the experimental data is very large, affecting the accuracy of the experimental data, and thus relation (5.3).

3. The results by Turner [1968] and Wolanski and Brush [1975] suggest a significant influence of the molecular diffusivity on the entrainment rate at low Reynolds number. At higher Reynolds numbers, mixing is dominated by turbulent processes. This would imply that the actual entrainment rate occurring in nature is expected to be significant larger than those observed during small scale laboratory experiments.

The theory outlined above is valid for weakly stratified flow, i.e. low Richardson numbers (see Lawrence et al [1990] and Smyth et al [1990]). The dynamic instabilities then lead to the formation of a periodic train of vortex-like structures, known as Kelvin-Helmholz waves. This is shown in a photograph copied from Lawrence et al [1990] - see Figure 5.10.
For highly stratified conditions (high Richardson number), the relative thickness of the shear layer δ_u (δ_u = thickness of layer with velocity gradient) with respect to the thickness of the mixing layer δ_ρ (δ_ρ = thickness of layer with density gradient) becomes important. If $\delta_u \approx \delta_\rho$, instabilities in the flow are damped due to buoyancy effects and the flow becomes more stable with increasing Ri. This situation probably occurs in stratified flows were the lower, denser layer flows underneath a stagnant fresh water layer, as is the case for turbidity currents.
If $\delta_u >> \delta_\rho$, instabilities in the high speed upper layer can develop more easily. These instabilities will form spanwise vortices, that interfere with the internal waves on the interface. As a result the internal waves tend to cusp, injecting denser water into the upper layer. If the cusps become very pronounced, the waves may break, injecting even more sediment into the upper layer. This also explains why only one-way entrainment is observed: no vortices are generated in the denser lower layer. Figure 5.11 (from Lawrence et al [1990]) shows these cusping internal waves observed during experiments on a fresh-saline water two-layer flow. The resemblance with the photograph shown in Figure 5.9a is striking.

This picture is quantified by Lawrence et al [1990] in the form of the stability diagrams shown in Figure 5.12. The internal wave heigth ζ can described by:

$$\zeta(x,z,t) = \zeta_o(z)\, e^{ik(x - \sigma t)} \qquad (5.4)$$

where k = wave number, $k = 2\pi/\lambda$ and

σ = complex group celerity, $\sigma = \sigma_r + i\sigma_i$

From equ (5.4) it can be seen that for $\sigma_i < 0$, ζ will decrease with time: the flow is stable. For $\sigma_i > 0$, ζ will increase with time and the flow is unstable.

The Richardson number Ri_δ (=J) on the vertical axis and α on the horizontal axis of Figure 5.12 and the parameter ε are defined as:

$$Ri_\delta = J = \frac{g \Delta \delta_u}{U^2}$$

$$\alpha = k \delta_u \qquad (5.5)$$

$$\varepsilon = \frac{\delta_u - \delta_\rho}{\delta_u}$$

On the basis of these parameters, Lawrence gives the following analysis. For $\varepsilon = 0$, $\delta_u = \delta_\rho$, i.e. the classical case (see Figure 5.12) with two distinct modes of instability. The first mode with $c_r = 0$ only occurs at $Ri < 0{,}07$ and is commonly referred to as the Kelvin-Helmholz mode. The second mode is a dispersive, overstable mode and is known as the Holmboe mode. It occurs at all Ri. For $0 < Ri < 0{,}07$ both instabilities occur, but the Kelvin-Helmholz mode has the higher amplification rate. Curves of constant amplification rate for the Holmboe mode form closed loops.

The case studied by Lawrence is characterised by $\varepsilon \to 1$, $\delta_u >> \delta_\rho$ (see Figure 5.8c, d and e). The character of the diagram changes as the zone of instability bifurcates into two branches. The lower, unstable branch retains the characteristics of the Holmboe mode, the second branch is an extension of the Kelvin-Helmholz mode, but with two roots. The consequence of this behaviour is very interesting. Let α and ε be constant, for example $\alpha = 0{,}6$ and $\varepsilon = 0{,}8$ (these values are close to those for the present tidal experiments) and let Ri decrease from infinity down to zero. The stability diagrams show that for high Ri, the flow is stable ($c_i = 0$). For $1 < Ri < 0{,}5$ c_i increases up to about 0,3 yielding progressively more unstable flow. A further decrease shows first a decrease in c_i, then an increase, again a decrease and finally a rapid increase again when Ri approaches zero (no buoyancy effects). Though this picture is idealized, as it is based on linear perturbation theory, it clearly demonstrates the effect of other modes on the stability of stratified flows. In Paragraph 5.6 it will be shown that this picture may help to understand the phenomena observed in the annular flume during the tidal experiments.

5.4 Series 1 Tidal experiments ($\tau b,max$ = 0,2 Pa).

A detailed view of the depositional and erosional phase for the experiments with sediments from the Western Scheldt are shown in the Figures 5.13a and 5.13b, and for the Eems-Dollard experiments in the Figures 5.14a and 5.14b. The figures show the bed shear stress τ_b, the sediment concentration measured in the suspension c_s, and the deposition and erosion rates D and E. These latter are defined as:

$$D = h \frac{dc_s}{dt}$$

$$E = h \frac{dc_s}{dt} \qquad (5.6)$$

From D the effective settling velocity W_s can be derived:

$$W_s = - D/c_s \qquad (5.7)$$

W_s is plotted against c in the Figures 5.15a and 5.16a. No correlation is observed. However, it is noted that for the sediments from the Western Scheldt, W_s is about twice the values for the sediments from the Eems-Dollard. Measurements with the sedimentation balance (Table 2.1) show the opposite trend. This difference might be due to segregation effects in the annular flume during the tidal experiments.
The effective settling velocity is plotted against τ_b in the Figures 5.15b and 5.16b. It is shown that W_s decreases with increasing τ_b. For both sediments the same correlation was found:

$$W_s \propto \tau_b^{-1,7} \qquad (5.8)$$

It should be kept in mind that the effective settling velocity differs from settling velocities measured in still water (i.e. sedimentation balance, Owen tube, etc.): the effective settling velocity implicitly includes the effects of turbulence (vertical diffusion) on the deposition rate. This effect can only be corrected for when the vertical sediment profile is measured.

The maximum shear stress applied amounted to 0,2 Pa. The steady state experiments showed that at these small values of τ_b only very little erosion is to be expected. This was also observed during the tidal experiments. For the Western Scheldt sediments, c_s increased from about 0,1 to 0,35 kg/m^3, and for the Eems-Dollard sediments from about 0,12 to

0,2 kg/m^3. Assuming a bed concentration of 50 kg/m^3, this would yield the erosion of about 1 mm of the bed or less. However, within this 1 mm, the bed, a pronounced gradient in strength is present. This can be seen from the Figures 5.13b and 5.14b, which show that E first increases and then decreases, though τ_b increases continuously. The strength distribution within such a thin layer cannot be established at present. It is proposed that in a next phase of this research, this will be elaborated further through numerical simulations with "DELWAQ-Slib" and some realistic guesses of this strength distribution; the latter based on the further analyses of the steady state experiments described in Chapter 4.

5.5 Series 2 Tidal experiments ($\tau b,max$ = 0,4 Pa): Deposition.

A part of the measured concentration-time curves, shown in the Figures 5.3 and 5.7, are given in the Figures 5.17 and 5.18. These figures focus on the deposition period and include the deposition rate D. D is obtained from the mass balance (see section 5.4):

$$D = h \frac{dc_s}{dt} \qquad (5.6)$$

The deposition curve in Figure 5.18 is much smoother than the curve in Figure 5.17. This is due to a numerical smoothing of the c_s-t curve of Eems-Dollard mud prior to determining the time derivative.

The settling velocity W_s of the sediments can be established from the deposition rate. This is done using two different definitions:

1. Using Krone´s law (Krone [1962]):

$$D = - W_s c_s \left(\frac{\tau_{d,K} - \tau_b}{\tau_{d,K}}\right) \qquad \text{for } \tau_b < \tau_{d,K} \qquad (5.9)$$

where $\tau_{d,K}$ = Krone´s critical shear stress for deposition, which is defined as a threshold shear stress below which all sediments eventually settle, and beyond which no sediment settles at all. For graded sediments, also a minimum critical shear stress for deposition τ_d exists, defined as the threshold shear stress below which all sediments eventually settle. From the steady state experiments this was found to be τ_d = 0,06 ± 0,01 Pa for Western Scheldt mud, and τ_d = 0,03 ± 0,01 Pa for Eems-Dollard mud. Applying these figures in

Krone´s law would yield no deposition before t = 330 min and t = 340 min for Western Scheldt mud and Eems-Dollard mud, respectively (see the Figures 5.17 and 5.18). From the graphs, deposition is observed to start much earlier, i.e. at $\tau_b < 0,15$ Pa and $\tau_b < 0,09$ Pa respectively. Therefore, these values are used in equ (5.9): for Western Scheldt mud $\tau_{d,K} = 0,15$ Pa and for Eems-Dollard mud $\tau_{d,K} = 0,09$ Pa. The resulting settling velocity W_s is shown in the Figures 5.19a and 5.20a. The large values of W_s around t ≈ 380 min. are attributed to the inaccuracy of the data when D becomes zero.

2. Using the "effective settling velocity concept":

$$D = - W_s c_s \qquad (5.7)$$

The results are shown in the Figures 5.19b and 5.20b.

The two sets of figures show that the effective settling velocity is generally smaller than W_s determined with Krone´s law. Considerable differences occur during the beginning of deposition, when $\tau_b \approx \tau_{d,K}$, i.e. when $(\tau_{d,K} - \tau_b)/\tau_{d,K}$ is small.
In the following analysis, the concept of effective settling velocity is used.

The Figures 5.21a and 5.22a show the variation of W_s with the sediment concentration c_s. The same pictures are shown on logarithmic scale in the Figures 5.21b and 5.22b. The large scatter in W_s at the lower concentrations is due to the inaccuracy of the results at low c_s. The very rapid drop at c_s = 10 kg/m^3 has another cause. The maximum concentration measured during the experiments is about 10 kg/m^3. So this value is an asymptote yielding the W_s-c relation at the beginning of deposition when W_s is small. This means that (some) data in the left part and in the right part of the figures should be omitted.
When this is done, the data can be compared with data for the Severn estuary (Thorn [1982]) and Tampa Bay (Ross [1988]). Both sets of data were obtained with a settling column; Ross used a column of 2 m length and 10 cm diameter. Hence, these settling velocities differ in definition from the effective settling velocities used in the present analysis. However, the phenomena of flocculation and hindered settling should occur in both cases. The figures show an initial increase of W_s with c due to flocculation effects, next a subsequent stabilization and then a decrease due to hindered settling. These effects were captured by Mehta [1986] with the following formula:

$$W_s = k_1 c_s^n \qquad \text{flocculation effect}$$

$$W_s = W_{s0} (1 - k_2 c_s)^{\beta} \qquad \text{hindered settling effect} \qquad (5.10)$$

For Severn mud: $k_1 = 0{,}513$, $n = 1{,}29$, $W_{s0} = 2{,}6$ mm/s, $k_2 = 0{,}008$ and $n = 4{,}65$. For Tampa Bay mud: $k_1 = 0{,}11$, $n = 1{,}6$, $W_{s0} = 0{,}37$ mm/s, $k_2 = 0{,}008$ and $n = 5$.
The agreement with these data and the present data is good for Western Scheldt mud, but much less for Eems-Dollard mud. No explanation for this difference in character between the two sediments was found but the difference in the definition of W_s.

Plotting W_s versus τ_b, as in the Figures 5.15b ad 5.16b showed graphs comparable to the W_s vs t plots in the Figures 5.19a and 5.20a, thus no correlation at all. This is because of the large influence of the flocculation effect on W_s during the first half hour of the deposition phase, obscurating all other effects. These plots are therefore not presented here.
Finally, the variation of the settling velocity according to Krone´s law with sediment concentration is given in Figure 5.23, showing the same trend as the effective setting velocity.

5.6 Series 2 Tidal experiments ($\tau_{b,max} = 0{,}4$ Pa): Erosion/re-entrainment.

A part of the measured concentration-time curves, shown in the Figures 5.3 and 5.7, are given in the Figures 5.24 and 5.25. These figures focus on the erosion/re-entrainment period and include the erosion rate E. E is obtained from the mass balance:

$$E = h \frac{dc_s}{dt} \qquad (5.6)$$

For the analysis of the experiments, the photographs made during the re-entrainment phase are used. The photographs taken during the experiments with Eems-Dollard mud do not include a vertical scale, and can therefore not be quantified. Hence, the following analysis is restricted to the experiments with sediment from the Western Scheldt.
Directly after the start of re-entrainment, E becomes very large, with a maximum around 420 min, and then drops to an almost constant level (see Figure 5.24). The analysis of this behaviour is presented in two steps:

first the erosion rate is estimated using the model by Parchure and second the concept of entrainment of stratified two-layer flows is used. For both methods the concentration profile within the bed should be known. This profile is estimated with the consolidation curves described in the Chapters 2 and 3. It is assumed that these consolidation relations may also be applied to estimate the concentration distribution within the fluid mud layer. Possible errors will be due to for instance sorting effects (the consolidation curve is affected by the presence of sand in the original sample - no (little) sand is expected in the fluid mud layer). The consolidation relation for Western Scheldt mud reads[5]:

$$c_b(z)/\bar{c}_b = 0,6\ (z/H)^{-0,4} \qquad (5.11)$$

From the interface-time curves measured during the consolidation tests, a bed thickness of H = 70 mm is expected after 6,5 hours (6 hours consolidation + 0,5 hour before erosion starts). The initial concentration was c_s = 56 kg/m^3, so that the mean bed concentration $\bar{c}_b$ becomes $\bar{c}_b$ = 240 kg/m^3.

The photographs taken during the tidal experiments show that the non-erodible layer has a thickness H_1 = 31 mm, and the fluid mud layer just prior to erosion has a thickness H_{fm} = 50 mm. The maximum concentration of the suspension just prior to deposition is c_s = 10 kg/m^3, so that $\bar{c}_{fm}$ = 54 kg/m^3. The bed concentration curve (Cb-predicted) thus obtained is shown in Figure 5.26a. It is the basis for the further analyses, and it is therefore recommended that in future experiments this curve is measured directly.
Figure 5.26a also shows the erosion depth, based on the measured suspension concentration and the predicted fluid mud concentration.

The fluid mud concentration varies between about 30 and 180 kg/m^3. This means that τ_e cannot be established from the steady state experiments described in Chapter 4. Therefore an empirical relation by Owen [1970] is adapted:

$$\tau_e \propto c_b^{2,3} \qquad (5.12)$$

5. For the present analysis it is necessary that the total amount of sediment in the fluid mud layer is correct. Hence $\alpha + \beta$ should be unity, as explained on page 21 (equ (3.3)). Consequently, equ (5.11) does not necessarily yield the best overall empirical fit.

The maximum bed shear stress during the tidal cycle is τ_b = 0,4 Pa. It is therefore reasonable to assume that the erosion strength τ_e = 0,4 Pa at the interface between the fluid mud layer and the non-erodible bed (z ≈ 0,031 m). Then equ (5.12) becomes for Western Scheldt mud:

$$\tau_e = 2{,}6.10^{-6}\ c_b^{2,3} \qquad (5.13)$$

This relation is given in Figure 5.26b, together with the bed concentration distribution. Note that the left hand vertical axis has a linear scale and the right hand vertical axis a logarithmic scale.

Using the common erosion formula by Parchure [1984], [1985], the erosion potential E_p of the bed can be established. The coefficients α and β were deduced by Kuijper et al [1990], and the floc erosion E_f is obtained through data-fitting, yielding:

$$E_p = 2.10^{-6} \exp\{10\sqrt{(\tau_b - \tau_e(z))}\} \qquad (5.14)$$

In Figure 5.27 E_p is compared with the actual measured entrainment rate E. It is shown that beyond t = 440 min the agreement is fair, indicating that the erosion during this period can be described with common theory established from steady state experiments. Before t = 440 min. however, E is much larger than E_p. Apparently other processes play a role initially. The erosion in this phase of the tide should be attributed to the instability and entrainment processes between the fluid mud layer and the overflowing fluid, as discussed in paragraph 5.3.

These instability processes are related in general to the Richardson number. Though the velocity gradient in the shear layer and the density gradient in the mixing layer were not measured, a fair estimate of the gradient Richardson number can be obtained. This is done by approximating Ri as follows:

$$Ri = -\frac{g\ (\partial\rho/\partial z)}{\rho\ (\partial u/\partial z)^2} \approx -\frac{g\ \Delta\rho}{\rho\ U^2}\ (\delta_u^2/\delta_\rho) \qquad (5.15)$$

Δρ can be obtained from the predicted concentration profile c_{fm} in the fluid mud layer, δ_u from velocity measurements in the annular flume (see Karelse [1990]), and δ_ρ from the photographs of the tidal experiments. An average value for δ_u ≈ 7 mm, with a minimum of 5 mm and a maximum of 10 mm, and for δ_ρ ≈ 1,5 mm, with a minimum of 1 mm and a maximum of 2 mm. Figure 5.28 gives the resulting Ri as a function of time showing an

initial decrease due to the increase in flow velocity U, followed by an increase, due to the increase in bed density. From theoretical analyses a critical value of Ri = 0,25 is known, indicating that for Ri > 0,25, disturbances cannot grow. From experimental work however it is known that unstable interfaces may occur for Ri up to unity. Figure 5.28 shows that the estimated Richardson numbers for the present experiments lie in the range where interfacial instabilities may be expected to grow.
It should be noted that the effects of cohesion, which certainly will augment the stability of the mixing layer, have not been taken into account in this analysis. This probably can be done with a modified Richardson number. It is recommended to elaborate on this further in a next study.

One of the first extensive experimental studies on interfacial instabilities was carried out by Keulegan [1949]. His description of the interfacial behaviour (cusped, sharp crested waves that break and injection of eddies from the crests into the moving flow) shows a striking resemblance with the present observations and those by Srinivas and Mehta [1990]. Another interesting observation, again consistent with the present results, is that the wave length λ was hardly affected by the flow velocity, implying that λ is determined by the stability behaviour of the interface. Hence, Keulegan could estimate the maximum possible wave length from the wave equation:

$$k_{min} = \frac{2\pi}{\lambda_{max}} = \frac{2\,g}{U_c^2}\,\frac{\Delta\rho}{\rho} \qquad (5.16)$$

in which U_c is the critical velocity at which the instabilities start to grow (i.e. when entrainment starts). From Figure 5.27 it can be seen that $\tau_c \approx 0{,}07$ Pa, hence $U_c \approx 0{,}08$ m/s (see Karelse [1990] for the relation between τ_b and U). Substituting for $\Delta\rho = 20$ kg/m^3 ($c_b \approx 30$ kg/m^3) and $\rho = 1025$ kg/m^3, $\lambda_{max} \approx 0{,}1$ m, which is only a little larger than the observed wave lengths of 5 to 8 cm.

To analyse experimental data, an overall Richardson number Ri_o is used in general, defined as (see Chapter 5.3):

$$Ri_o = \frac{g\,\Delta\rho\,\ell}{\rho\,\chi^2} \qquad (5.2)$$

where ℓ is a typical length scale and χ a typical velocity scale. Various definitions are used in literature. First the approach by Kato and Phillips [1969] and Kantha, Phillips and Azad [1977] is followed, as

their experiments with fresh-saline stratified water in an annular flume (N.B. with only upper lid rotation) highly resemble the present experiments. They defined the following overall Richardson number:

$$Ri_* = \frac{g\ \Delta\rho\ h}{\rho\ u_{*,u}^2} \qquad (5.17)$$

Here h = water depth [m] and $u_{*,u}$ = the shear velocity [m/s] at the upper lid. The entrainment rate E_{v*} is also related to $u_{*,u}$ and reads:

$$E_{v*} = \frac{u_e}{u_{*,u}} = \frac{E}{c_b\ u_{*,u}} \qquad (5.18)$$

where u_e is the vertical entrainment velocity and E the erosion rate defined in equ (5.6). The present tidal experiments can be compared with those by Kato and Phillips and by Kantha et al when $u_{*,u}$ for the Delft annular flume is known. For this purpose, the flow in the flume is considered to be (quasi-)steady. Let τ_u be the shear stress on the upper lid, τ_w the shear stress on the side wall of the flume, τ_b the shear stress on the water-sediment interface (the bed), h the height of the flume (h = 0,3 m) and B the width of the flume (B = 0,2 m). Then because of equilibrium of forces:

$$B.\tau_u = B.\tau_b + 2.h.\tau_w \qquad (5.19)$$

If it is assumed that $\tau_b \approx \tau_w$, then $\tau_u \approx 4.\tau_b$. Hence, $u_{*,u} \approx 2.u_*$, i.e. the shear velocity at the upper lid is about twice the shear velocity at the bed. Using this value, the variation of Ri_* with time is plotted in Figure 5.29. A behaviour similar to that observed with the gradient Richardson number is found (see Figure 5.28), though more pronounced. Next, the variation of E_{v*} with Ri_* for the present experiments in the period $390 < t < 440$ min. is shown in Figure 5.30, together with the results by Kato and Phillips ($E_{v*} = 2{,}5/Ri_*$ for $20 < Ri_* < 400$) and with the results by Kantha, Phillips and Azad.

Next, a comparison is made with the recent results by Srinivas and Mehta [1990], obtained in a "race-track" flume with kaolinite and bentonite clay. The results are shown in Figure 5.31. Ri_o and E_v are defined slightly different:

$$Ri_u = \frac{g\ \Delta\rho\ h}{\rho\ U^2} \qquad (5.20)$$

$$E_v = \frac{u_e}{U} = \frac{E}{c_b U} \qquad (5.21)$$

The Figures 5.30 and 5.31 lead to several observations:

1. An inverse trend is observed around $Ri_* \approx 170$ (and to a lesser extend around $Ri_u \approx 5{,}5$).
2. The slope of the data agrees only for a very small part with the results by Kantha et al and well with the results by Srinivas and Mehta.
3. For decreasing Ri, the data show a rapid drop when $Ri_* < 170$, or $Ri_u < 5{,}5$.

The inverse trend in E_{v*} around $Ri_* = 170$ is due to an inverse trend in Ri_* itself, which is shown as a kink in the Ri_* - t curve around t = 420 min. (Figure 5.29). This is probably due to a deviation of the c_b profile that is used (equ (5.11)) from the actual concentration profile; this is elaborated a little further below.

The difference between the present results and those by Kantha et al and Srinivas and Mehta is significant. Though cohesion (augmented viscosity and yield strength) may play a role, its effect is probably small, as μ and τ_y are small at the concentrations of interest ($c_b \approx 30$ kg/m^3; see Figures 2.3 and 2.5), and the experiments by Srinivas and Mehta were also carried out with cohesive material. This conclusion is consistent with the arguments by Turner on the role of viscosity. A second difference between the present experiments and the others is that the present experiments are tidal experiments; interface and concentration may not respond instantaneously to variations in bed shear stress, hence show a time lag. The other experiments are based on equilibrium conditions. A third problem is that neither τ_b nor u_* are known properly for the various studies. This should be elaborated upon further.

There are some uncertainties on the actual values of the E_{v*} vs Ri_* curve around $Ri_* = 170$. However, the results show qualitatively that E_{v*} first increases and then decreases again with increasing Ri_*. Two explanations exist for this behaviour, which are both fairly speculative however.
From the visual observations and the kink in the c vs t curve, the soft, high concentrated sediment layer on the bed can be regarded to consist of two parts. The upper, softer layer behaves as a fluid (viscous part) and is eroded through interfacial instabilities. The lower (plastic?)

layer is only exposed to surface erosion; no waves can be formed on its interface. As a result of the erosion, the upper layer becomes thinner, and the waves cannot penetrate as far down into the bed as during the initial phase, and therefore decrease in wave height. As the transfer from one erosion mode to the other is fairly abrupt, some discontinuity in the $c_b(z)$ and/or $\tau_e(z)$ is to be expected. This discontinuity may be formed during the consolidation process around slack tide. This, however is not very likely, as no such behaviour was observed during the simultaneous consolidation experiments. Possibly, the cyclic loading by the interfacial instabilities themselves may cause additional compaction of the lower layer, causing a discontinuity in the density profile, and thus in the erosion mode. This compaction is not taken into account in equ (5.11). It also explains the doubts on the inverse trend shown in Figure 5.29. It is therefore recommended to measure the (variation in) density distribution in this layer in detail during further experiments.

The increase and subsequent decrease in E_{v*} is possibly also due to the character of the interfacial instabilities. At low Ri, i.e. large kinetic energy and/or small buoyancy effects, strong mixing between two layers of fluid may take place. When Ri increases, the mixing decreases. This is the classical picture. However, Holmboe [1962] and later f.i. Lawrence [1987] observed a second mode of instability when $\delta_u >> \delta_\rho$. Then vortices can develop in the shear layer, not hindered by buoyancy effects. These vortices interfere with the waves on the interface, which become cusped, sharply crested. These waves are known as Holmboe waves, and these are the waves observed in the present experiments, but also by Keulegan [1949], Narimousa et al [1987], Srinivas and Mehta [1990] and many others. When these waves steepen up, they may overtop and inject large quantities of sediment into the flow. It is clear that in that case, Ri is not the sole parameter anymore that describes the stability of the interface. Hence, the entrainment may seem to increase with Ri. This picture was quantified by Lawrence [1987] in a stability analysis, showing that the amplification factor is governed by Ri, a wave number, and the ratio δ_u/δ_ρ - see Paragraph 5.3 and Figure 5.12. A crude estimation for the present experiments yields $\lambda \approx 5$ cm, and $\delta_u \approx 5$ mm, so that α and ε can be established at $\varepsilon \approx 0{,}8$ and $\alpha \approx 0{,}6$. Figure 5.12d shows a remarkable agreement with Figure 5.30b: for decreasing Ri_o E_v first increases and decreases (N.B. Ri_o and $J = Ri_\delta$ are defined differently).

Figure 5.32 finally shows the correlation between the erosion rate E and the bed shear stress τ_b. This figure includes the relation found by

Umita et al [1984], who also performed tidal experiments with a natural mud. They did not report the occurrence of fluid mud; probably due to much lower sediment concentrations (much lower erosion rates). As a result, there is no agreement between the present results and those by Umita.

Acknowledgements.

This research is performed in commission of Rijkswaterstaat (Ministry of Transport and Public Works, The Netherlands). It is also part of "The Netherlands Integrated Soil Research Programme".
We like to acknowledge Kees Koree, Erik van Velzen and Frans de Vreede for their skilful contribution in running the facilities and instrumentation and executing the experiments.

References.

K. Ashida, S. Egashira, [1975], "Basic study on turbidity currents", Hydraulic and Sanitary Engineering Division, Transactions of JSCE, Vol 7, pp 83 - 86.

C. Blom, R.J.J. Jongschaap, J. Mellema, [1986], "Inleiding in de reologie; Reometrie, Dispersiereologie, Polymeerreologie", Technisch Hogeschool Twente, Kluwer Technische Boeken .

J.M. Cornelisse, C. Kuijper, J.C. Winterwerp, [1990], "Sedimentatie en erosie van China-clay onder getijomstandigheden; Verkennend onderzoek in de carrousel", Waterloopkundig Laboratorium, Rapport Z159, maart 1990.

S. Egashira, [1980], "Basic research on density stratified flows and the mixing mechanism", PhD thesis, Kyoto Univerity, Japan.

A. Einstein, [1906], "Eine neue Bestimmung der Moleküldimensionen", Annalen der Physiek, Leipzig (4) 19.

T.H. Ellison, J.S. Turner, [1959], "Turbulent entrainment in stratified flows", Journal of Fluid Mechanics, Vol 6, pp 423 - 448.

M.H. Garcia, [1989], "Depositing and eroding sediment-driven flows: turbidity currents", A thesis submitted to the Faculty of the Graduate School of the University of Minnesota.

J. Holmboe, [1962], "On the behaviour of symmetric waves in stratified shear layers", Geo Fysiske Publikasjoner, Vol 24, pp 67 - 113.

A.E. James, D.J.A. Williams, P.R. Williams, [1987], "Direct measurement of static yield properties of cohesive suspensions", Rheologica Acta, Vol. 26, pp 437-446.

L.H. Kantha, O.M. Phillips, R.S. Azad, [1977], "On turbulent entrainment at a stable density interface", Journal of Fluid Mechanics, Vol 79, Part 4, pp 753 - 768.

M. Karelse, [1990], "Experimenteel onderzoek naar de snelheids- en schuifspanningsverdeling in de carrousel", Waterloopkundig Laboratorium, Notitie Z159-52, November 1990.

H. Kato, O.M. Phillips, [1969], "On the penetration of a turbulent layer into stratified fluid", Journal of Fluid Mechanics, Vol 37, Part 4, pp 643 - 655.

G.H. Keulegan, [1949], "Interfacial instability and mixing in stratified flows", Journal of Research of the National Bureau of Standards, Vol 43, November 1949, Research Paper RP2040, pp 487 - 500.

R.B. Krone, [1962], "Flume studies of the transport of sediment in estuarial shoaling processes", Hydraulic Engineering Laboratory and Sanitary Engineering Research Laboratory, University of California, Berkeley, June 1962.

R.B. Krone, [1963], "A study of rheological properties of estuarial sediments", Hydraulic Engineering Laboratory and Sanitary Engineering Research Laboratory, University of California, Berkeley, Technical Bulletin No 7, September 1963.

R.B. Krone, [1986], "The significance of aggregate properties to transport processes", in Lecture Notes on Coastal and Estuarine Studies, Estuarine Cohesive Sediment Dynamics, Proceedings of a Workshop on Cohesive Sediment Dynamics with Special Reference to Physical Processes in Estuaries, Tampa, Florida, November 12-14, 1984, Springer-Verlag, pp 66-84.

C. Kuijper, J.M. Cornelisse, J.C. Winterwerp, [1990], "Erosion and deposition characteristics of natural muds; Sediments from the Hollandsch Diep (Sassenplaat)", Rijkswaterstaat, Delft Hydraulics, Cohesive Sediments Report 27, November 1990.

C. Kuijper, J.M. Cornelisse, J.C. Winterwerp, [1990], "Erosion and deposition characteristics of natural muds; Sediments from the Hollandsch Diep (Moerdijkbrug)", Rijkswaterstaat, Delft Hydraulics, Cohesive Sediments Report 28, November 1990.

C. Kuijper, J.M. Cornelisse, J.C. Winterwerp, [1990], "Erosion and deposition characteristics of natural muds; Sediments from the Western Scheldt (Breskens)", Rijkswaterstaat, Delft Hydraulics, Cohesive Sediments Report 29, November 1990.

C. Kuijper, J.M. Cornelisse, J.C. Winterwerp, [1990], "Erosion and deposition characteristics of natural muds; Sediments from Lake Ketel",

Rijkswaterstaat, Delft Hydraulics, Cohesive Sediments Report 30, November 1990.

C. Kuijper, J.M. Cornelisse, J.C. Winterwerp, [1990], "Erosion and deposition characteristics of natural muds; Sediments from the River Meuse (Belfeld)", Rijkswaterstaat, Delft Hydraulics, Cohesive Sediments Report 32, November 1990.

C. Kuijper, J.M. Cornelisse, J.C. Winterwerp, [1990], "Erosion and deposition characteristics of natural muds; Sediments from the Eems-Dollard (Delfzijl Harbour)", Rijkswaterstaat, Delft Hydraulics, Cohesive Sediments Report 35, November 1990.

C. Kuijper, J.M. Cornelisse, J.C. Winterwerp, [1991], "Erosion and deposition characteristics of natural muds; Sediments from Loswal Noord (North Sea)", Rijkswaterstaat, Delft Hydraulics, Cohesive Sediments Report 37, February 1991.

C. Kuijper, J.M. Cornelisse, J.C. Winterwerp, [1991], "Erosion and deposition characteristics of natural muds; Sediments from the Biesbosch (Spijkerboor)", Rijkswaterstaat, Delft Hydraulics, Cohesive Sediments Report 36, May 1991.

J.W. Lavelle, H.O. Mofjeld, E.T. Baker, [1984], "An in situ erosion rate for a fine-grained marine sediment", Journal of Geophysical Research, Vol 89, No C4, pp 6543-6552.

G.A. Lawrence, J.C. Lasheras, F.K. Browand, [1987], "Shear instabilities in stratified flow", Proceedings of the Third International Symposium on Stratified Flows, February 1987, Pasadena, California, ed. by E.J. List and G.H. Jirka, ASCE, pp 15 - 27.

D.I. Lee, [1969], "The viscosity of concentrated suspensions", Transactions of the Society of Rheology, Vol 13, No 2.

K. Lofquist, [1960], "Flow and stress near an interface between stratified liquids", Physics of Fluids, Vol 3, pp 158 - 175.

A.J. Mehta, T.M. Parchure, J.G. Dixit, R. Ariathurai, [1982], "Resuspension potential of deposited cohesive sediment beds", in: Estuarine Comparisons, ed. by V.S. Kennedy, Acadamic Press, New York, pp 591-609.

A.J. Mehta, [1986], "Characterization of cohesive sediment properties and transport processes in estuaries", in Lecture Notes on Coastal and Estuarine Studies, No 14, Proceedings of a Workshop on Cohesive Sediment Dynamics with Special Reference to Physical Processes in Estuaries, ed. by A.J. Mehta, Tampa, Florida, November 1984, pp 290 - 326.

A.J. Mehta, [1991], "Review notes on cohesive sediment erosion", Proceedings of a Speciality Conference on Quantitative Approaches to Coastal Sediment Processes, Seattle, Washington, June 1991, ed. by N.CX. Kraus et al, Coastal Sediments 1991, Volume 1, pp 40-53.

C. Migniot, [1968], "A study of the physical properties of various forms of very fine sediments and their behaviour under hydrodynamic action", Communication présenté au Comité Technique da la Société Hydrotechnique de France, la Houille Blanche, Vol 23, No 7, pp 591-620.

C. Migniot, [1989], "Tassement et rhéologie des vases; Première Partie", la Houille Blanche, No 1, pp 11-29.

C. Migniot, [1989], "Tassement et rhéologie des vases; Deuxième Partie", la Houille Blanche, No 2, pp 95-111.

S. Narimousa, H.J.S. Fernado, [1987], "On the sheared density interface of an entraining stratified fluid", Journal of Fluid Mechanics, Vol 174, pp 1 - 22.

K. Otsubo, K. Muraoka, [1985], "Resuspension rate function for cohesive sediment in stream", Journal of Hydroscience and Hydraulic Engineering", Vol 3, No 2, November 1985, pp 1-13.

M.W. Owen, [1975], "Erosion of Avonmouth Mud", Report No INT 150, Hydraulics Research Station, Wallingford, September 1975.

T.M. Parchure, [1984], "Erosional behaviour of deposited cohesive sediments", University of Florida, Coastal and Oceanographic Engineering Department, Gainesville, Florida, Report UFL/COEL/001, Dissertation.

T.M. Parchure, A.J. Mehta, [1985], "Erosion of soft cohesive sediment deposits", ASCE, Journal of Hydraulic Engineering, Vol 111, No 10, pp 1308 - 1326.

G. Parker, H.M. Pantin, Y. Fukushima, [1985], "Self-accelerating turbidity currents", Proceedings of the Euromech 192 Conference, Transport of Suspended Solids in Open Channels, Munich, June 1985, paper D9, pp D9-1 - D9-7.

J.F. Price, [1979], "On the scaling of stress-driven experiments", Journal of Fluid Mechanics, Vol 90, Part 3, pp 509 - 529.

M.A. Ross, [1988], "Vertical structure of estuarine fine sediment suspensions", University of Florida, Coastal and Oceanographic Engineering Department, Gainesville, Florida, Report UFL/COEL/TR-079, Dissertation.

G.C. Sills, D.M. Elder, [1984], "The transition from sediment suspension to settling bed", in Lecture Notes on Coastal and Estuarine Studies, Estuarine Cohesive Sediment Dynamics, Proceedings of a Workshop on Cohesive Sediment Dynamics with Special Reference to Physical Processes in Estuaries, Tampa, Florida, November 12-14, 1984, Springer-Verlag, pp 192-205.

W.D. Smyth, G.P. Klaassen, W.P. Peltier, [1987], "The nonlinear evolution of Holmboe waves", Proceedings of the Third International Symposium on Stratified Flows, February 1987, Pasadena, California, ed. by E.J. List and G.H. Jirka, ASCE, pp 45 - 54.

R. Srinivas, A.J. Mehta, [1990], "Observations on estuarine fluid mud entrainment", International Journal of Sediment Research, Vol 5, No 1, January 1990, pp 15 - 22.

R.O.R.Y. Thompson, [1979], "A re-interpretation of the entrainment processes in some laboratory experiments", Dynamics of Atmospheres and Oceans, Vol 4, pp 45 - 55.

M.F.C. Thorn, J.G. Parsons, [1980], "Erosion of cohesive sediments in estuaries: an engineering guide", Third International Conference on Dredging Technology, Bordeaux, France, BHRA, Fluid Engineering, paper F1, pp 349-358.

M.F.C. Thorn, [1982], "Physical processes of siltation in tidal channels", in Hydraulic Modelling in Maritime Engineering, Thomas Telford Ltd, London.

A. Toet, [1991], "Meetopstelligen en bemonsterigen Ketelmeer, 1988 t/m 1990", Rijkswaterstaat, Direktie Flevoland, Lelystad, 1991.

J.S. Turner, [1968], "The influence of molecular diffusivity on turbulent entrainment across a density interface", Journal of Fluis Mechanics, Vol 33, Part 4, pp 639 - 656.

J.S. Turner, [1973], "Buoyancy effects in fluids", Cambridge University Press.

T. Umita, T. Kusuda, Y. Awaya, M. Onuma, T. Futawatari, [1984], "The behaviour of suspended sediments and muds in an estuary", Water Science Technology, Vol 17, pp 915 - 927.

G. Verreet, J. Beralmont, [1988], "Rheology and non-Newtonian behaviour of sea and estuarine mud", Encyclopedia of Fluid Mechanics, Vol VII, N.P. Cheremisinoff, Gulf Publishing Co.

J.C. Winterwerp, [1989], "Flow induced erosion of cohesive beds; A literature survey", Rijkswaterstaat, Delft Hydraulics, Cohesive Sediments Report 25, February 1989.

E.J. Wolanski, L.M. Brush, [1975], "Turbulent entrainment across stable density step structures", Tellus, Vol27, No 3, pp 259 - 268.

C.E. Zobell, [1946], "Studies on the redox-potential of marine sediments", Bulletin of the American Association of Petroleum Geologists, Vol 30, No 4, pp 477-513.

Table 2.1: Physical-chemical properties of the water and sediment.

	SEDIMENT TYPE							
FIELD SAMPLING	H'Diep-Spl	H'Diep-Mbr	Breskens	Lake Ketel	Meuse	E-D:Delfz	Loswal-N	Biesbosch
Sampling date [-]	June 26/89	Sept. 4/89	Oct. 4/89	Nov. 8/89	Nov. 3/89	Febr 8/90	Sept 28/90	June 28/91
Water depth [m]	11	7	6,4	3,4	3,5	3,8	21	2,5
Conduct. [mS/cm]	0,9	1,0	39,0	1,2	0,61	33,3		0,57
Chlorinity [kg/m³]	0,16	0,20	17,1	-	-	20,5	18	0,088
Water temp. [°C]	22,5	19,0	16,6	11,4	14,6	6,6	14,9-15,8	20
Oxyg. cont.[kg/m³]	0,0072	0,0080	0,0068	0,0086	0,0055	0,009	0,008	0,007-0,01
,, [%]	79	-	82	-		77	82	73
Redox pot: [mV]								
- fluid	+130	-	-	-	+94	228	202	184
- sediment	-290	-170	-	-	-106	-164 (8,1C	-190a-230	-290
pH: [-]								
- fluid	7,8	7,7	8,1	7,8	7,42	8,04	8,2	7,4
- sediment	-	-	-	-	-	7,2	7,7	6,9
Secchi disk [m]	-	-	-	1,2	-	0,4		0,4

	SEDIMENT TYPE							
SEDIMENT PROPERTIES	H'Diep-Spl	H'Diep-Mbr	Breskens	Lake Ketel	Meuse	E-D:Delfz	Loswal-N	Biesbosch
Conduct. [mS/cm]	0,75	0,49	7,8	0,30	0,42	36	22,9	0,69
Chlorinity [mg/kg]	320	270	6500	310	87	14 E+3	12 E+3	
Ox. cont. [kg/m³]	0	0,0032	0,0025	0	0	<0,1 E-3		
,, [%]	0	39	30	0	0	<0,1		
Redox pot. [mV]	-300	-280	-310	-210	-230	-23		
pH [-]	6,99	7,36	7,63	7,63	7,21	7,77	7,46	7,1
Organic cont. [%]	9,5	8,5	5,3	12	8	1,9	1,7	7,7
Cations:[meq/100g]								
- Fe [g/kg]	32	26	18	33	26	12	12	33
- Na [meq/100gds]	0,22	0,20	2,8	0,3	0,1	3,8	1,2	0
- K ,,	0,53	0,38	1,3	0,5	0,3	1,2	0,6	0,3
- Mg ,,	33	2,2	8,4	1,6	1,2	14	2,9	1,8
- Ca ,,	2,37	16	14	16	13	37	19	46,6
CEC total	22	11	10	11	10	14	5,9	12,9
CEC clay	73,6	43,7	41,8	39,7	60,9	91,3	42,1	45,8
Spec. area [m²/g]	118,5	83,2	111,5	83,4	51,6	42,9	35,9	92,2
Sand > 63 µm [%]	8,70	22,60	26,64	6,67	36,34	59,86	69	7,67
Silt < 63 µm [%]								
Clay < 16 µm [%]	75,04	59,19	54,68	66,68	42,14	30,17	23	65,27
Lutum < 2 µm [%]	29,90	25,19	23,92	27,73	16,42	15,34	14	28,13
Mineral. comp. [%]								
- smectite	< 3	3	≈ 3	≈10	-	-		
- chlorite	10	8	7	20	15	5		++
- illite	20	20	20	15	10	10	10	++
- kaolinite	5	< 5	< 3	< 5	< 5	< 2		
- quartz	30	35	33	30	45-50	55	40	++++
- feldspar	20	16	20	15	15	25	10	++
- calcite	7	8	12	5	5	5	10	++
- dolomite	3	2	3	-	5	< 2		+

PHYSICAL PROPERTIES	SEDIMENT TYPE							
	H'Diep-Spl	H'Diep-Mbr	Breskens	Lake Ketel	Meuse	E-D:Delfz	Loswal-N	Biesbosch
Settling velocity:								
*Malvern [mm/s]:								
- Ws10	0,03	0,02	0,01	0,03	0,04	0,02-1,37	0,03	0,06
- Ws50	0,28	0,25	0,10	0,28	0,38	0,14-9,42	0,21	0,55
- Ws90	1,19	2,18	2,36	4,03	4,15	0,85-21,86	1,55	4,78
*Sedigraph [mm/s]:								
- Ws10	-	-	-	-	-			
- Ws50	0,02	0,15	0,12	-	-	5,5 ?	8,3	0,05
- Ws90	2,45	-	-	-	-		20,4	2,96
*Sedim. balance:								
- Ws50	0,18	0,22 0,32	0,23	0,36	0,85 0,94	1,3		0,25
Rheological prop.:								
*dyn. visc. [mPas]								
c=150 kg/m3	5,5	5,0	4,2	5,0	3,6	3,6	3,5	5,2
c=300 kg/m3	22,7	-	13,1	18,5	10,3	10,2	10	26
*yield str [Pa]								
c=150 kg/m3	0,39	0,23	0,2	0,31	0,14	0,13	0,15	0,17
c=300 kg/m3	4,26	-	3,0	2,39	0,33	0,45	0,58	4,5

DEPOSITION EXP.	SEDIMENT TYPE							
	H'Diep-Spl	H'Diep-Mbr	Breskens	Lake Ketel	Meuse	E-D:Delfz	Loswal-N	Biesbosch
Initial	0,19	0,18		0,21	0,11		0,2	0,17
concentr. [kg/m3]	0,84	0,72	0,76	1,01	0,76	0,69	1,0	0,83
[Pa]:	0,10	0,08	0,06	0,08	0,06	0,03±0,01	0,08±0,01	0,04±0,01
[-]:	1,18	2,10	1,78	2,22	3,87	11,3	1,91	3,9±0,01
[-]:	0,73	0,81	0,65	0,57	0,62	0,74	0,68	0,39
Conduct. [mS/cm]:	1,07 1,14	1,02 0,89	34,3	1,19	0,95	33	49	0,75
Chlorinity [kg/m3]	0,21 0,26	0,24 0,21	18	0,32	0,13	12	18	0,11
Ox. cont. [kg/m3]	0,0065	0,0046	0,0034	0,0081	-	6,7 E-3		
	0,0036	0,0027						
,, [%]	80 44	43 32	40	93	-	80		
Redox potent. [mV]	100 200	160 23	-60	200	130	+80		
pH [-]	7,74 7,71	7,76 7,83	7,90	7,92	8,31	8,07		7,6
Org. content [%]	- -	5,1 14	9,8	10	6,1	-		-
SAR [(meq/l)$^{\frac{1}{2}}$]	1,8 2,3	3,6 3,4	37,6	3,5	1,5	44	43	1,6

	SEDIMENT TYPE							
EROSION EXP. 1	H'Diep-Spl	H'Diep-Mbr	Breskens	Lake Ketel	Meuse	E-D:Delfz	Loswal-N	Biesbosch
Initial concentr. [kg/m³]	57 57	49	56	56	53	60	134 ?	55
Dry density:								
*top [kg/m³]	140 - 170	175	110	100	140	160-180	100	60-110
*bottom [kg/m³]	350	350	650	450	500	1200-1300	1500	ca 400
τ_c [Pa]:	0,35-0,40	0,35-0,45	0,2 - 0,3	0,1 - 0,3	0,2	0,15	0,1-0,25	0,14
M^e [kg/m²/s] (*10⁻³)	0,3 - 1,1	0,2 - 0,5	0,05 - 0,2	0,01 - 0,4	0,01-0,03	,006-,019	,001-,048	0,009-0,10
τ_c [Pa]:	5.2	7,1	10,4	10,1	7,3	7,1	14,3±0,2	15,7±1,0
Conduct. [mS/cm]		1,14	35,8	1,54	0,96	38	48	0,88
Chlorinity [kg/m³]		0,22	17,5	0,44	0,16	13	19	0,13
Ox. cont. [kg/m³]		0,0067	0,0053	0,0013	0,0043	0,0051		
,, [%]		78	60	15	51	53	60-87	
Redox pot. [mV]	+100	104	192	-180	150	+98	+150-+220	+100-+170
pH [-]	7,47	7,53	7,24	7,12	7,36	7,77	7,43	6,3-7,0
Org. cont. [kg/m³]	16,0	9,8	5,0	10	6,3	1,8	0,93	8,4
SAR [(meq/l)$^{\frac{1}{2}}$]		2,9	35,6	4,6	1,9	44	32,1	1,29

Consolidation period: 1 day

	SEDIMENT TYPE							
EROSION EXP. 2	H'Diep-Spl	H'Diep-Mbr	Breskens	Lake Ketel	Meuse	E-D:Delfz	Loswal-N	Biesbosch
Initial concentr. [kg/m³]	57	47						55
Dry density:								
*top [kg/m³]	250	215		160	155		100	160
*bottom [kg/m³]	350	350		450	600		1500	ca 450
τ_c [Pa]:	0,45-0,50	0,35-0,45		0,1 - 0,3	0,45-0,5		0,25-0,38	0,28
M^e [kg/m²/s] (*10⁻³)	0,2 - 0,8	0,1 - 0,3		0,01 - 0,4	0,05-0,1		,021-,105	0,04-0,21
τ_c [Pa]:	6,1	7,4		10,0	7,6		9,6±1,6	9,3±2,9
Conduct. [mS/cm]	1,21	1,26					48	0,87
Chlorinity [kg/m³]	0,24	0,23					19	0,12
Ox. cont. [kg/m³]	0	0,0018						ca 4
,, [%]	0	21					55-80	40-50
Redox pot. [mV]	- 70	100					+130-+220	+179-+70
pH [-]	7,30	7,49					7,33	6,7
Org. cont. [kg/m³]	8,9	4,8					0,94	8,1
SAR [(meq/l)$^{\frac{1}{2}}$]	1,4	3,6					29,9	1,18

Consolidation period: 7 days

Specific surface
versus lutum fraction

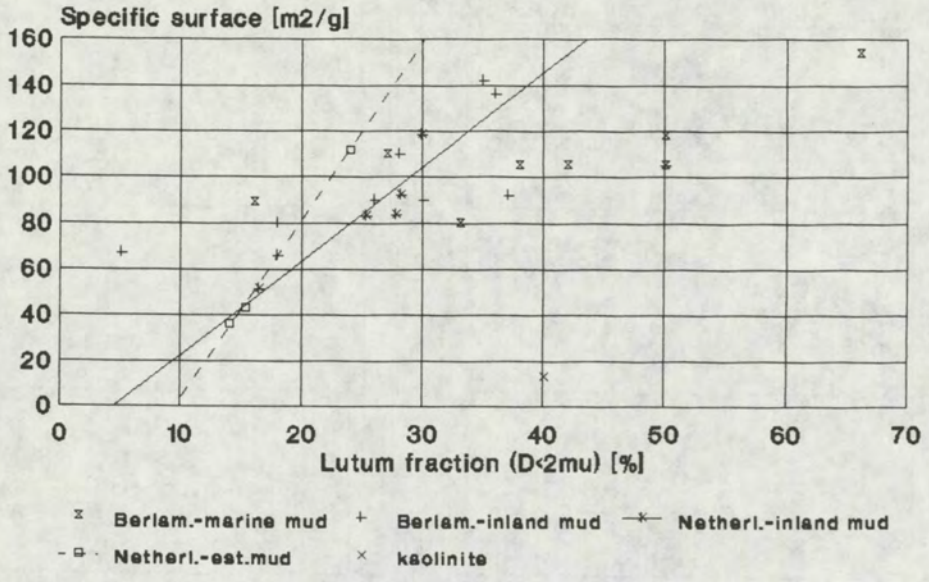

Fig 2.1

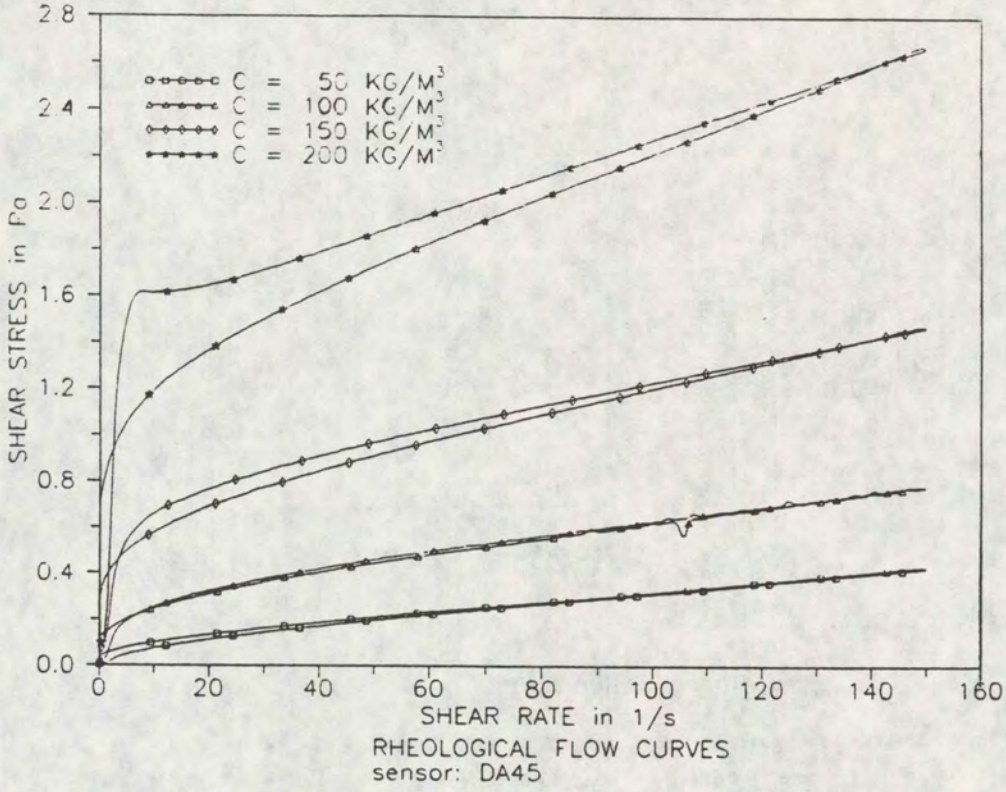

RHEOLOGICAL FLOW CURVES
sensor: DA45

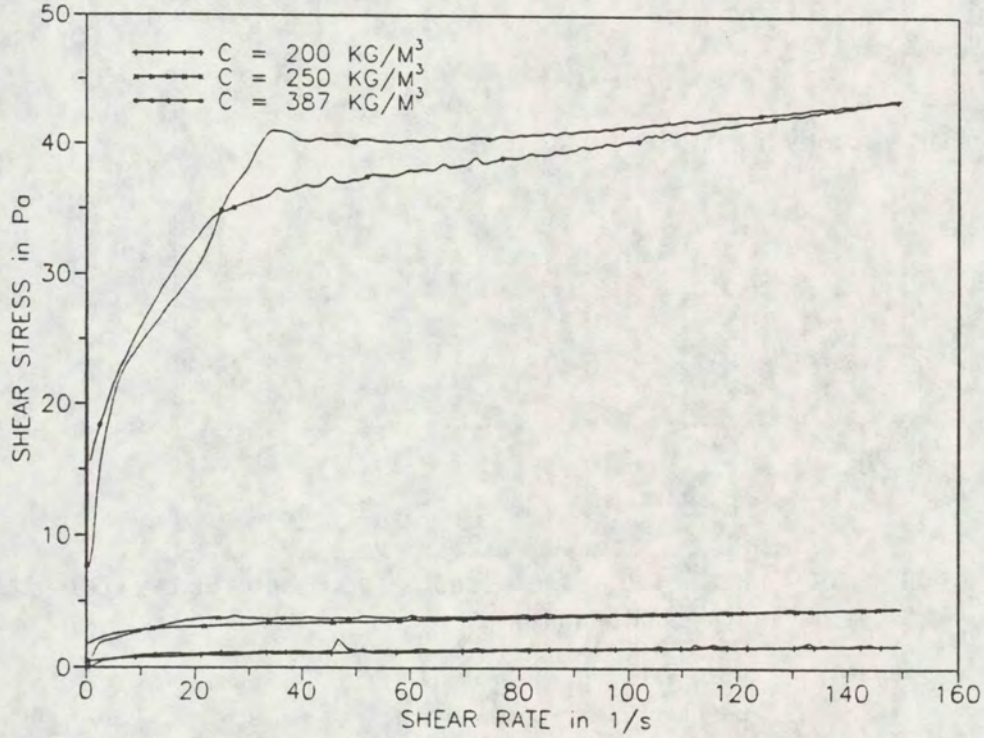

RHEOLOGICAL FLOW CURVES
sensor: ME15

Rheological flow-curves.	H'Diep. S.plaat	
DELFT HYDRAULICS		Fig. 2.2

Dynamic viscosity
versus concentration

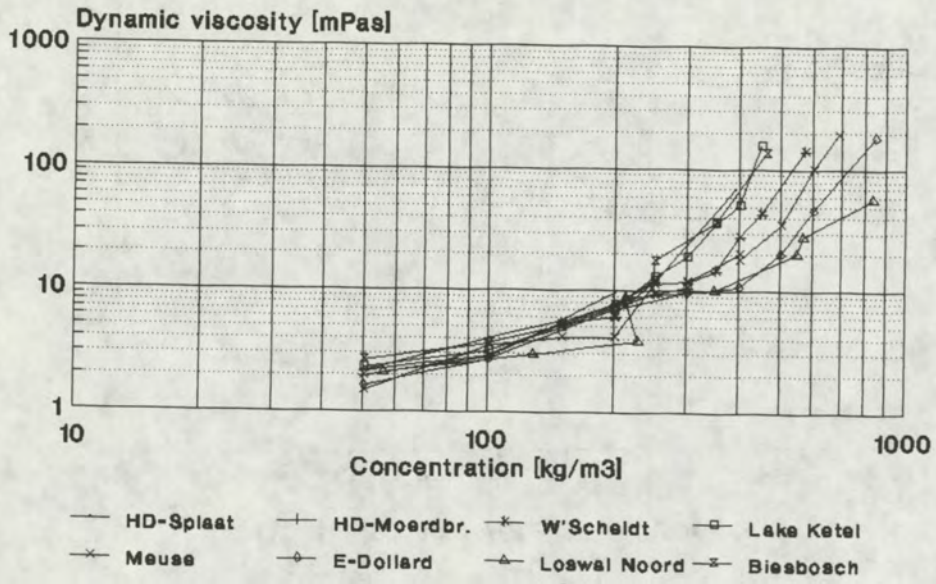

Fig 2.3a

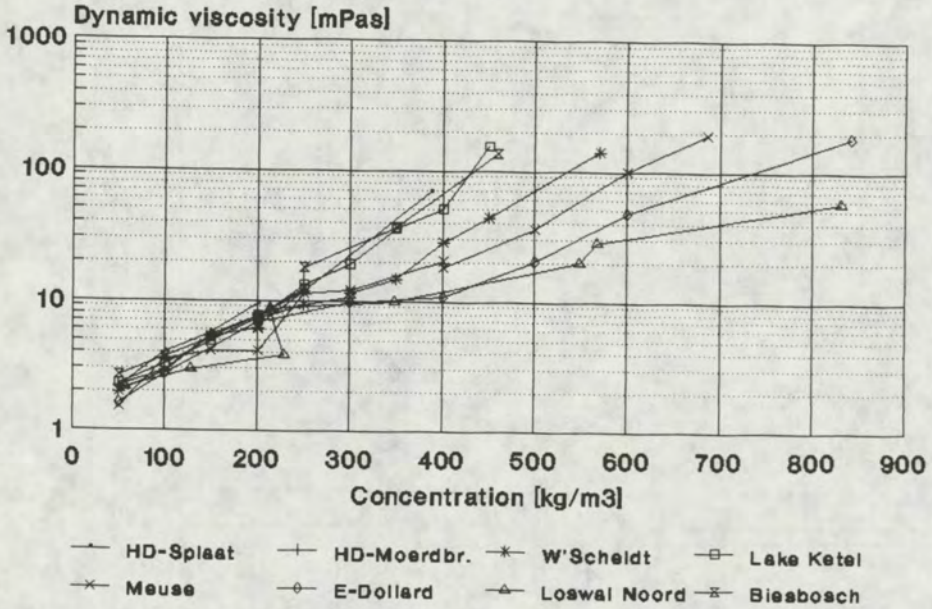

Fig 2.3b

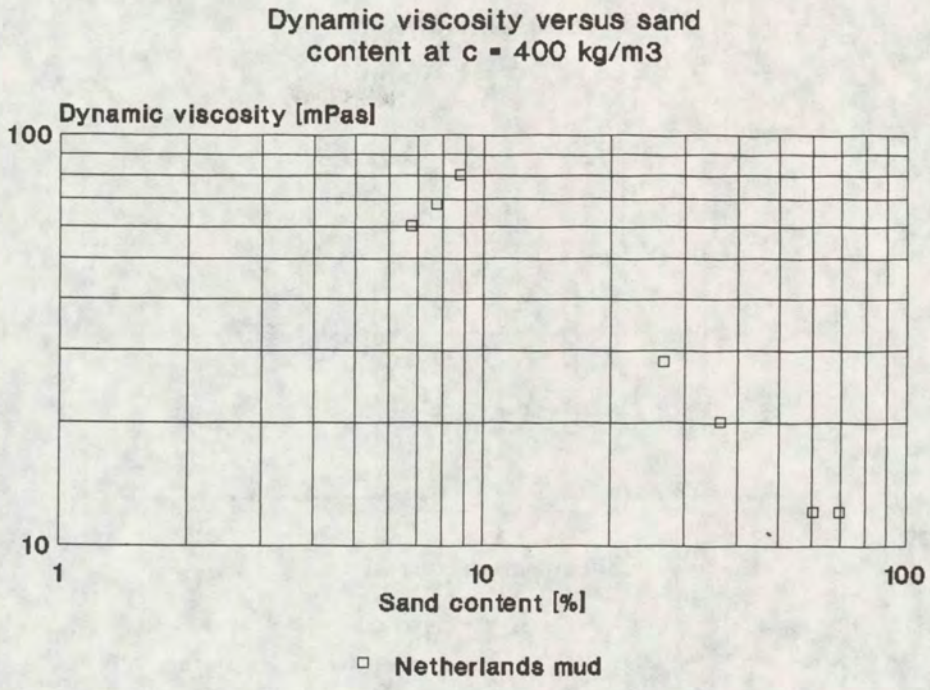

Fig 2.4a

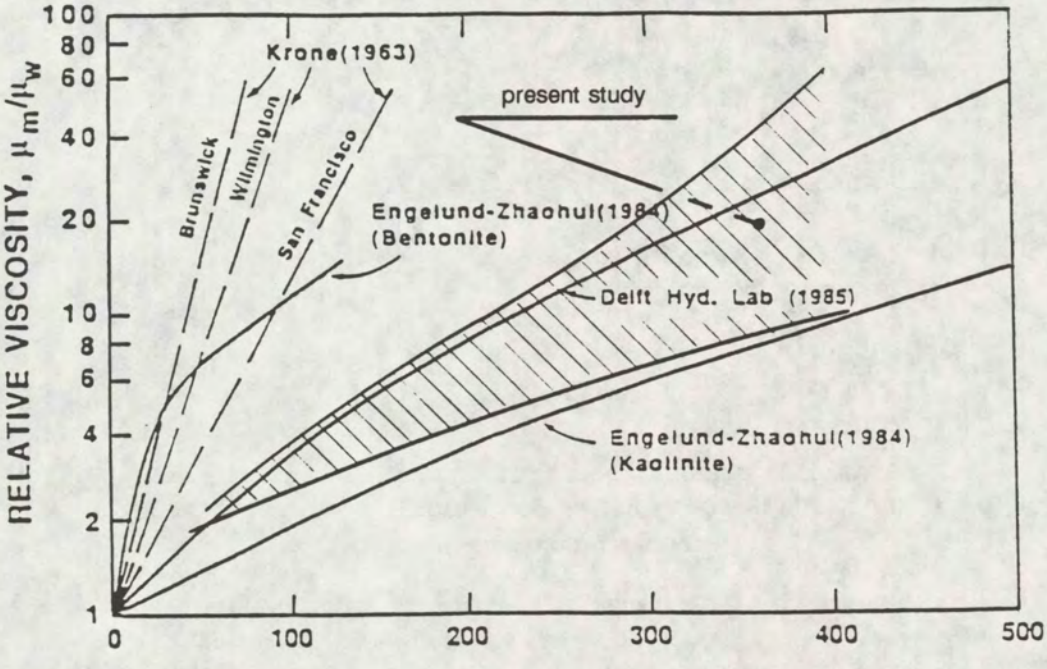

Fig. 2.4 b SUSPENDED SEDIMENT CONCENTRATION (g/l)

DELFT HYDRAULICS

Yield strength
versus concentration

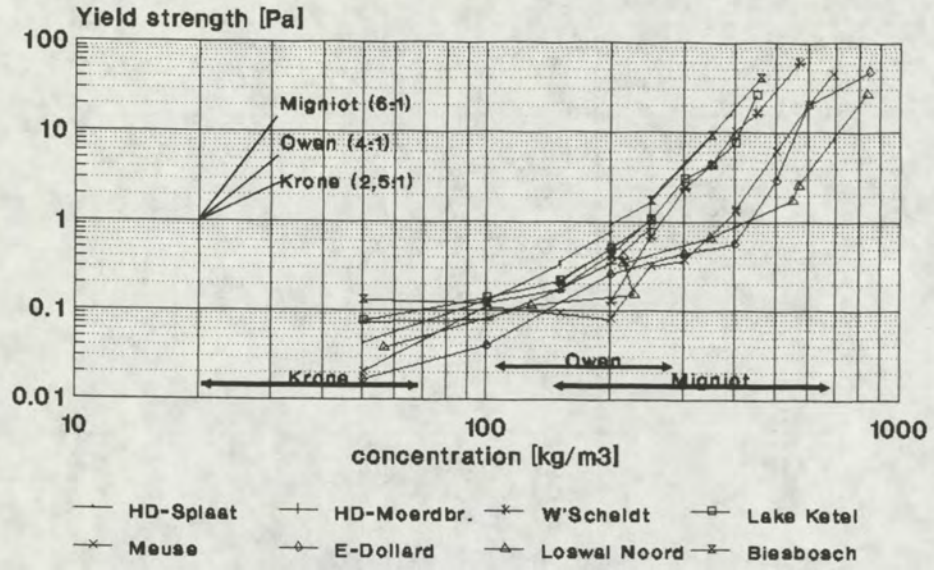

Fig 2.5a

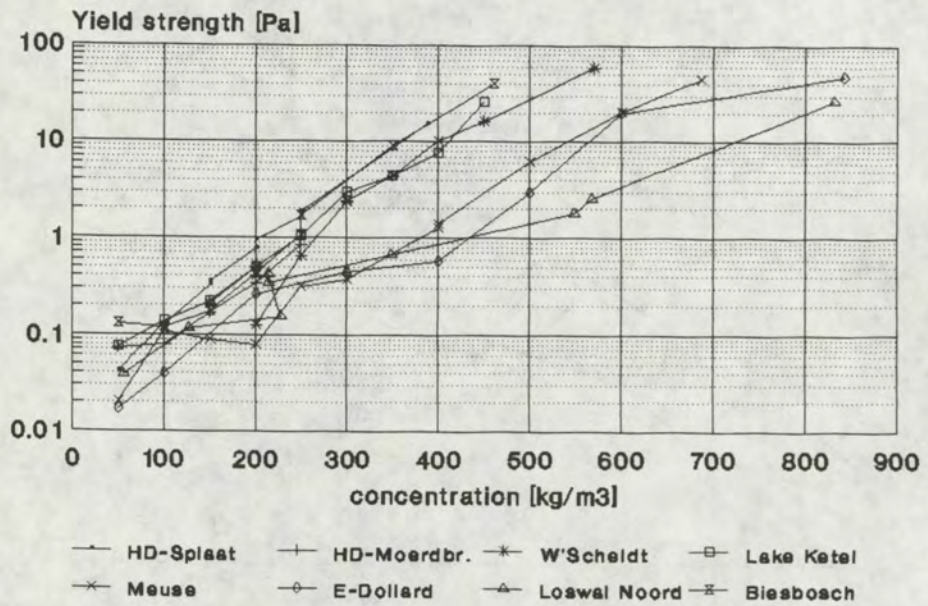

Fig 2.5b

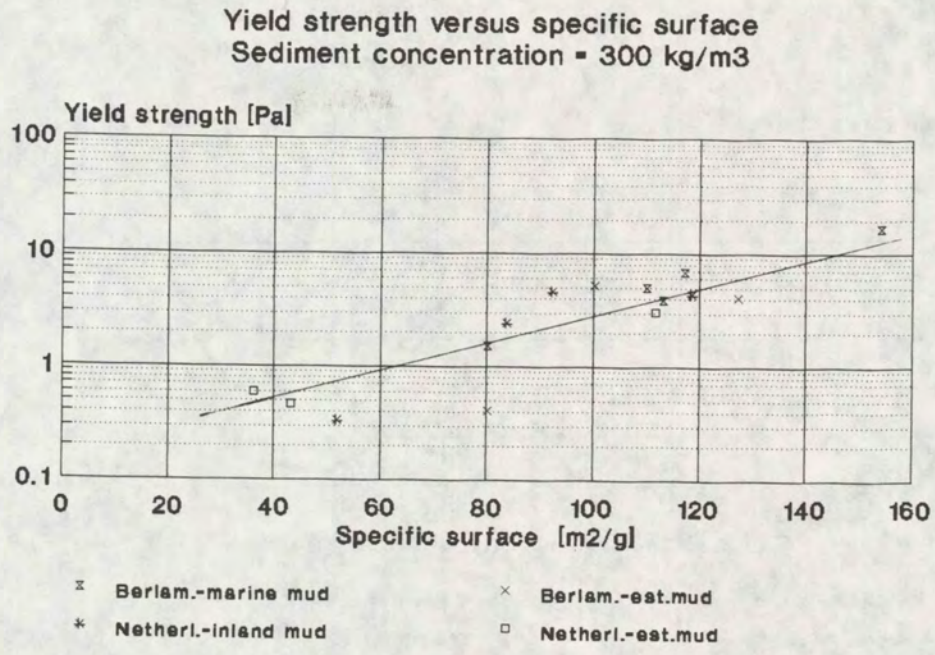

Fig 2.6 Berlammont: Bingham strength

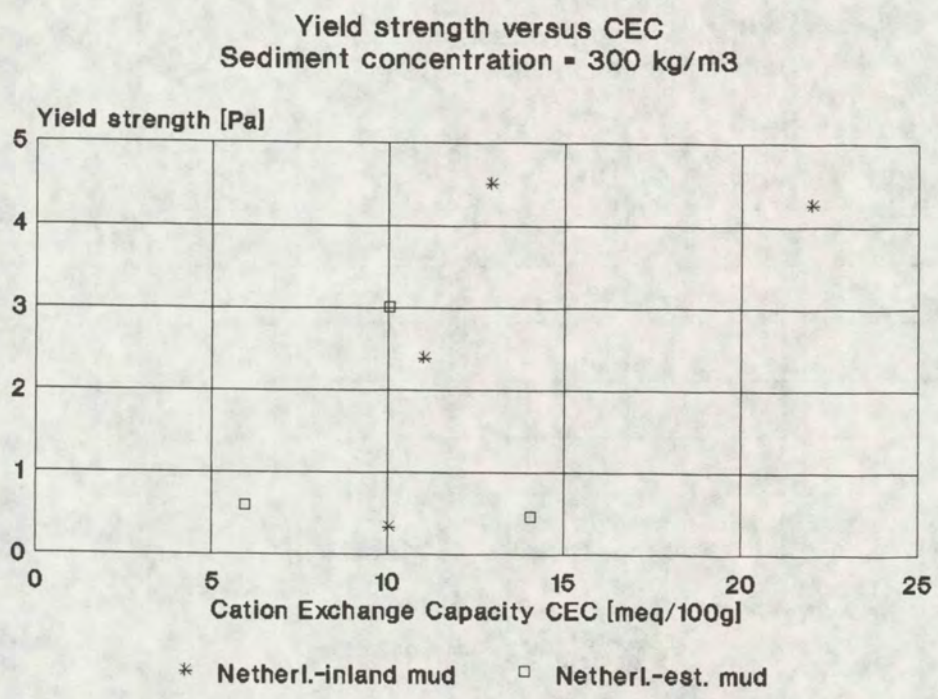

Fig 2.7

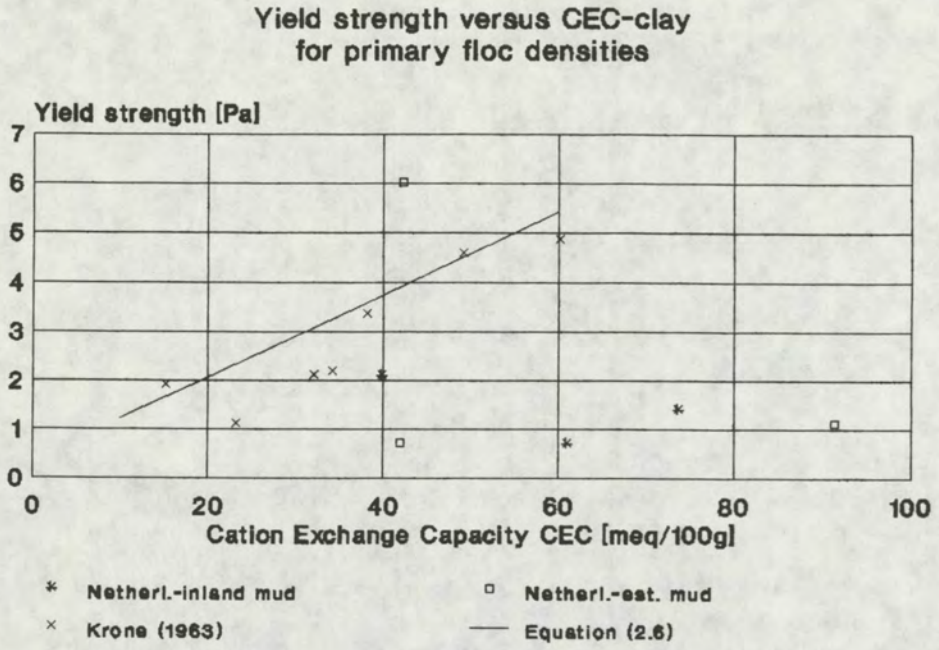

Fig 2.8 Krone: Bingham strength

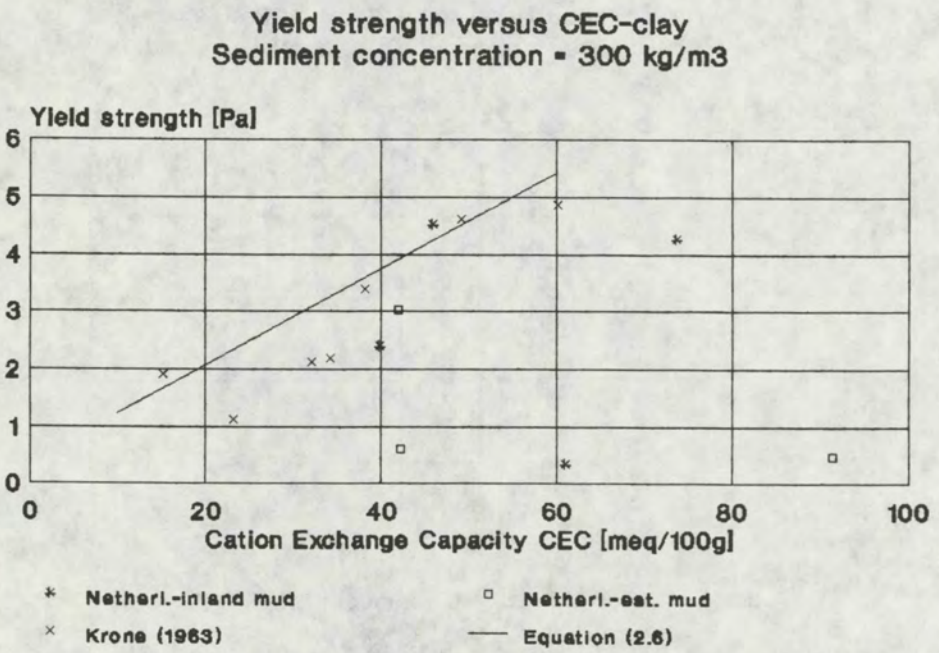

Fig 2.9 Krone: primary flocs, Bingh.str

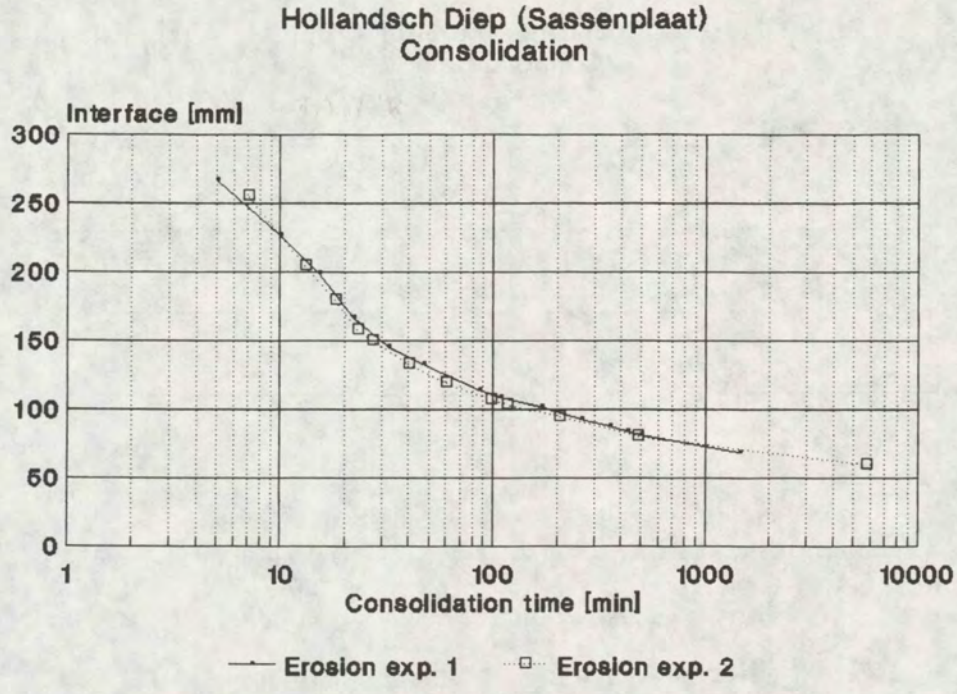

Fig 3.1a

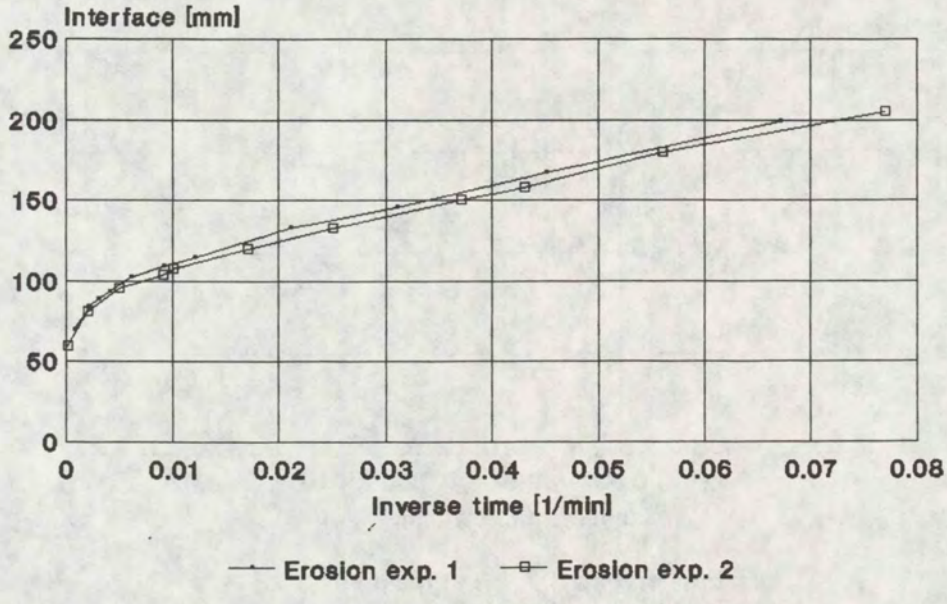

Fig. 3.1b

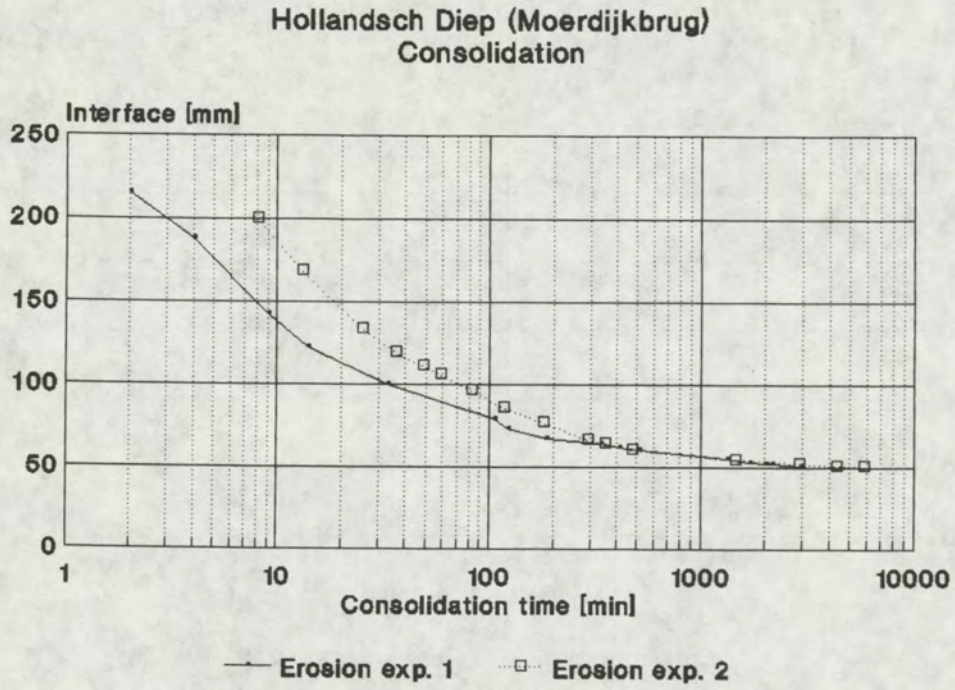

Fig 3.2a

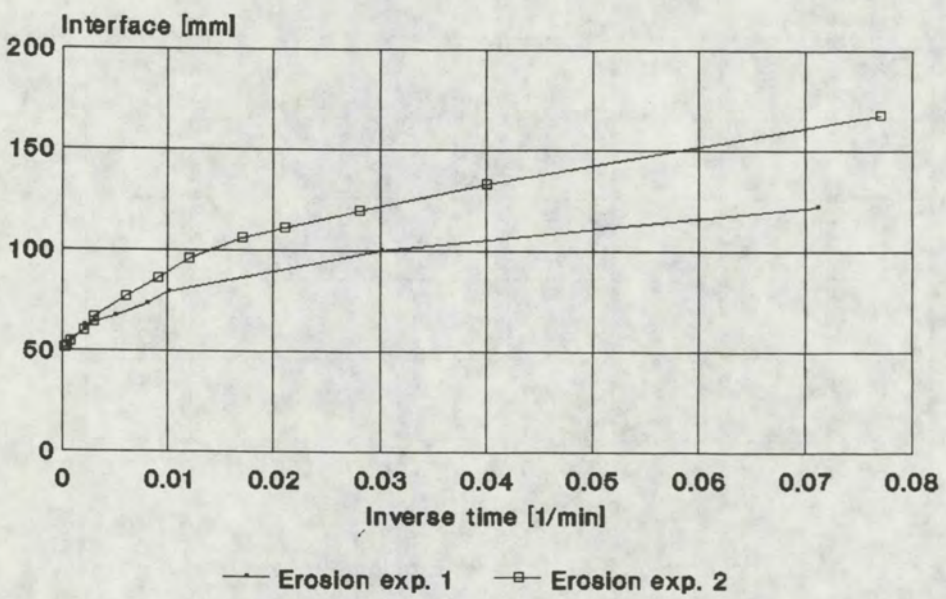

Fig. 3.2b

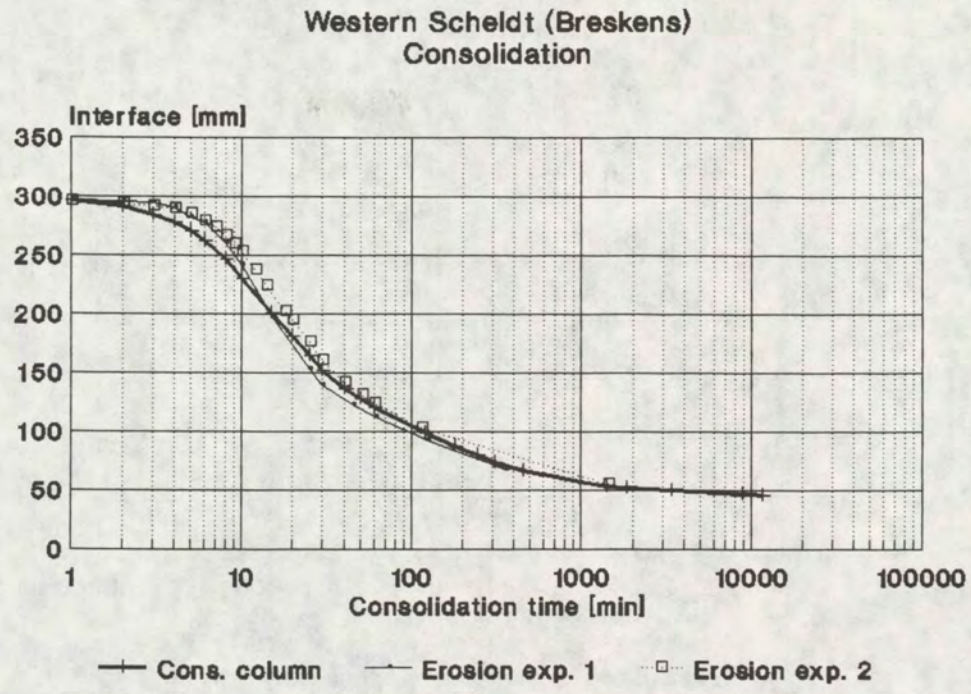

Fig 3.3a

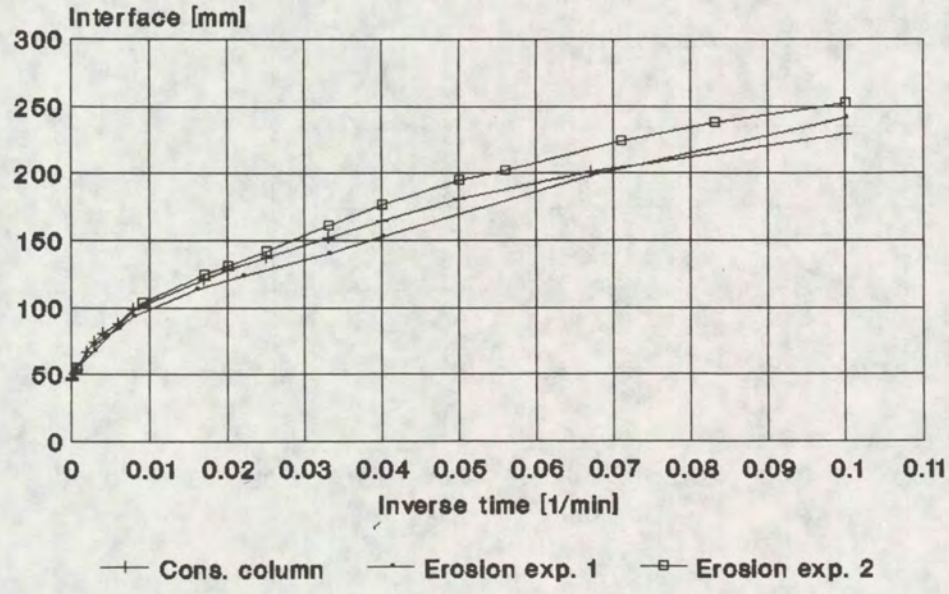

Fig 3.3b

DELFT HYDRAULICS

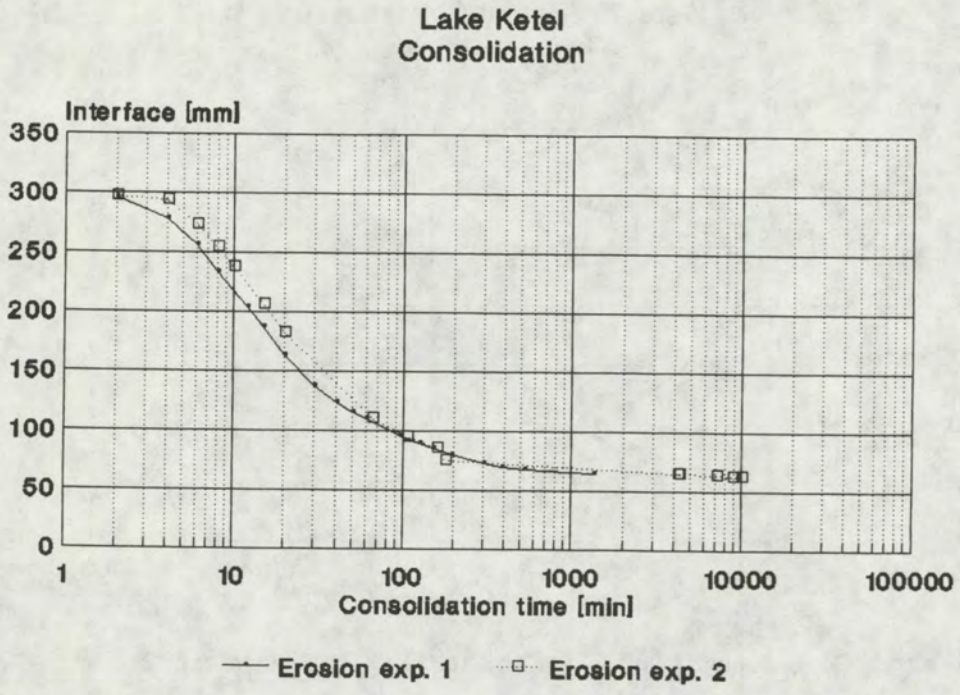

Fig 3.4a

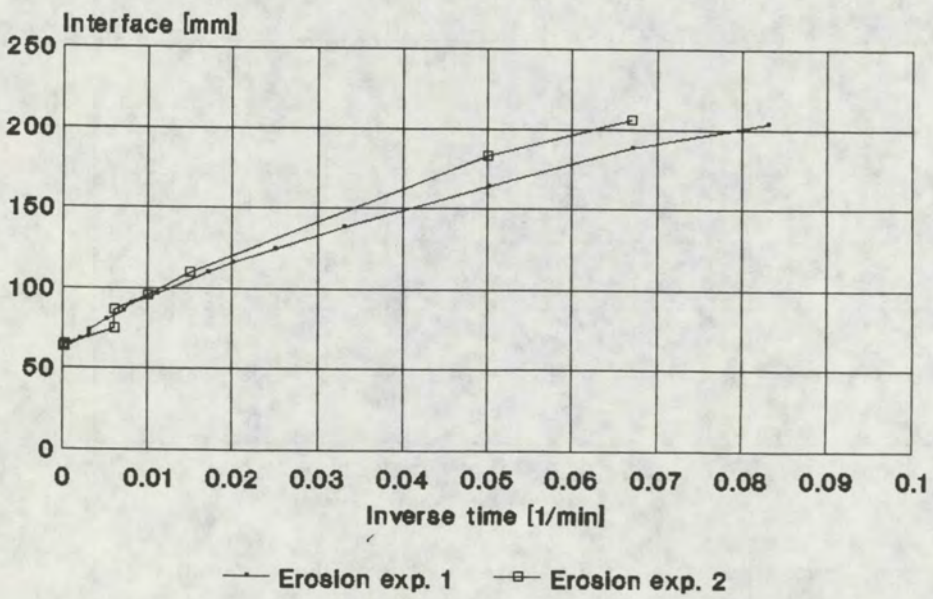

Fig. 3.4b

DELFT HYDRAULICS

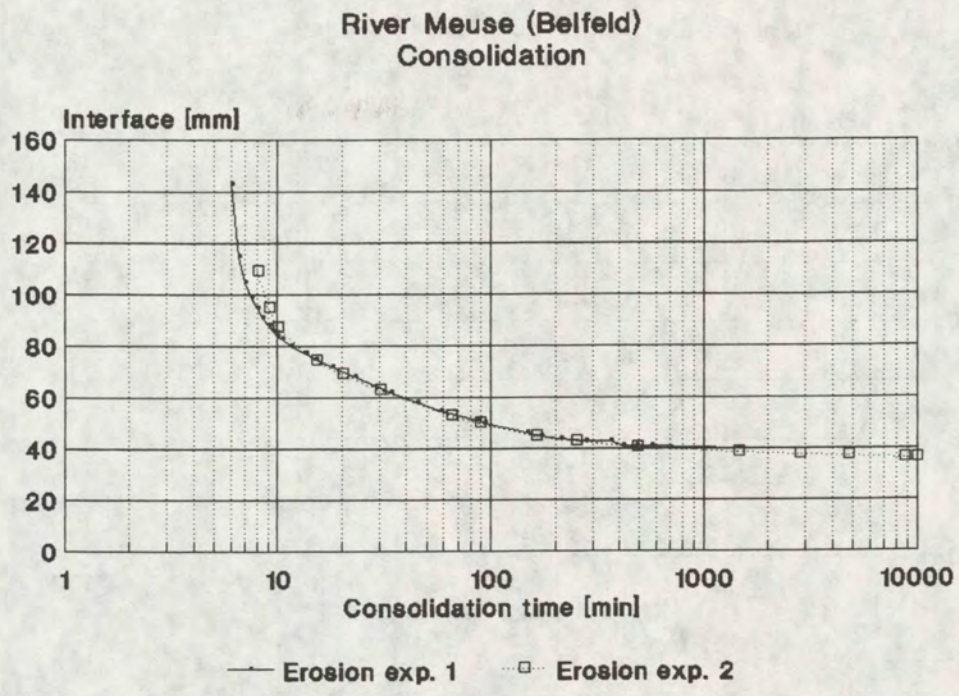

Fig 3.5a

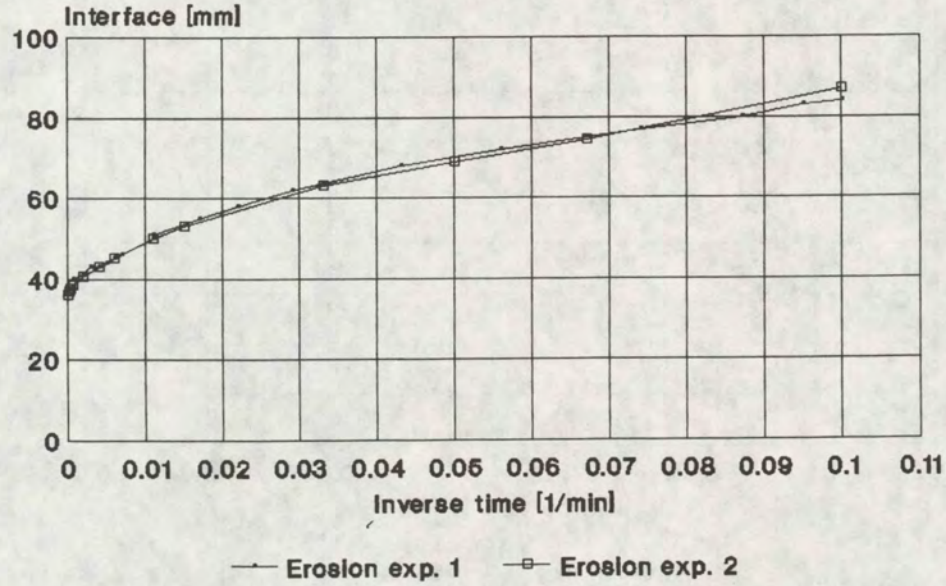

Fig. 3.5b

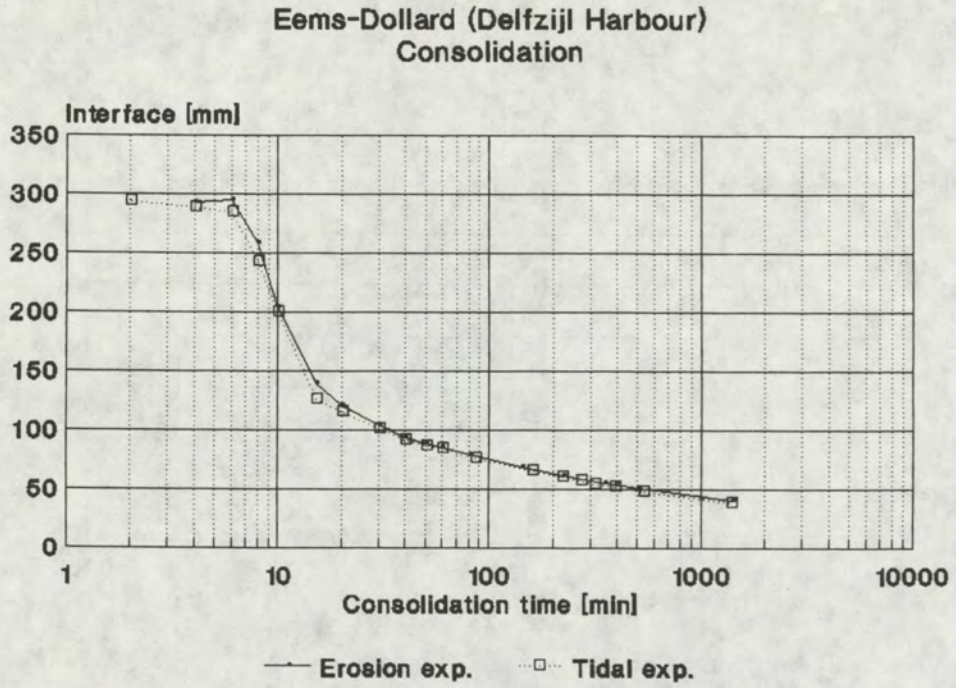

Fig 3.6a

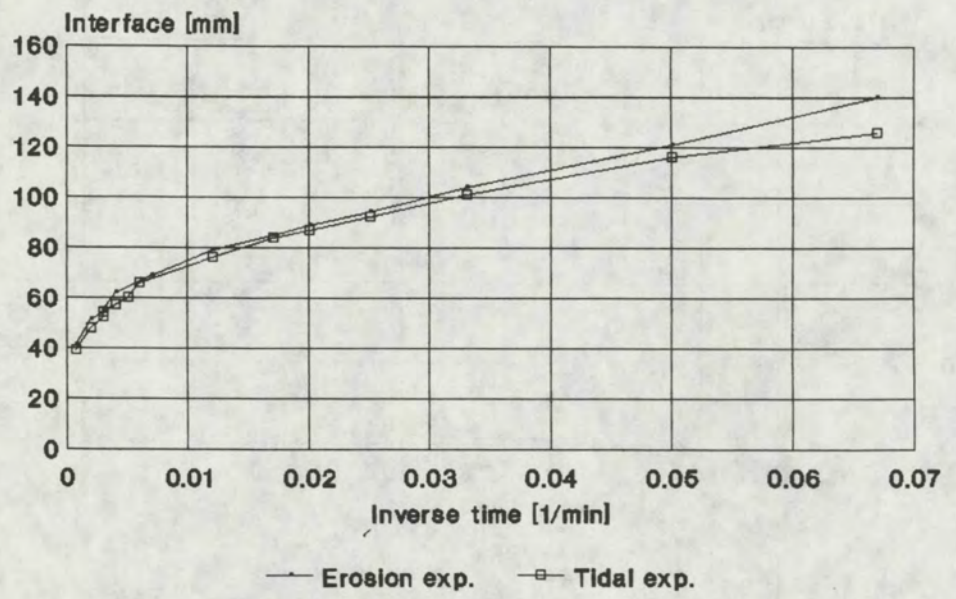

Fig. 3.6b

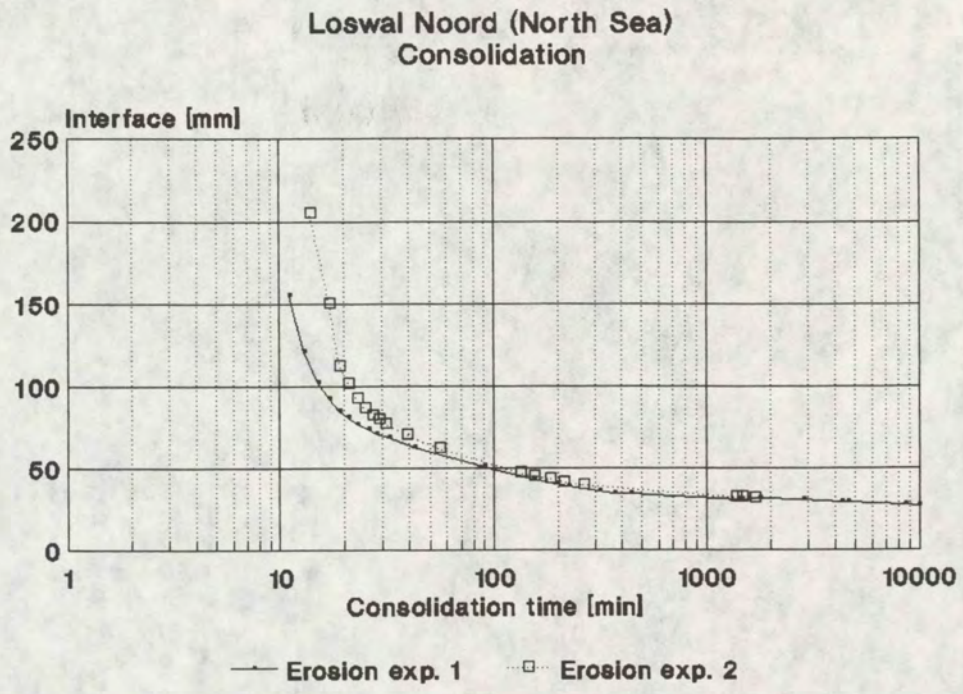

Fig 3.7a

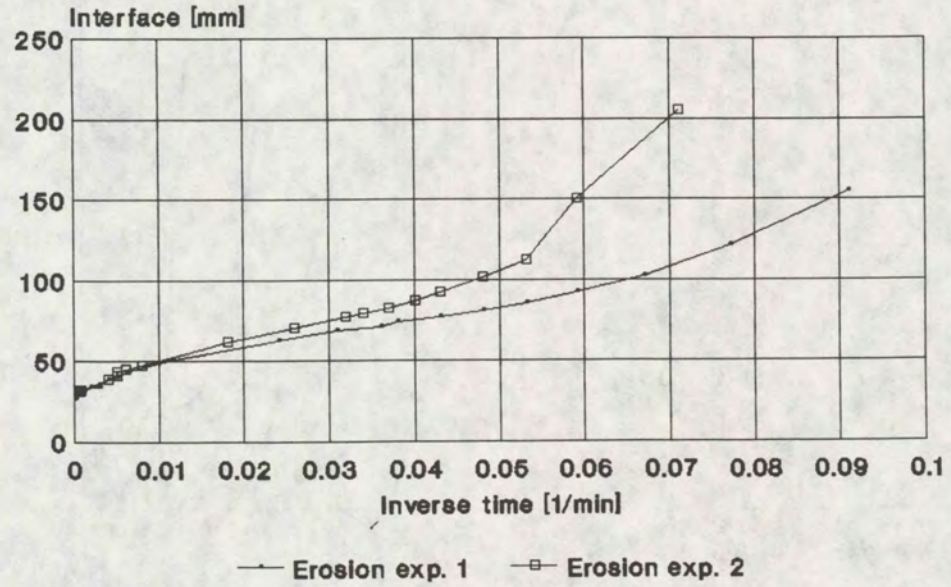

Fig. 3.7b

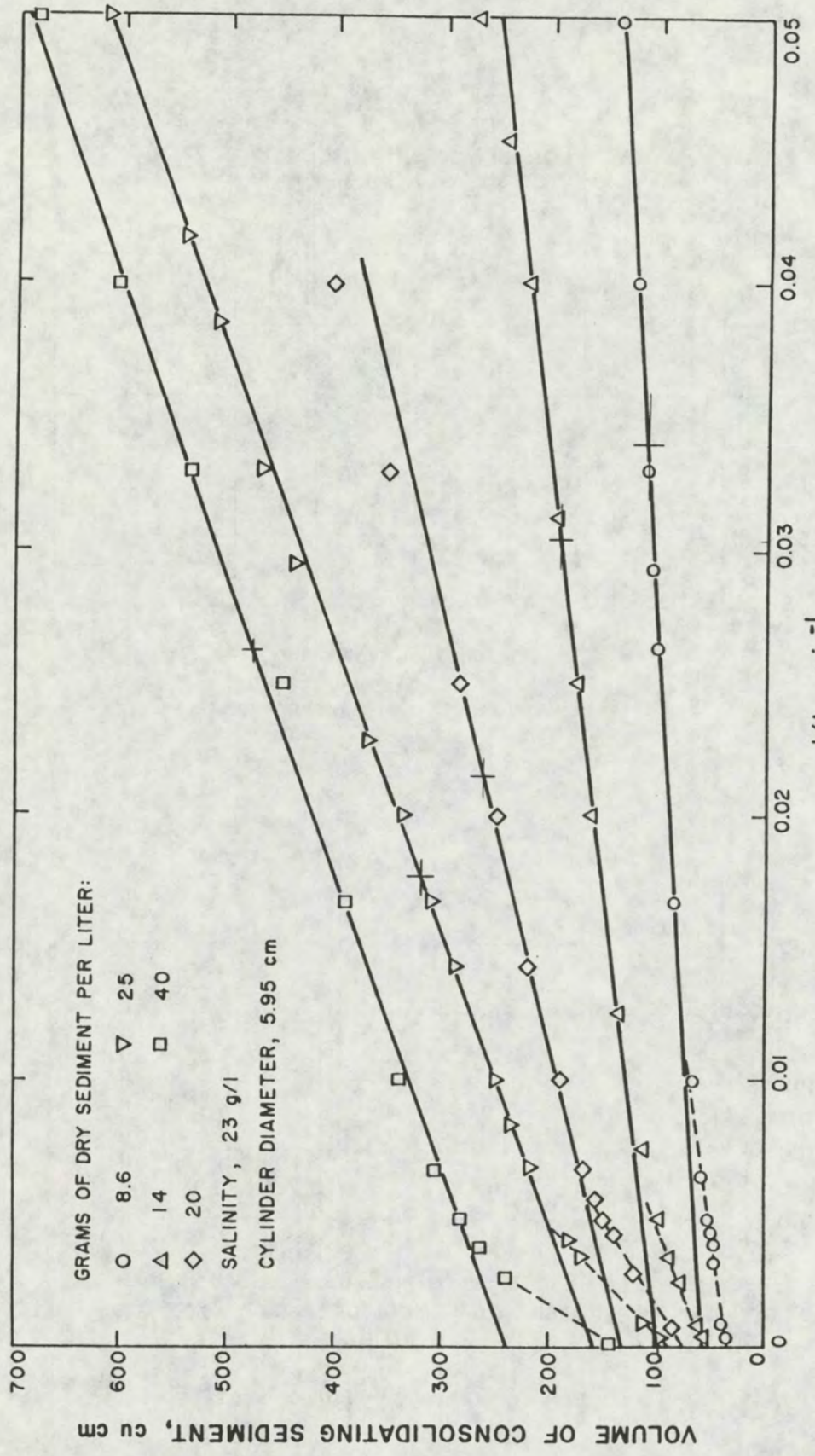

Consolidation of San Francisco Bay Mud	Krone [1962]	
DELFT HYDRAULICS	Fig. 3.8	

Hollandsch Diep (Sassenplaat)
Sediment-water interface H(t)

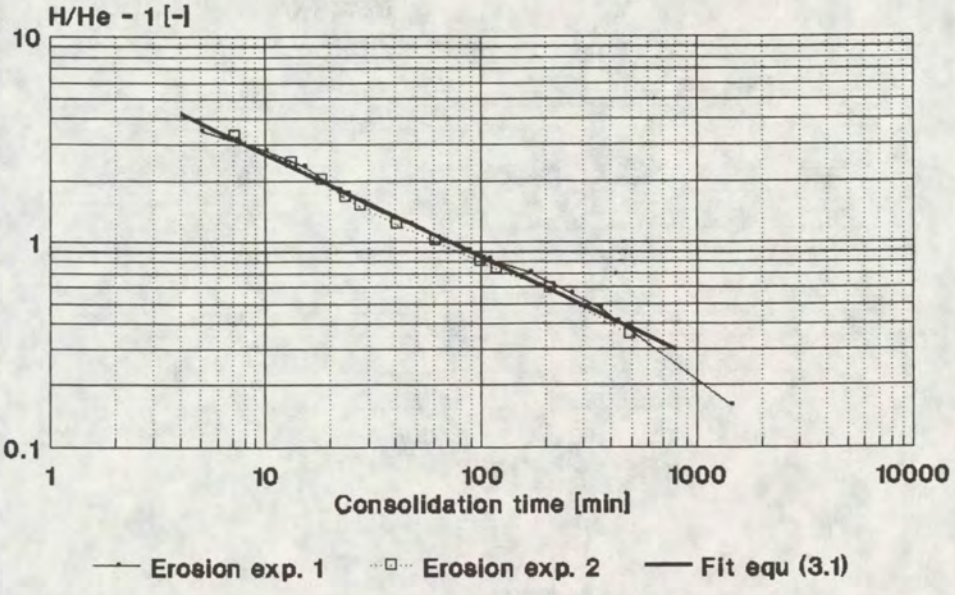

Fig 3.9

Hollandsch Diep (Moerdijkbrug)
Sediment-water interface H(t)

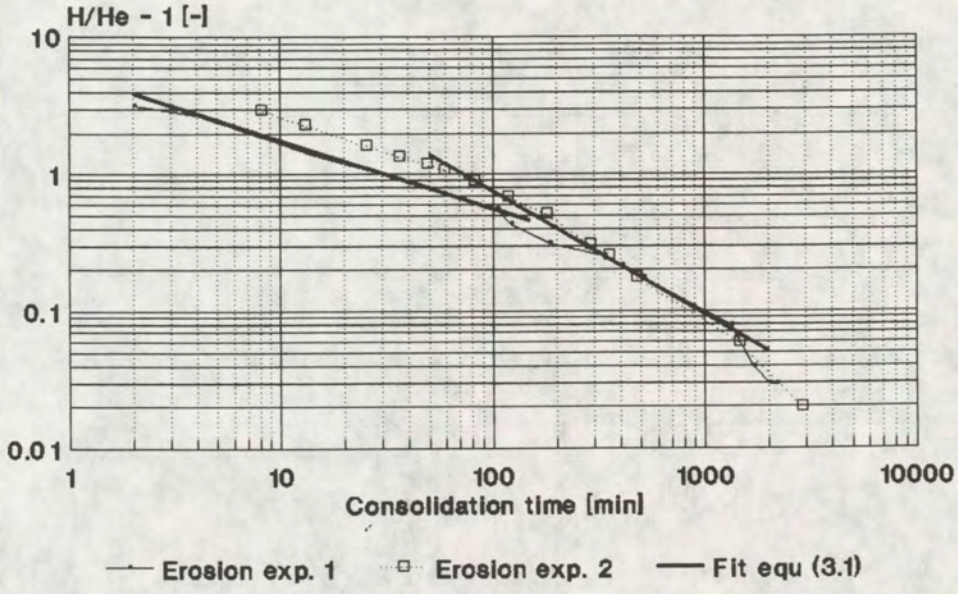

Fig 3.10

Western Scheldt (Breskens)
Sediment-water interface H(t)

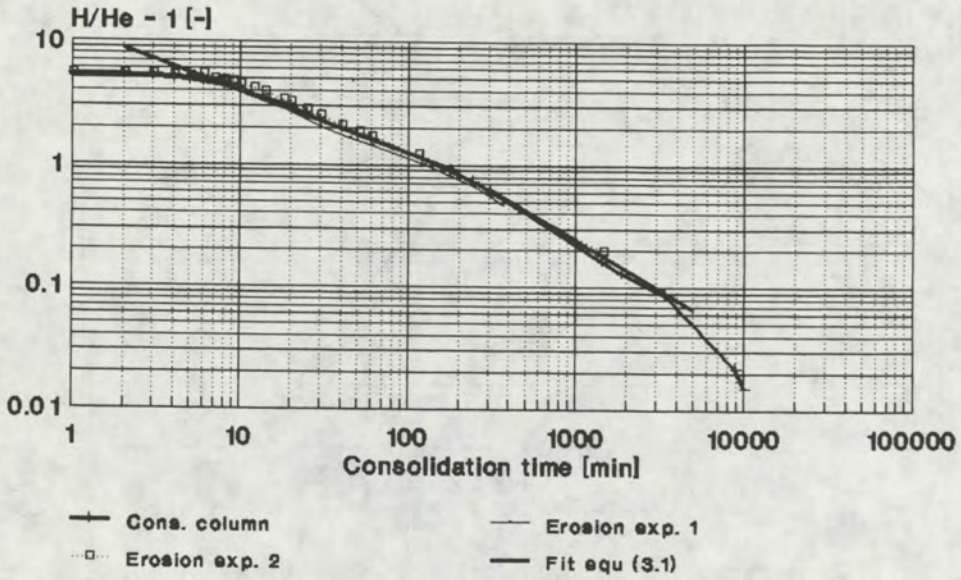

Fig 3.11

Lake Ketel
Sediment-water interface H(t)

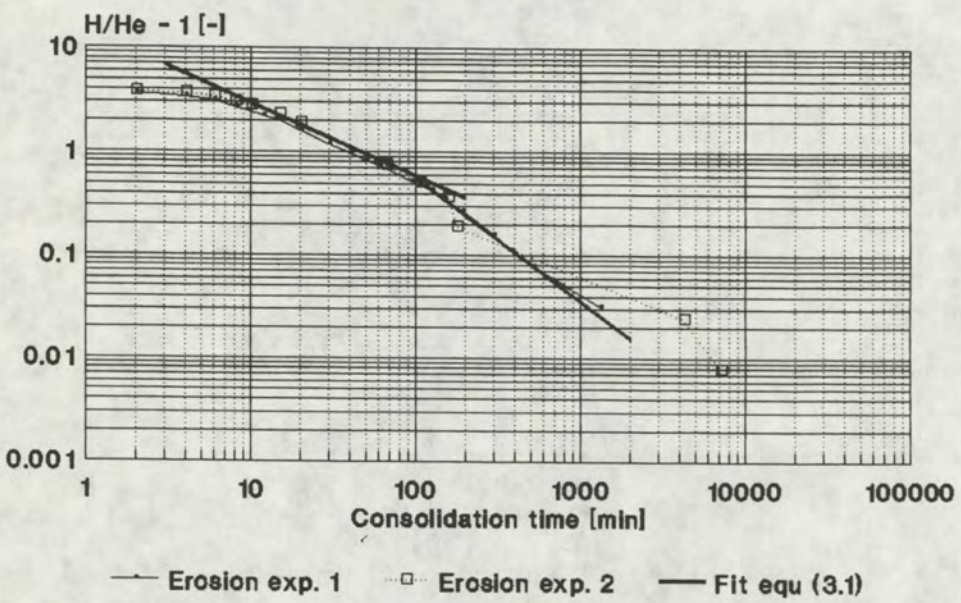

Fig 3.12

River Meuse (Belfeld)
Sediment-water interface H(t)

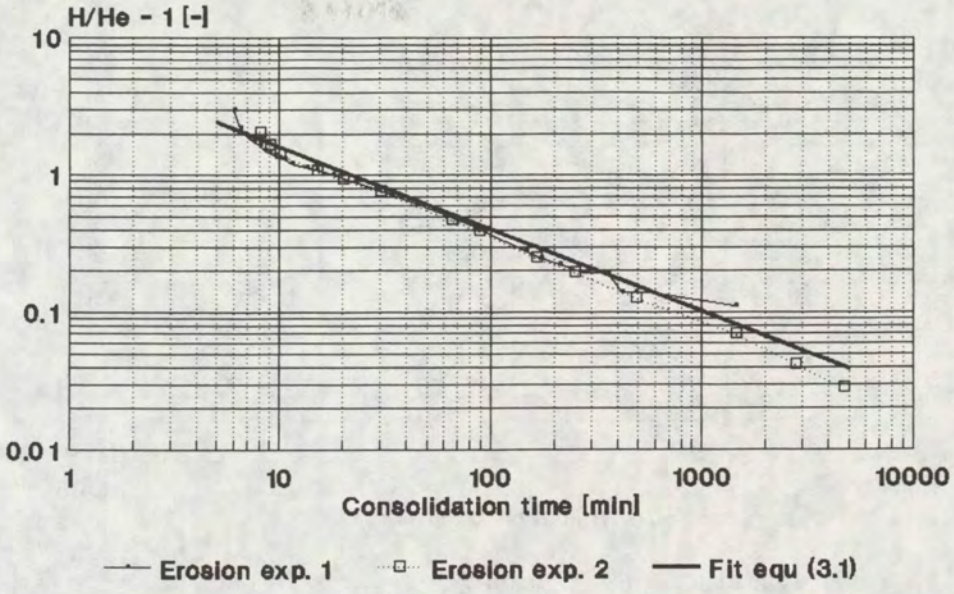

Fig 3.13

Eems-Dollard (Delfzijl Harbour)
Sediment-water interface H(t)

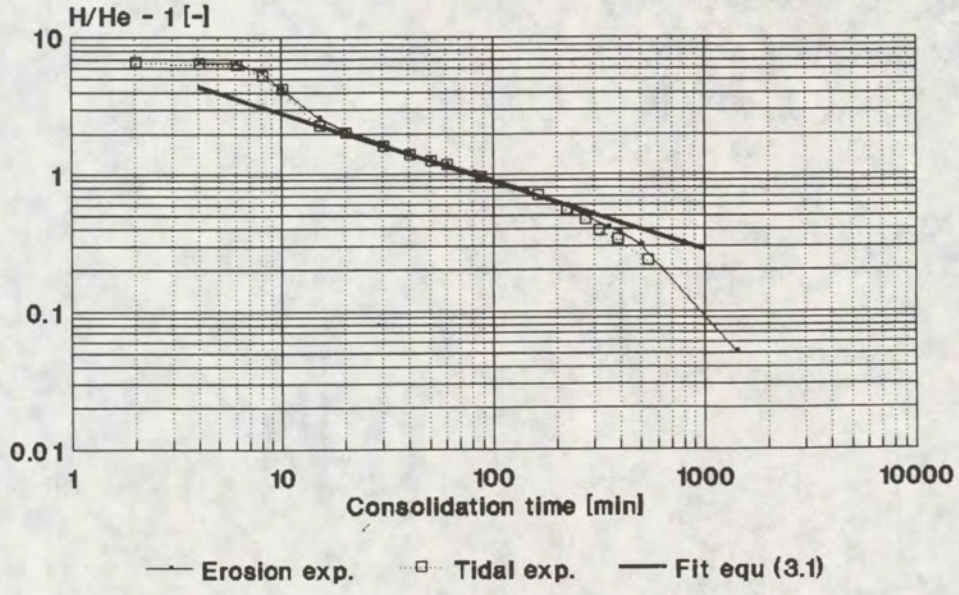

Fig 3.14

Loswal Noord (North Sea)
Sediment-water interface H(t)

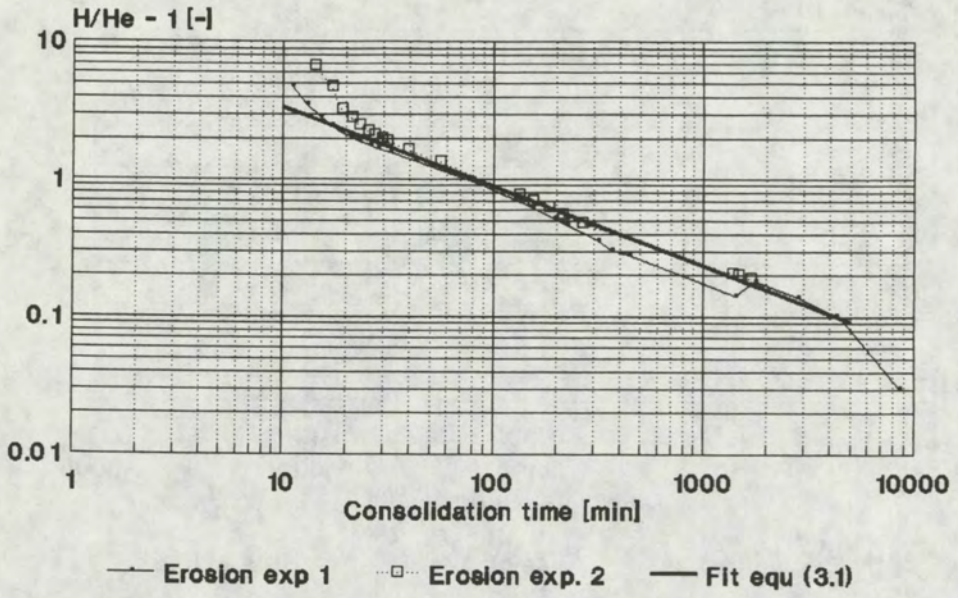

Fig 3.15

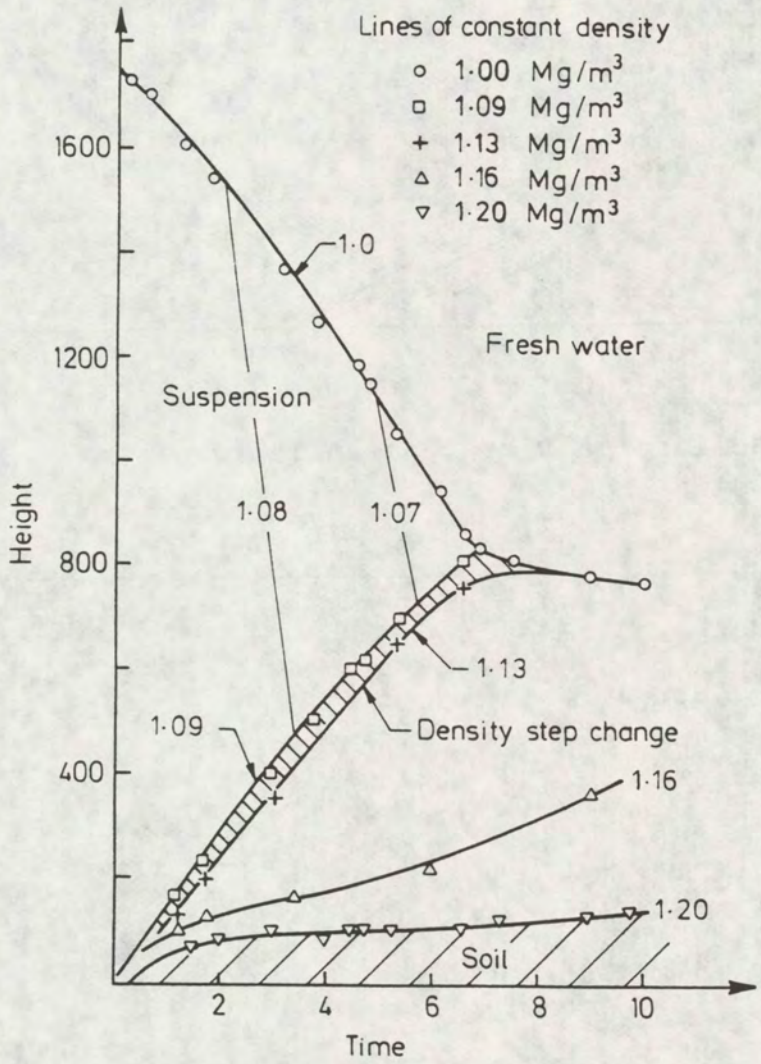

Contraction during consolidation	Sills [1986]	
DELFT HYDRAULICS	Fig. 3.16	

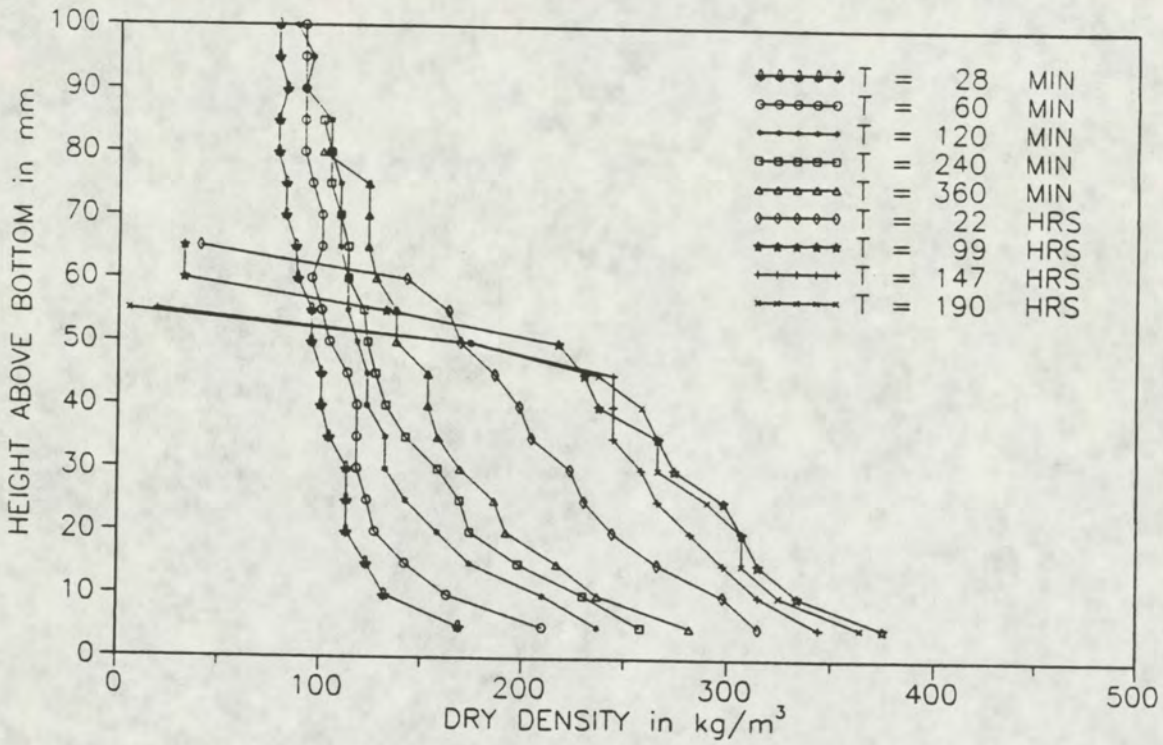

Fig. 3.17 Hollandsch Diep (Sassenplaat)

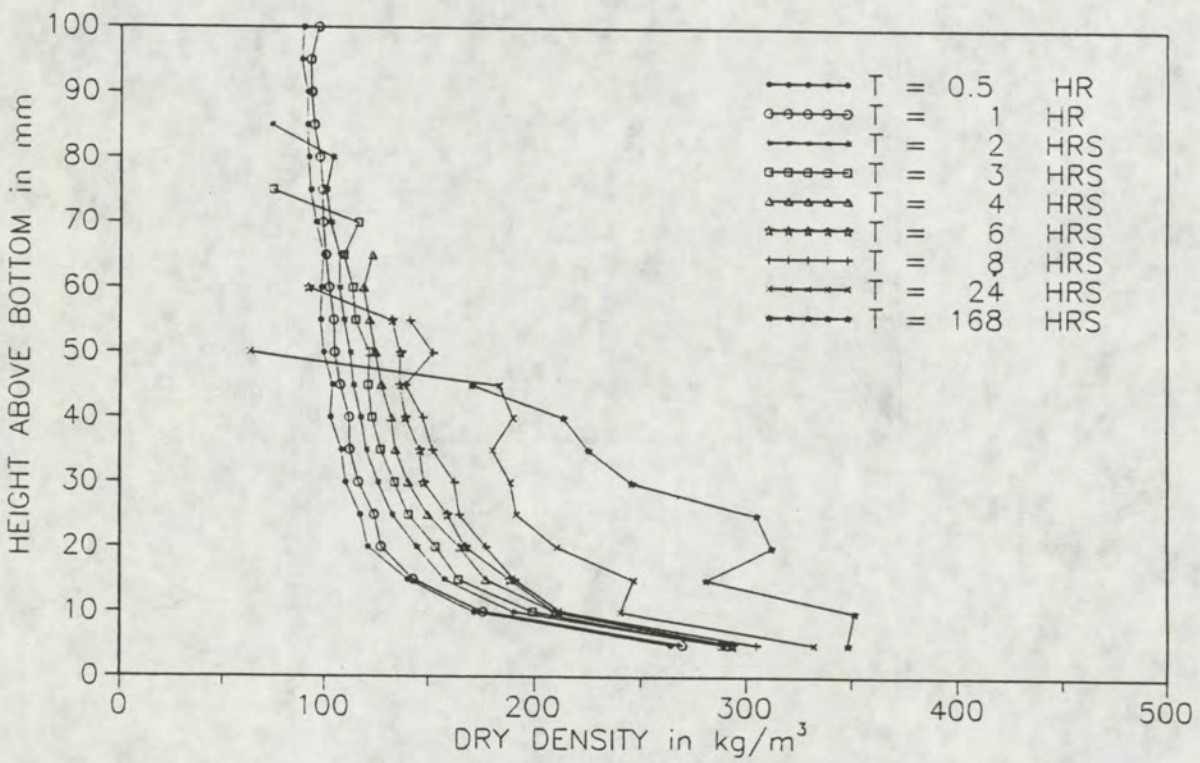

Fig. 3.18 Hollandsch Diep (Moerdijkbrug)

Bed concentration profiles during consolidation.

DELFT HYDRAULICS

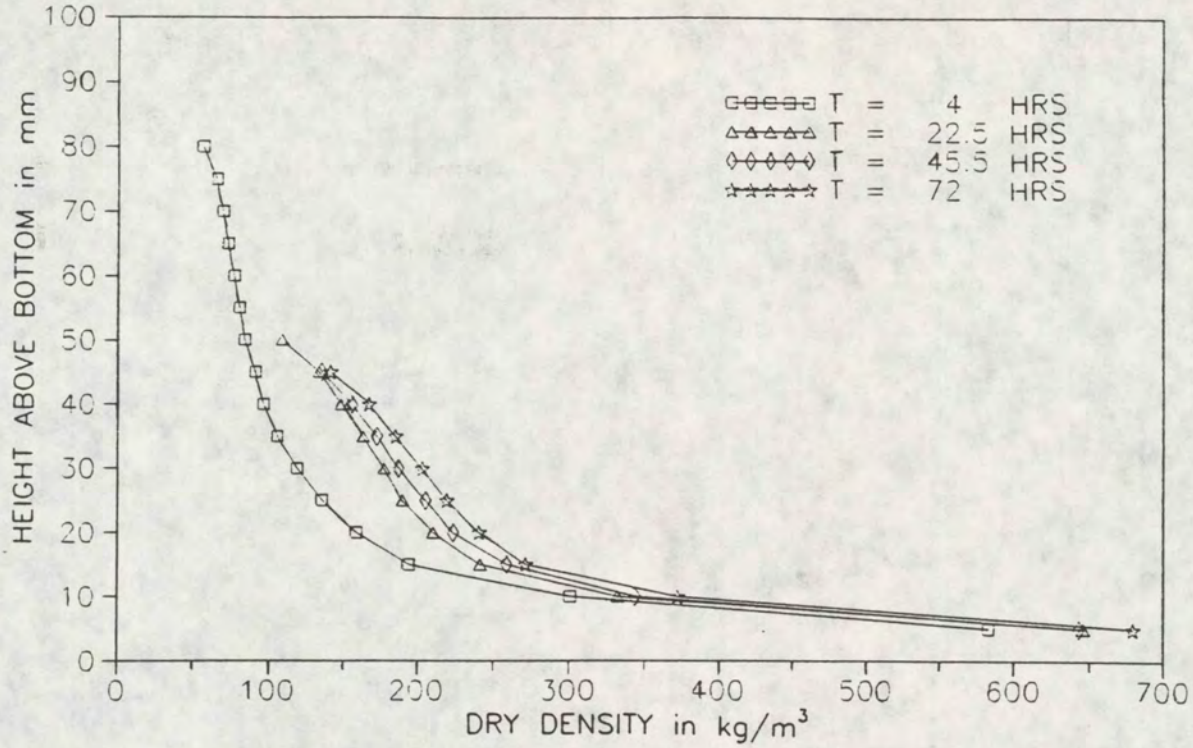

Fig. 3.19 Western Scheldt (Breskens)

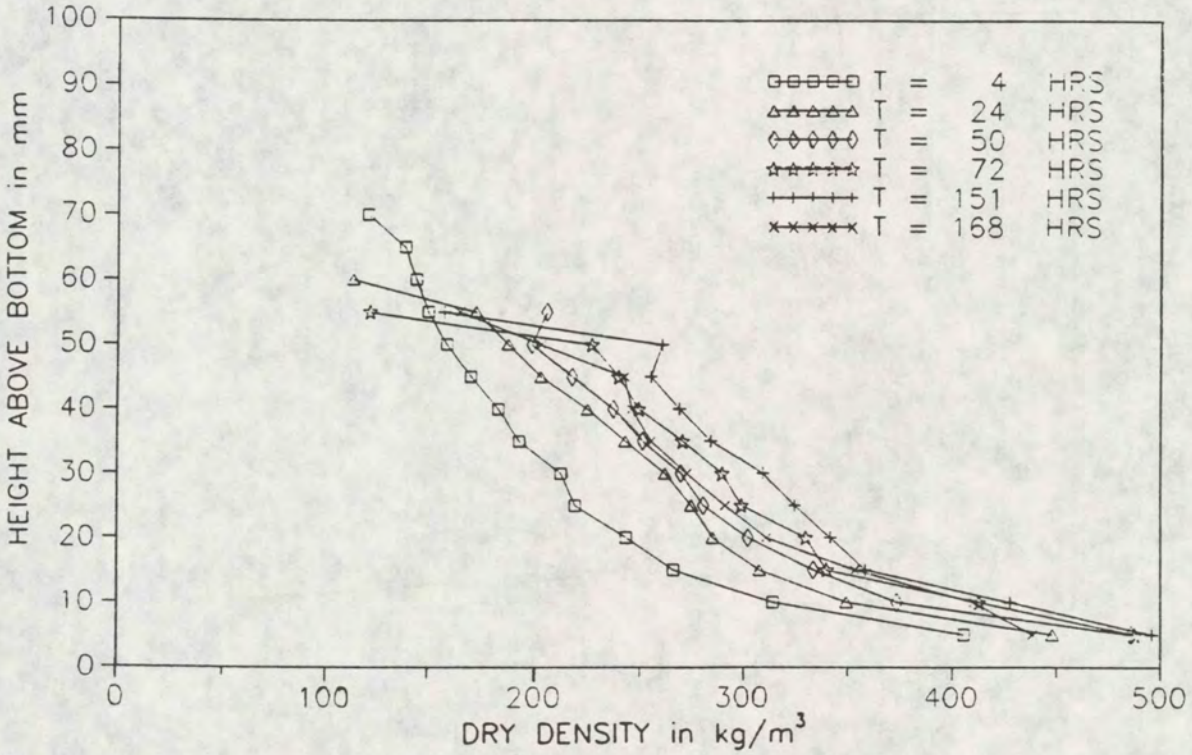

Fig. 3.20 Lake Ketel

Bed concentration profiles during consolidation.		
DELFT HYDRAULICS		

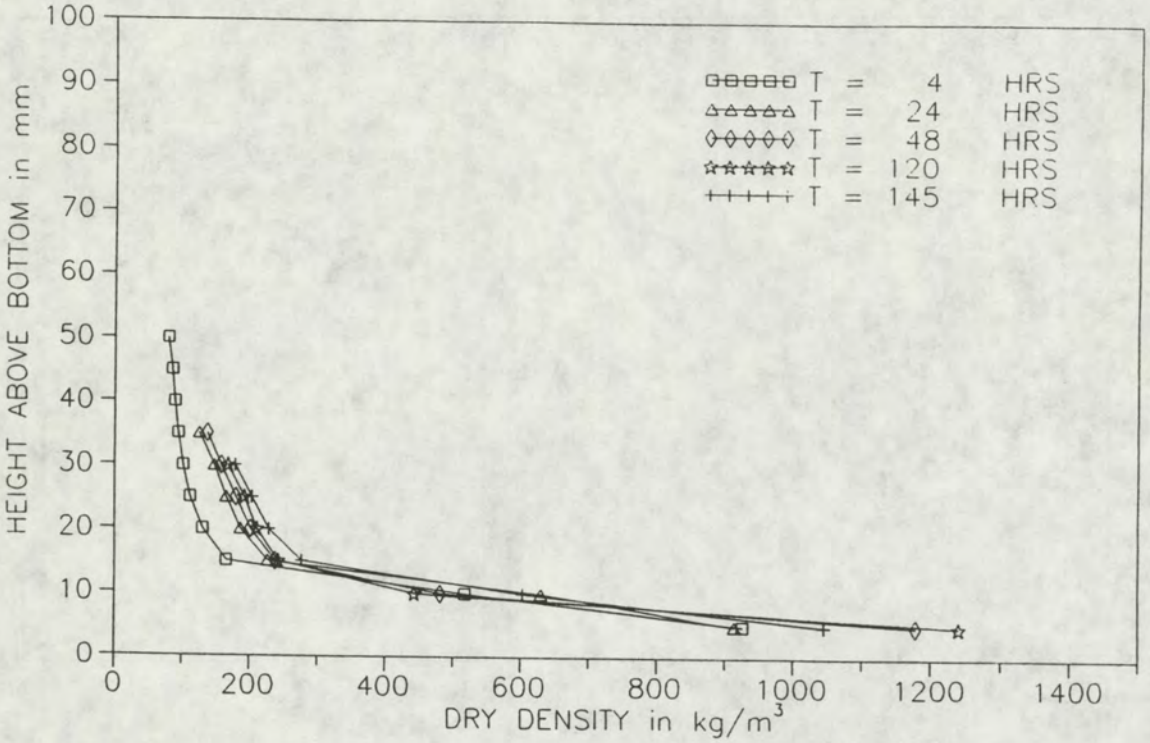

Fig. 3.21 Meuse (Belfeld)

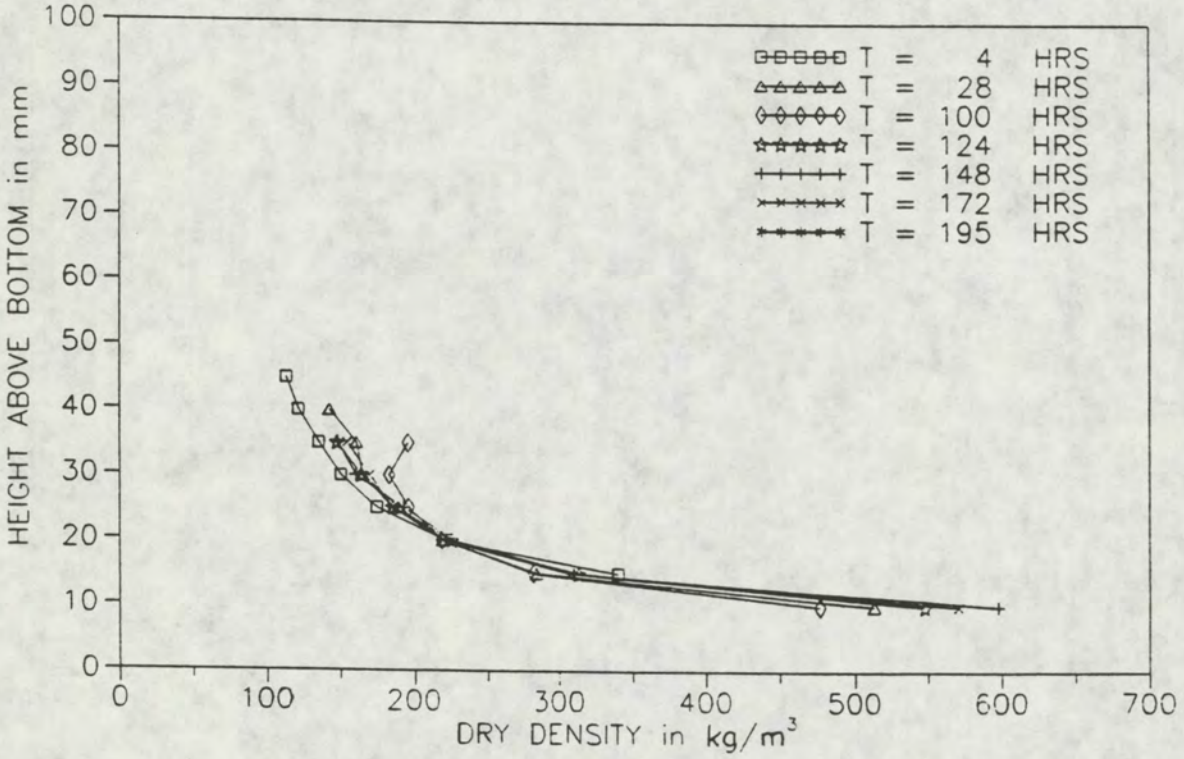

Fig. 3.22 Eems-Dollard (Delfzijl)

Bed concentration profiles during consolidation.		
DELFT HYDRAULICS		

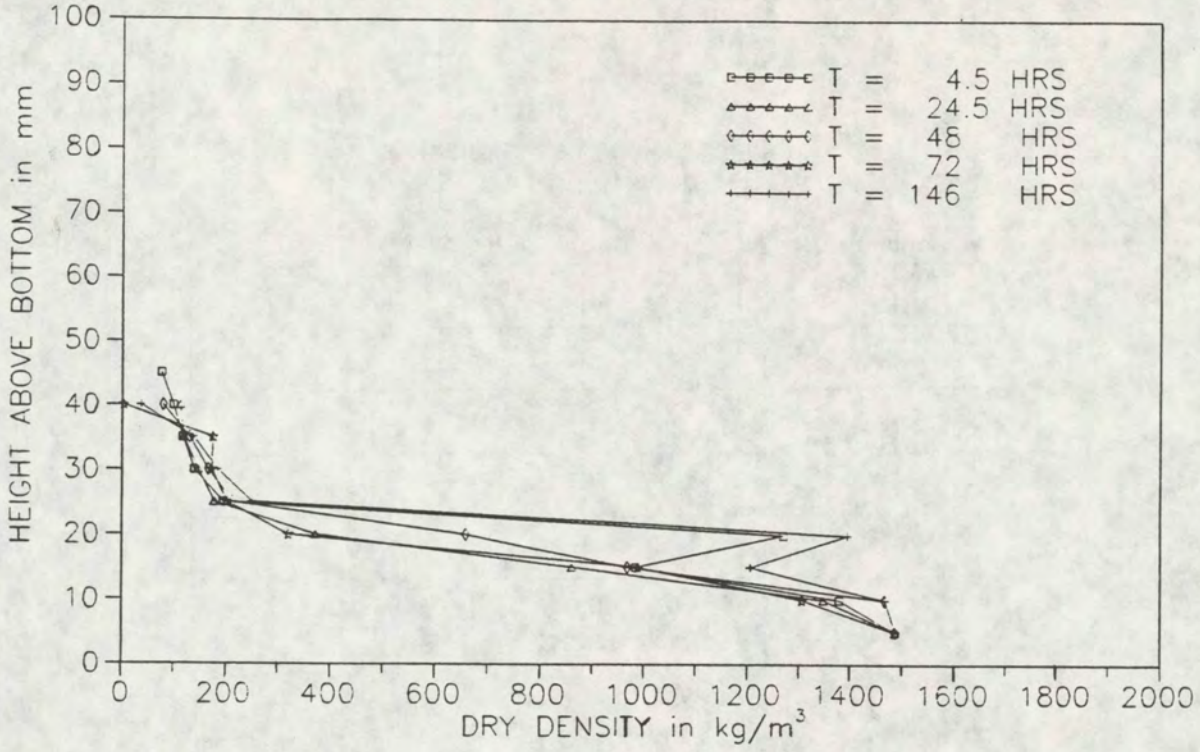

Fig. 3.23 Loswal Noord (North Sea)

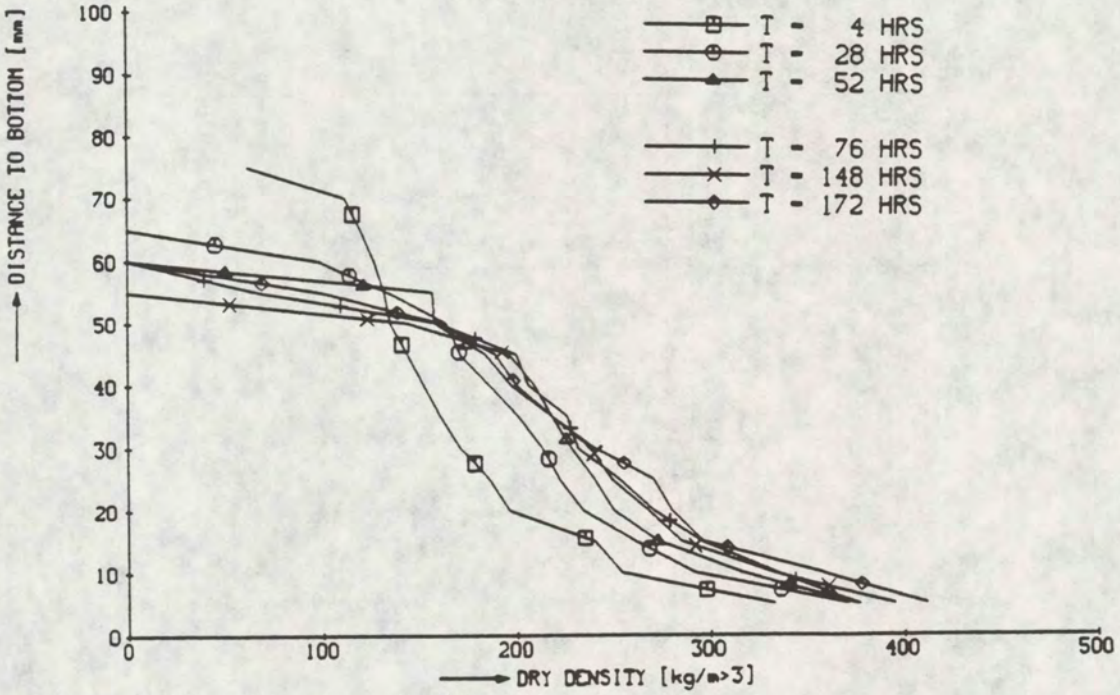

Fig. 3.24 Biesbosch (Spijkerboor)

Bed concentration profiles during consolidation.

DELFT HYDRAULICS

Hollandsch Diep (Sassenplaat)
Bed density profiles

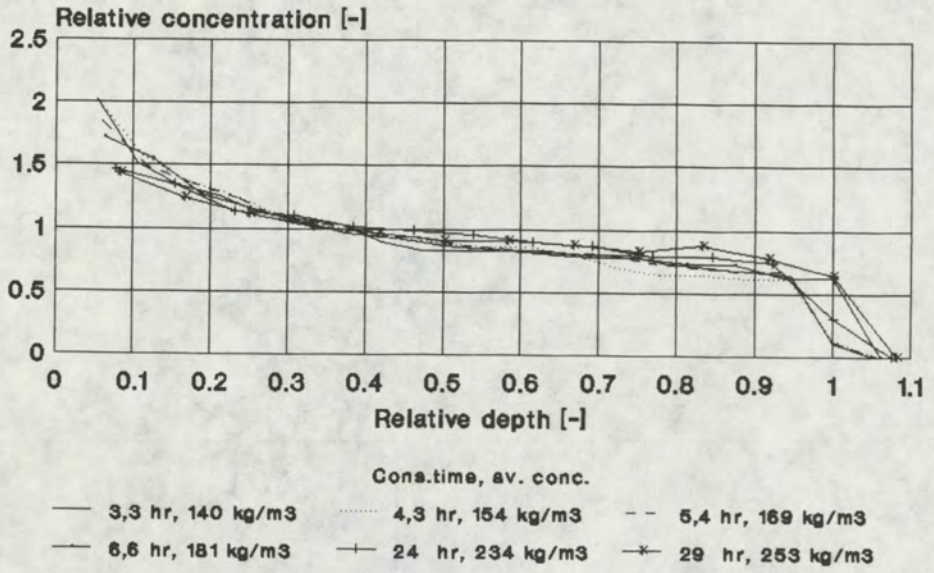

Cons.time, av. conc.

3,3 hr, 140 kg/m3 — 4,3 hr, 154 kg/m3 — 5,4 hr, 169 kg/m3

6,6 hr, 181 kg/m3 — 24 hr, 234 kg/m3 — 29 hr, 253 kg/m3

Fig 3.25a

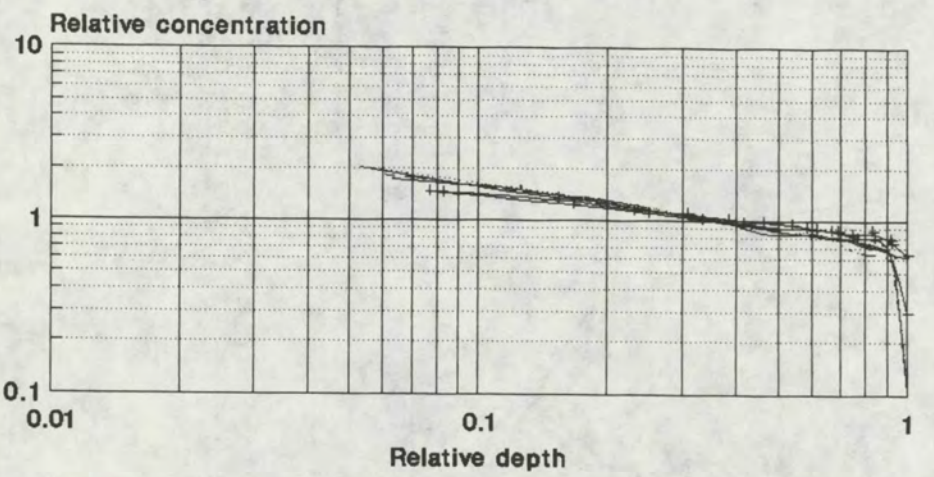

Cons.time, av.conc.

3,3 hr, 140 kg/m3 — 4,3 hr, 154 kg/m3 — 5,4 hr, 169 kg/m3

6,6 hr, 181 kg/m3 — 24 hr, 234 kg/m3 — 29 hr, 253 kg/m3

Fig 3.25b

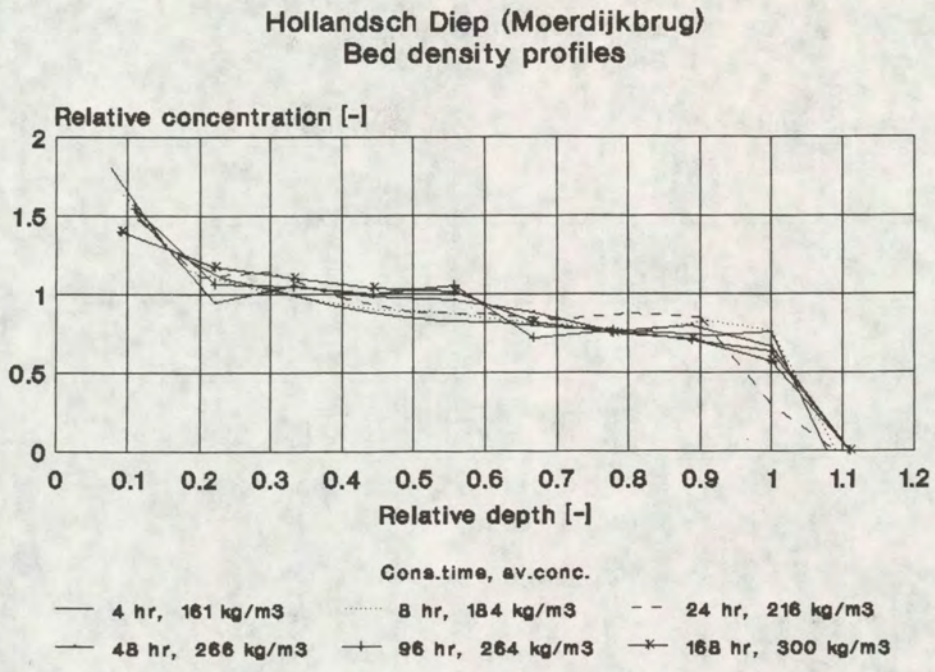

Fig 3.26a

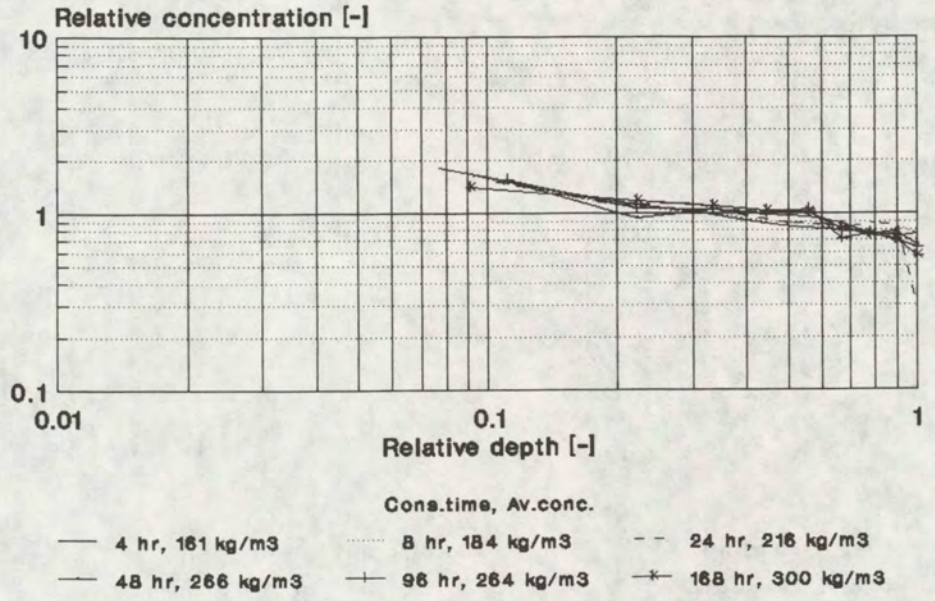

Fig 3.26b

Western Scheldt (Breskens)
Bed density profiles

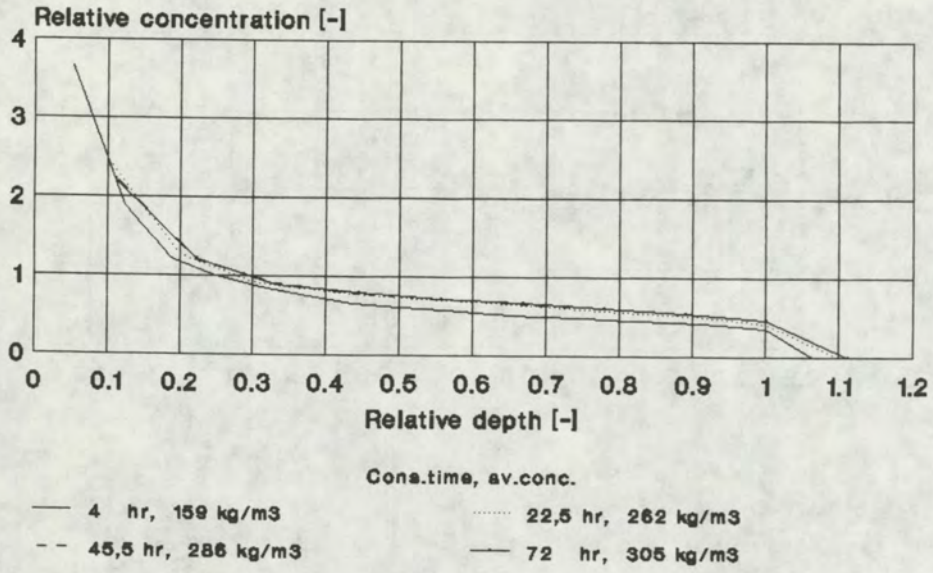

Cons.time, av.conc.

4 hr, 159 kg/m3
22,5 hr, 262 kg/m3
45,5 hr, 286 kg/m3
72 hr, 305 kg/m3

Fig 3.27a

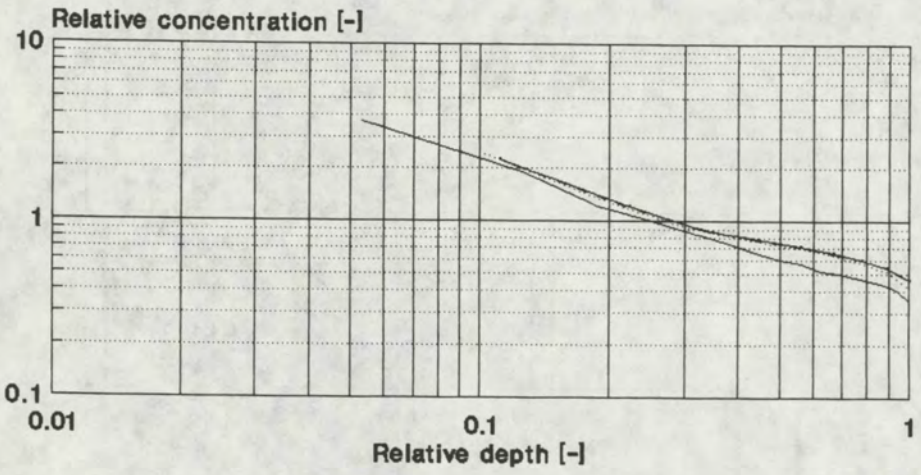

Cons.time, av.conc.

4 hr, 159 kg/m3
22,5 hr, 262 kg/m3
45,5 hr, 286 kg/m3
72 hr, 305 kg/m3

Fig 3.27b

Lake Ketel
Bed density profiles

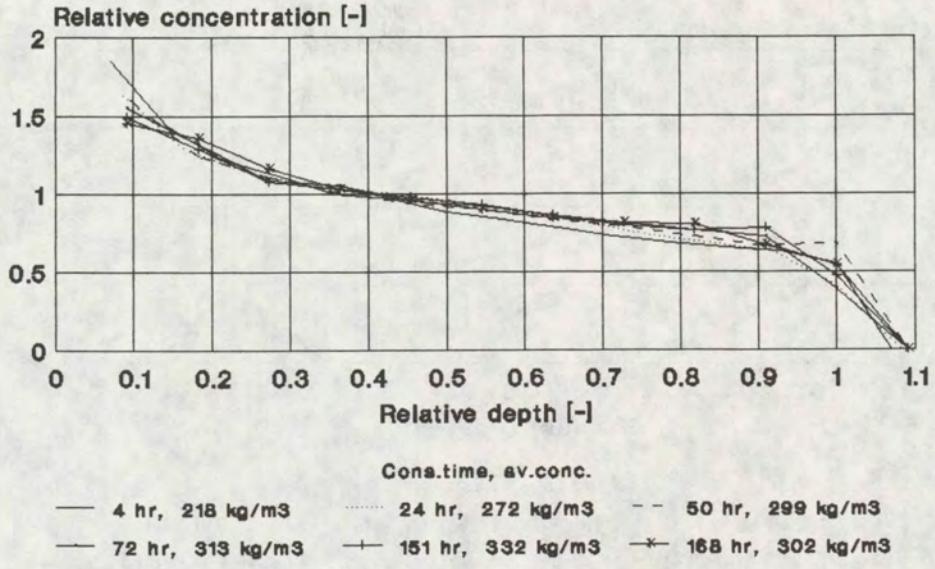

Fig 3.28a

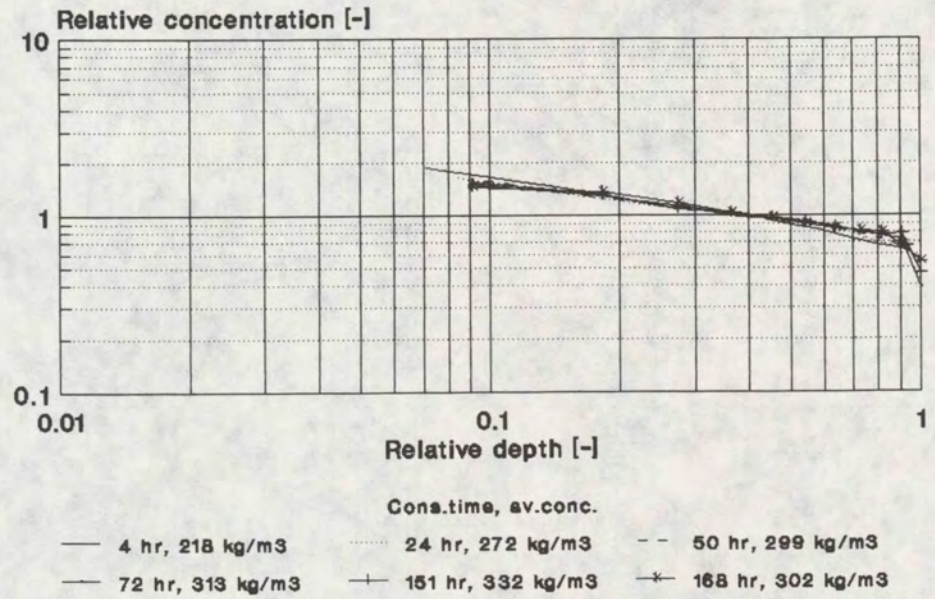

Fig 3.28b

Meuse (Belfeld)
Bed density profiles

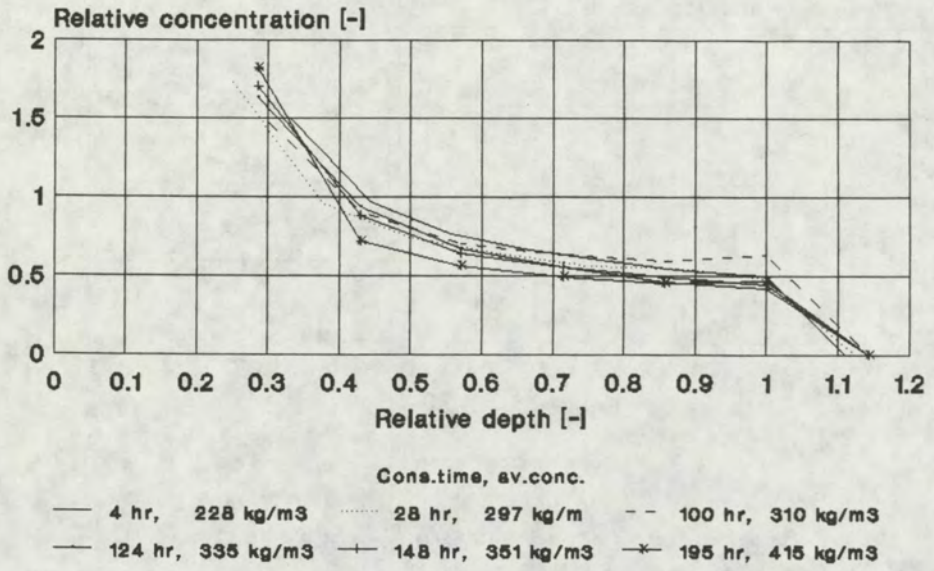

Cons.time, av.conc.

4 hr, 228 kg/m3 — 28 hr, 297 kg/m — 100 hr, 310 kg/m3
124 hr, 335 kg/m3 — 148 hr, 351 kg/m3 — 195 hr, 415 kg/m3

Fig 3.29a

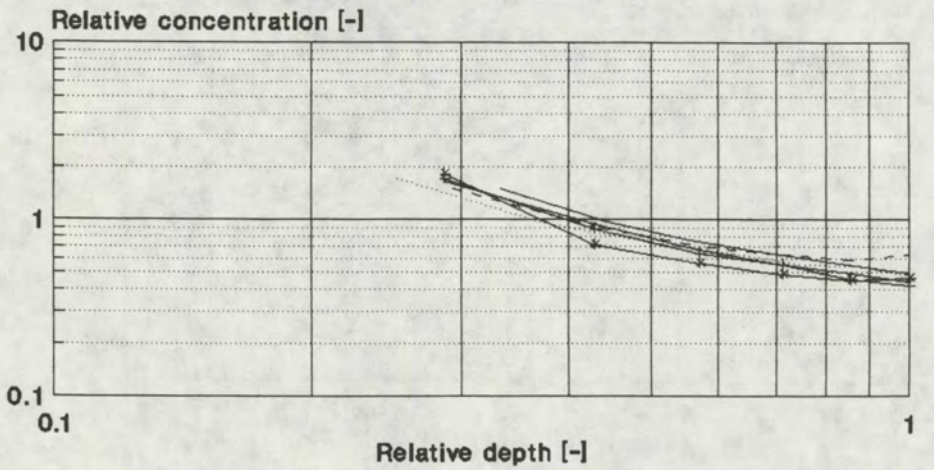

Cons.time, av.conc.

4 hr, 228 kg/m3 — 28 hr, 297 kg/m3 — 100 hr, 310 kg/m3
124 hr, 335 kg/m3 — 148 hr, 351 kg/m3 — 195 hr, 415 kg/m3

Fig 3.29b

Eems-Dollard (Delfzijl Harbour)
Bed density profiles

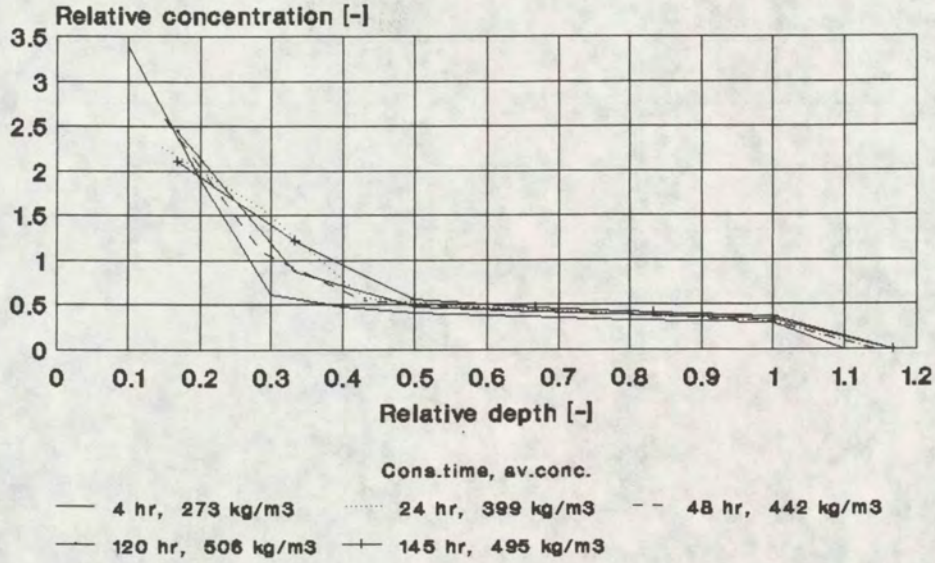

Fig 3.30a

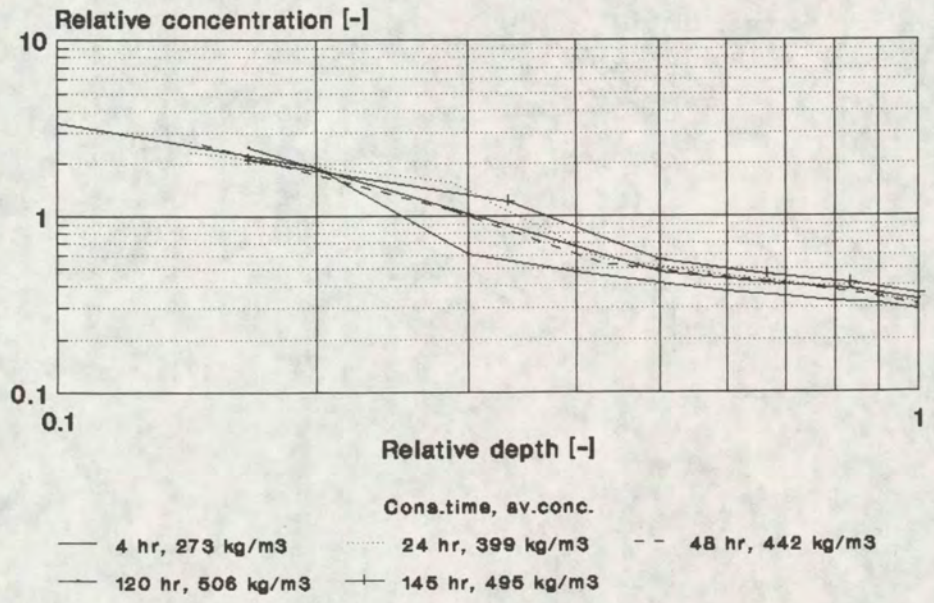

Fig 3.30b

Loswal Noord (North Sea)
Bed density profiles

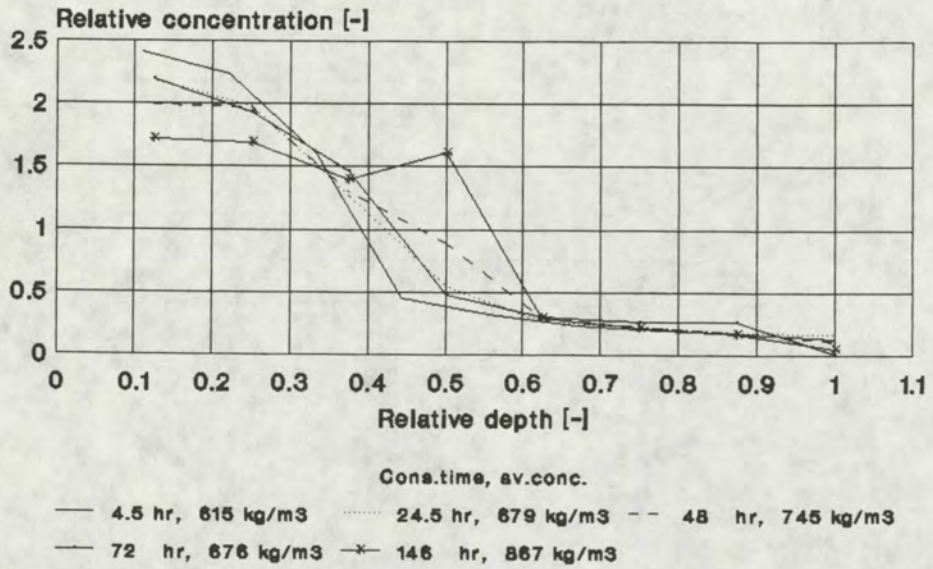

Fig 3.31a

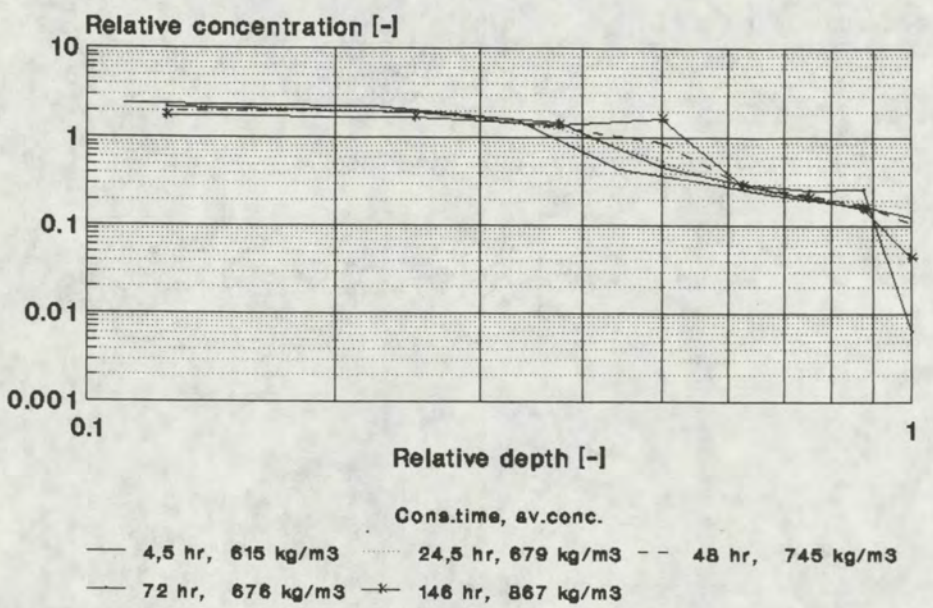

Fig 3.31b

Biesbosch (Spijkerboor)
Bed density profiles

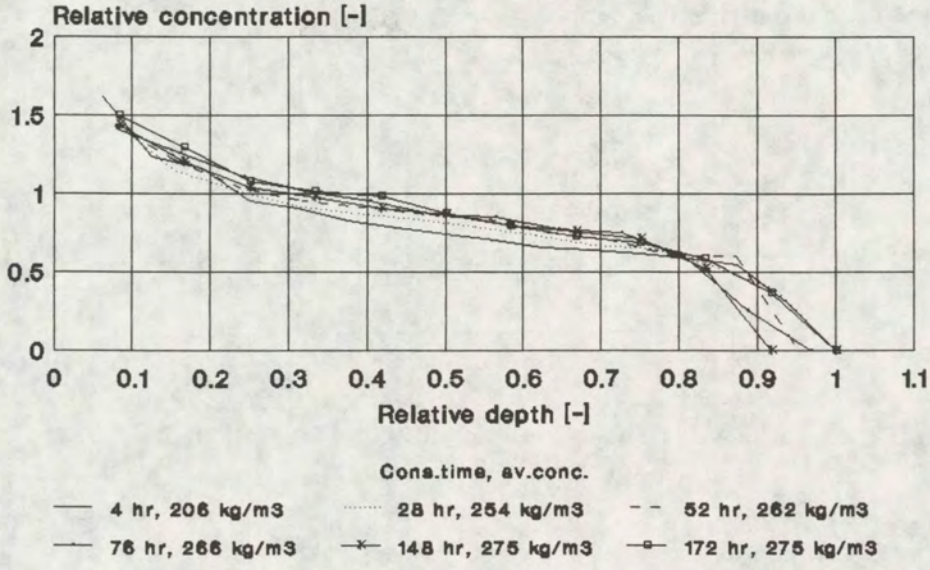

Fig 3.32a

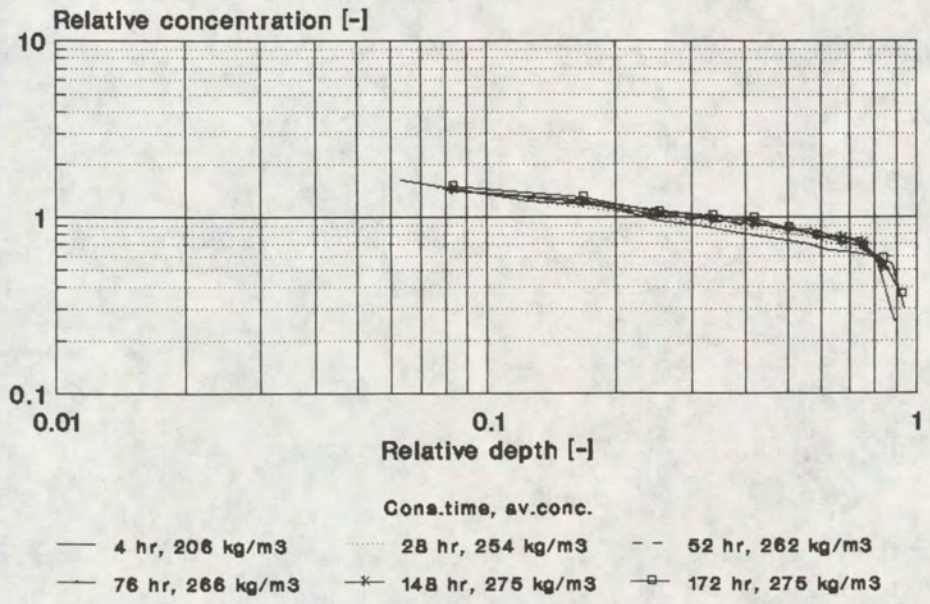

Fig 3.32b

Hollandsch Diep (Sassenplaat)
Bed concentration

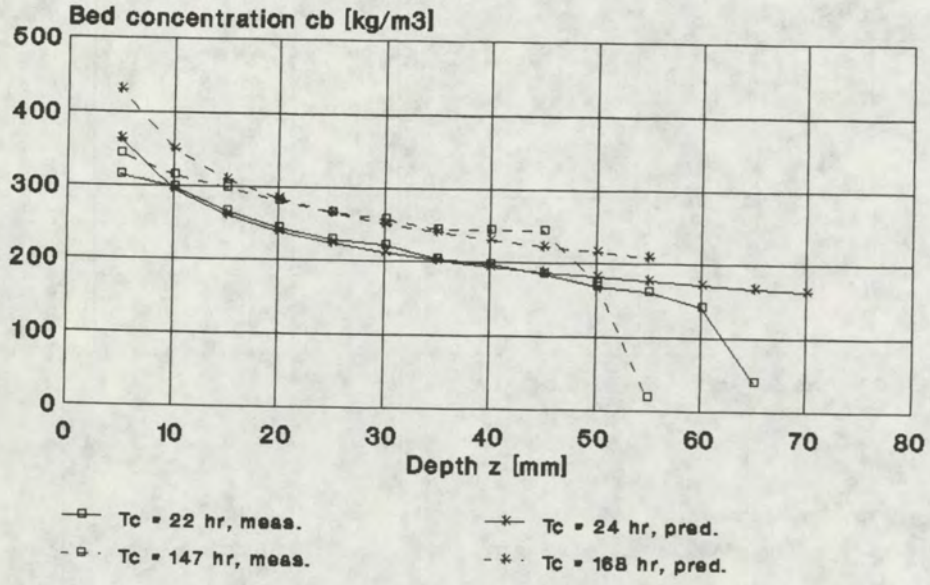

Fig 3.33

Hollandsch Diep (Moerdijkbrug)
Bed concentration

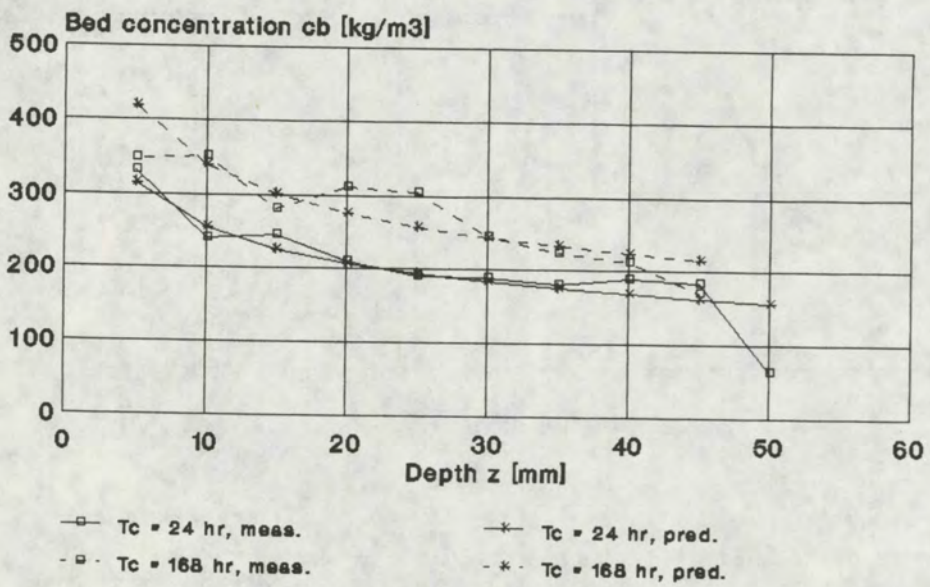

Fig 3.34

Western Scheldt (Breskens)
Bed concentration

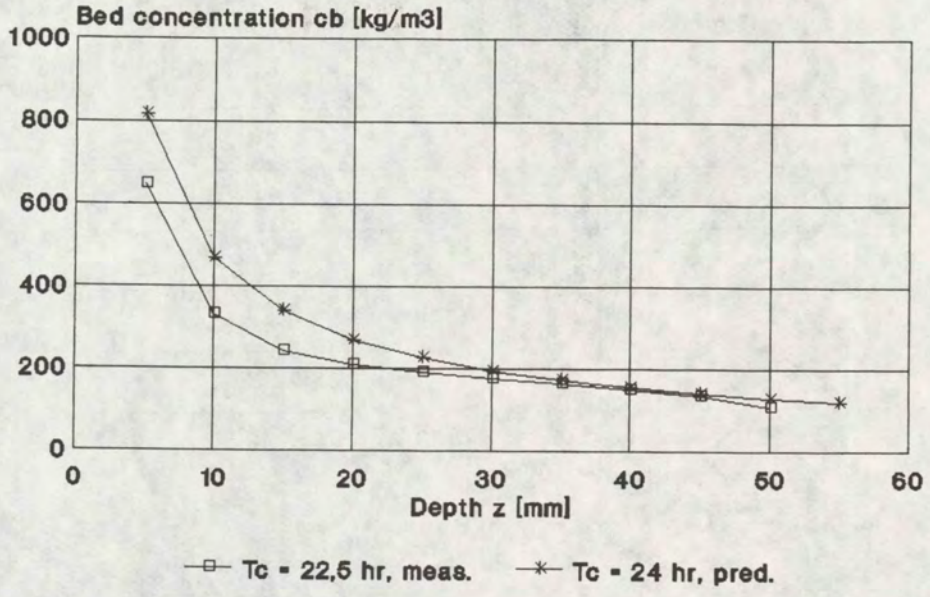

Fig 3.35

Lake Ketel
Bed concentration

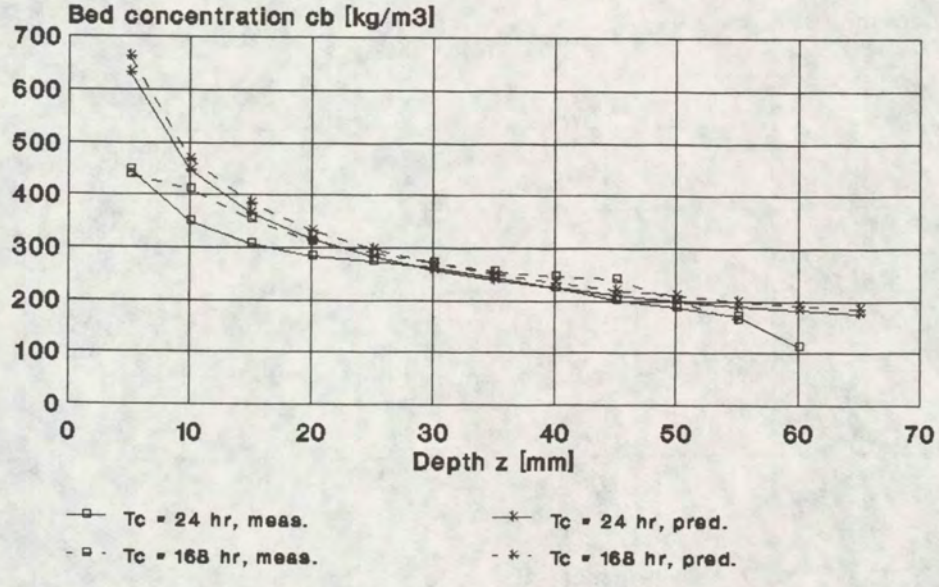

Fig 3.36

Meuse (Belfeld)
Bed concentration cb [kg/m3]

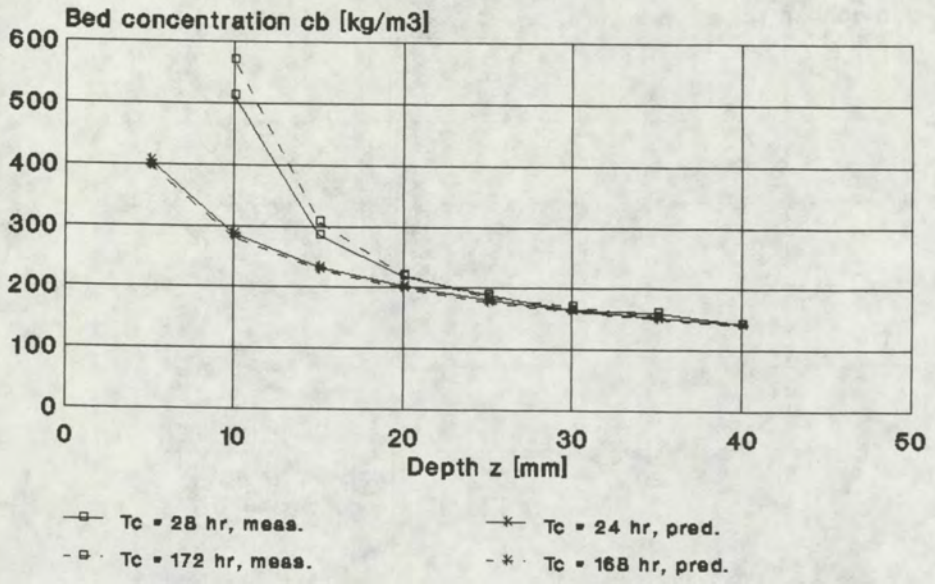

Fig 3.37

Eems-Dollard (Delfzijl Harbour)
Bed concentration

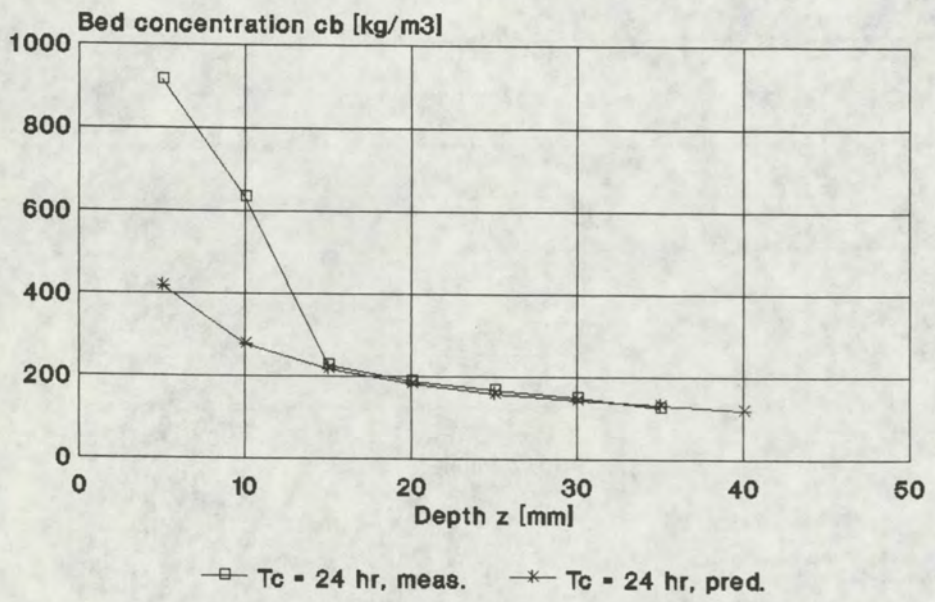

Fig 3.38

Loswal Noord (North Sea)
Bed concentration

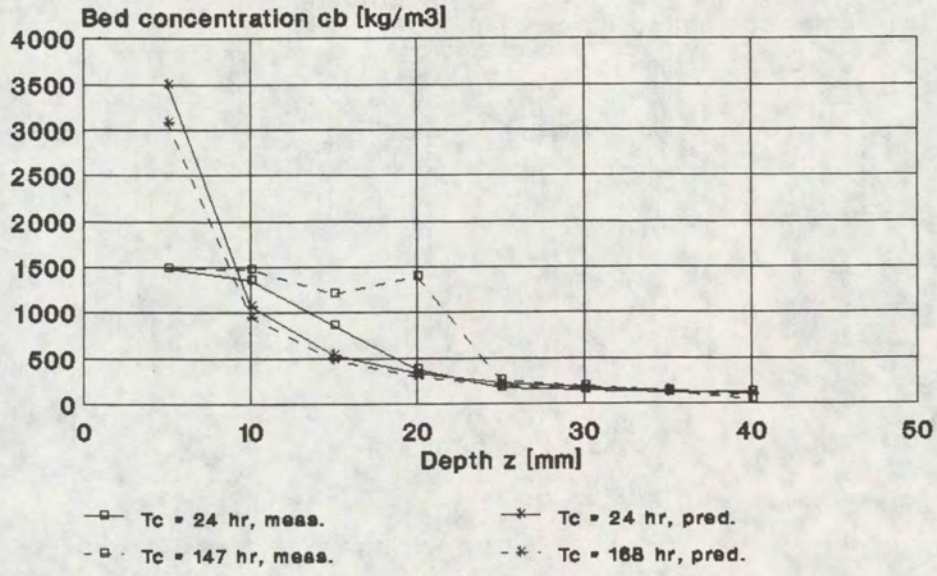

Fig 3.39

Biesbosch (Spijkerboor)
Bed concentration

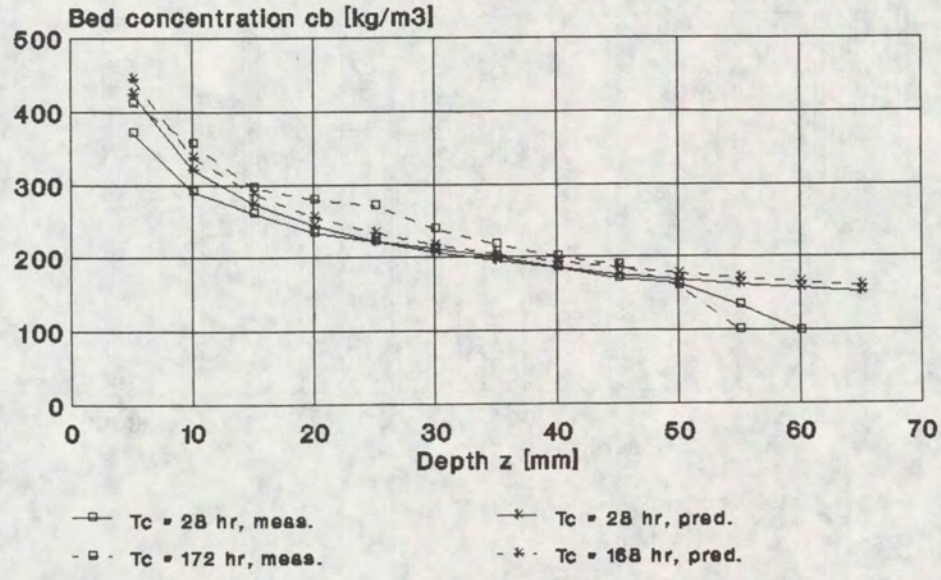

Fig 3.40

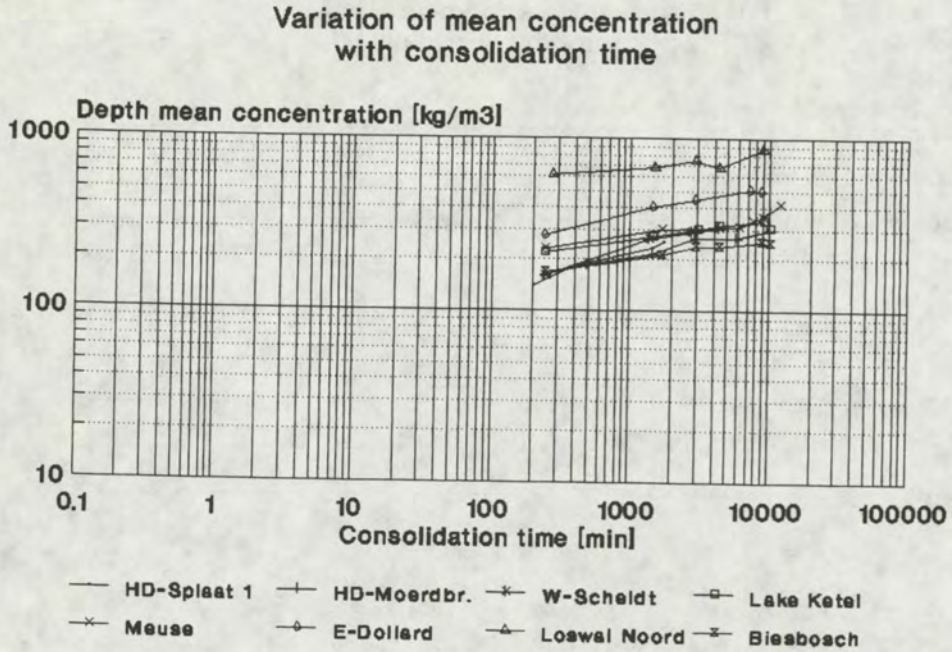

Fig 3.41a; from acoustic measurements

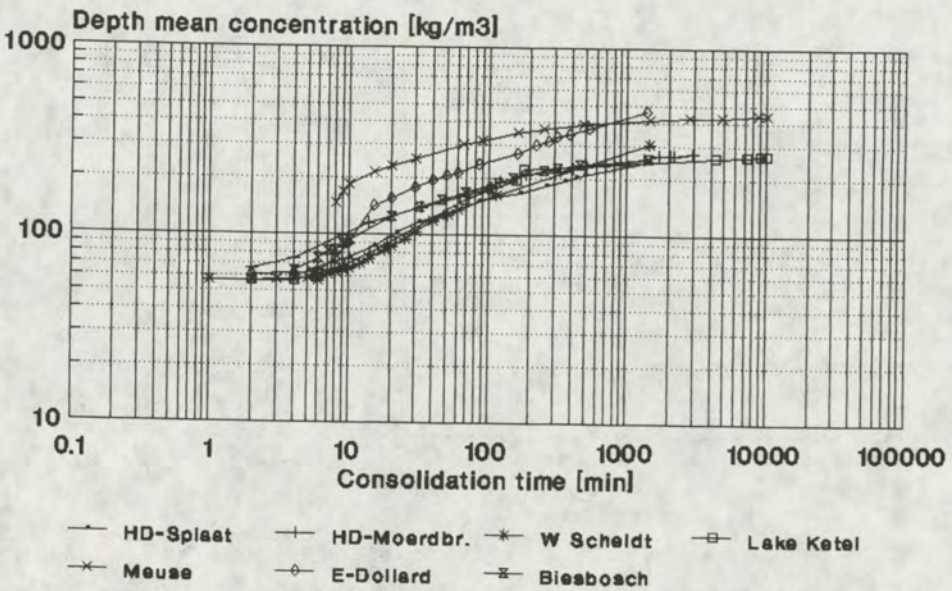

Fig 3.41b; from interface

Slope of bed density vs
original sand content

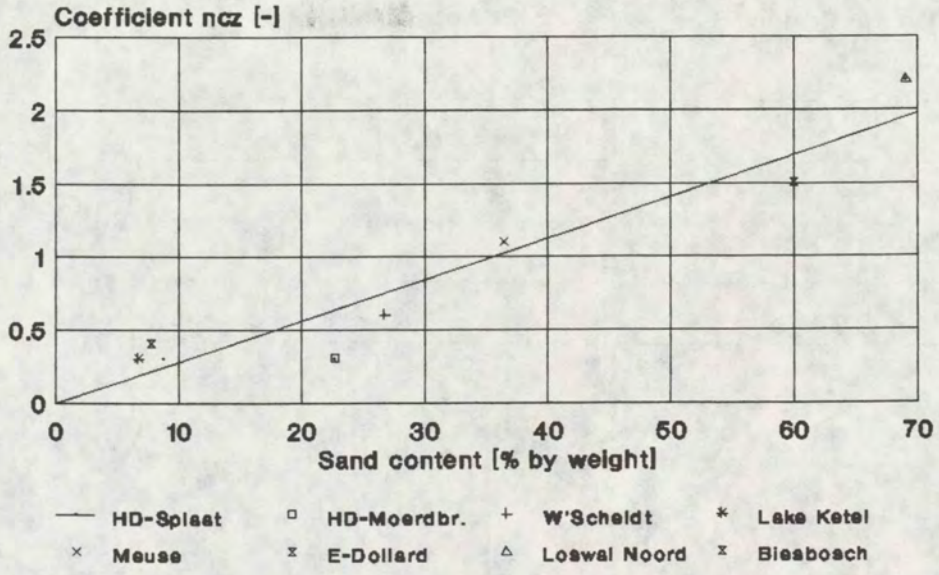

Fig 3.42

Variation of mean concentration
with consolidation time

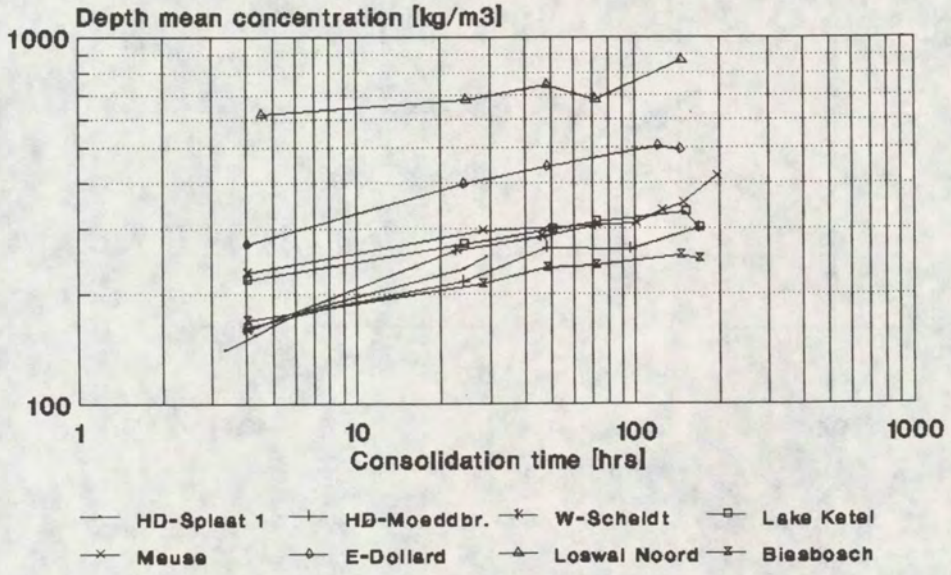

Fig 3.43

Hollandsch Diep (Sassenplaat)
Strength distribution

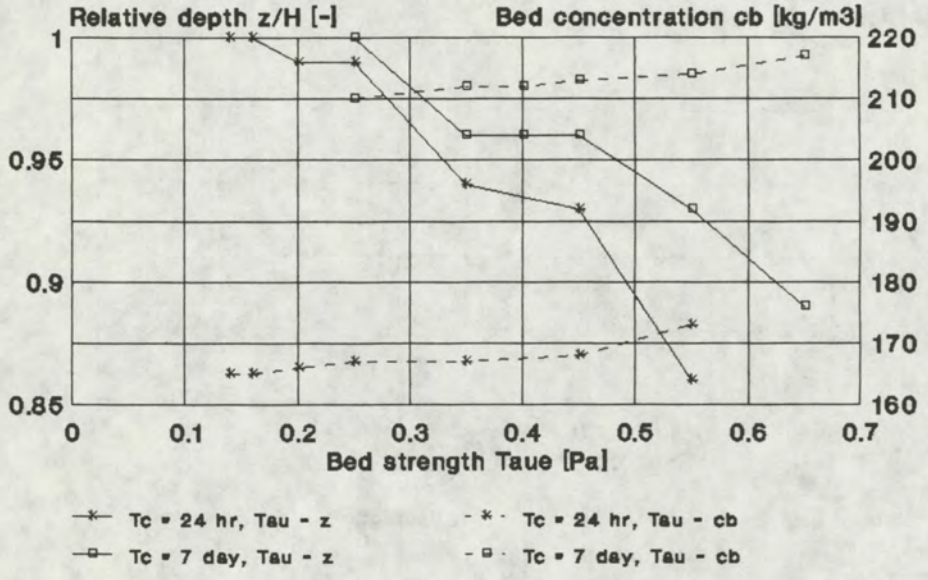

Fig 4.1

Hollandsch Diep (Moerdijkbrug)
Strength distribution

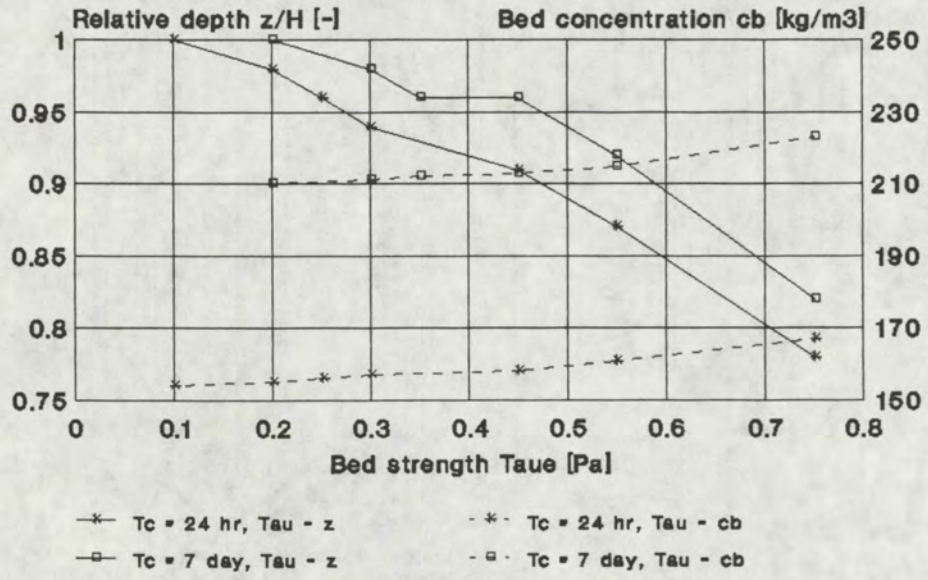

Fig 4.2

Western Scheldt (Breskens)
Strength distribution

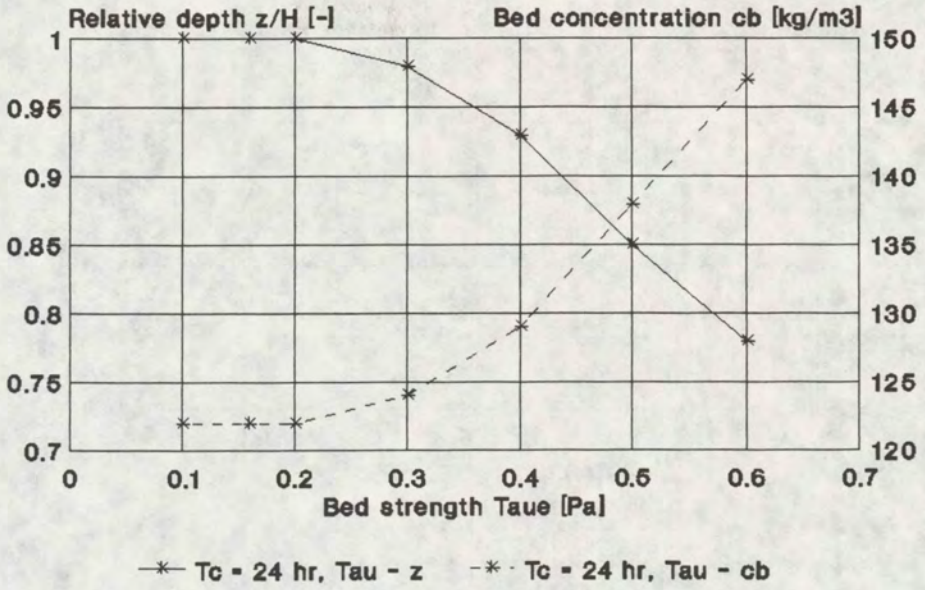

Fig 4.3

Lake Ketel
Strength distribution

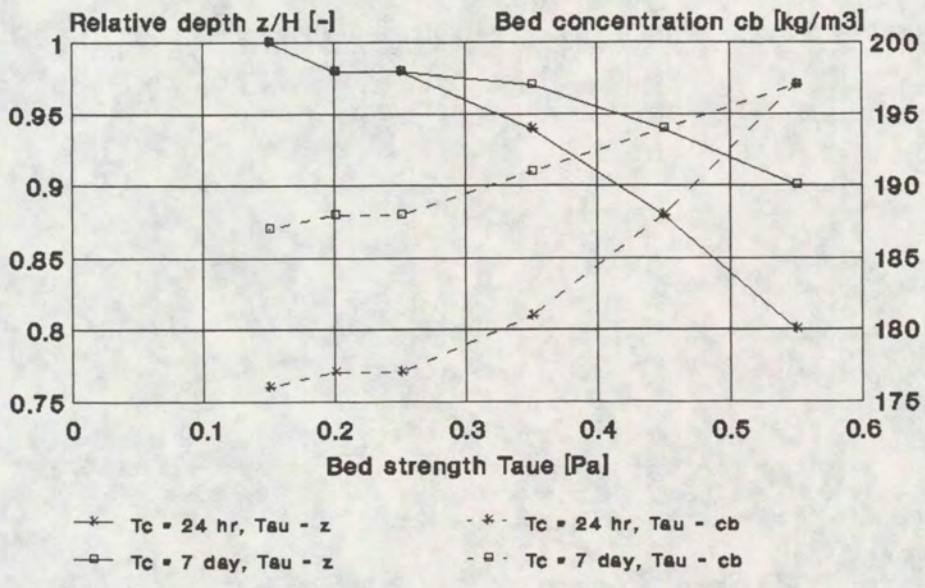

Fig 4.4

Meuse (Belfeld)
Strength distribution

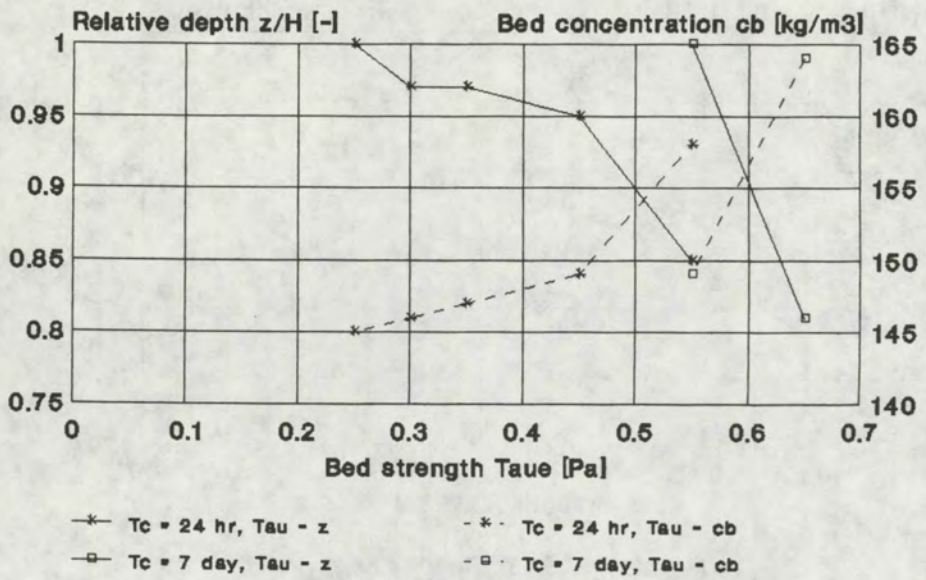

Fig 4.5

Eems-Dollard (Delfzijl)
Strength distribution

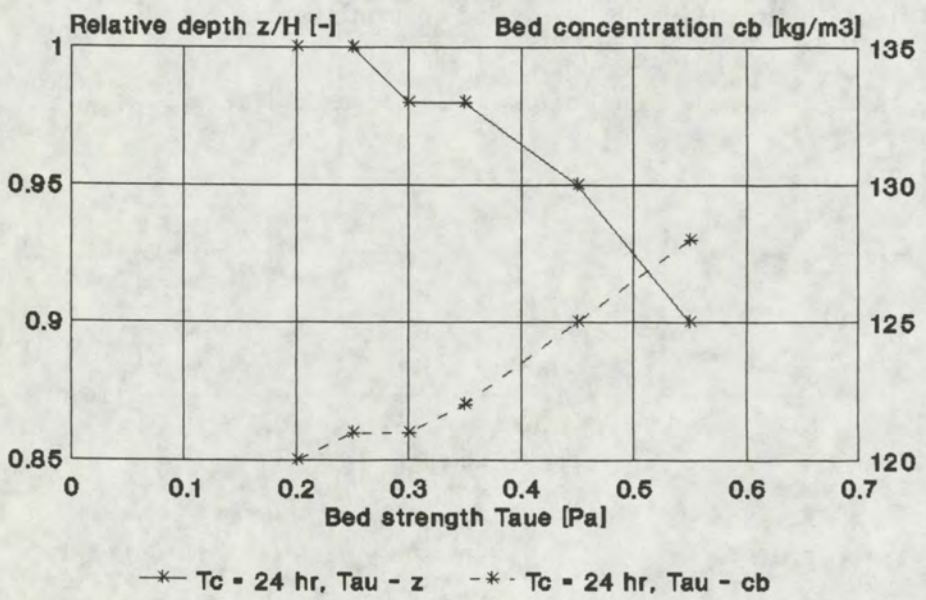

Fig 4.6

Loswal Noord (North Sea)
Strength distribution

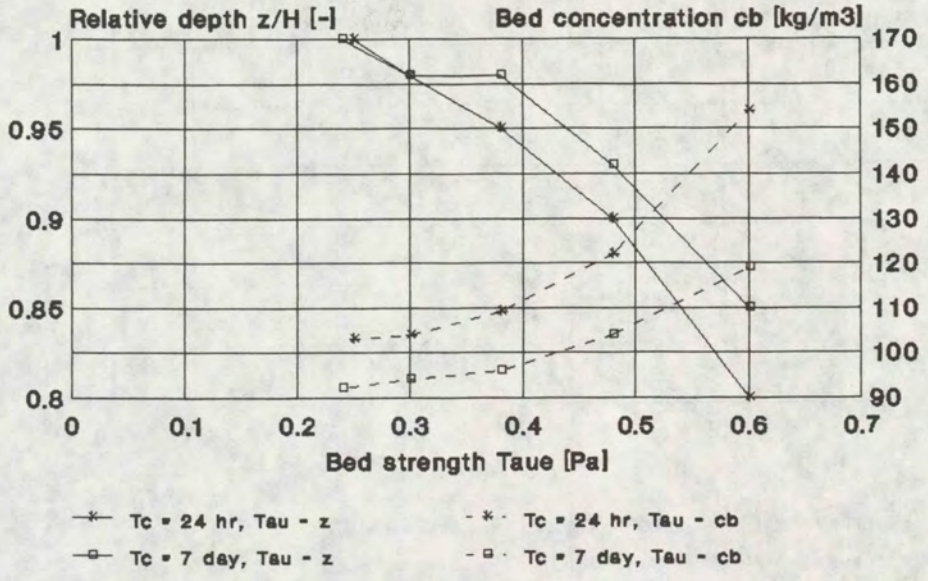

Fig 4.7

Biesbosch (Spijkerboor)
Strength distribution

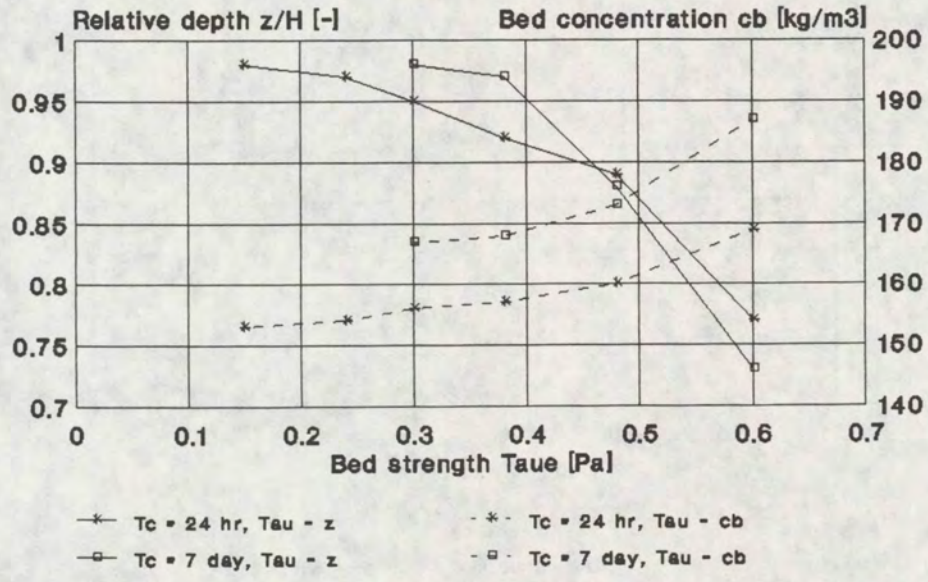

Fig 4.8

Strength distribution
Consolidation time Tc = 24 hrs

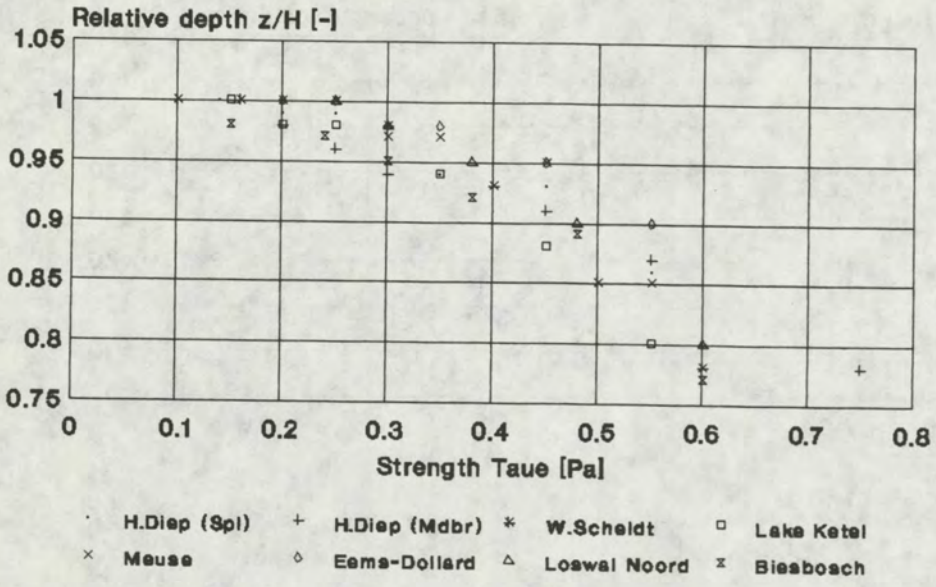

Fig 4.9

Strength distribution
Consolidation time Tc = 7 days

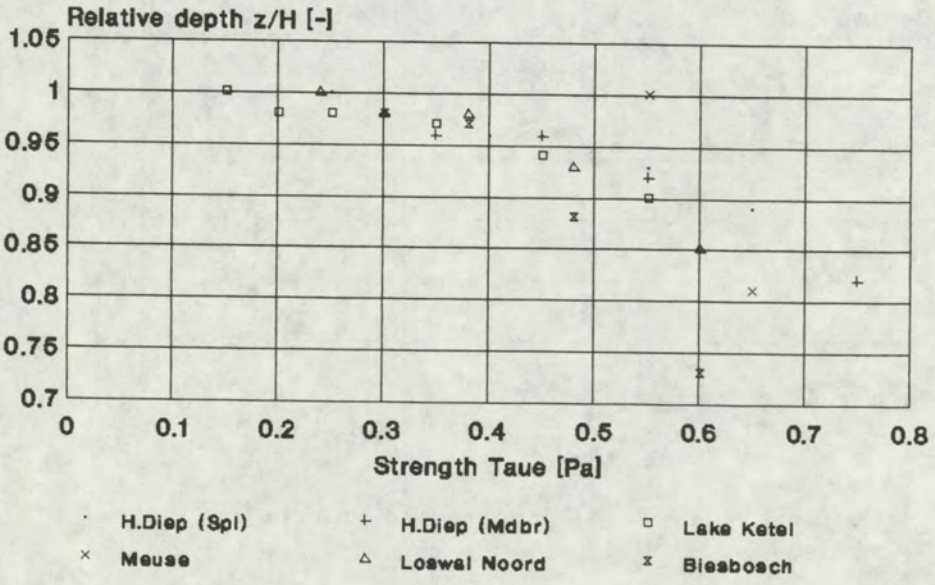

Fig 4.10

Strength distribution
Consolidation time Tc = 24 hrs

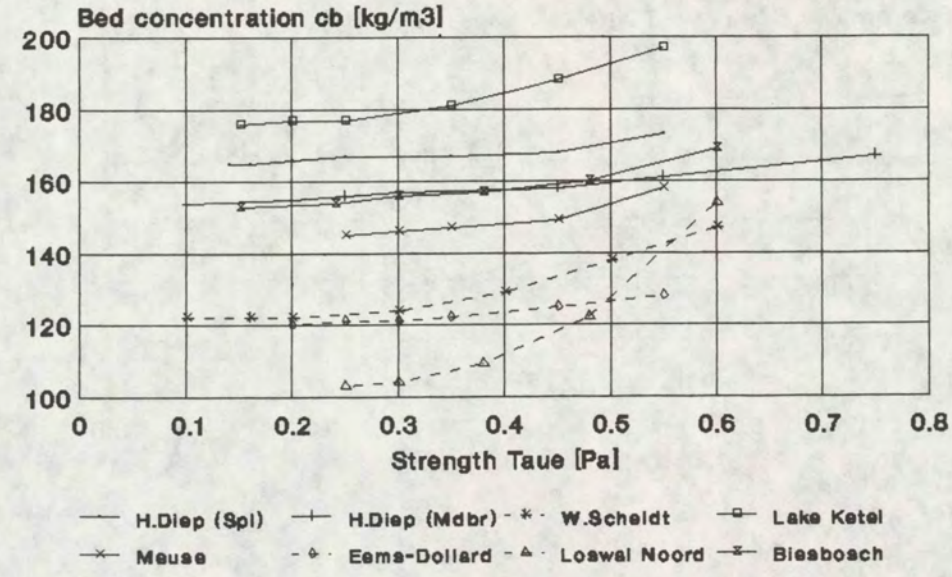

Fig 4.11

Strength distribution
Consolidation time Tc = 7 days

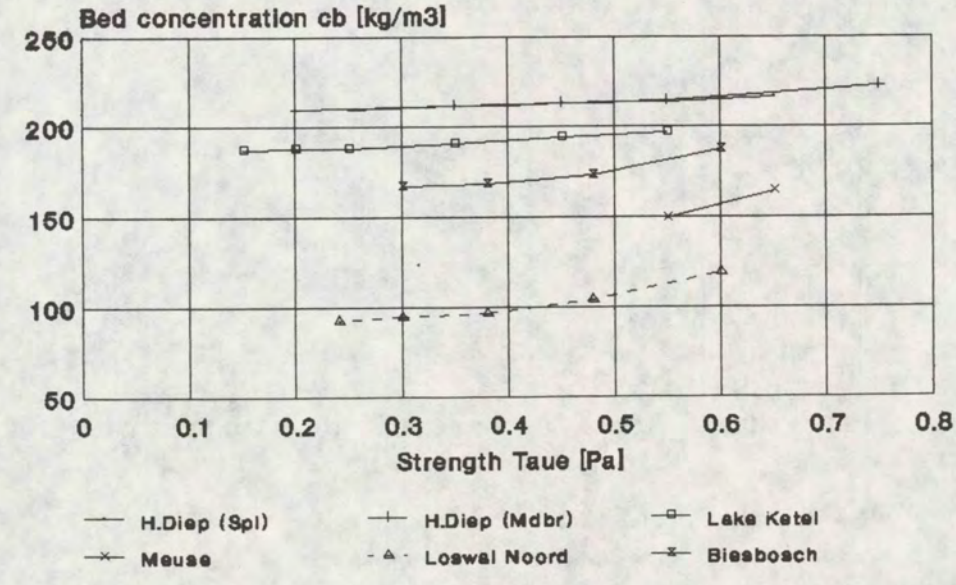

Fig 4.12

Variation of floc erosion rate
with bed shear stress (Tc = 24 hrs).

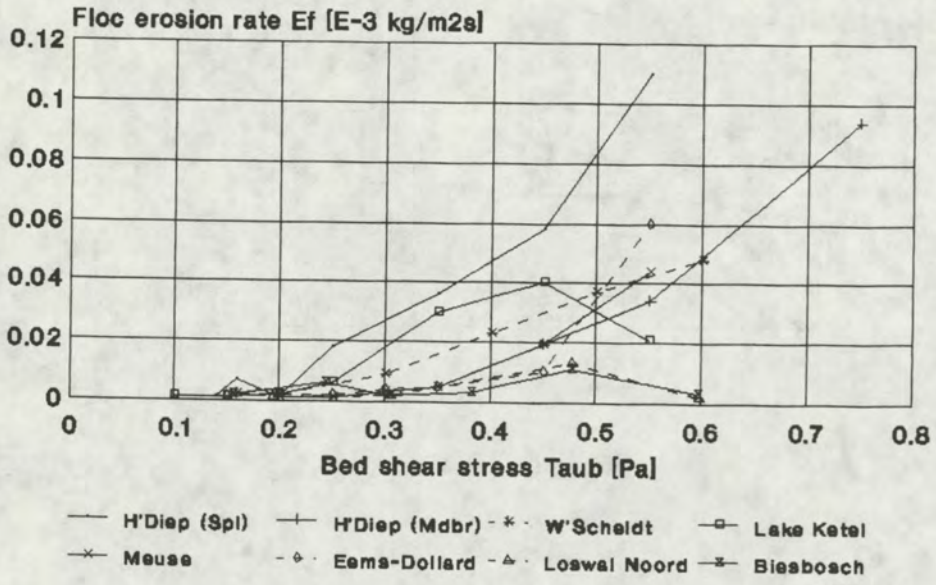

Fig 4.13a

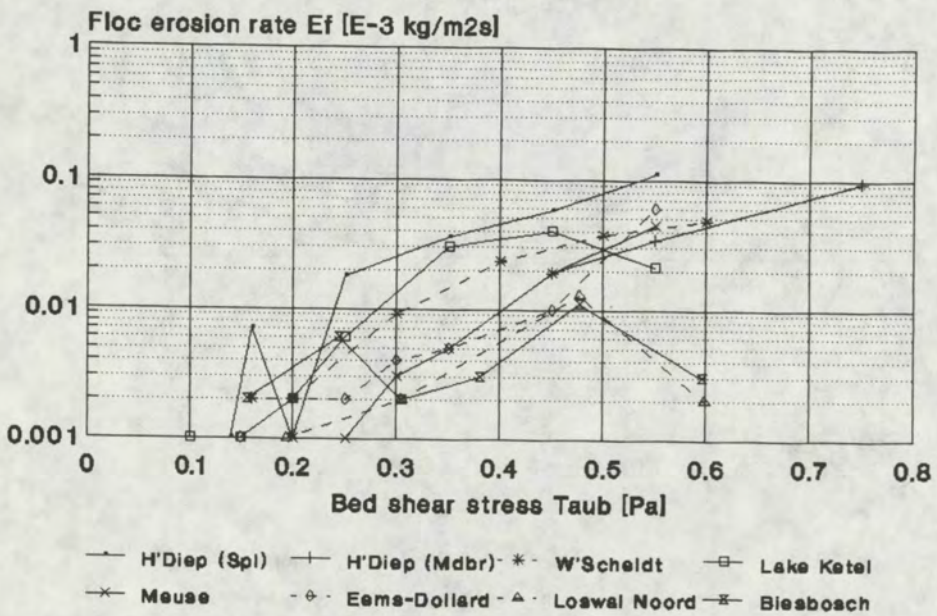

Fig 4.13b

Variation of floc erosion rate
with bed shear stress (Tc = 7 days).

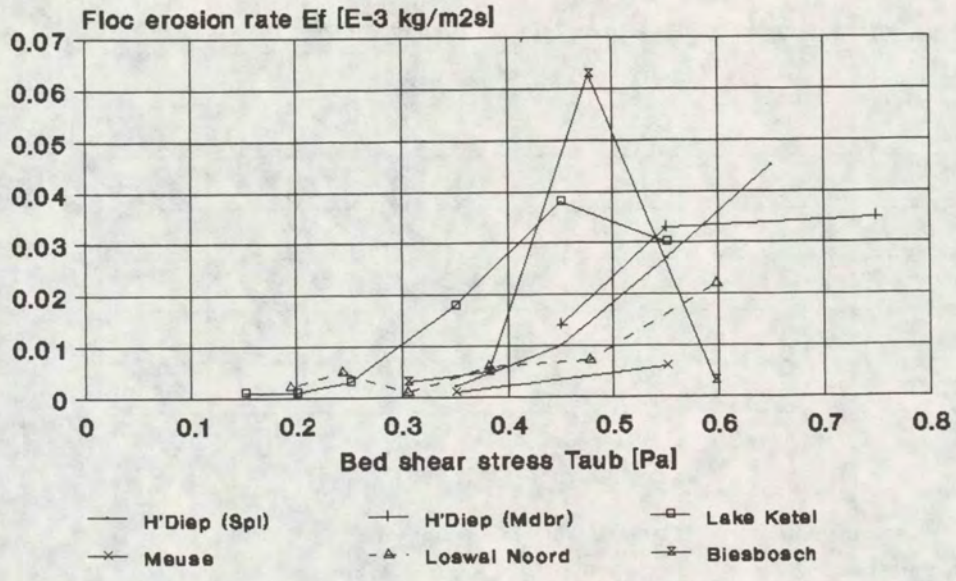

Fig 4.14a

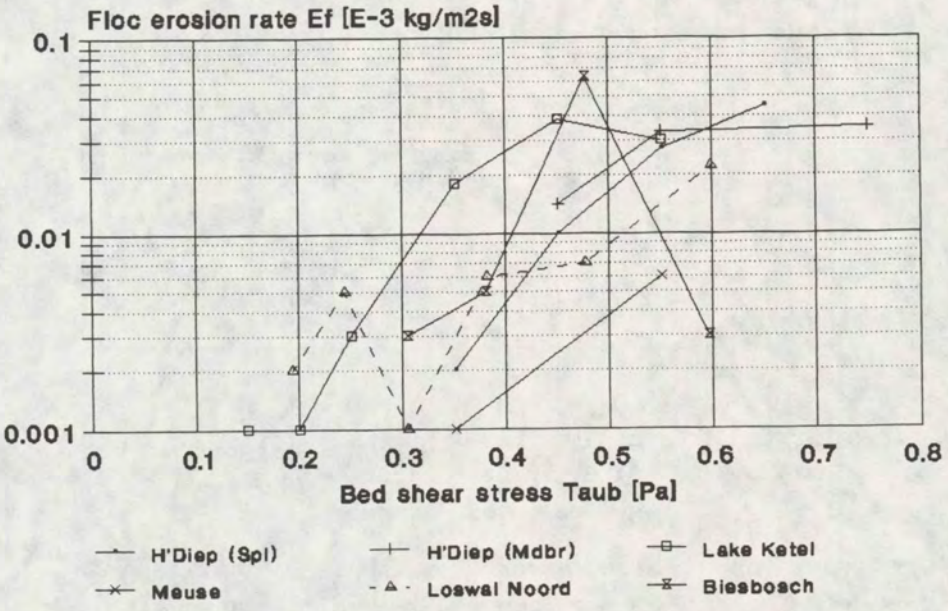

Fig 4.14b

Variation of maximum erosion rate
with bed shear stress (Tc = 24 hrs).

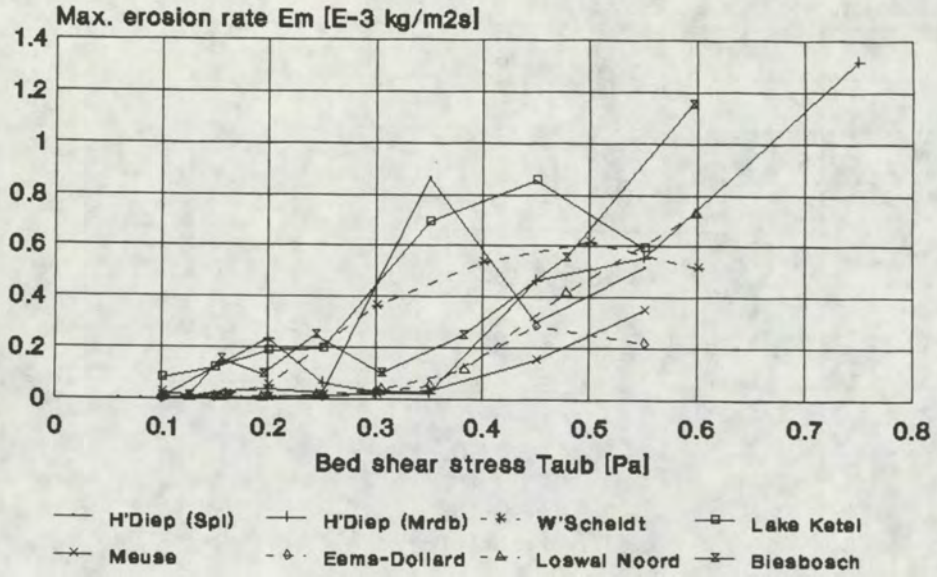

Fig 4.15a

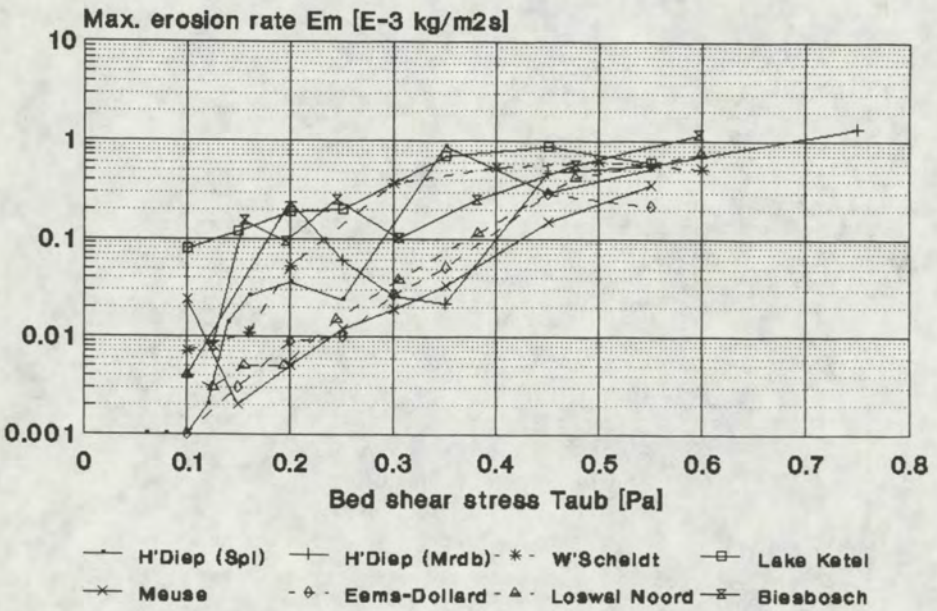

Fig 4.15b

Variation of maximum erosion rate
with bed shear stress (Tc = 7 days).

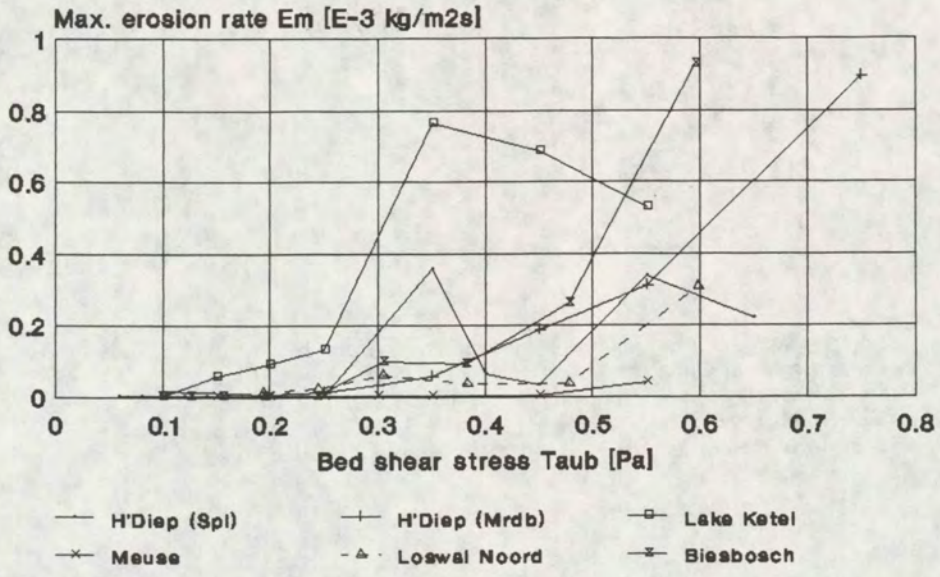

Fig 4.16a

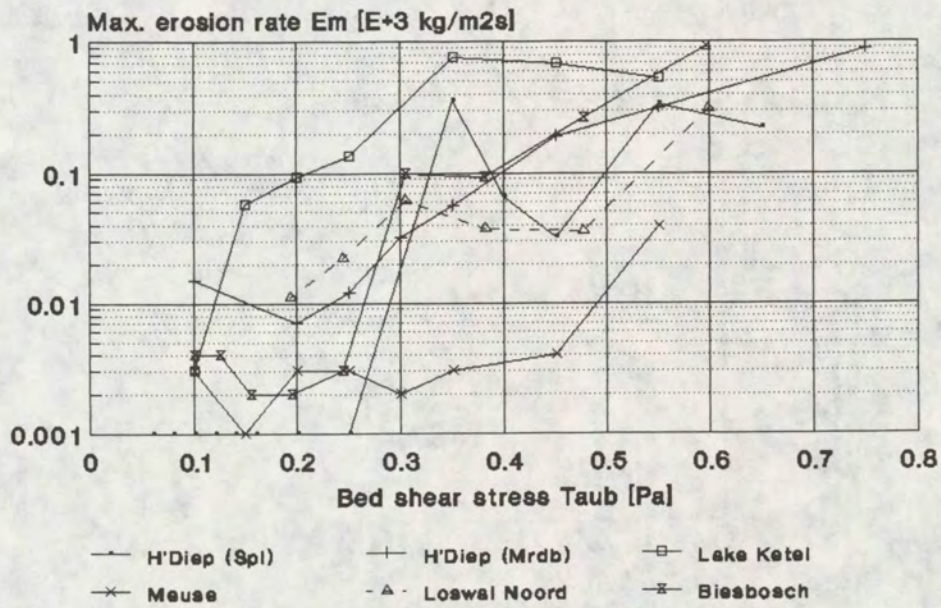

Fig 4.16b

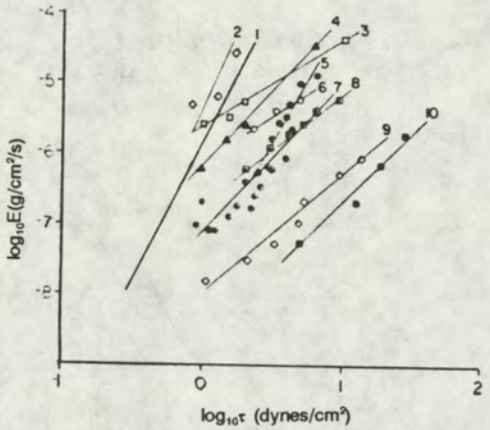

Fig. 4.17a Rates of erosion versus bottom stress from laboratory flume experiments and from measurements in Puget Sound. Limitations of space do not permit the presentation of all laboratory results. Numbers refer to the references in Table 3. The lines are least squares fits of the erosion law $E = \alpha|\tau|^{\eta}$: the resulting values of α and η are given in Table 3.

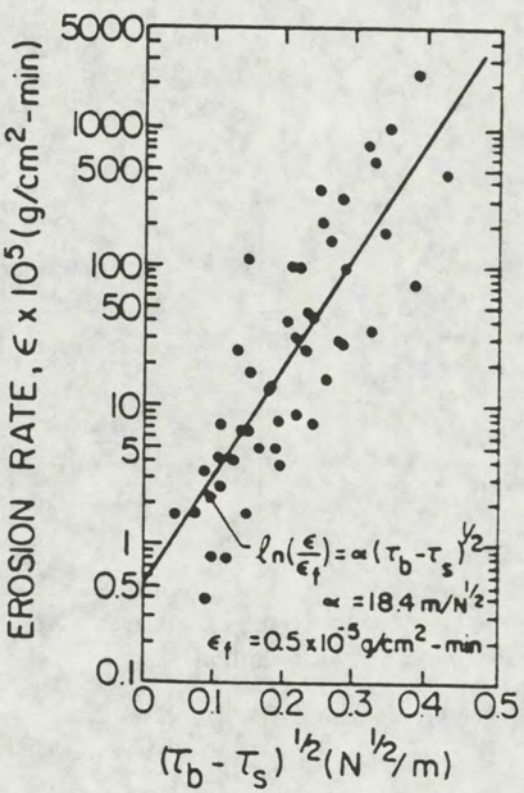

FIG. 4.17b—**Variation of** $\ln(\epsilon/\epsilon_f)$ **with** $(\tau_b - \tau_s)^{1/2}$, **Series LM**

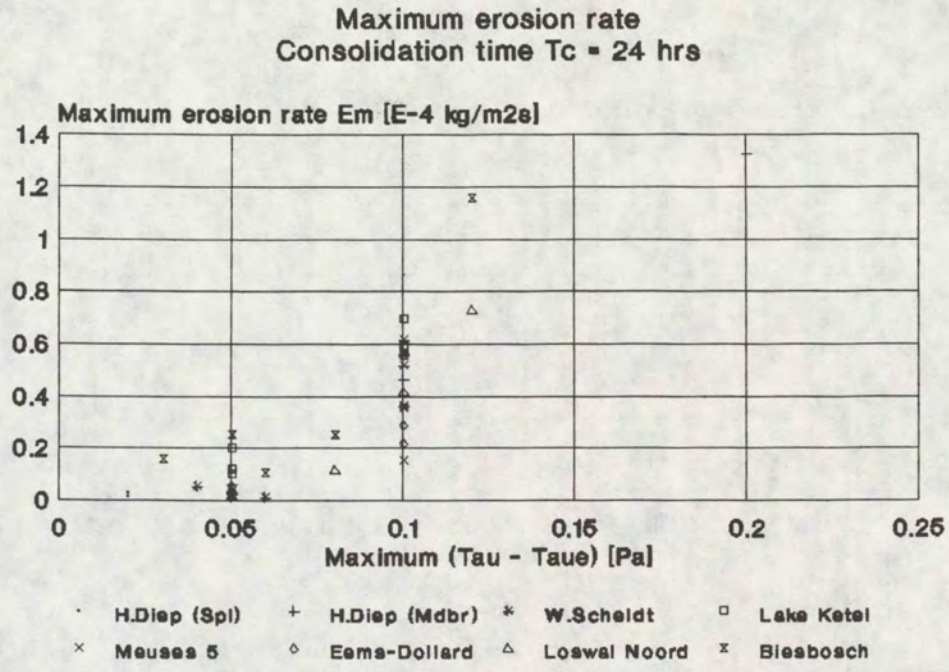

Fig 4.18a

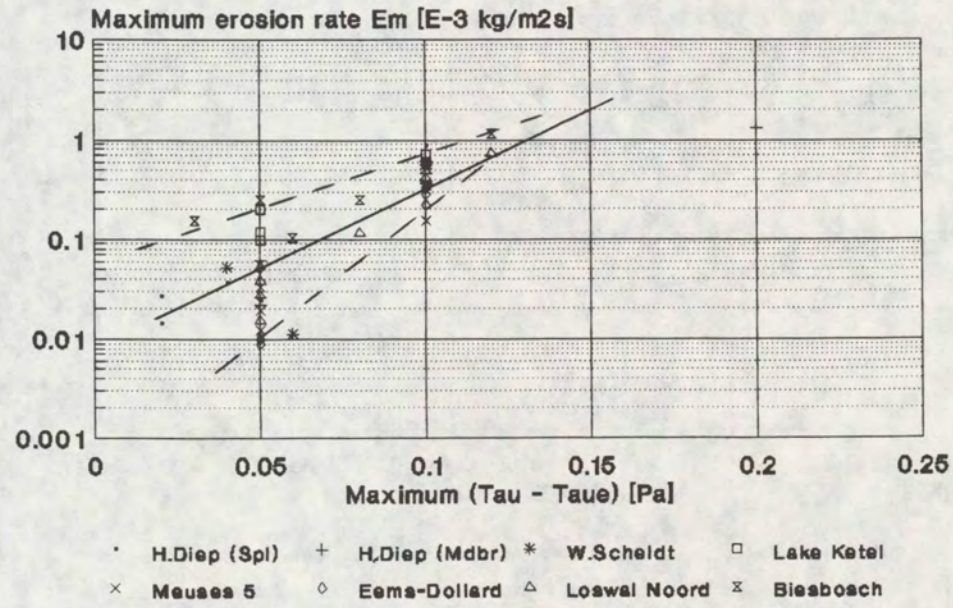

Fig 4.18b

Maximum erosion rate
Consolidation time Tc = 7 days

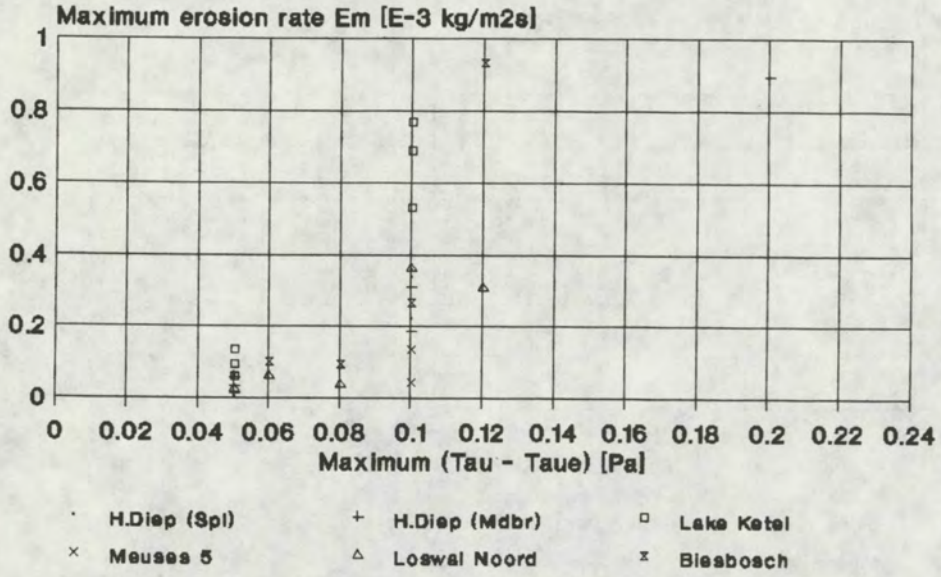

Fig 4.19a

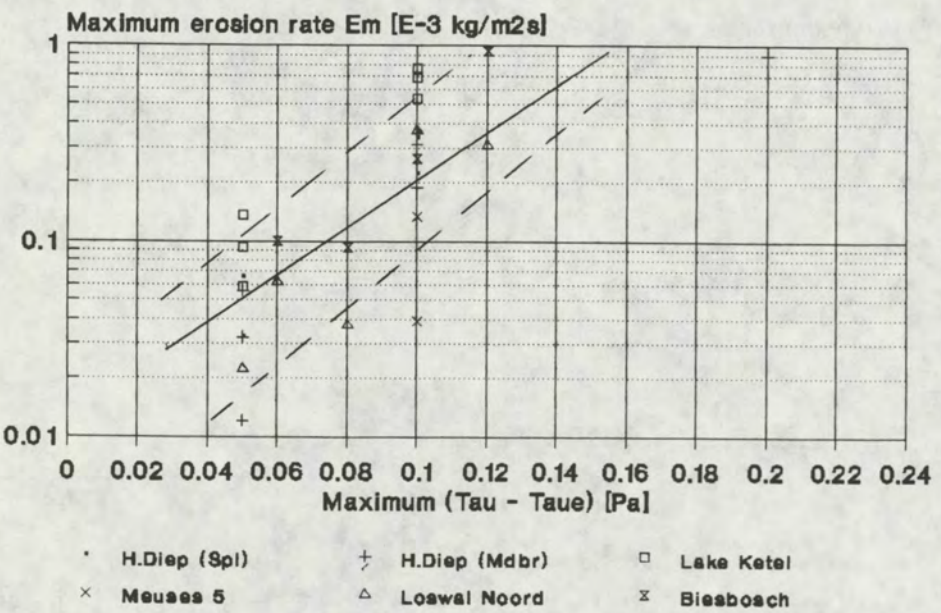

Fig 4.19b

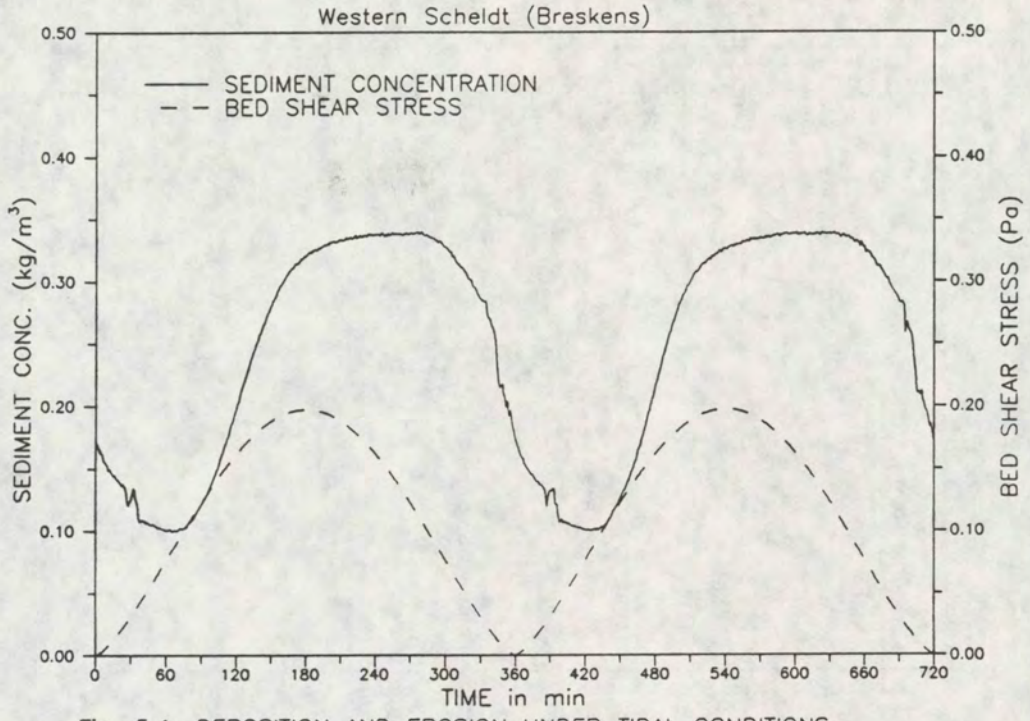

Fig. 5.1: DEPOSITION AND EROSION UNDER TIDAL CONDITIONS
maximum bed shear stress: 0,2 Pa

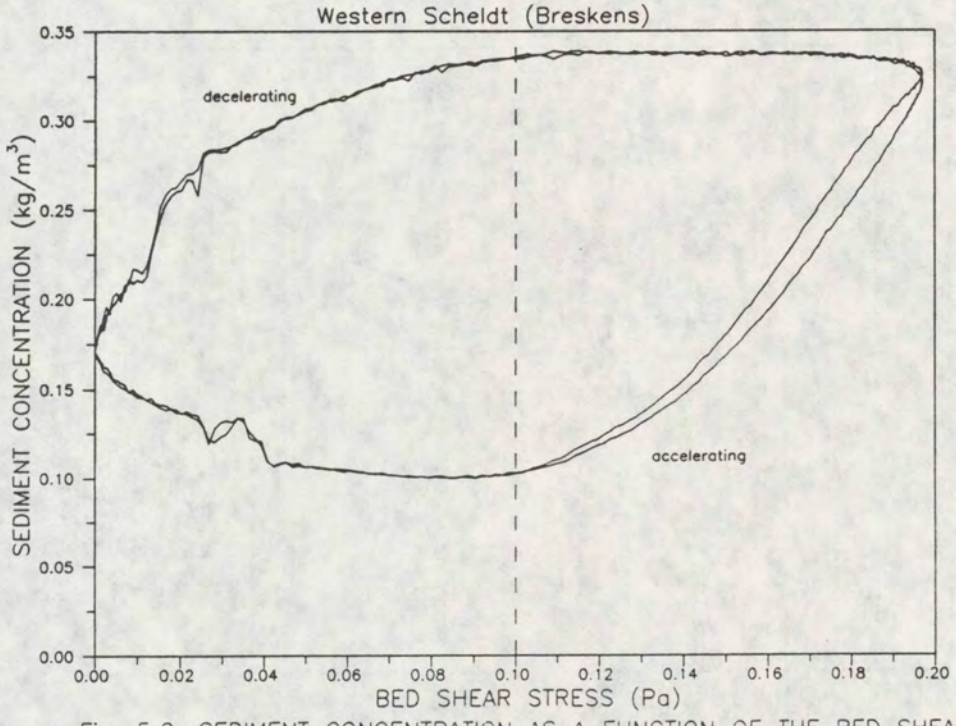

Fig. 5.2: SEDIMENT CONCENTRATION AS A FUNCTION OF THE BED SHEAR STRESS
maximum bed shear stress: 0,2 Pa

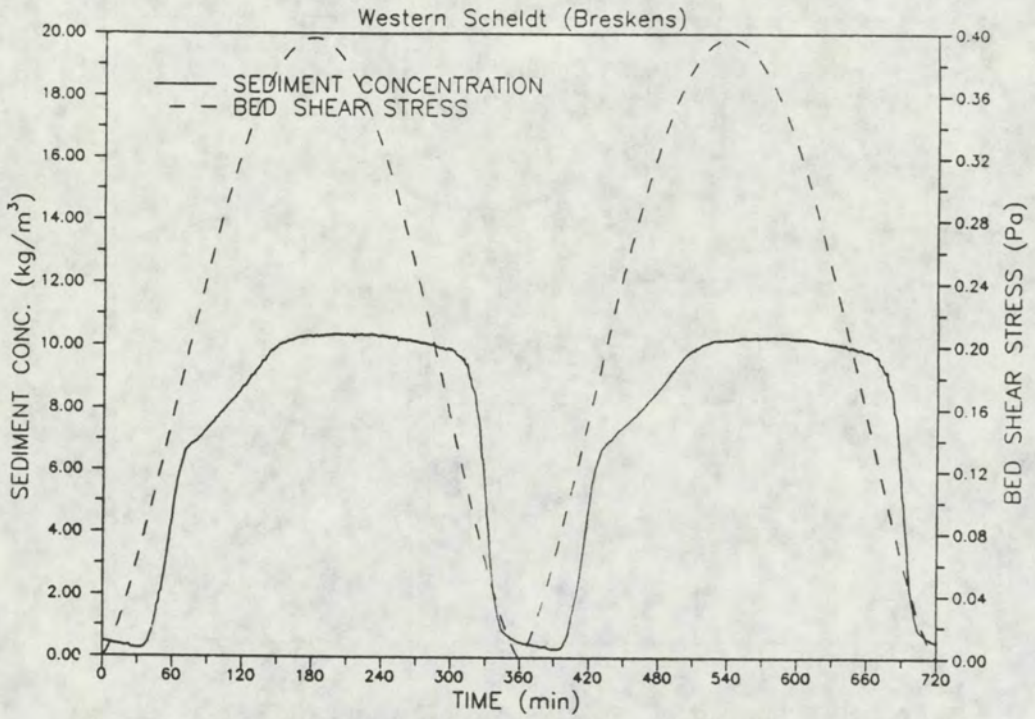

Fig. 5.3: DEPOSITION AND EROSION UNDER TIDAL CONDITIONS
maximum bed shear stress: 0,4 Pa

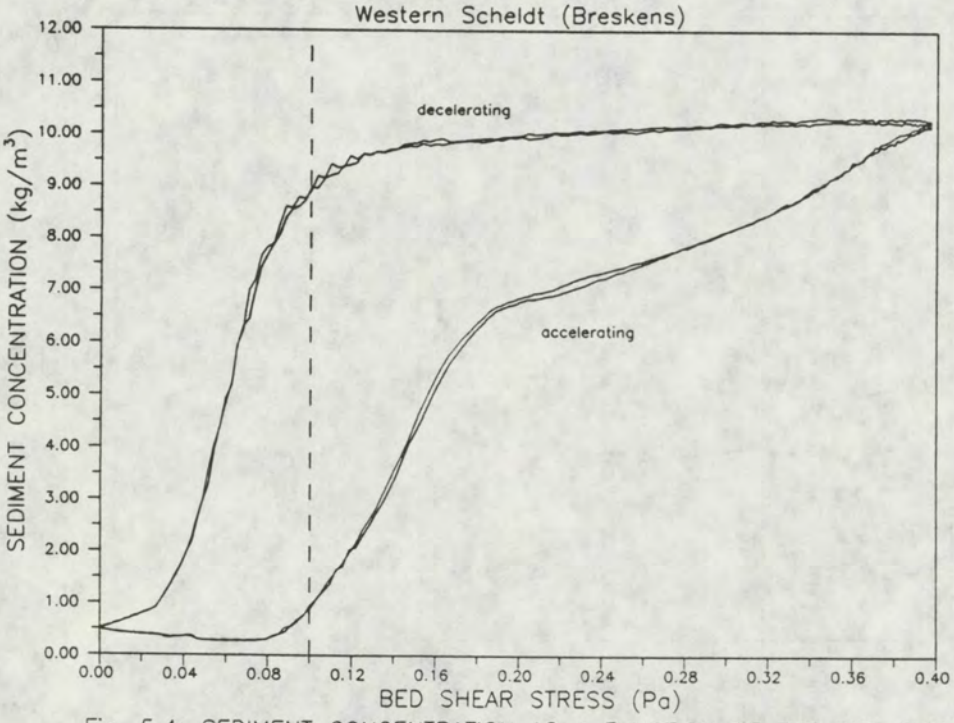

Fig. 5.4: SEDIMENT CONCENTRATION AS A FUNCTION OF THE BED SHEAR STRESS
maximum bed shear stress: 0,4 Pa

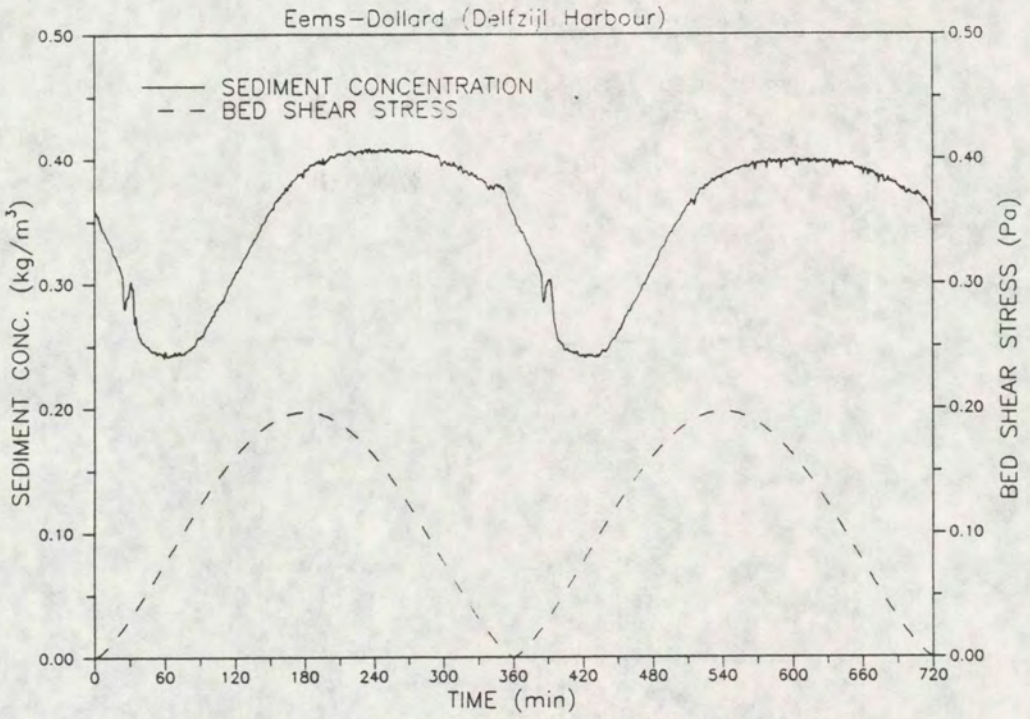

Fig. 5.5: DEPOSITION AND EROSION UNDER TIDAL CONDITIONS
maximum bed shear stress: 0,2 Pa

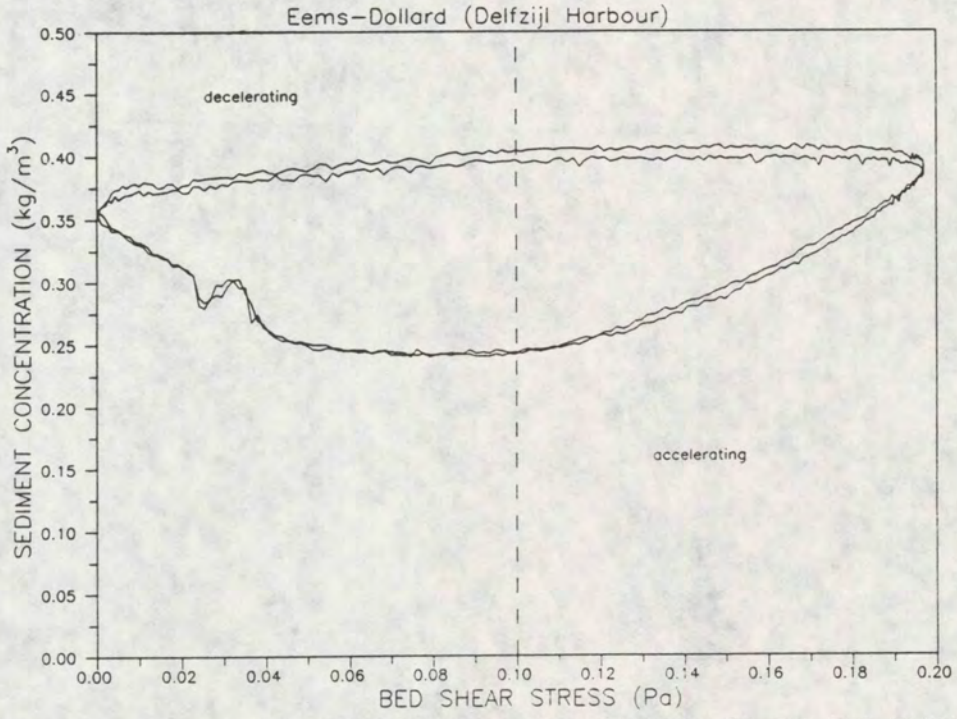

Fig. 5.6: SEDIMENT CONCENTRATION AS A FUNCTION OF THE BED SHEAR STRESS
maximum bed shear stress: 0,2 Pa

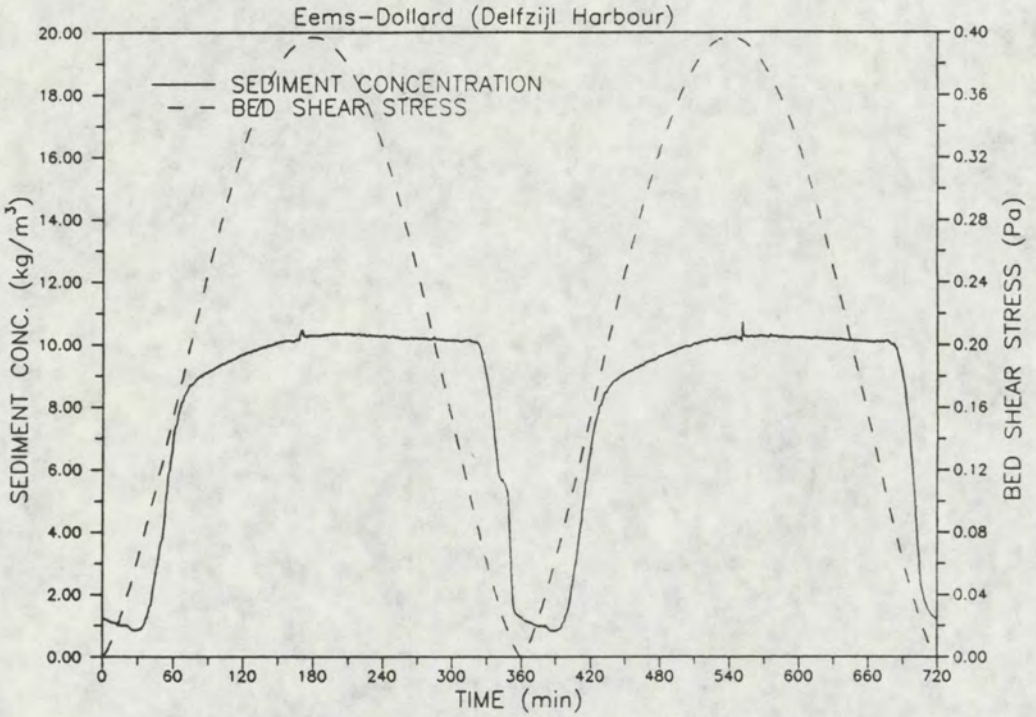

Fig. 5.7: DEPOSITION AND EROSION UNDER TIDAL CONDITIONS
maximum bed shear stress: 0,4 Pa

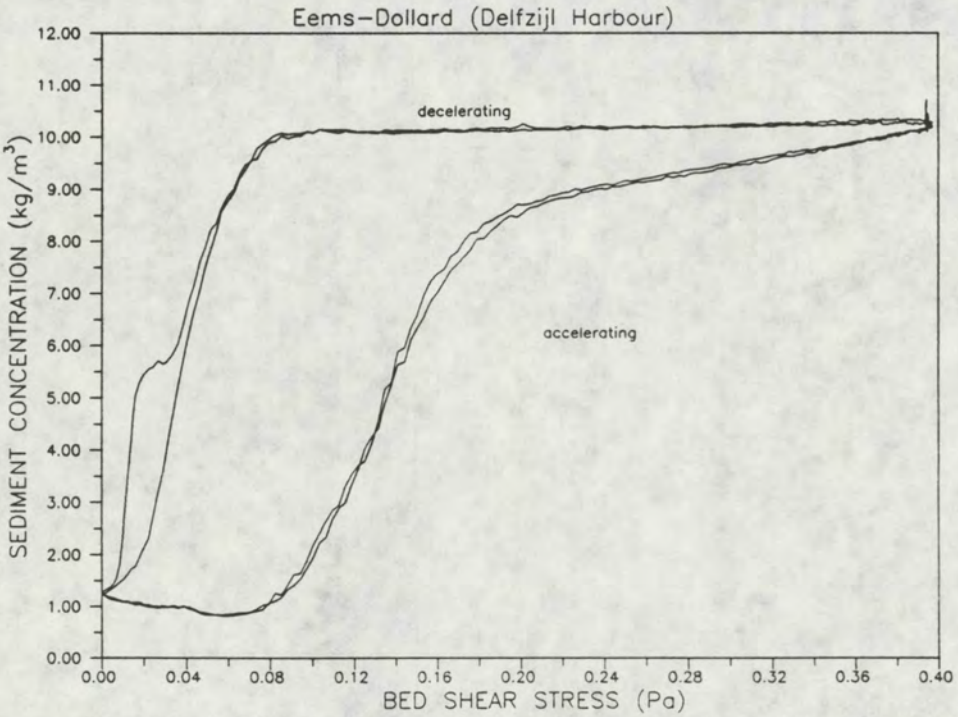

Fig. 5.8: SEDIMENT CONCENTRATION AS A FUNCTION OF THE BED SHEAR STRESS
maximum bed shear stress: 0,4 Pa

Fig. 5.9 a Interfacial instability at t ≈ 420 min.

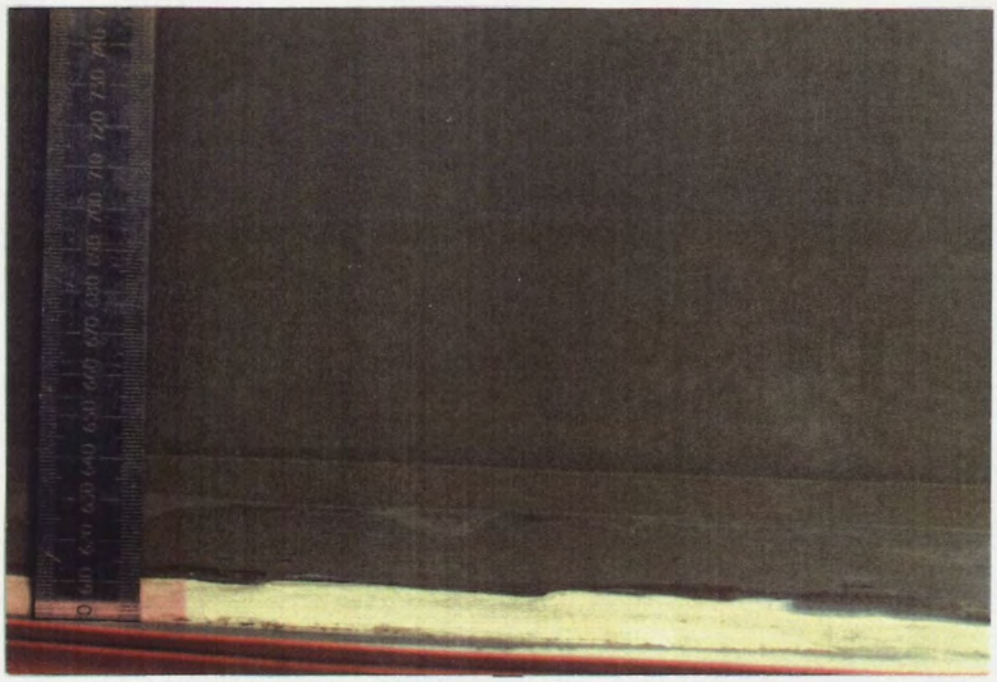

Fig. 5.9 b Interface at t ≈ 430 min.

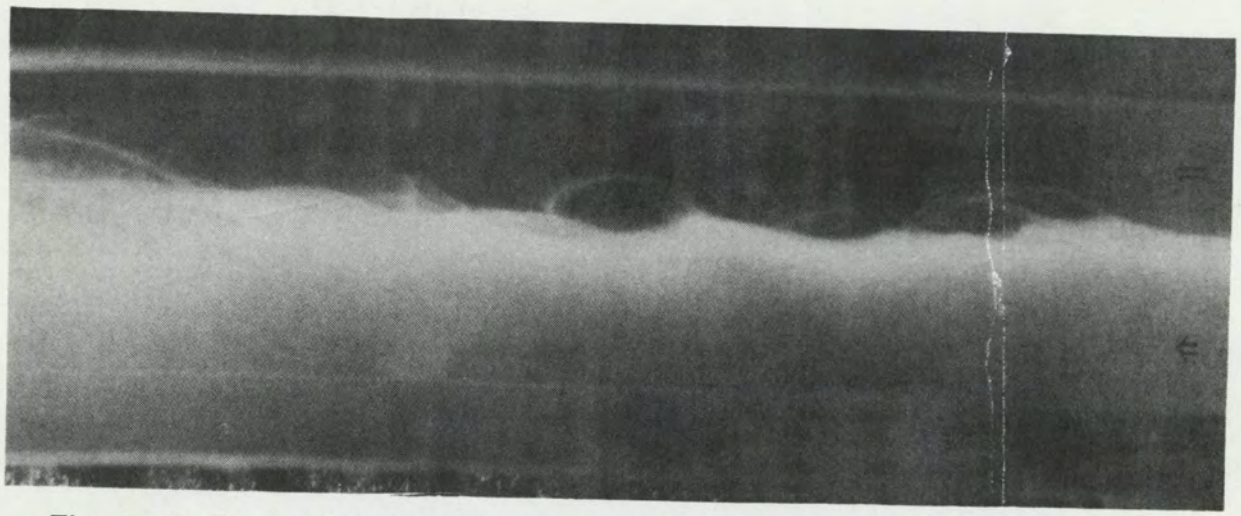

Fig. 5.10 Kelvin-Helmholtz like billowing but with very thin wisps of fluid in the billows

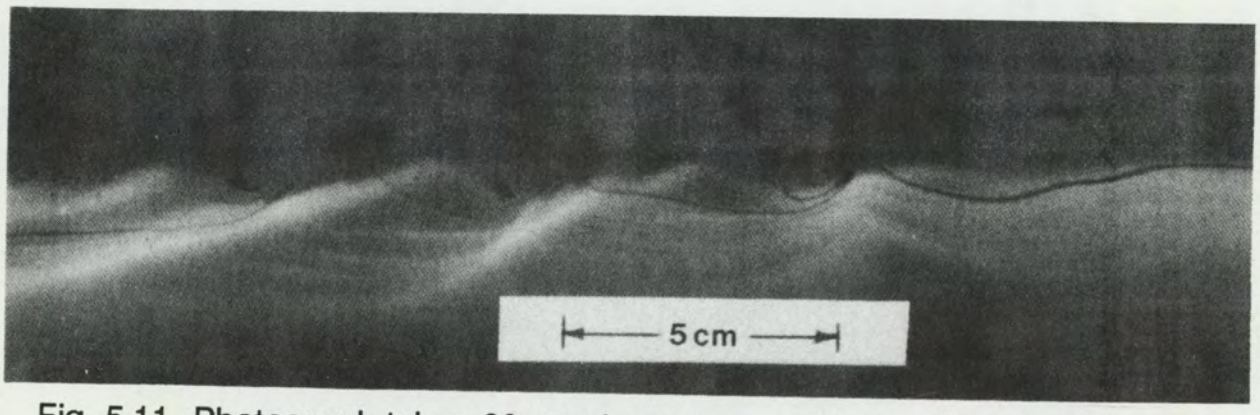

Fig. 5.11 Photograph taken 30 cm downstream of the splitter plate showing the concentration of vorticity above the interface

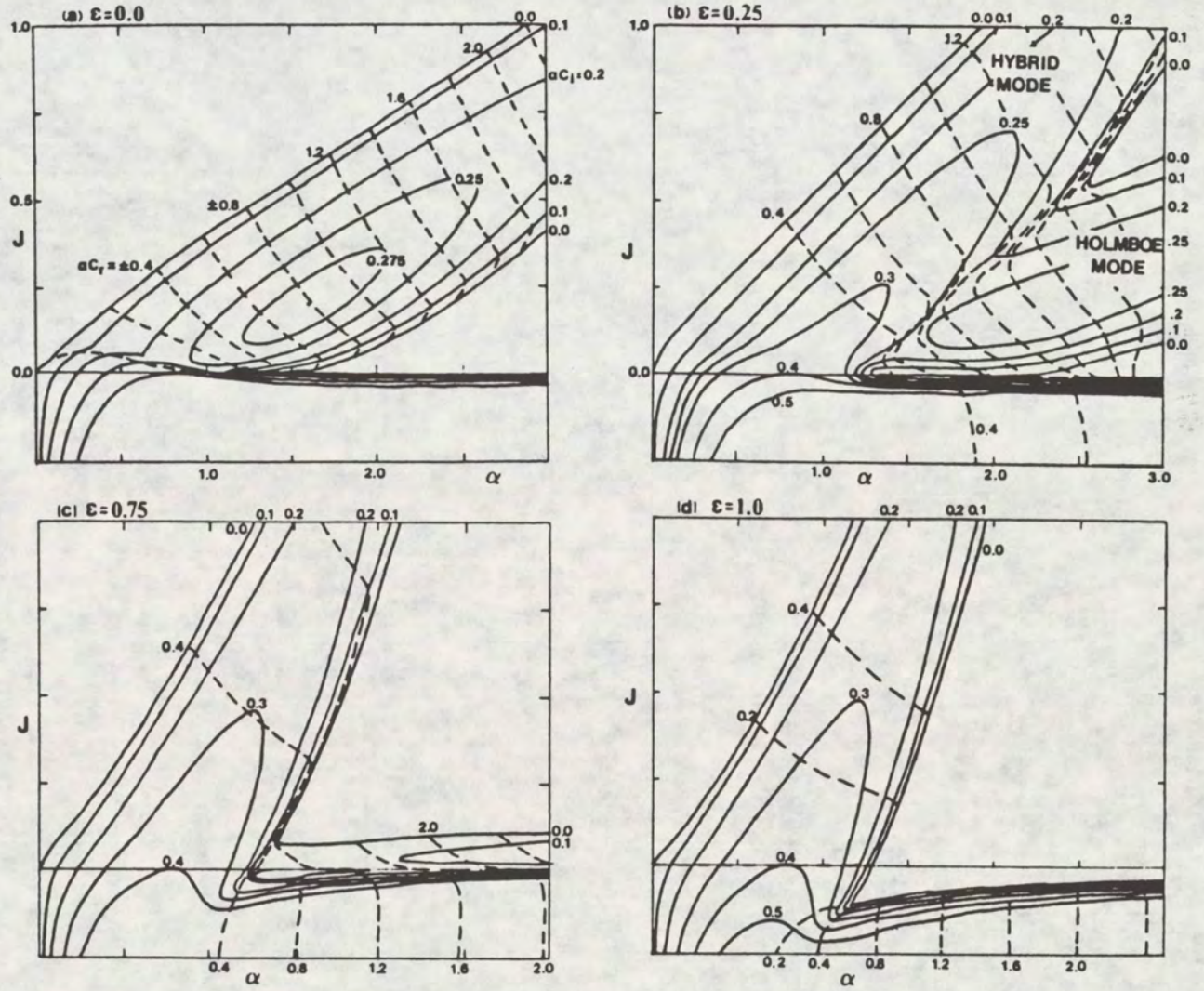

Fig. 5.12 **Stability diagrams for ε = 0.0, 0.25, 0.75, and 1.0**

Tidal experiments (Taub,max = 0,2 Pa)
Western Scheldt (Breskens)

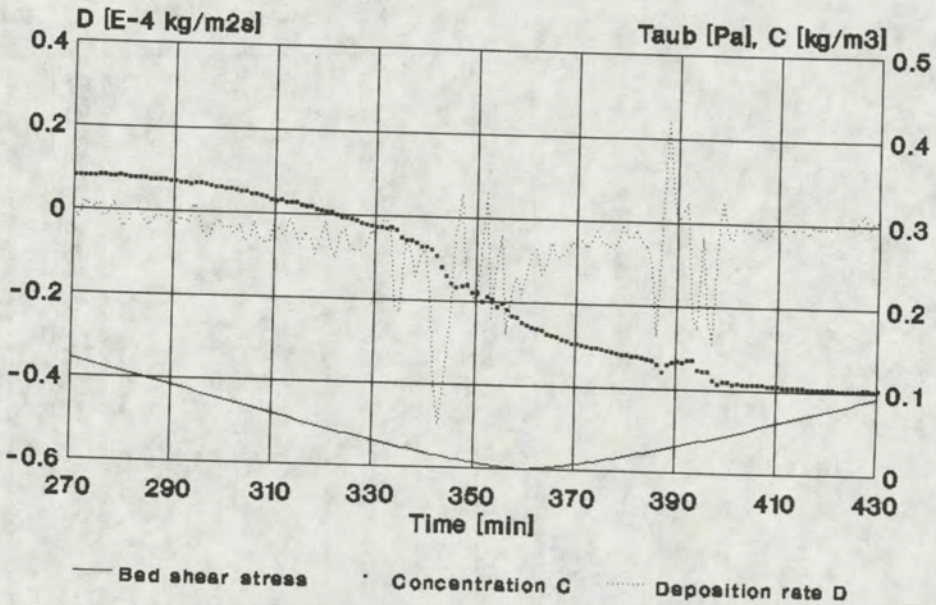

Fig 5.13a

Western Scheldt (Breskens)

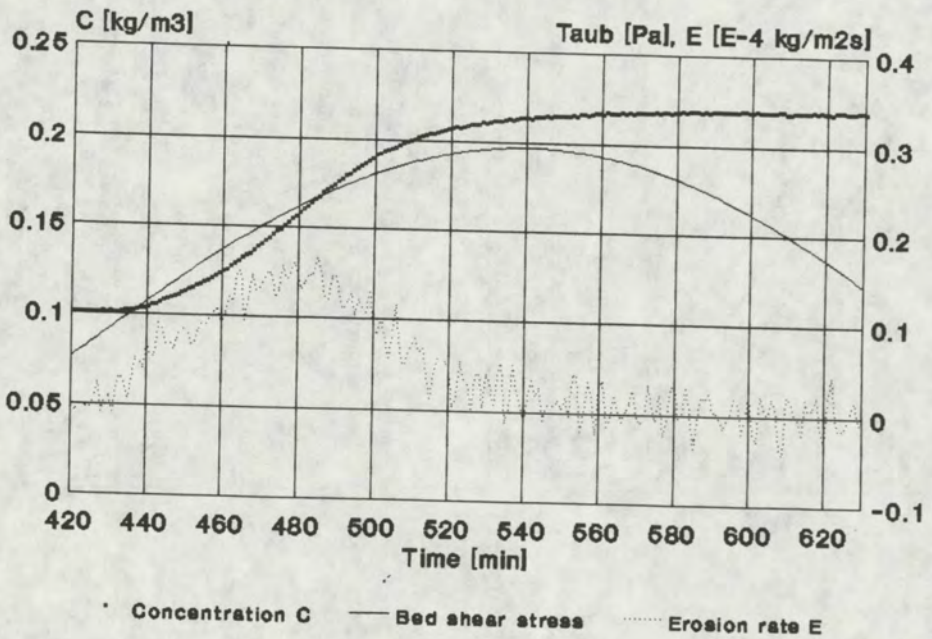

Fig 5.13b

Tidal experiments (Taub,max = 0,2 Pa)
Eems-Dollard (Delfzijl Harbour)

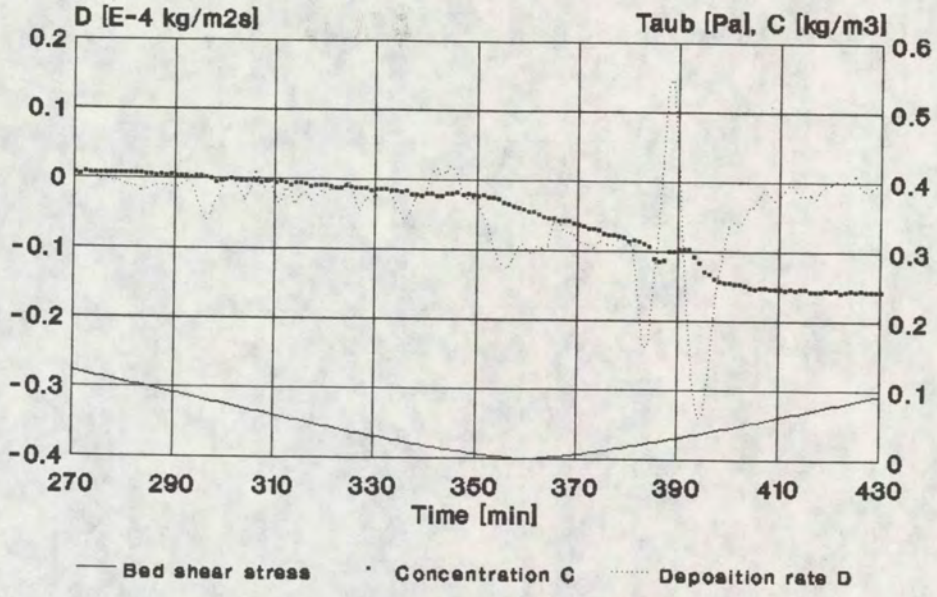

Fig 5.14a

Eems-Dollard (Delfzijl Harbour)

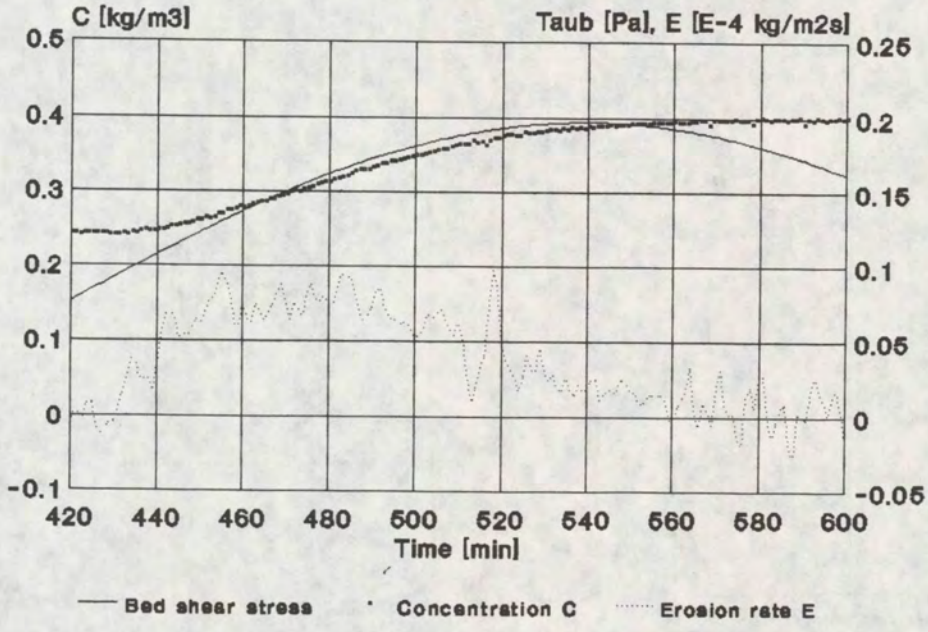

Fig 5.14b

Tidal experiments (Taub,max = 0,2 Pa)
Western Scheldt (Breskens)

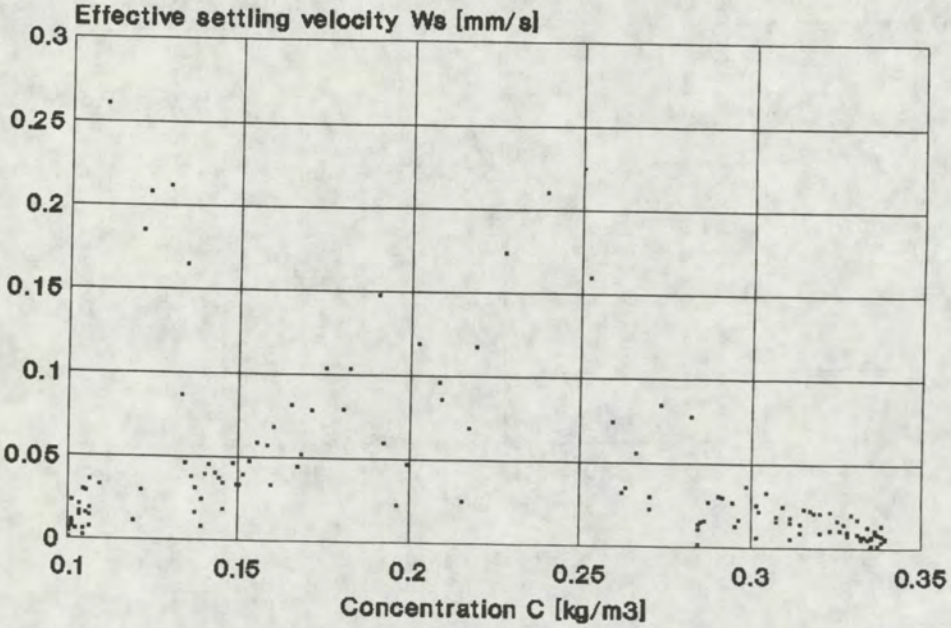

Fig 5.15a

Western Scheldt (Breskens)

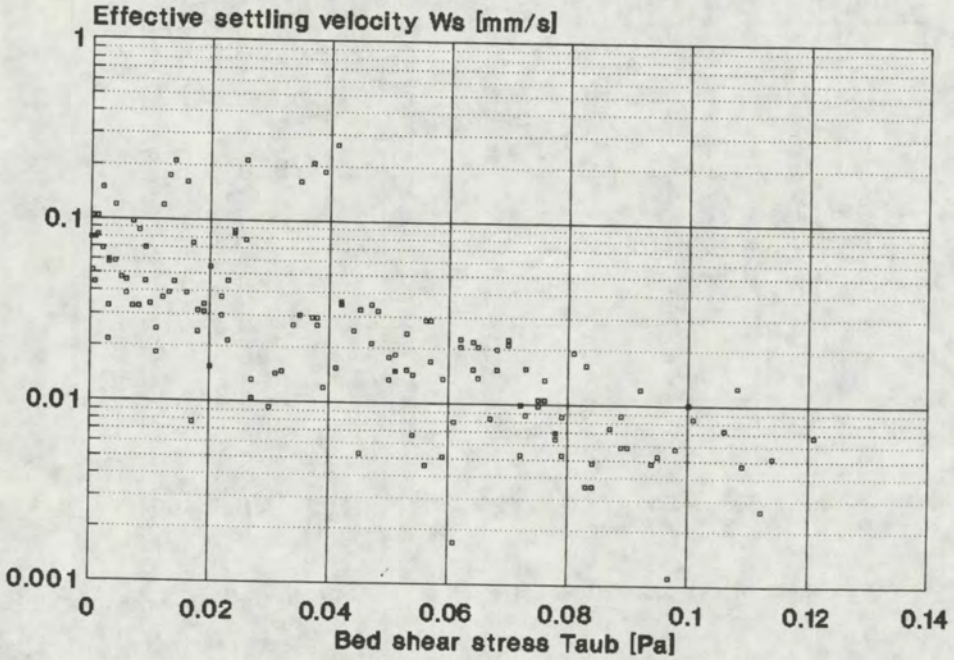

Fig 5.15b

Tidal experiments (Taub,max = 0,2 Pa)
Eems-Dollard (Delfzijl Harbour)

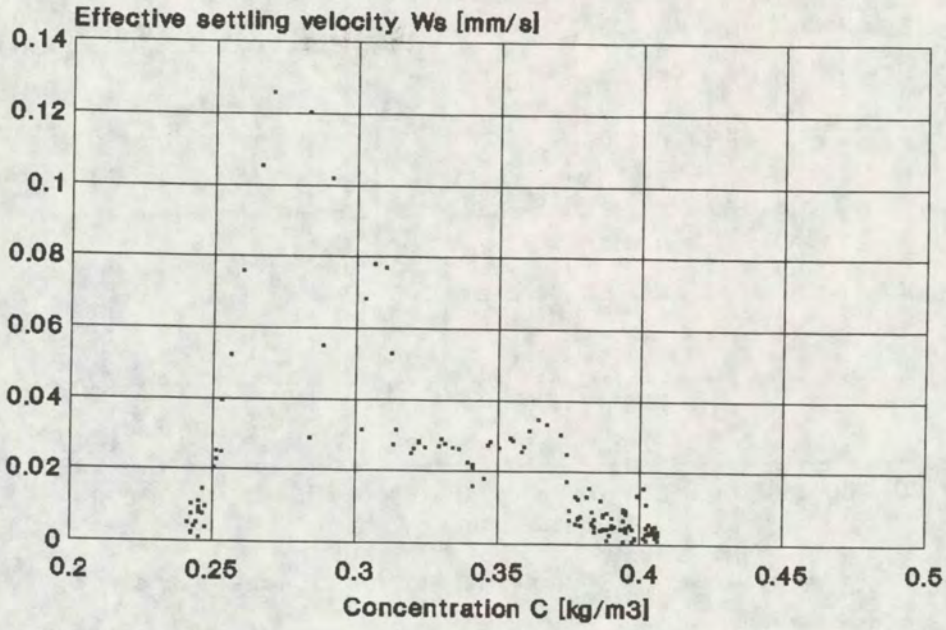

Fg 5.16a

Eems-Dollard (Delfzijl Harbour)

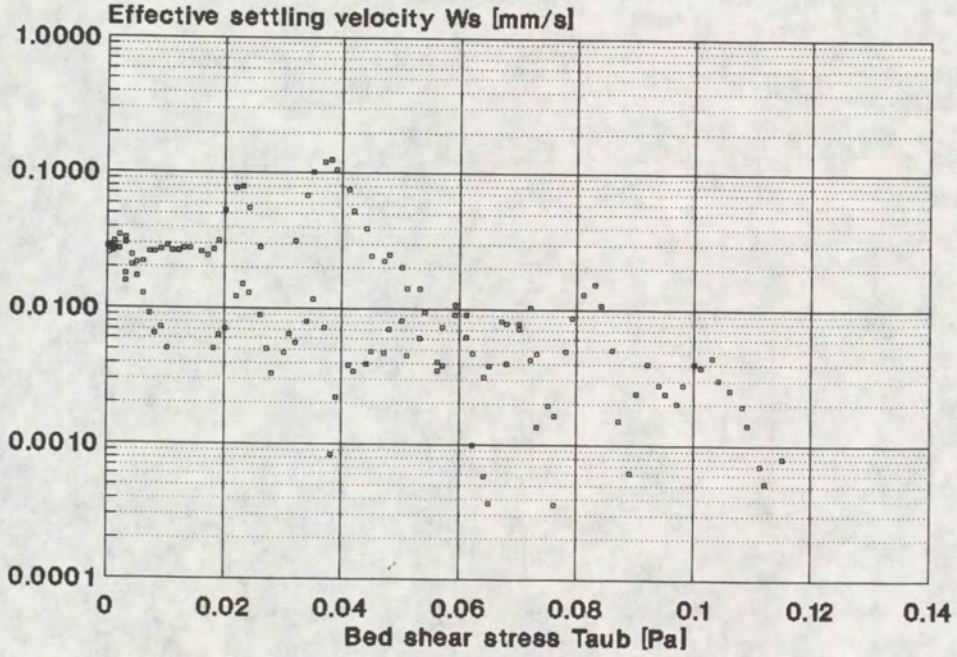

Fig 5.16b

Western Scheldt (Breskens)
Tidal experiments

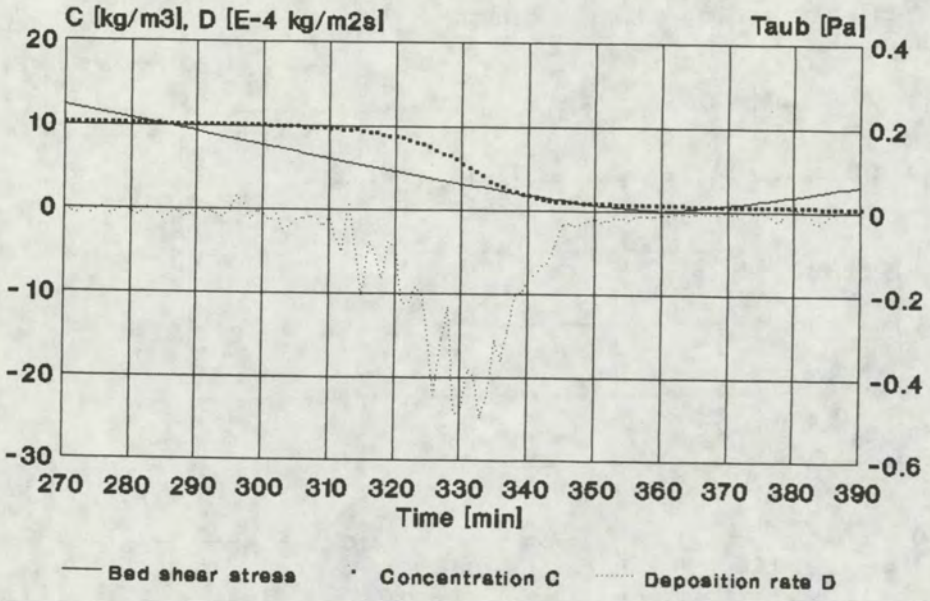

Fig 5.17

Eems-Dollard (Delfzijl Harbour)
Tidal experiments

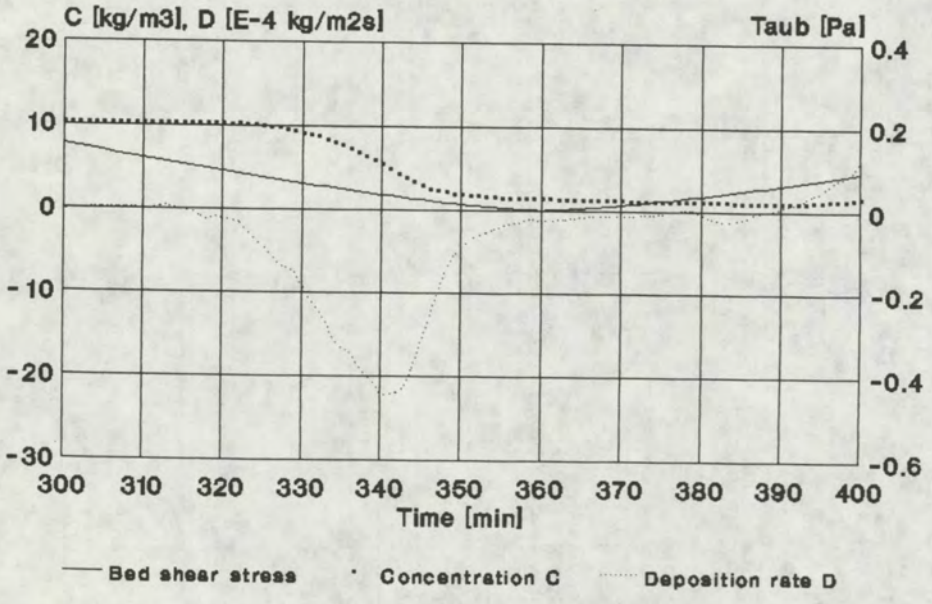

Fig 5.18

Western Scheldt (Breskens)
Tidal experiments

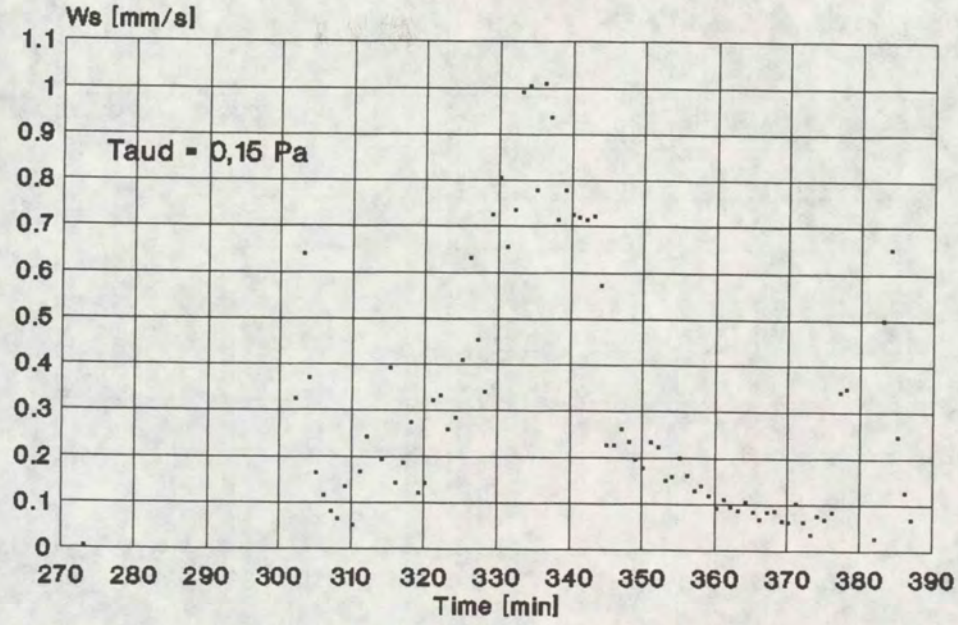

Fig 5.19a: Ws from Krone's law

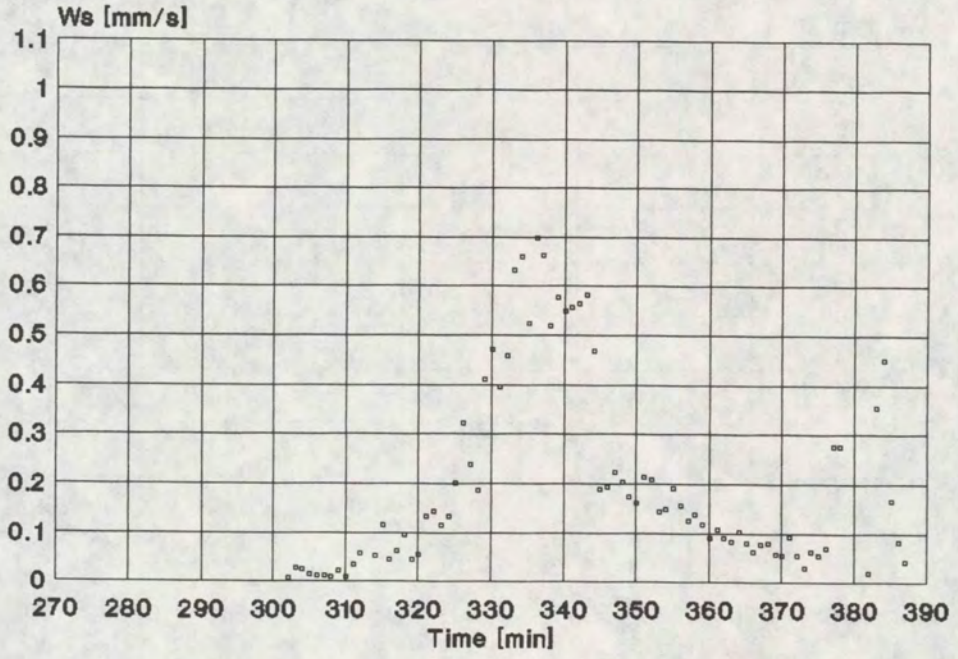

Fig 5.19b: Eff. settl. velocity

Eems-Dollard (Delfzijl Harbour)
Tidal experiments

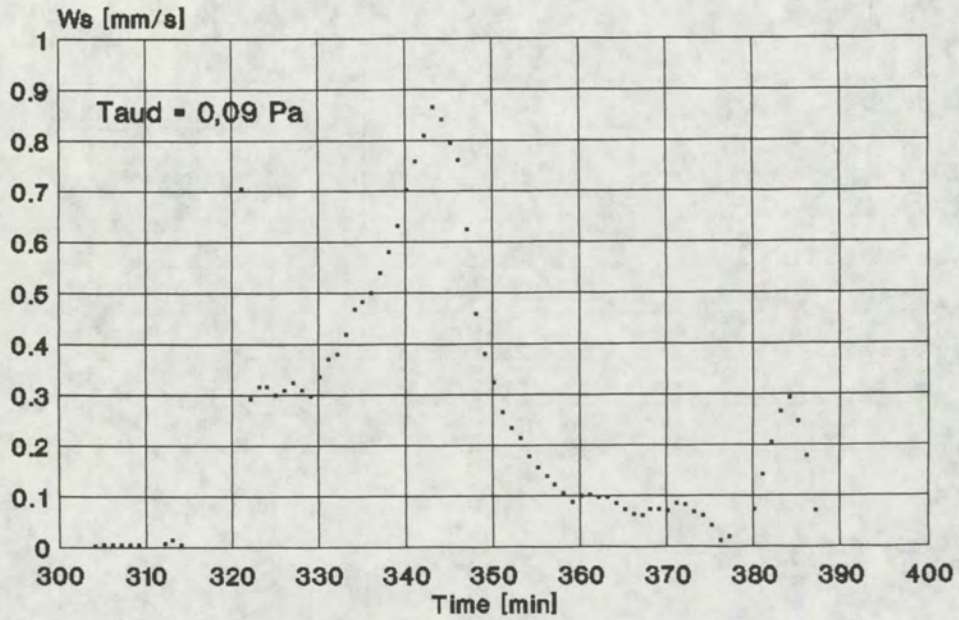

Fig 5.20a: Ws from Krone's law

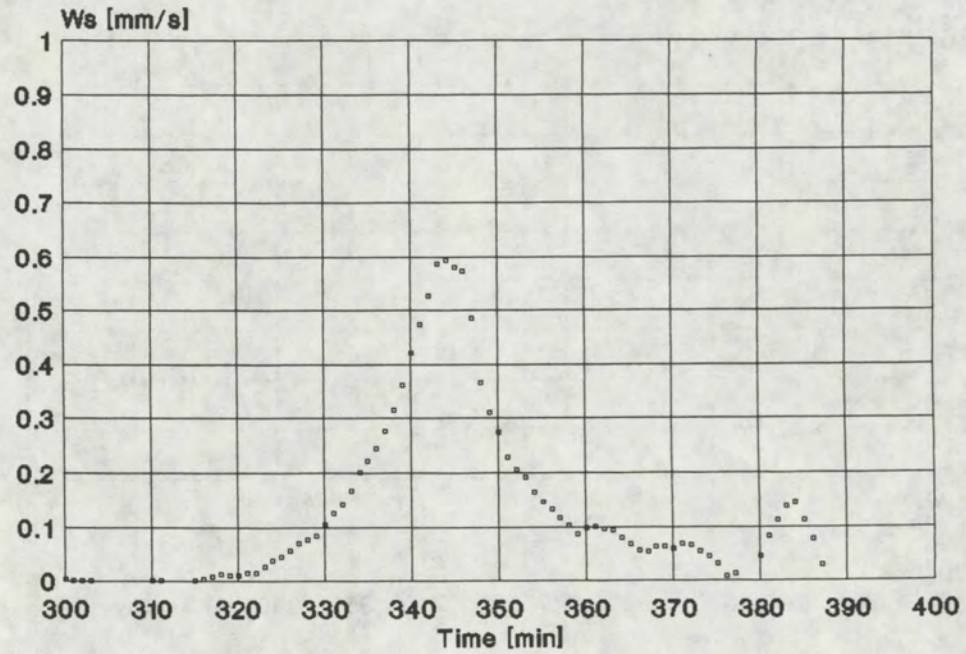

Fig 5.20b: Eff. settl. velocity

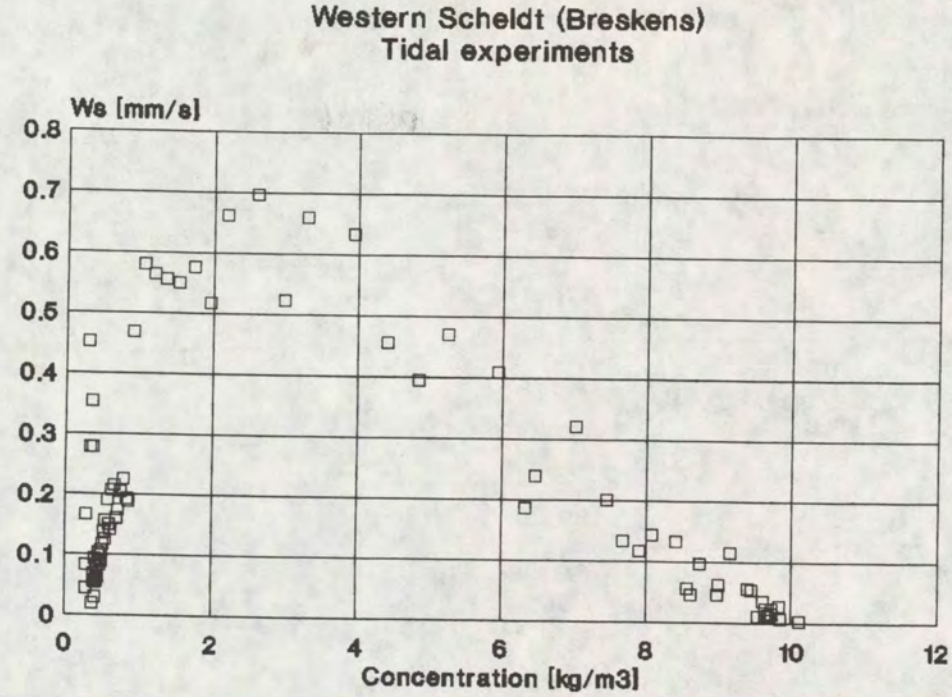

Fig 5.21a Effective settling velocity

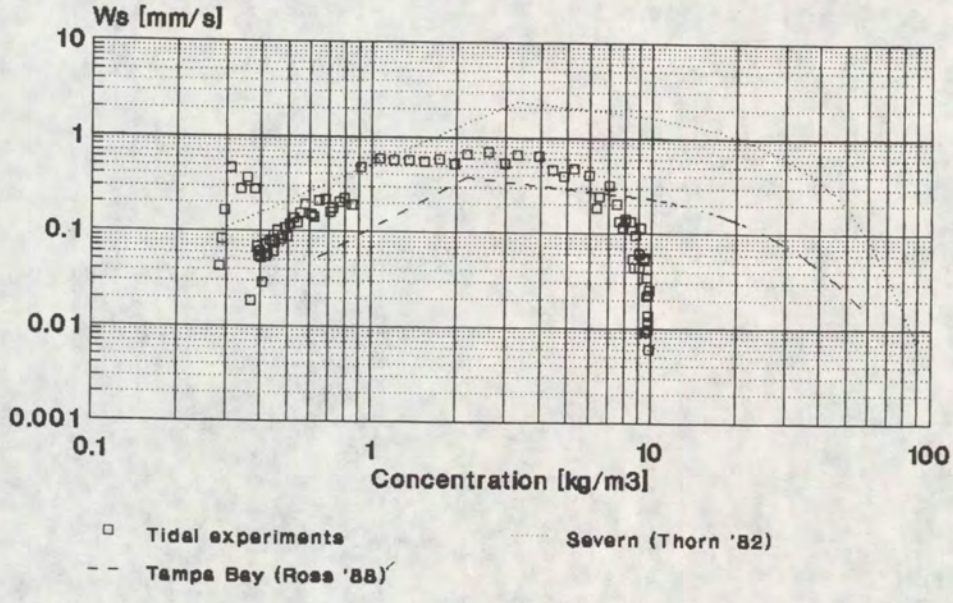

Fig 5.21b Effective settling velocity

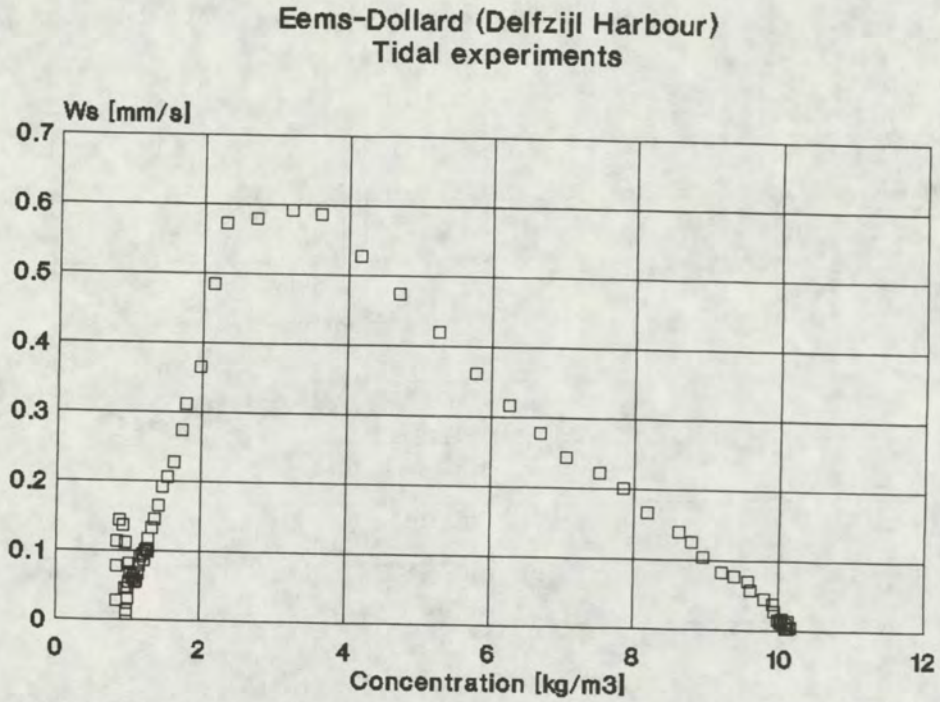

Fig 5.22a Effective settling velocity

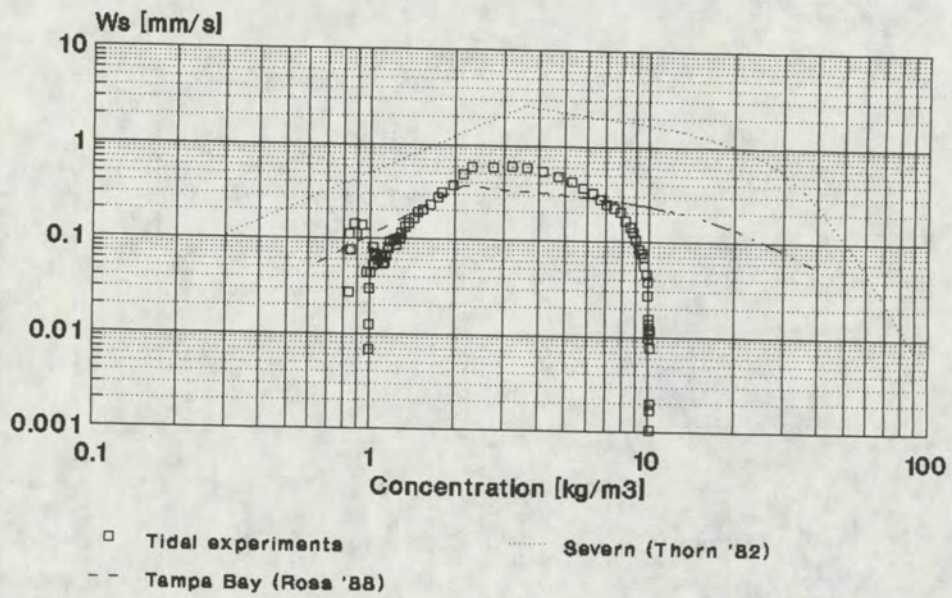

Fig 5.22b Effective settling velocity

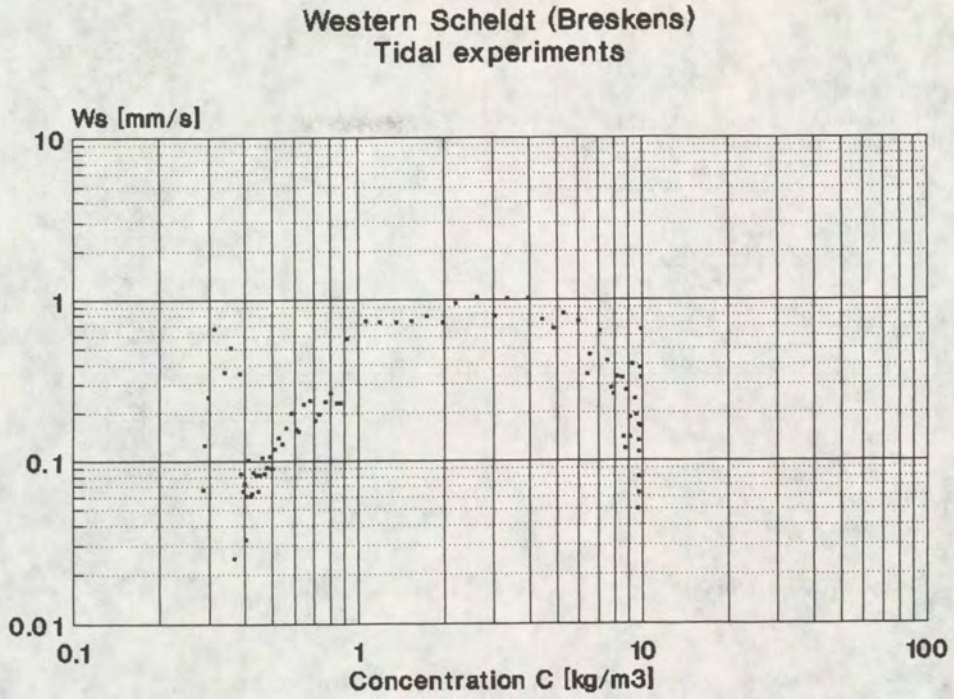

Fig 5.23a: Ws from Krone's law

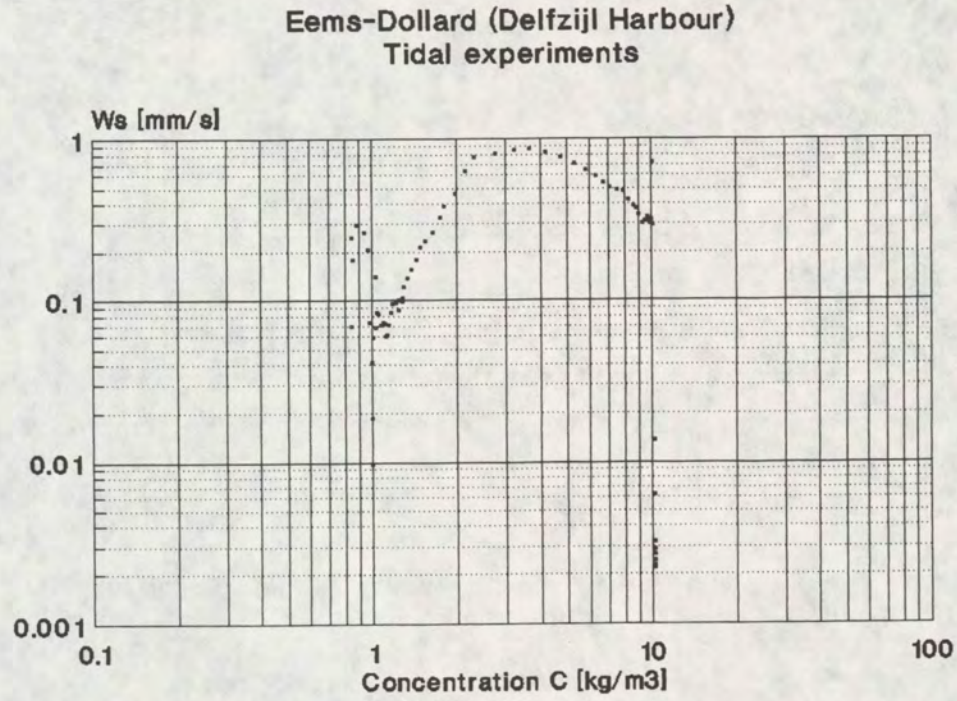

Fig 5.23b: Ws from Krone's law

Western Scheldt (Breskens)
Tidal experiments

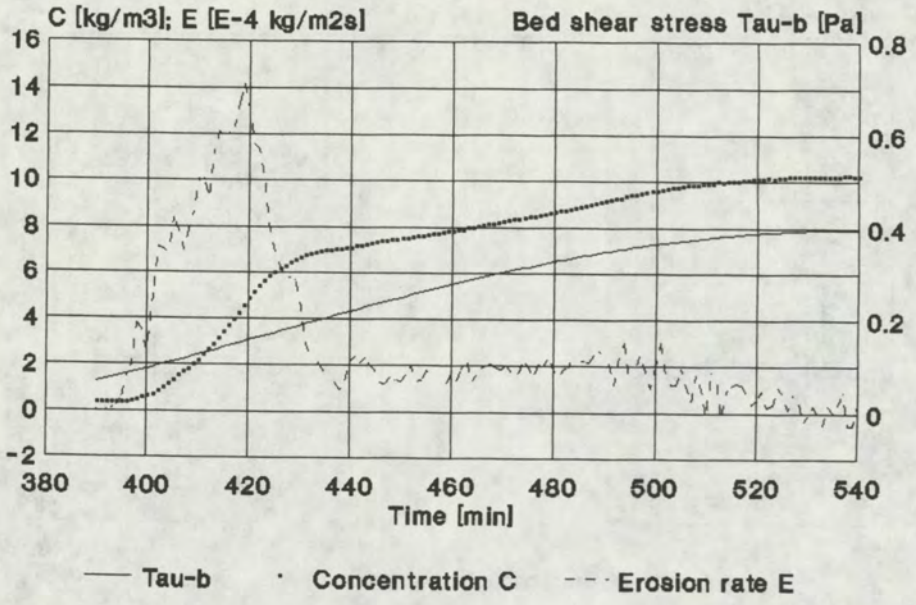

Fig 5.24

Eems-Dollard (Delfzijl Harbor)
Tidal experiments

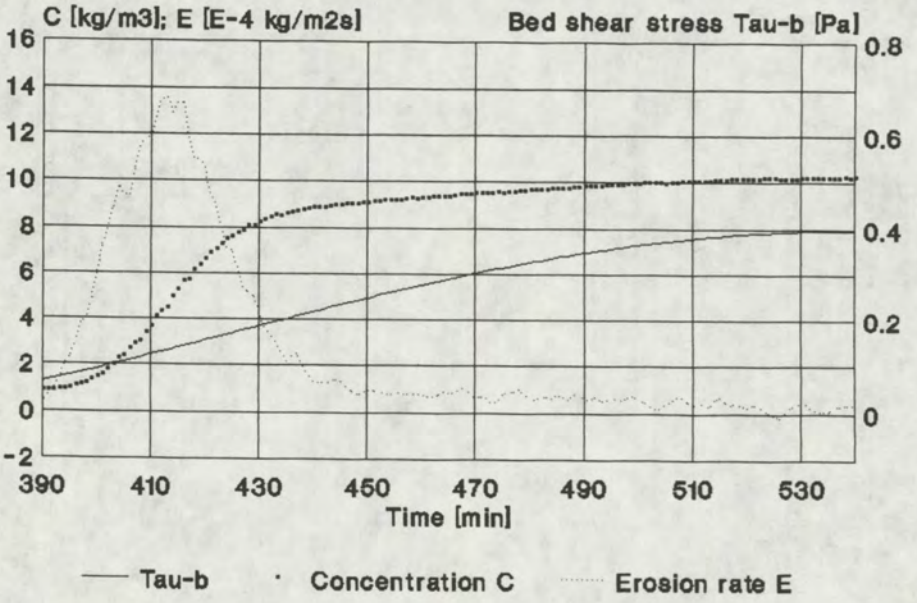

Fig 5.25

Western Scheldt (Breskens)
Tidal experiments

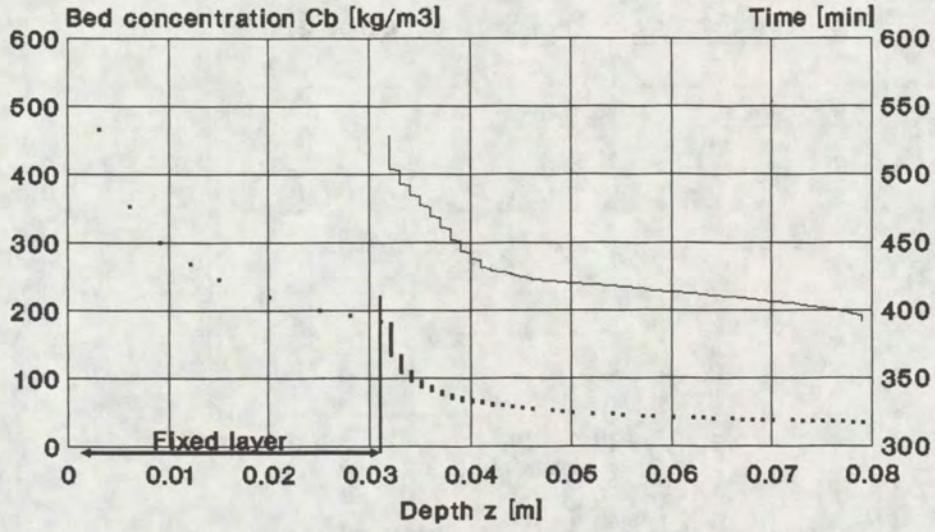

Fig 5.26a

Predicted shear strength distribution

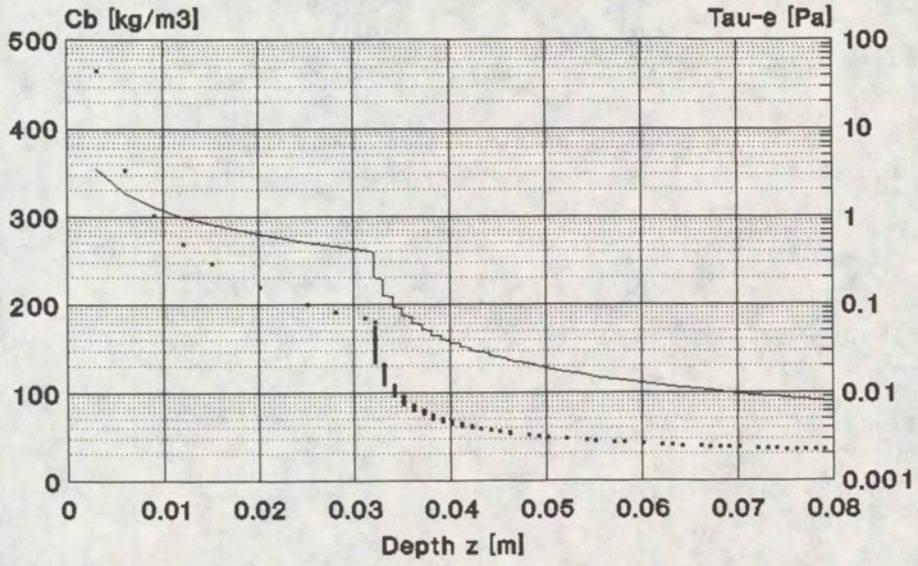

Fig 5.26b

Western Scheldt (Breskens)
Tidal experiments

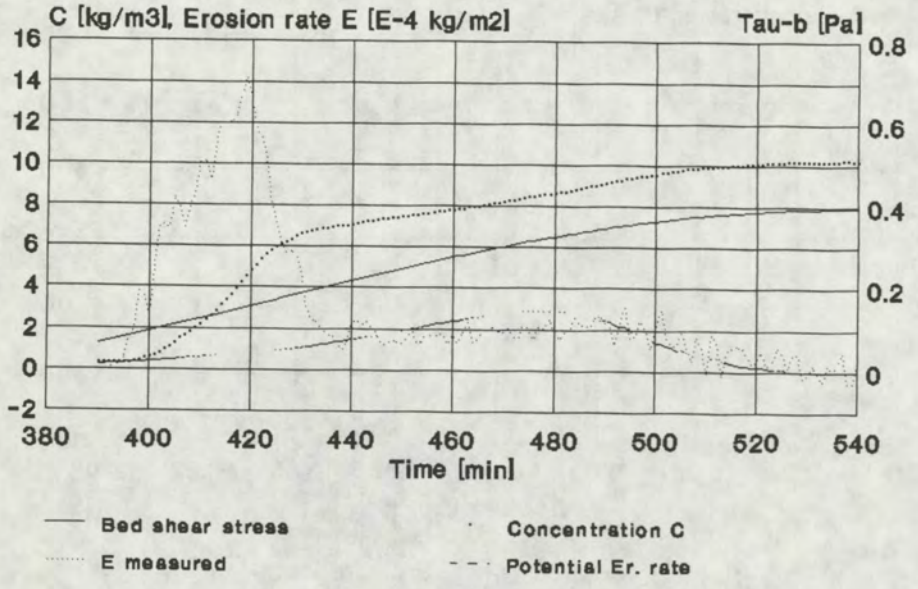

Fig 5.27

Variation of gradient
Richardson number with time

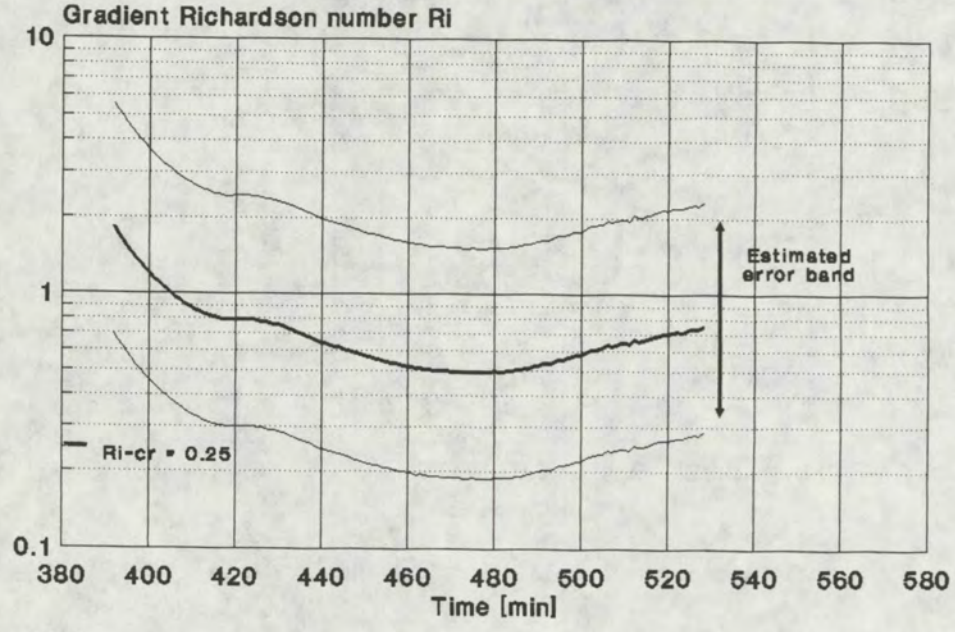

Fig 5.28

Western Scheldt (Breskens)
Tidal experiments

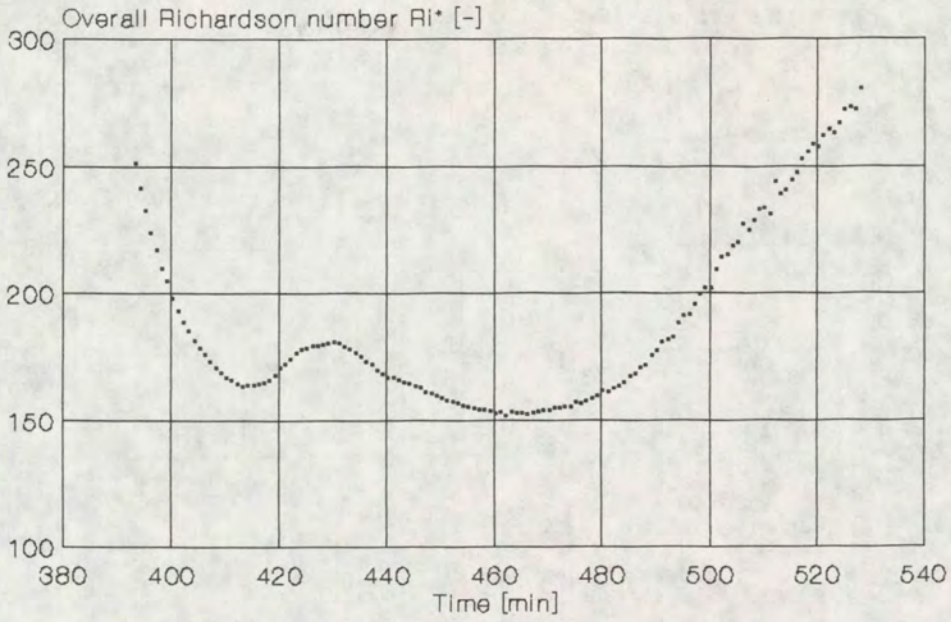

Fig 5.29 (N.B. u* upper lid)

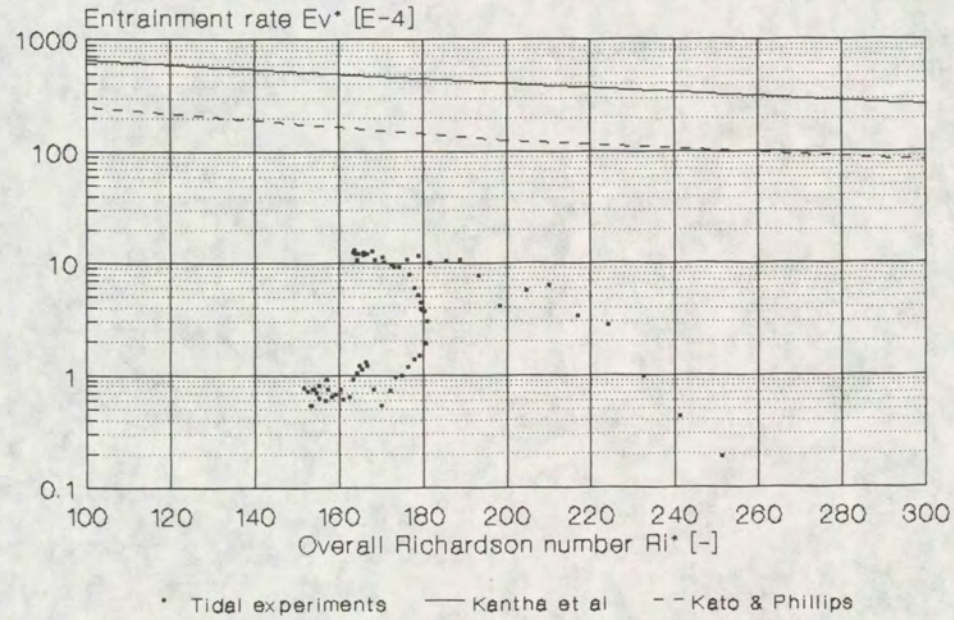

Fig 5.30 (N.B. u* upper lid)

Western Scheldt (Breskens)
Tidal experiments

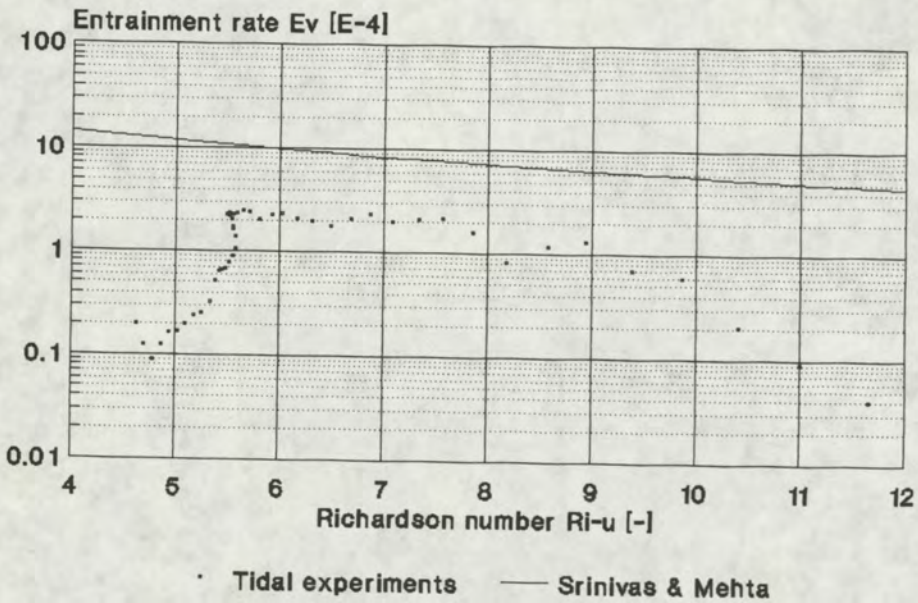

Fig 5.31

Variation of erosion rate with
bed shear stress

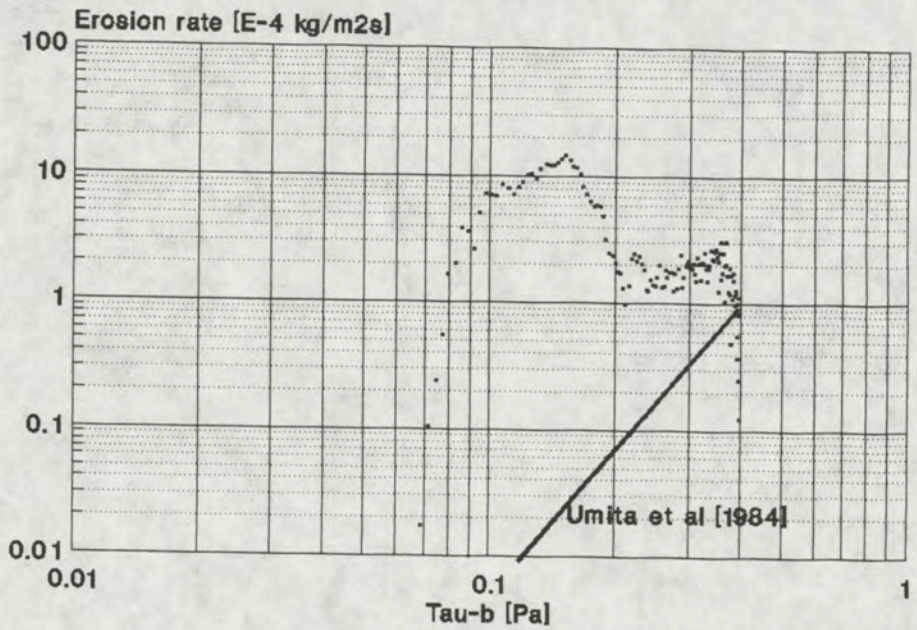

Fig 5.32

DELFT HYDRAULICS		

Appendix A:

Test programme to determine the flow induced erosion and sedimentation behaviour of natural muds encountered in the Netherlands.

Test programme to determine the flow induced erosion and sedimentation behaviour of natural muds encountered in the Netherlands.

1. Sampling.

a. Selection and description of the location.

b. Sample about 30 kg dry bed material (e.g. about 100 kg wet material) from a sedimentation area with a small "Van Veen" grab sampler; probably the sediments in a sedimentation area are representative for the sediments in the selected location, whereas in an eroding area, the finer particles may have been washed out.
The sampler should be small to obtain mainly sediments from the surface layer, i.e. not from one deep pit. The sediment should be brought ashore as fast as possible and transported and stored in a cooling box.
Sample simultaneously also 500 ltr water under quiet weather conditions; this water can be transported and stored in 25 l jerrycans.

c. Describe the area and the local conditions, take photographs at the site and of the mud. Measure the temperature, salinity (if relevant) and oxygen content of the water, and the redox potential of the water and the mud.

2. Determine the physical-chemical properties.

a. The composition of the mud:
-Deflocculate the mud and determine the grain size distribution with the MALVERN and with the sedimentation balance.
-Determine the specific surface of the mud (by GD, Delft Soil Mechanics).
-Determine the mineralogical composition of the mud (GD).
-Determine the organic content, the O_2 content, and the redox potential.
-Determine the pH, temperature and salinity.
-Measure the SAR and CEC (GD).
-Make some photographs of the sediments with the microscope.

b. The properties of the mud:

-Determine the distribution of the settling velocity of the mud in the sedimentation balance (without de-flocculant).

-Determine the up-going and down-going flow curve (viscosity and yield strength) with the Haake-viscometer at concentrations of 0 (50) $c_{natural}$ g/l up to a shear rate of 150 s^{-1} and a temperature of 20 C. Use the natural water.

-Determine the consolidation behaviour in a column by measuring the height of the interface and the water over pressure. Measure the vertical dry density profile within the consolidation column with a conductivity and/or accoustic probe (and measure the vane shear strength at the end of the test at various depths).

3. Determine the erosion and sedimentation behaviour in the caroussel.

a. General tests for all samples:

-Perform a sedimentation test at an initial concentration of 1 g/l by lowering the bed shear stress from about 0,40 to about 0,05 Pa in small steps of about 0,02 to 0,10 Pa. Each sub-test will be continued until equilibrium is attained. During the tests, the variations in suspended sediment concentration will will be measured continuously with the OSLIM (optical concentration measuring probe); samples will be taken at regular intervals to calibrate the OSLIM recordings and to determine the organic content and grain size distribution.

-Carry out an erosion test. A so-called deposited bed will be formed in still water from the deposition of a homogeneous suspension of c_0 = 60 g/l. A consolidation time of 24 hours (after stopping the annular flume) is used. The dry density profile within this bed will be deduced from the consolidation test described above. The erosional behaviour is determined by increasing the bed shear stress from 0 to about 0,7 Pa in steps of o,02 to 0,1 Pa.; each sub-test is continued for about one hour. During the tests, the variations in suspended sediment concentration will will be measured continuously with the OSLIM; samples will be taken at regular intervals to calibrate the OSLIM recordings and to determine the organic content and grain size distribution.

b. Sediments from non-tidal locations;

Next to the tests mentioned under 3.a. the following tests will be performed:

-A sedimentation test as described above with an initial concentration of c_0 = 0,2 g/l.

-An erosion test as described above with a consolidation time of 7 days.

c. Sediments from tidal locations:

Next to the tests mentioned under 3.a. the following tests will be performed:

-A test with a sinusoidal varying bed shear stress on a deposited bed (see 3.a), with a consolidation time of 6 hours. The tidal period will amount to 12 hours, and the amplitude of the bed shear stress to 0,4 Pa. The test will be continued until equilibrium is achieved. During the tests, the variations in suspended sediment concentration will will be measured continuously with the OSLIM; samples will be taken at regular intervals to calibrate the OSLIM recordings and to determine the organic content and grain size distribution.

-A similar tidal test with a shear stress amplitude of 0,2 Pa.

4. Reporting.

The results and experimental data of the composition, properties and tests will be summarized in a report. These results will be used to determine the critical shear strength for erosion and sedimentation of the mud and its erosion rate.

5. Determination of the flocculation properties in the settling column (p.m.)

Determine the distribution of the settling velocity and floccualation properties at a grid frequency of 0,05 Hz (amplitude = 0,075 m) and initial concentrations of c_0 = 0,1 and 0,5 g/l. Samples will be taken from 13 locations over the entire height of the column at regular time intervals. The settling mud flocs will be monitored with a CCD-camera at the bottom of the column.

APPENDIX B:

Method of analysis of erosion experiments.

In this Appendix the method of analysis described in Chapter 4.2 is elaborated a little further. It was shown that the sediment concentration in suspension c_s, as measured in the annular flume, is directly related to the concentration distribution within the bed c_b through:

$$c_s.(h - z_b) \approx h.c_s = Ms(z) = \int_{z_b}^{H} c_b \, dz \qquad (B.1)$$

in which h = height of annular flume, H = initial thickness of bed and $z_b(t)$ is erosion depth. By differentiating (B.1) with respect to time t, one obtains the erosion rate E:

$$E = \frac{d}{dt} h \, c_s = \frac{d}{dt} \int_{z_b}^{H} c_b \, dz = - c_b(z_b).\frac{dz_b}{dt} \qquad (B.2)$$

If $c_b(z)$ is known, dz_b/dt can be assessed from (B.2), as c_s is measured. For instance, by substituting equ (3.4), one obtains:

$$E = - \alpha \, \bar{c}_b \exp \{\frac{\beta \, z_b}{H}\}.\frac{dz_b}{dt} \qquad (B.3)$$

from which it follows that E is an exponential function of z_b. If it is further assumed that the critical shear stress for erosion $\tau_e(z)$ varies linearly with depth z, (B.3) shows that E is an exponential function of τ_e. The Figures 4.9 and 4.10 show that this assumption is not too bad.
For each sub test, τ_e is only known at the beginning of this sub test and at the end. Additional data can be obtained through interpolation, using the $\tau_e(z)$ relation mentioned above. However, it follows, that this will only result in additional points on the exponential curve (B.3). Hence, no real additional information is added.
This can be illustrated clearly with the erosion curves obtained by Mehta et al [1982], showing almost straight curves in the E vs τ_e plane - see Figure B.1 - for each sub test. Only the points at the origin and the encircled points were measured directly, the other points were obtained through some interpolation procedure, the details of which are not given. However, probably some graphical interpolation procedure was used, which explains the small deviations of the "data points" from the straight (exponential) curve.

Hence, it can be concluded, that with the present experimental procedure, it is not possible to obtain additional, non-spurious data through interpolation within a sub test.

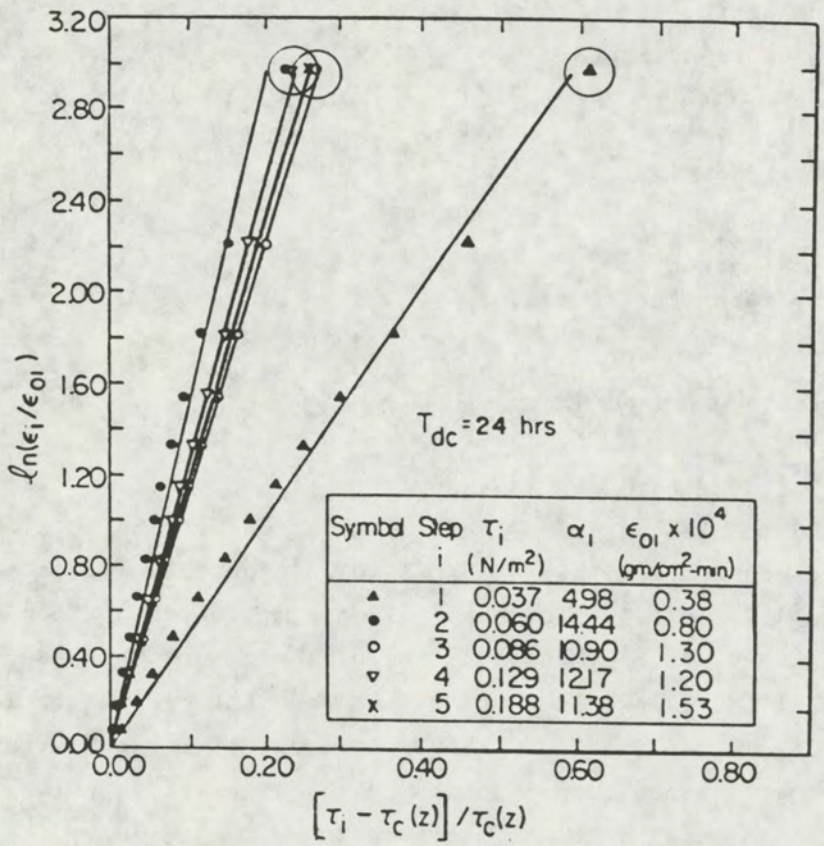

Figure B.1 *Normalized rate of erosion, ϵ_i/ϵ_{oi}, versus normalized excess shear stress, $[\tau_i - \tau_c(z)]/\tau_c(z)$, using kaolinite in tap water with T_{dc} = 24 hrs.*

(From Metha et al, 1982)

DELFT HYDRAULICS

APPENDIX C:

Correlations between erosion rate and some functions of the bed shear stress.

Maximum erosion rate
Consolidation time Tc = 24 hrs

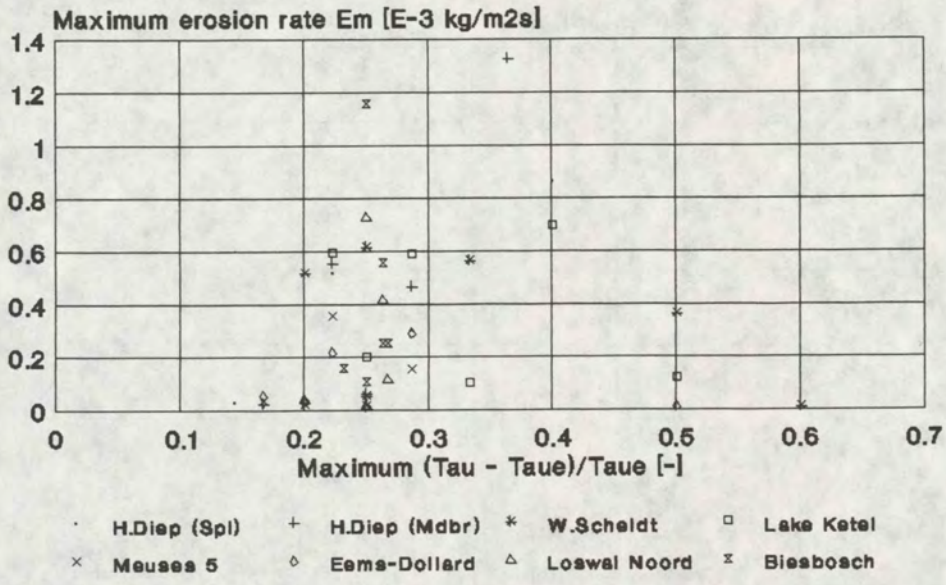

Fig C.1

Maximum erosion rate
Consolidation time Tc = 7 days

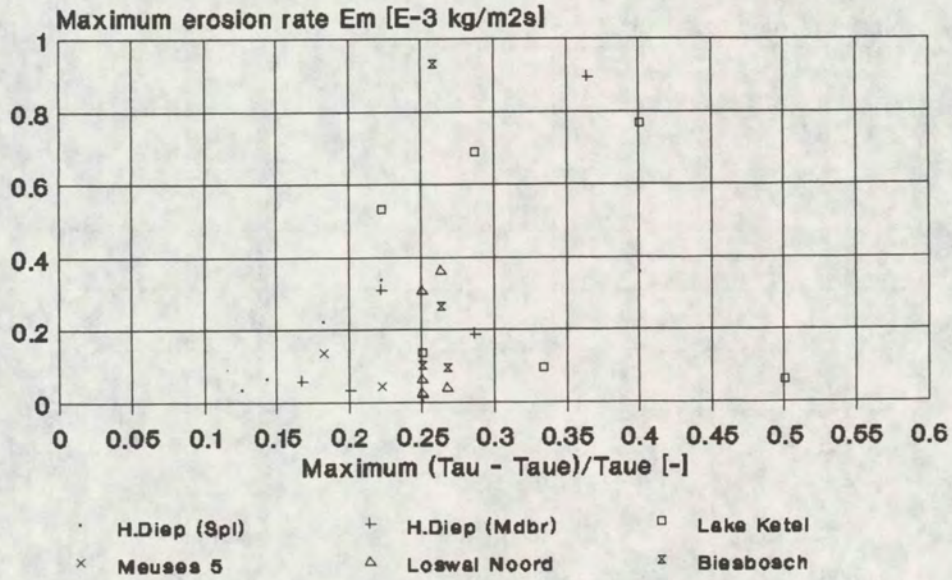

Fig C.2

Relative erosion rate
Consolidation time Tc = 24 hrs

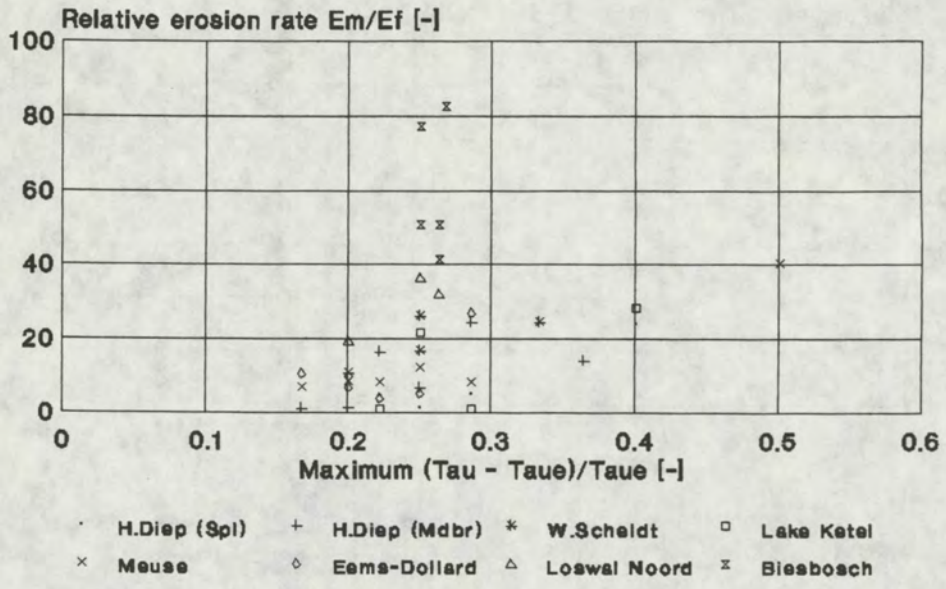

Fig C.3

Relative erosion rate
Consolidation time Tc = 7 days

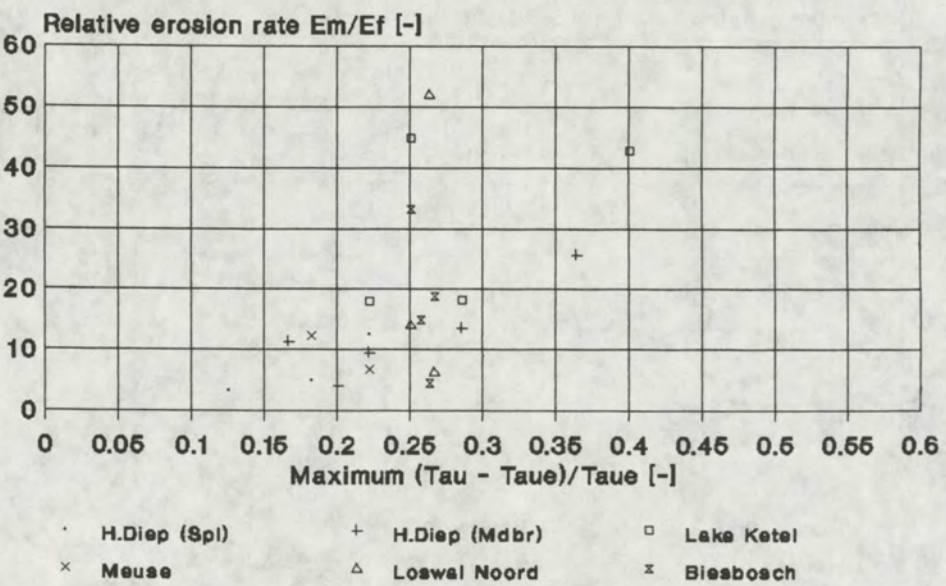

Fig C.4

APPENDIX D:

Summary of entrainment experiments described in literature.

Summary of entrainment experiments described in literature.

D.1 Experiments on fresh-water - saline-water experiments.

Ellison and Turner [1959].

Ellison and Turner performed two sets of entrainment experiments, referred to as "Surface jet experiments" and "Inclined plume experiments".
The surface jet experiments were carried out in a flume of 15 cm width, 20 cm depth and 2 m length. The lower saline layer was stagnant and had a depth of about 15 cm. The flowing upper layer had a depth of about 5 cm. The experiments describe the entrainment of saline water from a stagnant lower layer water into a flowing fresh water upper layer. An overall Richardson number Ri_o is defined as:

$$Ri_o = \frac{g\ \Delta\ h1}{U^2} \qquad (D.1)$$

where Δ = relative density difference ($\Delta = (\rho - \rho_0)/\rho_0$),
$h1$ = thickness flowing upper layer, and
U = velocity flowing upper layer.

During the experiments, Ri_o was varied between about 0,05 and 0,75. No other data on the experiments are given.

The inclined plume experiments were carried out in a 200 * 60 * 10 cm closed tank, which could be tilted to any desired angle. Saline water was injected through a slot near the bottom of the tank and fresh water was injected through a cloth cylinder mounted at the top of the tank. Thus the saline layer could flow underneath the fresh upper layer, driven by gravity. These experiments describe the entrainment of fresh water from a stagnant upper layer into a flowing saline lower layer.
A maximum velocity of about 0,15 m/s was recorded, the relative density difference was kept at 3 %, and the slope α was varied between 9^o and 90^o, and Ri_o was varied between 0,05 and 0,4. The overall Richardson number Ri_o is now defined as:

$$Ri_o = \frac{g\ \Delta\ h2\ \cos\alpha}{U^2} \qquad (D.2)$$

The results are presented in a E_v versus Ri_o graph, E_v defined as:

$$E_v = V_e/U \qquad (D.3)$$

with E_v = entrainment rate [-]
V_e = entrainment velocity ($V_e = dh/dt$) [m/s].

This graph, given in Figure D.1 shows that $E_v = f(1/Ri_o)$. This relation is not specified further in the paper. However, it shows no significant difference between the results of the two experiments. This is remarkable, as it would be expected because of the differences in velocity profile, that the processes of the entrainment of fresh water into a flowing saline lower layer are different from those of the entrainment of saline water into the fresh upper layer.

Kato and Phillips [1969].

Kato and Phillips carried out experiments with fresh and salt water in an annular flume. The outer diameter of this flume amounted to 1,524 m, the inner diameter to 1,067 m, thus the width of the flume was 0,228 m. A maximum depth of 0,28 m could be attained.
A linear density gradient was obtained by injecting water of varying salinity through 20 orifices equally spaced over the depth of the flume. The upper layer always contained fresh water. During the experiments the entire water column was flowing. But, as the flow was driven at the water surface, the upper part of the flow was more turbulent than the lower part, and the experiments describe the entrainment of more saline water from the lower layers into the less saline water in the upper part of the flow.
Three series of experiments were carried out with three different density differences: 1000 to 1042 kg/m^3, 1000 to 1084 kg/m^3, and 1000 to 1092 kg/m^3.
The flow velocity was typically varied between 0,25 and 0,35 m/s. During the experiments the Richardson number Ri_* was varied between 15 and 350. Ri_* is defined as:

$$Ri_* = \frac{g\ \Delta\ \delta}{u_*^2} \qquad (D.4)$$

with δ = depth of mixed layer (intermediate turbulent layer); this depth increases during the experiments from 0 to about 15 cm.

u_* = shear velocity at the rotating upper lid.

From the experiments the following empirical relation was derived:

$$Ev_* = \frac{V_e}{u_*} = \frac{2,5}{Ri_*} \qquad (D.5)$$

Thomson [1979] re-analysed the data by Kato and Phillips and obtained a somewhat different relation by correcting the experimental correlations for the Froude number. This resulted in:

$$Ev_* \propto \frac{1}{\sqrt{Ri_*}} \qquad (D.6)$$

Also Price [1979] apparently was inspired by the experiments of Kato and Phillips and also did some re-analysis. He corrected the original data for the effects of the drag of the side-wall of the flume. Through this exercise he obtained a relation similar to equ (D.6).

Kantha, Phillips and Azad [1977].

Kantha, Phillips and Azad carried out another series of experiments in the annular flume described by Kato and Phillips. This time however, the flume initially contained two homogeneous layers of different density. The relative density difference ($\Delta\rho/\rho_o$) was varied between about 0,1 and 0,4 and the shear stress (at the water surface) between 0,2 and 0,37 Pa. The overall Richardson number Ri_* (see (D.4)) was varied between 30 and 1100.

The results of these experiments are shown in Figure D.2 together with the results by Kato and Phillips. The latter found an entrainment rate of about half of that found by Kantha et al. Kato and Phillips used a linear stratified density gradient, so that energy could be lost from the turbulent layer by radiation as well as internal waves (explanation from Kantha et al).

A further observation is that the entrainment rate has no simple power-law dependence on Ri_* over the whole range studied. For $Ri_* < 400$ the slope is about Ri^{-1}, but beyond that the decrease in Ev_* is much larger.

Lofquist [1960].

Lofquist carried out experiments in a straight flume with a length of 24 m and a width 23,3 cm. The lower, saline water was circulated underneath a still layer of fresh water at a velocity between 2 and 10 cm/s. The depth of the lower layer h2 was varied between 18 and 20 cm, and the total depth of the two layers amounted to about 46 cm. The experiments describe the entrainment of fresh water from a stagnant upper layer into a flowing, saline lower layer.
Observed entrainment rates were correlated against the densimetric Froude number, which is the inverse of the overall Richardson number:

$$F_i = \frac{1}{Ri_o} = \frac{U^2}{g\ \Delta\ h2} \qquad (D.7)$$

During the experiments Ri_o was varied between about 8 and 100, and a relation similar to Ellison and Turner was found:

$$E_v = \frac{V_e}{U} \propto \frac{1}{Ri_o} \qquad (D.8)$$

Narimousa and Fernando [1987].

Narimousa and Fernando carried out experiments with fresh and saline water in a "disk flume, or race-track-flume". This is a recirculating flume in which the flow (in the upper layer) is driven by rotating disks mounted above each other. The test section of the flume has a length of 2 m, its width is 15 cm and its depth 60 cm. The velocity of the upper layer was varied between 5 and 15 cm/s; the variation of the density difference is not given. The overall Richardson Ri_δ number was varied between about 1 and 20, where Ri_δ is defined as:

$$Ri_\delta = \frac{g\ \Delta\ \delta}{U^2} \qquad (D.9)$$

where δ = thickness of mixed layer.

At low Richardson number ($Ri_\delta < 5$) the interface was observed to consist of regularly spaced billows. These billows break down to form regions containing irregular small features. Over a wide range of higher Richardson numbers ($5 < Ri_\delta < 20$) breaking internal waves were observed in which wisps of fluid are ejected to the mixed layer. The frequency of

these breaking waves decreases with increasing Richardson number. At 10 $< Ri_\delta <$ 20 large amplitude solitary waves were observed, which travel without breaking. At $Ri_\delta > 20$ molecular processes seem to take over the entrainment mechanism.

D.2 Experiments on entrainment of turbidity currents.

Ashida and Egashira [1975].

Ashida and Egashira studied the entrainment of stagnant, clear water into a turbidity current. They carried out experiments in a tank of 20 m length, 0,55 m depth and 0,5 m width. The turbid water was obtained by mixing fresh water with fine sand with a median diameter of about 30 μm. The thickness of the flowing lower layer varied between 7 and 13 cm, the density difference between upper and lower layer varied between 5 and 22 kg/m^3, and lower layer velocities of 8 to 19 cm/s were measured. During the experiments the overall Richardson number was varied between about 0,8 and 8.

Parker, Pantin and Fukushima [1985].

Parker et al describe the analysis by Egashira [1980] of the entrainment experiments described above and those by Ellison and Turner, Lofquist and Kato and Phillips (again after a re-analysis). They obtained the following relation:

$$E_v = \frac{V_e}{U} = \frac{0,0015}{Ri_o} \qquad (D.10)$$

Using the same data, Garcia [1989] found a somewhat different relation:

$$E_v = \frac{V_e}{U} = \frac{0,075}{(1 + 718\ Ri_o^{2,4})^{0,5}} \qquad (D.11)$$

Data and equ. (D.10) and (D.11) are shown in Figure D.3.

Srinivas and Mehta [1990].

Srinivas and Mehta report on experiments carried out in a "race-track flume" similar to that used by Narimousa et al. The test section of this flume is about 2 long, its width 10 cm, and the flume height 50 cm. The experiments were carried out with kaolinite and bentonite in tap water. The initial bulk density was varied between 1030 and 1080 kg/m^3; the velocity is estimated at about 10 cm/s, though no details are given. An overall Richardson number Ri_u was varied between 4 and 30 and is defined as:

$$Ri_u = \frac{g \Delta h}{U^2} \qquad (D.13)$$

where h = entire flow depth.

From the experiments the following relation was deduced:

$$E_v = \frac{0,27\ Ri_u^{-0,9}}{(400 + Ri_u^2)^{0,66}} \qquad (D.13)$$

Or, as a first approximation: $E_v \propto 1/Ri_u^{0,9}$, which is again consistent with the results of other experiments.

D.3 Effect of diffusivity.

Turner [1968].

Turner carried out entrainment experiments in a perspex tank, 25,4 cm square and 40 cm height with an oscillating grid mounted in either the lower layer or in both layers. The grid consisted of 1 * 1 cm strips aligned at 5 cm interval. The amplitude of the oscillations was kept constant at about 1 cm. Experiments were carried out with cold and hot water, with fresh and saline water, and a combination of these. The following overall Richardson number was defined:

$$Ri_o = \frac{g \Delta}{\ell f^2} \qquad (D.14)$$

in which ℓ is some arbitrary length scale and f is the frequency of the grid.

For density differences produced by heat alone, the entrainment rate appeared closely dependent on Ri^{-1}, except at small values of Ri. For experiments with a salinity difference across the interface, the mixing rate appeared the same as in the heat experiments at low values of Ri, but becomes proportional to $Ri^{-3/2}$ when Ri is increased. As a result, the entrainment rate differed by almost an order of magnitude at the higher Richardson number experiments.
Turner attributes this difference in behaviour to the differences in molecular diffusivity. At low Reynolds number, it is the molecular diffusivity that mixes packages of fluid, ejected from one layer into the other, with its environment. At higher Reynolds number, the mixing will be dominated by small scale turbulent motions.
The viscosity varied only slightly and can therefore not play a significant role, according to Turner.

Wolanski and Brush [1975].

Wolanski and Brush carried out entrainment experiments in a device with the same dimensions as the one used by Turner [1968]. The amplitude of the oscillations was kept constant at about 1 cm, its frequency was varied between 120 and 360 rpm. The density difference was kept small at about 0,005 kg/m^3. This was attained by using cold and hot water, fresh and saline water, fresh water and a sugar solution and fresh water and suspensions of Silica spheres and kaolinite clay. The Reynolds number Re, defined as:

$$Re = \frac{u_* D}{\nu} \qquad (D.15)$$

where D = depth lower layer = depth upper layer. Re was varied between $4\ 10^3$ and $12\ 10^3$. The molecular diffusivity of these fluids varied from $10^{-14}\ m^2/s$ for the kaolinite suspension to $1.4\ 10^{-7}\ m^2/s$ for hot water. From the experiments the following relation was deduced:

$$Ev_* = \frac{V_e}{u_*} \propto Ri_*^{-n} \qquad (D.16)$$

with n varying from about 1 for hot water, 1,3 for saline water, up to 4 for the kaolinite suspension. This is shown in Figure D.4. The Richardson number Ri_* is now defined as:

$$Ri_* = \frac{4\,\pi^2\,g\,\Delta\,h}{u_*^2} \qquad (D.17)$$

with $u_* = 2\,\pi\,a\,f$, where a and f are the amplitude and frequency of the oscillating grid. These experiments agree with the hypothesis by Turner on the significant role of the molecular diffusivity at low Reynolds number.

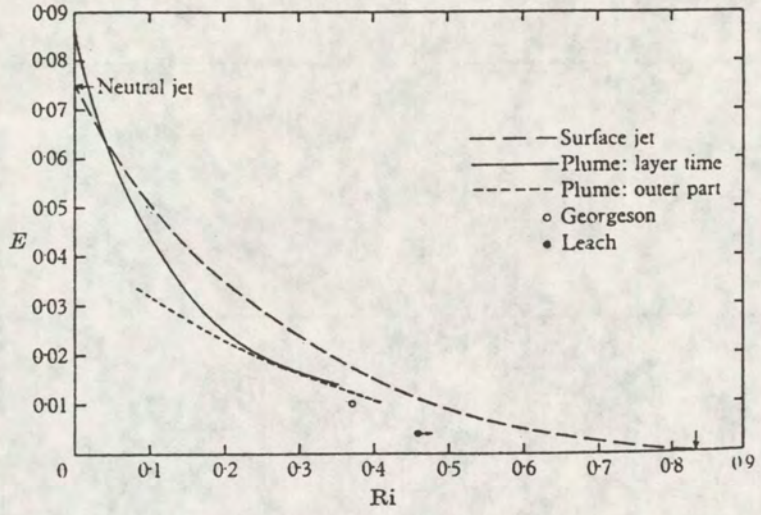

Fig. D 1 Ellison and Turner

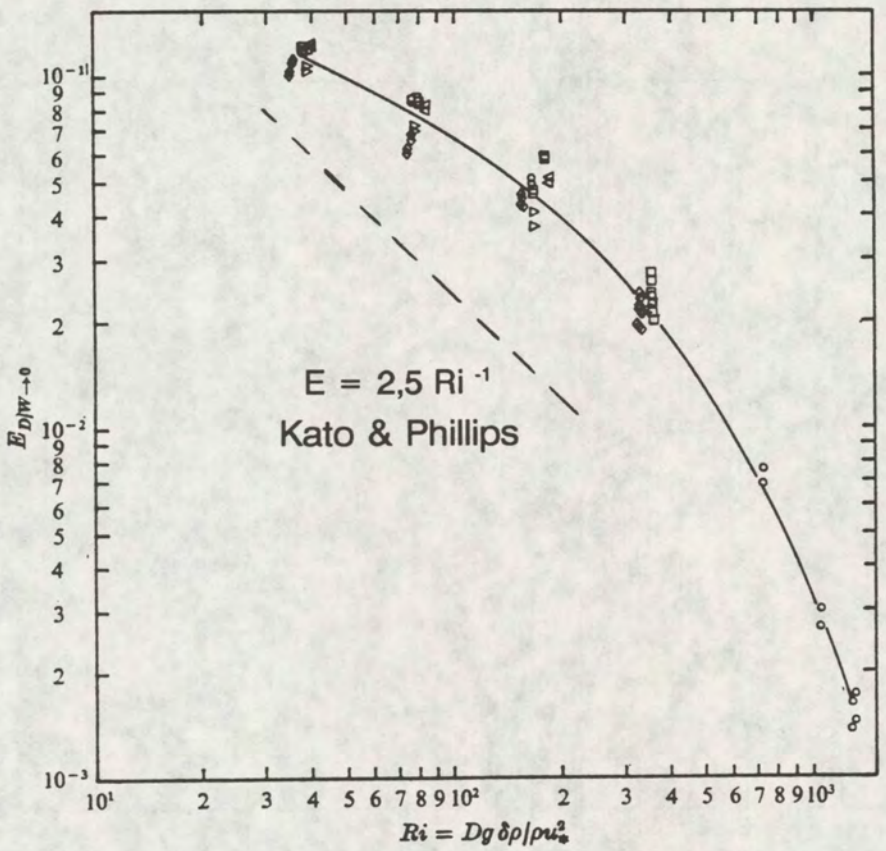

Fig. D 2 Kantha , Phillips and Azad

Entrainment rates		
DELFT HYDRAULICS		Fig. D 1,2

DELFT HYDRAULICS

Entrainment rates

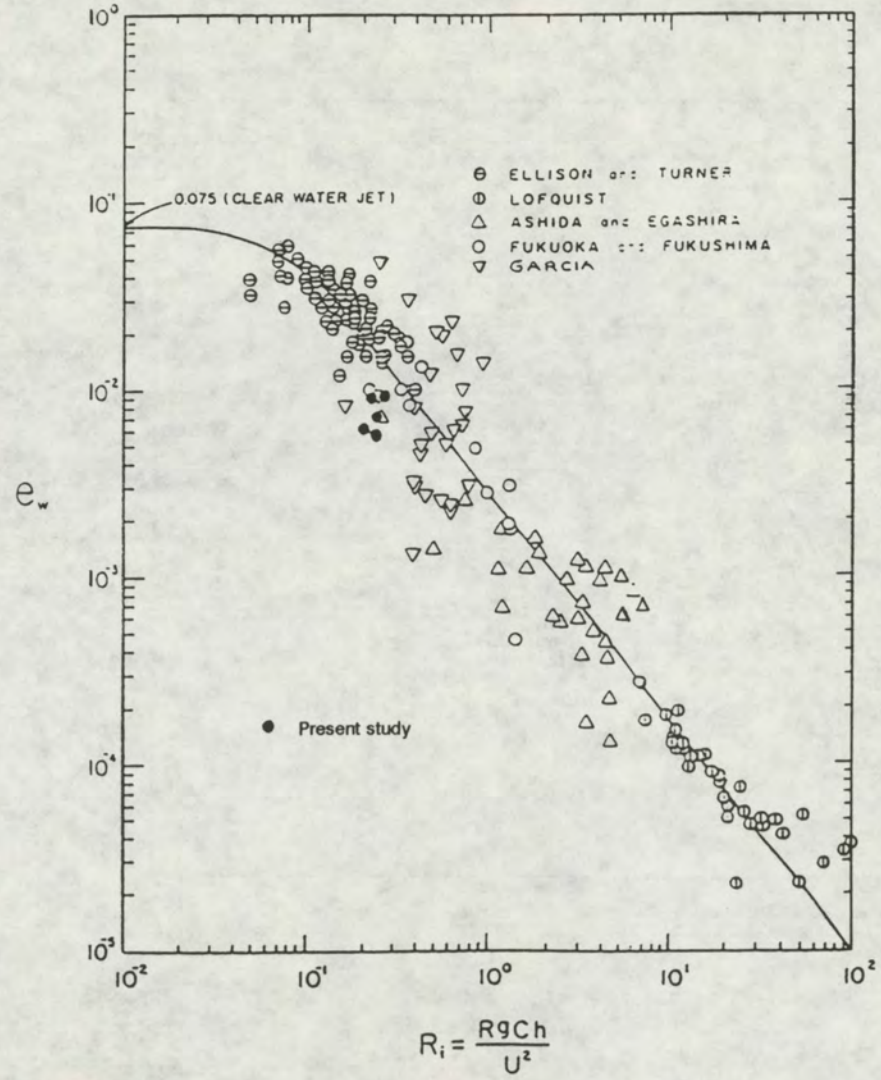

Fig. D 3 Garcia

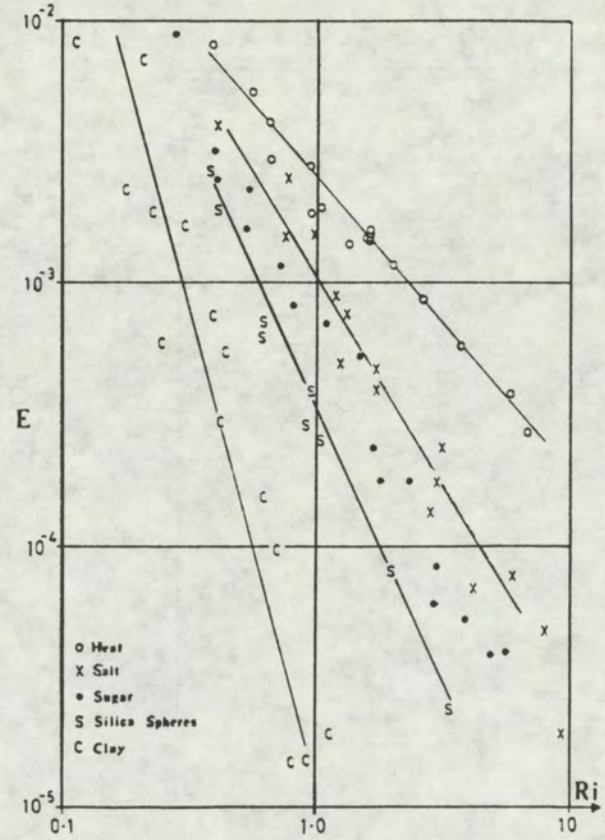

Fig. D 4 Wolanski and Brush

Fig. D 3,4